ENGINEERING RIBONUCLEASE-BASED

CANCER THERAPEUTICS

by

Thomas John Rutkoski

A dissertation submitted in partial fulfillment

of the requirements for the degree of

Doctor of Philosophy

(Biochemistry)

at the

UNIVERSITY OF WISCONSIN–MADISON

2008

A dissertation entitled

ENGINEERING

RIBONUCLEASE-BASED

CANCER THERAPEUTICS

submitted to the Graduate School of the
University of Wisconsin-Madison
in partial fulfillment of the requirements for the
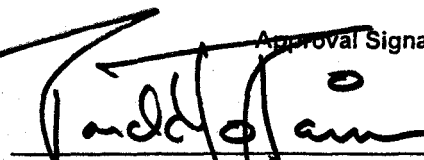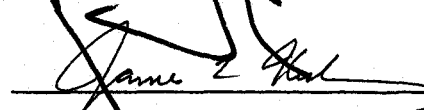degree of Doctor of Philosophy

by

Thomas J. Rutkoski

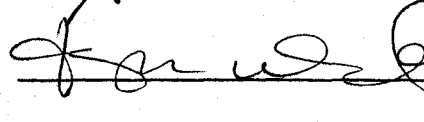**Date of Final Oral Examination:** March 6, 2008
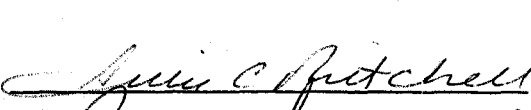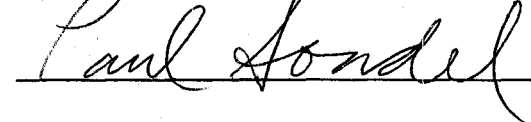
Month & Year Degree to be awarded: **December**   **May** 2008 **August**

****

Approval Signatures of Dissertation Committee

Signature, Dean of Graduate School

ENGINEERING RIBONUCLEASE-BASED CANCER THERAPEUTICS

Thomas John Rutkoski

Under the supervision of Professor Ronald T. Raines

at the University of Wisconsin–Madison

Bovine pancreatic ribonuclease (RNase A) was perhaps the most-studied enzyme of the 20th century. It was quickly established as a popular model system partly due to its ready availability following the purification of one kilogram of pure crystalline RNase A in the 1950's by Armour, Inc., a meat packing company in Chicago that freely distributed the material to interested researchers. The role that RNase A has played in the field of protein biochemistry is evidenced by four Nobel laureates, C. B. Anfinsen, S. Moore, W. H. Stein (Chemistry '72), and R. B. Merrifield (Chemistry '84), having chosen this now storied protein as the object of their investigations.

Originally thought to serve solely as a digestive enzyme for the degradation of bacterial RNA produced in the ruminant gut, the physiological role of RNase A might have been dismissed by some as mundane. In recent decades, however, other members of this enzyme superfamily have been shown to participate in a greater number of biological functions including angiogenesis, innate immunity, and sperm maturation. Additionally, homologues of RNase A isolated from oocytes and early embryos of frogs as well as one from bovine seminal plasma (BS-RNase) have been shown to exert selective toxicity to human cancer cells. In particular, Onconase® (ONC), isolated from the Northern leopard

frog, *Rana pipiens*, has recently been granted both orphan-drug and fast-track status by the U.S. Food and Drug Administration for the treatment of malignant mesothelioma.

Thus, ribonucleases represent an exciting new class of cancer therapeutics. Mammalian ribonucleases such as RNase A and its human homologue, RNase 1, are not toxic to cancer cells as a result of their potent inhibition by the cytosolic ribonuclease inhibitor (RI). However, they exhibit a number of properties that make them otherwise more desirable as therapeutics. The natural cytotoxic activity of ONC and BS-RNase is largely attributed to their inherent insensitivity to RI. Using a variety of protein engineering strategies, RNase A and RNase 1 have been endowed with cytotoxic activity by reducing their high endogenous affinity (femtomolar) for RI. These strategies, as well as the structural basis for the natural RI-insensitivity of ONC and BS-RNase, are reviewed in CHAPTER 1.

One approach to engineering an RI-evasive ribonuclease has been the use of site-directed mutagenesis to make disruptive amino acid substitutions in RNase A within the RI–ribonuclease interface. CHAPTER 2 describes the exploitation of an unbiased computational algorithm (FADE) to identify the regions of greatest shape-complementarity within the RI-RNase A interface. Guided by this analysis, several variants of RNase A were created that are more potent cytotoxins than ONC in vitro.

BS-RNase derives its cytotoxic activity from its unique dimeric quaternary structure. Inspired by this design, CHAPTER 3 describes the production of dimers and trimers of mammalian ribonucleases resulting from the restrictive tethering of these enzymes to

preclude RI-binding. These semi-synthetic conjugates are shown to reduce the growth of tumor cells both in vitro and in vivo.

The parenteral administration of therapeutic proteins, as well as their potential immunogenicity, sensitivity to proteases, and greater production and formulation costs pose unique challenges to the development of biologics. The covalent attachment of large, inert polymers such as poly(ethylene glycol) (PEG) to candidate protein therapeutics (a process termed PEGylation) is a strategy proven to overcome many of these hurdles. The next two chapters describe the site-specific PEGylation of RNase A (CHAPTER 4) and RNase 1 (CHAPTER 5) to simultaneously enhance RI-evasion and increase the persistence of these proteins in the circulation of animals.

The final chapter (CHAPTER 6) explores future directions and ideas for the area of ribonuclease-based cancer therapeutic development. This chapter is followed by several appendices that describe ancillary collaborative projects, including the optimization and miniaturization of a fluorescence-based competition assay (APPENDIX 1), which enabled the precise determination of RI-affinity for many of the ribonucleases and their conjugates prepared in CHAPTERS 2–5. APPENDIX 2 describes a means to enhance RNase A cytotoxicity through cationization of the protein ("arginine grafting") without altering its affinity for RI. And finally, APPENDIX 3 describes a collaboration aimed at producing a dual therapeutic/diagnostic for cancer treatment by appending a variant of RNase A with a MRI contrast agent. Taken together, this thesis describes progress toward the development of ribonuclease-based cancer therapeutics by using a number of strategies to reduce the sensitivity of mammalian pancreatic ribonucleases to RI.

Acknowledgements

This thesis represents the culmination of my education thus far as a scientist. Whatever personal sense of accomplishment I might derive from being able to present this tome to my committee, it would be a terrible injustice to do so without first expressing my most sincere and humble gratitude to the myriad of people throughout my life who have made my graduate career not only possible but enjoyable.

First and foremost I want to thank my parents, Eugene and Ann Rutkoski, for teaching my sisters and me the enormous value of education and for always making it a top priority in our family. Without their love and support, and that of my sisters, Jennifer and Sarah, I don't know how I would've navigated through the low points of the last four and a half years. This work is therefore dedicated to them. I am also especially grateful to the extended Gormican clan and their families who made Wisconsin an easy place to call home. And although blood is said to be thicker than water, my friends, both new and old, have helped me maintain a larger life perspective, and are a continuous source of inspiration, camaraderie, and encouragement.

I am thankful for all of my teachers, whose jobs are many times thankless, but especially those who cultivated my early interest in science, including J. Calvaresi, D. Dahms, H. Dean, T. Frey, and R. Ringler. Additionally, I have been fortunate to have had many fantastic mentors and advisors throughout my development as a scientist, including, D. R. McCaslin, B. T. Nixon, J. R. Rojas, and N. Watson.

My time in graduate school has been most strongly influenced by those individuals with whom I have had the pleasure of working next to at the bench in the Raines

Laboratory. Among them are T.-Y. Chao, K. A. Dickson, S. M. Fuchs, K. L. Gorres, G. J. Jakubczak, R. J. Johnson, J. Kalia, F. W. Kotch, V. M. Kung, L. D. Lavis, J. E. Lee, B. G. Miller, M. D. Shoulders, B. D. Smith, and R. F. Turcotte. In fact, all members of the Raines group past and present have shaped my time at the University of Wisconsin–Madison and I recognize that even in the microcosm of an individual lab my contributions have been made while standing on the shoulders and accomplishments of those before me.

In an age of ever-increasing specialization I have had the opportunity to benefit from the expertise of numerous exceptionally talented collaborators including: J. A. Kink, L. D. Lavis, J. C. Mitchell, L. E. Strong and others who are specifically acknowledged within individual chapters where appropriate.

I am grateful to the NIH Biotechnology Training Program, the William R. & Dorothy E. Sullivan Wisconsin Distinguished Graduate Fellowship Program, and Professor Raines for funding during my graduate training.

Finally, I would like to thank Professor Ronald T. Raines for allowing me to be a part of his research group, for his professionalism, and for conveying to me the importance of articulating and conveying one's scientific ideas clearly. He has made possible a number of unique opportunities throughout my graduate career including my participation in the 7th International Meeting on Ribonucleases in Stará Lesná, Slovakia in 2005. I thank him for assembling a diverse group of extremely talented scientists and establishing an environment where I have been continually challenged to grow as a scientist and have been provided the means to do so.

Table of Contents

CHAPTER 1

Introduction: Evasion of Ribonuclease Inhibitor as a Determinant of Ribonuclease

CHAPTER 3

Cytotoxic Dimers and Trimers of Mammalian Ribonucleases Generated via Site-Specific

CHAPTER 5

Site-Specific PEGylation of Recombinant Human Pancreatic Ribonuclease to Evade

CHAPTER 6

APPENDIX 1

APPENDIX 2

APPENDIX 4

Cover Art   318

List of Tables

List of Schemes

List of Figures

List of Abbreviations

ε	extinction coefficient
5-IAF	5-iodoacetamidofluorescein
6-FAM	6-carboxyfluorescein
6-TAMRA	6-carboxytetramethylrhodamine
ATCC	American Type Culture Collection
ATP	adenosine 5'-triphosphate
BCA	bicinchoninic acid
BMH	1,6-bis(maleimido)hexane
BMOE	1,2-bis(maleimido)ethane
BSA	bovine serum albumin
BS-RNase	bovine seminal ribonuclease
cDNA	complementary deoxyribonucleic acid
Da	dalton
ddH$_2$O	distilled de-ionized water
DEF	2',7'-diethylfluorescein
DEFIA	2',7'-diethylfluorescein-5-iodoacetamide
DMF	dimethylformamide
DMSO	dimethylsulfoxide
DNA	deoxyribonucleic acid
DO3A	1,4,7,10-tetraazacyclododecane-1,4,7-triacetic acid

DO3A-MAL	1,4,7,10-tetraazacyclododecane-1,4,7-triacetic acid-10-maleimidoethylacetamide
DOTA	1,4,7,10-tetraazacyclododecane-1,4,7,10-tetraacetic acid
DPBS	Dulbecco's phosphate buffered saline
dsRNA	double-stranded ribonucleic acid
DTNB	5,5'-dithiobis(2-nitrobenzoic acid)
DTPA	diethylenetriaminepentaacetic acid
DTT	dithiothreitol
E	enzyme
ECP	eosinophil cationic protein
EDN	eosinophil-derived neurotoxin
EDTA	ethylenediaminetetraacetic acid
EPR	enhanced persistence and retention
F	fluorescence
FACS	fluorescence-activated cell sorting
FADE	fast atomic density evaluation
FBS	fetal bovine serum
FDA	United States Food and Drug Administration
FPLC	fast performance liquid chromatography
FRET	Förster (fluorescence) resonance energy transfer
GCW	glomerular capillary wall
GSC	glomerular sieving coefficient

GSH	reduced glutathione
GSSG	oxidized glutathione
h	hour
HCl	hydrochloric acid
HOPO	hydroxypyridinone
HPLC	high-performance (pressure) liquid chromatography
hRI	human ribonuclease inhibitor
HSA	human serum albumin
I	inhibitor
i.p.	intraperitoneal
IgG	immunoglobulin gamma (γ)
IPTG	isopropyl-1-thio-β-D-galactopyranoside
k_{cat}	first-order enzymatic rate constant
K_d	equilibrium dissociation constant
kDa	kilodalton
K_i	inhibitor dissociation constant
K_m	Michaelis constant
λ_{em}	emission wavelength
λ_{ex}	excitation wavelength
λ_{max}	absorption or excitation maximum
LB	Luria–Bertani broth
MALDI–TOF	matrix assisted laser desorption/ionization–time of flight

MES	2-(*N*-morpholino)-ethanesulfonic acid
min	minute
MOPS	4-morpholinepropanesulfonic acid
mPEG	monomethoxy-poly(ethylene glycol)
mRNA	messenger ribonucleic acid
MW	molecular weight
MWCO	molecular weight cutoff
NaCl	sodium chloride
NEM	*N*-ethylmaleimide
NBS	non-binding surface
OD	optical density
ONC	Onconase®; ranpirnase; P-30; Pannon
OVS	oligo(vinylsulfonic acid)
PBS	phosphate-buffered saline
PCR	polymerase chain reaction
PDB	protein data bank
PDM	phenylenedimaleimide
PEG	poly(ethylene glycol)
PS	poly(styrene)
PTM	*N,N',N''*-(1,3,5-phenylene)trimaleimide
pK_a	log of the acid dissociation constant
poly(C)	poly(cytidylic acid)

pRI	porcine ribonuclease inhibitor
r_1	longitudinal water proton relaxation rate ($1/T_1$ vs. [Gd])
R_9	nonaarginine
rDNA	recombinant DNA
RI	ribonuclease inhibitor
RNA	ribonucleic acid
RNase A	unglycosylated bovine pancreatic ribonuclease
RNase 1	human pancreatic ribonuclease
rRNA	ribosomal ribonucleic acid
s	second
SDS–PAGE	sodium dodecyl sulfate–poly(acrylamide) gel electrophoresis
S–E	Stokes–Einstein
t	time
T_1	longitudinal relaxation time
TB	terrific broth
TGI	tumor growth inhibition
THF	tetrahydrofuran
TI	therapeutic index
TMEA	tris(maleimido)ethylamine
TNB	2-nitro-5-thiobenzoate
Tris	2-amino-2-(hydroxymethyl)-1,3-propanediol
Z	net molecular charge: Arg + Lys – Asp – Glu

CHAPTER 1

Introduction:

Evasion of Ribonuclease Inhibitor as a

Determinant of Ribonuclease Cytotoxicity

1.1 Abstract

Onconase® (ONC) is an amphibian member of the bovine pancreatic ribonuclease (RNase A) superfamily that exhibits innate antitumoral activity. ONC has been granted both orphan-drug and fast-track status by the U.S. Food and Drug Administration for the treatment of malignant mesothelioma and is poised to become the first chemotherapeutic agent based on a ribonuclease. Investigations into the mechanism of ribonuclease-based cytotoxicity have elucidated several important determinants for cytotoxicity, including efficient deliverance of ribonucleolytic activity to the cytosol and preservation of conformation stability. Nevertheless, the most striking similarity between ONC and bovine seminal ribonuclease (BS-RNase), another naturally cytotoxic ribonuclease, is their insensitivity to inhibition by the potent cytosolic ribonuclease inhibitor protein (RI). RI typically binds to its ribonuclease ligands with femtomolar affinity—an extraordinary feat considering the lack of sequence identity among the bound ribonucleases. Mammalian ribonucleases such as RNase A or its human homologue, RNase 1, have the potential to be more desirable chemotherapeutic agents than ONC owing to their higher catalytic activity, low potential for immunogenicity, favorable tissue distribution, and high therapeutic index, but are limited by their sensitivity to RI. These non-toxic mammalian ribonucleases can be transformed into potent cytotoxins by engendering them with RI-evasion using protein engineering strategies such as site-directed mutagenesis (See also CHAPTER 2 and APPENDIX 2), multimerization (See also CHAPTER 3), fusion to a targeting moiety, and chemical modification (See also CHAPTERS 4 and 5; APPENDIX 3). In several instances, these engineered ribonucleases exhibit greater cytotoxicity in vitro

than does ONC. Herein, we review the biochemical characteristics of RI·ribonuclease complexes and progress towards the development of mammalian ribonuclease-based chemotherapeutics through the elicitation of RI-evasion.

1.2 Introduction

Since its discovery over eighty years ago (Jones, 1920), bovine pancreatic ribonuclease (RNase A; EC 3.1.27.5) has provided chemical enzymologists, biophysical chemists, structural biologists, and evolutionary biologists with a highly tractable model system. The result has been a myriad of advances in numerous disciplines (Richards and Wyckoff, 1971; Blackburn and Moore, 1982; Raines, 1998; Marshall *et al.*, 2007). RNase A catalyzes the cleavage of RNA at a rate approaching the diffusion limit (Park and Raines, 2003) and putatively functions to break down the large amounts of RNA that accumulate in the ruminant gut (Barnard, 1969). In the last several decades, owing to the discovery of homologues of RNase A that exhibit cytotoxic activity at low concentrations both in vitro and in vivo (Floridi *et al.*, 1972; Dostál and Matoušek, 1973; Ardelt *et al.*, 1991), interest in this enzyme family has experienced a resurgence directed at exploiting these activities for therapeutic purposes (Leland and Raines, 2001; Matoušek, 2001; Makarov and Ilinskaya, 2003; Benito *et al.*, 2005; Arnold and Ulbrich-Hofmann, 2006; Lee and Raines, 2008).

Many of the details of the mechanism of ribonuclease-mediated cytotoxicity are unclear. Nonetheless, several major aspects of the pathway have been elucidated, allowing for the construction of the mechanism depicted in Figure 1.1 (Leland and

Raines, 2001; Haigis and Raines, 2003; Benito *et al.*, 2005). The first step in

ribonuclease-mediated cytotoxicity is the association of the cationic ribonuclease with the

anionic cell membrane (Figure 1.1A) (Futami *et al.*, 2001; Haigis and Raines, 2003). For

many members of the RNase A superfamily, this absorptive process has been shown to

be non-saturable and not receptor-mediated (Haigis and Raines, 2003), but is instead

governed by electrostatic association with either heparan sulfate proteoglycans (Fredens

et al., 1991; Soncin *et al.*, 1997; Fuchs and Raines, 2006) or the head groups of

phospholipids (Notomista *et al.*, 2006). The importance of Coulombic interactions in the

cellular association and subsequent internalization of ribonucleases has been

demonstrated by using both chemical modification (Futami *et al.*, 2001) and site-directed

mutagenesis (Fuchs *et al.*, 2007; Johnson *et al.*, 2007a). Notable exceptions exhibiting

more specific cellular interactions include the amphibian sialic acid-binding lectins

(SBLs) from *Rana catesbeiana* and *Rana japonica*, whose high affinity for sialic acid

groups enabled the initial isolation of these ribonucleases (Youle and D'Alessio, 1997).

Additionally, the amphibian ribonuclease, Onconase® (ONC; ranpirnase; P-30), has been

reported to bind to specific sites on cultured 9L glioma cells (Wu *et al.*, 1993), although

these putative receptors have never been identified and could be absent from other cell

types (Haigis and Raines, 2003). Furthermore, two proteins that bind to angiogenin

(ANG; RNase 5) have been identified on the surface of human endothelial cells (Hu *et

al.*, 1993; Hu *et al.*, 1997). Regardless of the exact nature of their cellular association, the

subsequent internalization and translocation of ribonucleases into the cytosol

(Figure 1.1B,C) has been shown to be an essential aspect of ribonuclease-mediated

cytotoxicity (Saxena *et al.*, 1991). Ribonuclease cytotoxicity has been correlated with the efficiency of endocytic internalization (Leich *et al.*, 2007), though its route to the cytosol is in dispute (Haigis and Raines, 2003; Rodríguez *et al.*, 2007).

Many protein toxins derived from bacteria and plants contain a separate domain for the express purpose of translocating across the vesicular membrane to their cytosolic site of action (Collier, 2001; Olsnes and Kozlov, 2001). In contrast, pancreatic ribonucleases are single-domain proteins for which the mechanism of translocation into the cytosol is understood only poorly. For cytotoxic variants of RNase A, escape from the acidifying endosome occurs prior to reaching the trans-Golgi network (Haigis and Raines, 2003) and is a relatively inefficient process, as ~95% of the internalized ribonuclease is degraded in lysosomal compartments without ever reaching the cytosol ((Davidson *et al.*, 1971; Bartholeyns and Baudhuin, 1976; Bosch *et al.*, 2004); Chao, T.-Y.; Lavis, L. D. and Raines, R. T., unpublished results). Ultimately, a few molecules of ribonuclease reach the cytosol, and there encounter the ribonuclease inhibitor protein (RI) (Figure 1.1D). Tightly bound ribonucleases are rendered harmless to the cell (Haigis *et al.*, 2003) (Figure 1.1E). In contrast, ribonucleases that are naturally RI-evasive, or have been engineered to be so, degrade cellular RNA and induce apoptosis (Figure 1.1F) (Ilinskaya and Makarov, 2005). Additional mechanisms unrelated to the disruption of protein synthesis have been proposed for the elicitation of an apoptotic response by ONC (Iordanov *et al.*, 2000; Ardelt *et al.*, 2003).

Considering this model of ribonuclease-mediated cytotoxicity, several attributes of a ribonuclease can be identified as determinants of cytotoxicity, and thus represent targets

for modification and optimization by the protein engineer. These properties include the ability to bind to the cell surface and be internalized efficiently (which includes the ability to reach the cytosol) (Johnson *et al.*, 2007a), the preservation of native three-dimensional structure (*i.e.*, conformational stability) (Klink and Raines, 2000), and the ability to catalyze the degradation of RNA (Kim *et al.*, 1995a), specifically in the presence of RI (*i.e.*, RI-evasion) (Leland *et al.*, 1998; Leland *et al.*, 2001; Lee and Raines, 2005; Rutkoski *et al.*, 2005). Protein design and engineering efforts aimed at modulating each of these characteristics with the goal of increasing cytotoxic activity have yielded impressive results, while informing our understanding of ribonuclease-mediated cytotoxicity (Rybak and Newton, 1999; Klink and Raines, 2000; Futami *et al.*, 2002; Fuchs *et al.*, 2007). Much of this work, including tumor cell-targeting (Daniels *et al.*, 2006; Hoshimoto *et al.*, 2006; Yagi *et al.*, 2006) and sub-cellular localization (Bosch *et al.*, 2004; Rodríguez *et al.*, 2006), is beyond the scope of this review but has been described elsewhere (Rybak *et al.*, 1991; Youle *et al.*, 1993; Schein, 1997; Rybak and Newton, 1999).

Here, we consider the anomalously high affinity of RI for its secretory ribonuclease ligands and the tremendous gains in cytotoxicity that can be made by disruption of this association. We review the strategies nature has used to achieve RI-evasive cytotoxic ribonucleases as well as the state of the art of engendering RI-evasion with the goal of developing ribonuclease-based chemotherapeutics. Before describing the explicit strategies used by nature and protein engineers to achieve RI-evasion, we review RI and

its protein complexes so as to provide a detailed understanding of the task at hand and to underscore just how daunting that task can be.

1.3 Ribonuclease Inhibitor

RI is a ~50-kDa protein found exclusively in the cytosol of mammalian cells. (For recent reviews of RI, see (Hofsteenge, 1997; Shapiro, 2001; Dickson *et al.*, 2005).) Its obligate cytosolic localization maintains its 29 (bovine RI), 30 (porcine RI), or 32 (human RI) cysteine residues in a reduced state, which is required for its function as an inhibitor (Blázquez *et al.*, 1996). Nevertheless, all known ligands of RI are secreted ribonucleases. This apparent paradox, in conjunction with its invariant high concentration of ~4 µM in the cytosol (Leland *et al.*, 1998; Haigis *et al.*, 2003), implies a biological role for RI as an intracellular "sentry" to safeguard the cell from the potentially damaging activity of adventitious ribonucleases (Roth, 1958; Beintema *et al.*, 1988b; Lee and Vallee, 1993; Haigis *et al.*, 2003). Further support of this hypothesis comes from experiments in which cytosolic RI is over-produced, diminishing the potency of toxic RNase A variants (Haigis *et al.*, 2003). Conversely, silencing of RI gene expression by RNA interference increases the sensitivity of cells to exogenous cytotoxic ribonucleases (Monti and D'Alessio, 2004). Other proposed biological roles for RI include the modulation of the biological function of various ribonucleases (*e.g.*, the angiogenic activity of ANG in promoting neovascularization) or as an oxidative sensor to monitor the redox status or age of a cell (Moenner *et al.*, 1998; Johnson *et al.*, 2007b; Monti *et al.*, 2007). Despite the uncertainty surrounding the precise physiological role of RI, its potent

inhibitory effects have had a strong influence on the natural and artificial evolution of cytotoxic ribonucleases.

1.4 RI·Ribonuclease Complexes

RI binds to members of the RNase A superfamily with a 1:1 stoichiometry, inhibiting completely their catalytic activity by steric occlusion of the enzymic active site (Kobe and Deisenhofer, 1996). The noncovalent complexes formed by RI and its ligands ($K_d =$ 0.3–2.7 × 10^{-15} M) are among the tightest known in biology (Table 1.1; Figure 1.2). The affinity of RI for its ligands is comparable to that of avidin for biotin (Green, 1975), protein trypsin inhibitor (PTI) for trypsin (Vincent and Lazdunski, 1972), tissue inhibitor of metalloproteinase (TIMP) for matrix metalloproteases (Hutton *et al.*, 1998), and barstar for barnase (Schreiber and Fersht, 1993). Astonishingly, RI has evolved anomalously high affinity towards protein ligands of low amino-acid sequence identity (≥23%; Table 1.2). During the last 15 years, many of the atomic details that enable these dichotomous, high affinity/broad specificity interactions have been illuminated by the determination of the three-dimensional structure of free RI (Kobe and Deisenhofer, 1993) as well as that of four RI·ligand complexes (Kobe and Deisenhofer, 1995b; Papageorgiou *et al.*, 1997; Iyer *et al.*, 2005; Johnson *et al.*, 2007c) (Table 1.3; Figure 1.3A,B).

The highly symmetrical but nonglobular horseshoe-shape of RI provides a broad platform for extensive protein–protein interactions, which is a hallmark of leucine-rich repeat (LRR)-containing proteins (Kobe and Deisenhofer, 1994). Few heterologous protein complexes bury more solvent accessible surface area (ASA) than do

RI·ribonuclease complexes, which bury 27–60% more surface area than do the average

inhibitor·enzyme complex and 54–105% more surface area than is observed in typical

antibody·antigen complexes (Table 1.1). Despite the expansive size of the interfaces

formed between RI and its ligands, much of the free energy of complex formation is

contributed by small regions or "hot spots" (Clackson and Wells, 1995; DeLano, 2002;

Moreira *et al.*, 2007), with the majority of the interface contributing little to complex

stability (Chen and Shapiro, 1997; Chen and Shapiro, 1999; Shapiro *et al.*, 2000;

Rutkoski *et al.*, 2005). For example, truncated variants of RI that lack residues 144–257

or 315–371 retain picomolar affinity for RNase A and ANG (Lee and Vallee, 1990).

Cursory inspection of the four known RI·ribonuclease structures suggests that RI

binds to each of its ligands in a similar manner. Approximately one-third of the kidney-

shaped ligand protrudes into the central cavity of RI, which is lined exclusively with

parallel β-strands contributed by 15 LRR domains. The active-site cleft of the bilobal

ribonuclease is nestled against the C-terminal portion of RI, with the remainder of the

ribonuclease spilling outside of the inner circumference of the horseshoe and onto the

face of the inhibitor molecule (Figure 1.3A).

Actually, RI interacts distinctly with its ligands (Table 1.3; Figure 1.3B), binding

each with extraordinary avidity despite their low sequence conservation. RI achieves this

feat by recognizing features that are unique to each of its ribonuclease ligands. Although

the 23–31 ribonuclease residues that mediate interactions with RI appear to be grouped in

similar regions along the enzymic amino-acid sequences (Figure 1.3B), this apparent

similarity of interaction is misleading because either the cognate contact residue on RI or

the nature of the interaction usually differs among the ribonuclease ligands (Iyer *et al.*, 2005). Further evidence for the unique means by which RI recognizes divergent ribonucleases has come from alanine-scanning mutagenesis studies, which demonstrate that both the location of the energetic "hot-spots" and the nature of the cooperativity between these regions vary greatly from one ligand to another (Chen and Shapiro, 1997; Chen and Shapiro, 1999; Teufel *et al.*, 2003; Iyer *et al.*, 2005). Another illustration of the divergence of interactions within the various RI·ribonuclease interfaces is provided by the ability to endow RI with selectivity for different ribonuclease ligands. For example, subtle remodeling of a single loop of RI provided >10^9-fold selectivity for ANG over RNase A (Kumar *et al.*, 2004). Finally, the lack of conservation among the modes of ligand-recognition is evidenced most succinctly by the retention of only two hydrogen-bond interactions and two van der Waals interactions in the four known structures of RI·ribonuclease complexes (Iyer *et al.*, 2005; Johnson *et al.*, 2007c) (Figure 1.4; Table 1.4).

The problem of preserving the integrity of intracellular RNA is not unique to vertebrates. The prokaryote *Bacillus amyloliquifaciens* produces the intracellular ribonuclease inhibitor barstar for protection from its cognate extracellular ribonuclease, barnase (Smeaton *et al.*, 1965). Thus, across two domains of life, nature has chosen to solve a fundamentally identical problem by using the same strategy—a cytosolic proteinaceous inhibitor with extraordinary affinity for its potentially lethal ligand. Though the bacterial barstar–barnase system bears no evolutionary or structural

relatedness to the RI–ribonuclease system, it is both interesting and informative to compare and contrast these two solutions to an ancient problem.

Barnase and barstar have a high affinity for one another ($K_d \sim 10^{-14}$ M (Schreiber and Fersht, 1993)), but the means by which this affinity is achieved differs significantly from that of RI and its ribonuclease ligands. Electrostatic interactions play a large role in the formation of both complexes, particularly in the use of electrostatic steering to enhance the association rate (Buckle and Fersht, 1994; Johnson et al., 2007c). The surface area buried at the interface of the barstar·barnase complex (1590 Å^2) is, however, dramatically less than that buried upon ligand binding by RI (2600–3400 Å^2). Also, buried solvent molecules play a much larger role in the barstar·barnase complex, filling otherwise deleterious voids at the interface and also increasing shape complementarity from $S_c = 0.70$ to $S_c = 0.82$. The latter value is significantly greater than the shape complementarity of, for example, the complex between porcine RI (pRI) and RNase A ($S_c = 0.58$). In addition, barstar comes much closer to mimicking the interactions with an RNA substrate than does RI (Buckle et al., 1994).

Compared to barstar, RI has the greater challenge of inactivating numerous divergent ligands and has evolved to do so with femtomolar affinity for each. In humans, RI has as many as 13 potential ribonuclease ligands. There are genes encoding 20 and 17 ribonucleases in the mouse and rat genomes, respectively (Cho et al., 2005). Exposure of human tumor cells to exogenous but homologous ribonucleases that are naturally RI-evasive, such as amphibian ribonucleases and BS-RNase has demonstrated their potential as cancer chemotherapeutic agents. Next, we review briefly the structural basis for the

natural evasion of the amphibian ribonucleases and BS-RNase. Finally, inspired by these naturally RI-evasive ribonucleases, we describe efforts to engineer otherwise non-toxic mammalian ribonucleases to evade RI, thereby unleashing their cytotoxicity and enabling the development of new chemotherapeutic agents.

1.5 Evasion of RI by Natural Cytotoxic Ribonucleases

The first observation of ribonuclease-mediated cytotoxicity occurred in the 1950's, when RNase A was shown to be toxic to tumor cells both in vitro (Ledoux and Baltus, 1954) and in vivo (Ledoux, 1955b; Ledoux, 1955a; Aleksandrowicz, 1958). Effects were observed only after milligram quantities of enzyme were injected into solid tumors—smaller doses of RNase A had no effect. Thirty years ago, BS-RNase, was discovered in bull seminal fluid and found to be cytotoxic at low concentrations (Floridi and D'Alessio, 1967; Dostál and Matoušek, 1973). In the last two decades, more cytotoxic homologues were isolated from the eggs of the bullfrog *Rana catesbeiana* (Lewis *et al.*, 1989; Liao, 1992), the Japanese rice paddy frog *Rana japonica* (Kamiya *et al.*, 1990), and the Northern leopard frog *Rana pipiens* (Ardelt *et al.*, 1991; Singh *et al.*, 2007). These amphibian ribonucleases are toxic to tumor cells in vitro with IC_{50} values <1 µM (Wu *et al.*, 1993; Nitta *et al.*, 1994; Liao *et al.*, 2000; Singh *et al.*, 2007). The ability of both BS-RNase and the amphibian ribonucleases to evade RI is a primary determinant of their cytotoxicity toward cancer cells. The aspects of their structures that enable them to evade RI are described below.

The *Rana pipiens* ribonuclease, ONC, deserves special attention as it is currently in a Phase IIIb confirmatory clinical trial as a second-line chemotherapeutic agent for malignant mesothelioma (Mikulski *et al.*, 2002), and has been granted both orphan-drug and fast-track status by the U.S. Food and Drug Administration. In this trial ONC is being administered to patients along with doxorubicin, and the life-extension is being compared to that from doxorubicin alone. ONC has also completed Phase II human clinical trials for the treatment of refractory breast cancer, prostate cancer, and metastatic kidney cancer (Pavlakis and Vogelzang, 2006). The enzyme is administered intravenously and is able to destroy cancer cells selectively. If the Phase IIIb trial is successful, ONC would be approved in 2008 for use as the first ribonuclease chemotherapeutic agent.

All amphibian ribonucleases characterized to date have been found to be toxic to mammalian tumor cells (Lou *et al.*, 2006; Singh *et al.*, 2007), which is in stark contrast to mammalian ribonucleases. For this reason the structural and biochemical differences between amphibian and mammalian ribonucleases are of particular interest. Amphibian ribonucleases, which are isolated from oocytes and early embryos, preferentially cleave RNA between pyrimidine and guanine residues instead of the pyrimidine–adenine substrates preferred by RNase A (Liao *et al.*, 2000). Like human RNase 4 and ANG, most amphibian ribonucleases (with the exception of the recently described "Amphinase" variants from *Rana pipiens* (Singh *et al.*, 2007)) contain an N-terminal pyroglutamate residue that, unlike in RNase 4 and ANG (Shapiro *et al.*, 1988), plays an important role in catalysis by pre-organizing active-site residues for binding to the rate-limiting transition state (Lee and Raines, 2003; Lou *et al.*, 2006). Despite ribonucleolytic activity being

required for cytotoxicity, amphibian ribonucleases typically exhibit markedly less ribonucleolytic activity than does RNase A (Liao *et al.*, 2000; Singh *et al.*, 2007).

The divergent, compact structure of the amphibian ribonucleases enables them to evade RI. The amphibian ribonucleases share three of the four conserved disulfide bonds of RNase A, lacking the cystine residue corresponding to Cys65–Cys72 and possessing instead a fourth disulfide bond near the C-terminus (Rosenberg *et al.*, 2001). Although amphibian ribonucleases and RNase A share a similar overall fold (Mosimann *et al.*, 1994; Hsu *et al.*, 2003; Lou *et al.*, 2006), they have low sequence identity. Moreover, the amphibian ribonucleases are typically shorter (104–111 amino-acid residues), giving rise to a more compact structure. The amino-acid deletions occur predominantly in surface loops, and decimate favorable interactions with RI (Wu *et al.*, 1993; Boix *et al.*, 1996; Kobe and Deisenhofer, 1996) (Figure 1.5). For example, of the 24 residues of RNase A that contact RI within the pRI·RNase A complex, only three are conserved in ONC, three are replaced with similar residues, nine with dissimilar residues, and the remaining nine contact residues are found in the surface loops of RNase A and have no structural counterparts on ONC (Kobe and Deisenhofer, 1996). These nine unique residues in the surface loops of RNase A are shown explicitly in Figure 1.5B.

BS-RNase is another member of the bovine pancreatic ribonuclease family that exerts selective toxicity toward cancer cells. The naturally dimeric nature of BS-RNase is unique among the members of the RNase A superfamily (D'Alessio *et al.*, 1997) and uses adverse steric interactions to preclude binding by RI (Murthy and Sirdeshmukh, 1992). The constituent RI-sensitive monomers (M) (Figure 1.6B) of the BS-RNase homodimer

are linked by two intermolecular disulfide bonds between Cys31 of one subunit and Cys32 of the other. At equilibrium, $^2/_3$ of the dimeric molecules are stabilized further by the swapping of N-terminal domains (denoted as "M×M") (Figure 1.6A). This additional degree of quaternary association affords greater protection against dissociation upon internalization into the reducing environment of the cytosol as compared to the non-domain swapped form ("M=M") (Piccoli *et al.*, 1992; Kim *et al.*, 1995b). The insensitivity of dimeric BS-RNase to inhibition by RI allows it to exert unique biological actions, including toxicity towards tumor cells as well as aspermatogenic, embryotoxic, and immunosuppressive activities (Vescia *et al.*, 1980; Murthy *et al.*, 1996). Thus, despite being >80% identical in sequence to RNase A, which is bound by RI with femtomolar affinity, the unique quaternary structure of BS-RNase renders it completely insensitive to RI.

Despite the discovery and characterization of these naturally-occurring cytotoxic ribonucleases, and the success of ONC in the clinic, the amphibian ribonucleases and BS-RNase exhibit at least five undesirable properties that could be circumvented by using related monomeric mammalian ribonucleases or their variants. (1) *Greater potential immunogenicity*. In general, exogenous proteins with a low degree of similarity to native homologues are immunogenic (De Groot and Scott, 2007). For example, RNase A shares 70% sequence identity with murine pancreatic ribonuclease (Rib1), whereas the amphibian ONC shares only 18% identity with Rib1, and mice produce neutralizing antibodies against ONC but not against RNase A (Matoušek *et al.*, 2003b). In a clinical study investigating the use of RNase A for the treatment of tick-borne encephalitis,

1 gram of RNase A was administered to 246 patients over a 6-day period and produced no evident toxic or allergic effects (Glukhov *et al.*, 1976). It should be noted, however, that numerous clinical studies have found ONC to possess an acceptable safety profile, being generally well-tolerated by most patients (Pavlakis and Vogelzang, 2006). The surprisingly low immunogenicity of ONC is perhaps a result of enhanced activation-induced apoptosis of lymphocytes exposed to ONC (Halicka *et al.*, 2002).

(2) *Unfavorable tissue distribution following administration*. A practical limitation of ONC as a potential chemotherapeutic agent stems from its dose-limiting renal toxicity (Mikulski *et al.*, 1993; Pavlakis and Vogelzang, 2006). Pharmacokinetic and biodistribution studies have revealed the renal retention of ONC to be 50- to 100-fold greater than that of mammalian members of the RNase A superfamily (Vasandani *et al.*, 1996). (3) *Rapid clearance from circulation*. Proteins having a low molecular mass ($\leq$40 kDa) are cleared rapidly from circulation by the kidneys via renal filtration (Maack *et al.*, 1979). RNase A administered intravenously to mice and rats was observed to possess a half-life in circulation of 3.5 and 5 min, respectively (Bartholeyns and Moore, 1974; Tarnowski *et al.*, 1976). ONC is cleared at a similar rate (Vasandani *et al.*, 1996). Considering that ONC is administered intravenously on a weekly basis in its current clinical trial (Pavlakis and Vogelzang, 2006), modification of a ribonuclease to possess an enhanced time in circulation could permit less frequent or lower dosing, which would translate to improved immunological tolerance, reduced cost, and greater patient compliance. (4) *Modest ribonucleolytic activity (amphibian ribonucleases)*. As mentioned above, ribonucleolytic activity is essential for cytotoxicity (Wu *et al.*, 1993;

Kim *et al.*, 1995a). The catalytic efficiency of RNase A, BS-RNase, and human

pancreatic ribonuclease (RNase 1) against known substrates is 10^4–10^5-fold greater than

that of ONC (Floridi *et al.*, 1972; Boix *et al.*, 1996; Lee and Raines, 2003), suggesting a

much greater cytotoxic potential. (5) *Dissociation of the BS-RNase dimer in the cytosol*

and subsequent inhibition by RI. The unique quaternary structure of BS-RNase, though a

powerful deterrent of RI, is metastable, and thus diminishes its potential as a cytotoxic

ribonuclease (Lee and Raines, 2005). Moreover, BS-RNase is <10-fold less cytotoxic

than ONC in a variety of assays (Matoušek *et al.*, 2003b).

Several microbial ribonucleases, including the prokaryotic RNase Sa3 from

Streptomyces aureofaciens and a ribonuclease from *Bacillus intermedius*, have been

found to be cytotoxic to human tumor cells (Ilinskaya *et al.*, 2001; Sevcik *et al.*, 2002).

Additionally, ribotoxins from the fungal genus *Aspergillus* (such as α-sarcin, restrictocin,

and mitogillin) exert cytotoxic activity toward mammalian cells by cleaving the 28 S

RNA of the large ribosomal subunit and thereby inhibiting protein synthesis (Olmo *et al.*,

2001). Not surprisingly, these microbial ribonucleases are not inhibited by RI (Cho and

Joshi, 1989; Sevcik *et al.*, 2002). The lack of cancer-cell selectivity of fungal

ribonucleases (Youle and D'Alessio, 1997), along with the high immunogenicity and

systemic toxicity of microbial enzymes (Bugelski and Treacy, 2004; Fu and Sakamoto,

2007), precludes their use as human chemotherapeutic agents.

These limitations of naturally cytotoxic ribonucleases could be overcome by the

development of new chemotherapeutic agents based on mammalian (especially human)

ribonucleases. A major hurdle in realizing the full cytotoxic potential of mammalian

ribonucleases is the potent inhibition of these enzymes by RI. The remainder of this

chapter will focus on the various protein engineering strategies from the literature that

have been applied towards thwarting the undesirable influence of RI on cytotoxicity.

Finally, the remainder of this thesis demonstrates the application and further extension of

these approaches toward the development of cytotoxic mammalian ribonucleases.

1.6 Engineering Evasion of RI

1.6.1 Site-Directed Mutagenesis

One especially successful strategy for attenuating the affinity of RI for mammalian

ribonucleases has been the use of site-directed mutagenesis to install steric or electrostatic

incompatibilities in the interface of the complex. Although site-directed mutagenesis has

elucidated the means by which RI recognizes its divergent ligands, this work has

primarily involved making single or multiple alanine substitutions in RI. The RI variants

have been characterized to reveal effects on the affinity of RI for native ribonuclease

ligands (Chen and Shapiro, 1997; Chen and Shapiro, 1999; Shapiro *et al.*, 2000; Teufel *et al.*, 2003; Iyer *et al.*, 2005). The focus of this review is to describe progress that has been

made through protein engineering toward the development of chemotherapeutic

ribonucleases and thus is concerned only with the disruption of RI–ribonuclease

interactions by the modification of ribonucleases.

Guided by the (then) recent report of the structure of the pRI·RNase A complex

(Kobe and Deisenhofer, 1996), our group first demonstrated the feasibility of

transforming a non-toxic ribonuclease into a potent cytotoxin. In the pRI·RNase A

complex, Gly88 was observed to reside in a hydrophobic pocket of pRI defined by Trp257, Trp259, and Trp314. By replacing Gly88 in the $\beta4$–$\beta5$ loop of RNase A with an arginine or aspartate residue, the affinity of RI was reduced by 10^4- and 10^3-fold, respectively. Because of the high sequence identity between pRI and hRI (23 of the 28 contact residues in pRI are identical in hRI, and 3 are replaced conservatively), these contacts were expected to be preserved in the hRI·RNase A complex, which has a K_d value nearly identical to that of the pRI·RNase A complex (Lee *et al.*, 1989; Vicentini *et al.*, 1990). The specific amino acids used for the substitution were chosen to introduce a bulky protrusion or "knob" that would not be well-accommodated by any "hole" on the surface of RI. In essence, this strategy is the converse of alanine-scanning mutagenesis, which seeks to truncate the side chain so as to discern its contribution to the binding interaction (Wells, 1991). Arginine and aspartate possess the two most polar side chains (Radzicka and Wolfenden, 1988), whose hydration imparts yet additional bulk. Furthermore, arginine is the second largest amino acid. Importantly, both G88R RNase A and G88D RNase A were found to inhibit the proliferation of a continuous human erythroleukemia line (K-562) with IC_{50} values of 7 and 30 μM, respectively (Leland *et al.*, 1998). Though G88R RNase A is ~25-fold less toxic than ONC, it has inspired numerous subsequent efforts to disrupt the RI–RNase A interface further (See Table 1.5). These efforts ultimately resulted in variants such as K31A/D38R/R39D/N67R/G88R RNase A, whose multiple amino-acid substitutions disrupt simultaneously several regions within the expansive interface (See CHAPTER 2). The five substitutions in this variant decrease affinity for RI by 60 million-fold, and endow RNase A with a greater ability

than ONC to inhibit the proliferation of human erythroleukemia cells in vitro. A related

variant, D38R/R39D/N67R/G88R RNase A, displays cytotoxicity equal to or greater than

that of ONC for four different human tumor cell lines (Rutkoski *et al.*, 2005). Similar

efforts to reduce the sensitivity of RNase 1 (Gaur *et al.*, 2001; Leland *et al.*, 2001),

RNase 1-immunotoxins (Erickson *et al.*, 2006), and monomeric BS-RNase (Antignani *et

al.*, 2001; Lee and Raines, 2005) to inhibition by RI have proven the broad utility of this

engineering strategy (Table 1.5).

Important considerations for selecting amino-acid substitutions to generate RI-

evasive, and thus cytotoxic, ribonuclease variants are evident from the work summarized

in Table 1.5 and reported elsewhere (Johnson *et al.*, 2007a; Johnson *et al.*, 2007c).

Substitutions should be chosen to minimize deleterious effects on either catalytic activity

or conformational stability (which is related to proteolytic susceptibility (McLendon,

1977; Klink and Raines, 2000)), as these attributes are themselves important determinants

of cytotoxicity (Bretscher *et al.*, 2000; Klink and Raines, 2000). In addition, positive

charge, manifested either as a high net molecular charge (Z) or in discrete regions of

cationicity, is crucial for the favorable Coulombic interactions with anionic components

of the cell surface (Futami *et al.*, 2002; Notomista *et al.*, 2006; Fuchs *et al.*, 2007; Huang

et al., 2007; Johnson *et al.*, 2007a).

Apparently, the site-directed mutagenesis approach has reached a limit (Rutkoski *et

al.*, 2005). The value of K_d for the complex of RI with highly evasive variants of

RNase A is close to the cytosolic concentration of RI (~4 µM (Leland *et al.*, 1998; Haigis

et al., 2003)). Additional evasion of RI does not lead to a substantial increase in the

concentration of free ribonuclease in the cytosol and hence does not increase cytotoxicity. Further increases in cytotoxicity are likely to be achievable, but will require modulating other parameters, such as cellular binding, uptake, and translocation.

1.6.2 Multimerization

The naturally dimeric nature of BS-RNase is unique in the RNase A superfamily (Figure 1.6). Pro19, Leu28, Cys31, and Cys32 were identified as the residues that enable BS-RNase to form its unique M=M ⇌ M×M structure (Di Donato et al., 1994; Di Donato et al., 1995; Ciglic et al., 1998). Replacement of the corresponding residues in RNase 1 (where necessary) with the aforementioned residues resulted in a variant that adopted a BS-RNase-like structure spontaneously (Piccoli et al., 1999). This dimeric RNase 1, also composed of a mixture of M=M and M×M forms, was selectivity toxic towards human tumor cells, albeit with a reduced potency compared to BS-RNase. Adding the E111G substitution does, however, lead to a dimeric RNase 1 that is more cytotoxic than BS-RNase to a SV40-transformed 3T3 fibroblast cell line. The quaternary structure of these RNase 1 dimers was essential not only for cytotoxicity, but also to reduce their sensitivity to RI (Di Gaetano et al., 2001) (Table 1.6).

Subsequent to the discovery of the antitumoral activity of BS-RNase, interest grew in generating chemically-linked dimers of RNase A in an attempt to reproduce by semisynthesis the unique biological activities of BS-RNase (Hartman and Wold, 1967; Wang et al., 1976). In contrast to BS-RNase or the noncovalent, domain-swapped oligomers of RNase A, which are metastable, dimers produced by chemical coupling are

not able to dissociate (Wang *et al.*, 1976). Dimers of RNase A that were cross-linked with bifunctional amine-reactive imido esters, inhibited tumor cell proliferation in vitro (Bartholeyns and Baudhuin, 1976), exhibited antitumoral activity in mice (Tarnowski *et al.*, 1976; Bartholeyns and Zenebergh, 1979), possessed both a newly acquired enzymatic activity against dsRNA, and had an enhanced persistence in the circulation of rats (Bartholeyns and Moore, 1974). Furthermore, these cross-linked dimers have a reduced affinity for RI (Bartholeyns and Moore, 1974). More recently, cross-linked trimers of RNase A generated with a dimethylsuberimidate linker displayed higher cytotoxic activity against a cervical carcinoma cell line than did cross-linked dimers of RNase A. The cross-linked trimers also possessed enhanced activity against dsRNA, compared to that of cross-linked dimers (Gotte *et al.*, 1997), conforming to the trend observed with the noncovalent domain-swapped oligomers of RNase A (Libonati and Gotte, 2004).

A marked disadvantage of utilizing amine-reactive linkers such as dimethylsuberimidate for the chemical cross-linking of RNase A is the heterogeneity of the products that derives from its eleven amino groups. This heterogeneity confounds biochemical characterization of the conjugates, making this methodology undesirable for the development of chemotherapeutic agents. Furthermore, modification of active-site lysine residues, such as Lys41, can reduce catalytic efficiency by up to 10^5-fold (Messmore *et al.*, 1995).

Homogeneous homodimers of both RNase 1 and eosinophil-derived neurotoxin (EDN; RNase 2) have been produced by introducing a cysteine residue via site-directed mutagenesis and reacting its thiol with 1,6-bis(maleimido)hexane to generate a

thioether-linked dimer (Suzuki *et al.*, 1999). The cysteine residues were introduced at

positions that were predicted to be the most disruptive to RI-binding. This site-specific

tethering resulted in dimeric conjugates that were $\geq 10^4$-fold less sensitive to inhibition by

RI, and effectively transformed these two non-toxic, RI-sensitive, monomeric

ribonucleases into cytotoxic dimers (Suzuki *et al.*, 1999).

Recently, the *in vacuo* incubation of lyophilized RNase A at 85 °C was shown to

promote the condensation of the side chains of Glu9 of one monomer and Lys66 of

another to form a dimer linked by an amide bond (Simons *et al.*, 2007). This dimer was

distinct from the noncovalent dimers prepared by lyophilization of RNase A from dilute

solutions of acetic acid (Libonati and Gotte, 2004). The covalent dimer exhibited a

slightly increased catalytic activity but was insensitive to RI at near-physiological

concentrations. No data have been reported on its cytotoxicity.

1.6.3 Fusion to a Targeting Protein

Mammalian ribonuclease-based immunotoxins have been engineered by linkage of

the N- or C-terminus of the enzyme to a targeting moiety, either by chemical coupling

(Rybak *et al.*, 1991) or by fusion to another protein (Rybak *et al.*, 1992; Newton *et al.*,

1994). Targeting moieties have included transferrin, growth factors, or antibody/antibody

fragments directed against cell-surface antigens or receptors abundant only on cancer

cells. The use of mammalian ribonucleases (especially human) as the effector portion of

the immunotoxin was intended to supplant more traditional plant or bacterial toxins

(*e.g.*, ricin and diphtheria toxin), which can elicit strong immunogenic responses and

promote vascular leak syndrome in patients (Pennell and Erickson, 2002). The resulting

conjugates had impressive toxicity for specific cell types but remained sensitive to RI

(Rybak et al., 1991; Rybak et al., 1992; Newton et al., 1994), limiting their potency

(Suzuki et al., 1999).

Semisynthesis has been used to link a targeting moiety to a ribonuclease residue in a

manner that enables evasion of RI. For example, a free cysteine residue was introduced

into the β4–β5 loop of both human RNase 1 (G89C) and EDN (T87C) to allow for

linkage via a thioether bond to either transferrin or an anti-human transferrin receptor

monoclonal antibody. Unlike other less-specific chemical coupling methods (e.g., via

multiple amino groups), these homogeneous conjugates preserved enzymatic activity and

displayed a 10^4-fold reduction in affinity for RI. The data suggest that gains in

cytotoxicity achieved through RI-evasion and cell-targeting were additive (Suzuki et al.,

1999), consistent with RI-evasion being an important consideration when designing

mammalian ribonuclease-based immunotoxins (Table 1.7).

Two immunotoxins have been prepared in which the C-terminus of the Δ1–7

fragment of RNase 1 is fused to the N-terminus of either hEGF or hFGF (Futami et al.,

1999; Hoshimoto et al., 2006). This truncated variant of RNase 1 possesses an attenuated

affinity for RI, which is accompanied by a substantial decrease in ribonucleolytic activity

(Futami et al., 1995). The fusion containing the Δ1–7 RNase 1 was more effective at

inhibiting the growth of A431 cells than was the fusion containing the full-length protein,

despite a 250-fold reduction in enzymatic activity (Hoshimoto et al., 2006). Apparently,

the reduced ability to degrade RNA is more than compensated by the decreased affinity

for RI—similar to what was observed for monomeric variants of RNase A (Bretscher *et al.*, 2000).

In RI·ribonuclease complexes, neither terminus of ribonuclease is in contact with RI. Accordingly, the tandem fusion of a ribonuclease to another protein is unlikely to enable the evasion of RI. To illustrate this point, tandem variants of RNase A were produced in which two enzymic moieties were co-expressed as a single polypeptide. The two catalytic entities were tethered through a short peptide linker (4–8 residues in length) with the aim of engendering RI-evasion—perhaps at the expense of one of the ribonuclease domains. In fact, these tandem variants of RNase A were still wholly sensitive to RI (Leich *et al.*, 2006). A new gene fusion technique—"insertional fusion"—overcomes this limitation (Russell, 1994). With this technique, human basic fibroblast growth factor has been inserted between Gly89 and Ser90 of RNase 1 (RNF89) to achieve cell-targeting and RI-evasion simultaneously. CL-RFN89, which contains an additional disulfide bond between Cys4 and Cys118, retained >85% of its enzymatic activity in the presence of a 200-fold molar excess of RI, and its interaction with cells was specific for the FGF receptor (Hayashida *et al.*, 2005). In contrast, constructs in which the insertional fusion was made outside of the RI–ribonuclease interface (RNF19, CL-RNF19; bFGF inserted between Pro19 and Ser20) retained sensitivity to RI and were >10-fold less cytotoxic than CL-RNF89 ((Tada *et al.*, 2004); Tada, H., personal communication).

1.6.4 Chemical Modification

The influence of random chemical cationization on the internalization of RNase A and RNase 1 has been studied in detail. These two ribonucleases have net charges of $Z = +4$ and $+6$, respectively. The basicity of these two proteins was enhanced by the amidation of the carboxyl groups (RNase A has 5 aspartate and 5 glutamate residues) with either ethylenediamine (Futami *et al.*, 2001) or polyethylenimine (PEI) (Futami *et al.*, 2005), and a positive correlation was observed between the value of Z and cytotoxic activity. The increase in cytotoxicity was due not only to enhanced internalization but also to diminished affinity for RI . Modification with either reagent was found to have a deleterious effect on enzymatic activity making the optimization of derivatization problematic (Futami *et al.*, 2002). The most cytotoxic preparation of RNase A ($Z = +15.6$) exhibited a $>4 \times 10^4$-fold reduced affinity for RI ($K_d = 19$ nM; Table 1.8).

The efficacy of biological chemotherapeutic agents is limited largely by their bioavailability and circulating half-life, which is in turn affected by rate of plasma clearance, degradation, and immunogenicity (Harris *et al.*, 2001). A common strategy to remedy these problems is to conjugate inert polymers such as poly(ethylene glycol) (PEG), which under normal dosing circumstances does not elicit an immune response (Harris and Chess, 2003). Instead, PEG acts to shield potentially immunogenic epitopes on the surface of the protein from the host immune system and also acts as a sheath to prevent proteolytic degradation (Greenwald *et al.*, 2003a). PEGylation serves by increasing dramatically the hydrodynamic radius of the species, thereby increasing serum half-life by reducing the rate of renal filtration. Indeed, plasma clearance time has been

shown to be directly proportional to PEG chain length (Yamaoka *et al.*, 1994). Other

water-soluble polymers such as poly(alkylene oxide), poly(oxyethylated polyols), and

poly(vinyl alcohols) have also been shown to achieve similar benefits (Harris and

Zalipsky, 1997).

First-generation PEG conjugates were produced through the modification of protein

amino groups. This strategy endowed RNase A with greater conformational stability and

resistance to proteolytic degradation (Monfardini *et al.*, 1995) as well as greater

antitumoral activity in vivo (Matoušek *et al.*, 2002; Matoušek *et al.*, 2004). RNase A has

also been modified with poly[*N*-(2-hydroxypropyl)methylacrylamide] (PHPMA),

producing a conjugate that inhibited tumor growth in nude mice (Poučková *et al.*, 2004).

Considering the cloaking effect that PEG imparts to a conjugated protein, it is tempting to

speculate that the enhanced biological activities of PEGylated RNase A are the result, at

least in part, of reduced affinity for RI (Maeda *et al.*, 2000; Matoušek *et al.*, 2002).

A disadvantage of amino-group PEGylation is its creation of a heterogeneous

population of conjugates. Moreover, the PEGylation of lysine residues can be deleterious

to the biological function of a protein. In addition, the PEGylation of amino groups

destroys positive charges, which has an adverse effect on the cellular internalization of

ribonucleases (Chapman, 2002). Therefore, recent generations of PEGylated conjugates

have had large PEG groups at one or two specific sites on the protein (Harris and Chess,

2003). For example, our group has prepared site-specifically PEGylated RNase A by

using maleimide-derivatized PEG and free thiol-containing variants of RNase A. We

have found that the affinity of RNase A for RI could be reduced by 10^6-fold through such

PEGylation and that the chain length, branching, and site of the PEG all influence the

evasion of RI and, consequently, the cytotoxicity (CHAPTER 4: Rutkoski, T. J.;

Kink, J. A.; Strong, L. E. and Raines, R. T., unpublished results).

Finally, we note that mammalian ribonucleases exhibit diverse *natural* chemical

modification in the form of glycosylation (Plummer and Hirs, 1963; Plummer, 1968).

The pendant carbohydrates could enhance bioavailability and circulating half-life

(Veronese and Pasut, 2005), as well as engender evasion of RI. For example, RNase 1 is

known to be glycosylated at an RI-contact residue, which is part of a consensus

N-glycosylation sequence: Asn88–Gly89–Ser90 (Beintema *et al.*, 1988a). Likewise, a

putative RI-contact residue in murine Rib1, residue 38 (Rutkoski *et al.*, 2005), is part of a

consensus N-glycosylation sequence: Asn38–Gly39–Ser40. Nothing is known about its

glycosylation. In addition, Trp7 of EDN, which is an RI-contact residue (Iyer *et al.*,

2005), undergoes an unusual post-translational modification with an α-mannopyranose

moiety (de Beer *et al.*, 1995). Finally, it is noteworthy that the glycosylation of ONC by

its heterologous production in *Pichia pastoris* increases its toxicity for human

erythroleukemia cells by 50-fold—presumably by increasing its conformational stability

and resistance to proteolysis—without compromising its cellular internalization (Kim *et*

al., 2004). Its amphibian homologue, Amphinase, is glycosylated naturally and is toxic

for submaxillary gland carcinoma cells (Singh *et al.*, 2007). Thus, the glycosylation of

ribonucleases could provide mammals with an endogenous toxin for cancer cells.

1.7 Prospectus

Ribonucleases represent a promising new class of chemotherapeutic agents (Leland and Raines, 2001; Matoušek, 2001; Makarov and Ilinskaya, 2003; Benito *et al.*, 2005; Arnold and Ulbrich-Hofmann, 2006; Lee and Raines, 2008). Mammalian ribonucleases, in particular human homologues of RNase A, are especially attractive because of their pronounced ribonucleolytic activity and selective toxicity for cancer cells (Piccoli *et al.*, 1999; Rutkoski *et al.*, 2005; Johnson *et al.*, 2007c). Moreover, mammalian ribonucleases are tolerated extremely well by humans. The primary hurdle in the development of mammalian ribonuclease-based chemotherapeutics is their inactivation by RI.

Some workers have reported on engineered ribonucleases that retain sensitivity to RI but demonstrate cytotoxicity, in apparent conflict with the work described above (Bosch *et al.*, 2004; Naddeo *et al.*, 2005; Leich *et al.*, 2006). There are at least three scenarios in which RI-evasion would not be essential for ribonuclease-mediated cytotoxicity. (1) *The mechanism of cytotoxicity is independent of enzymatic activity*. In these examples, which include bacteriocidal pore-forming mechanism of eosinophil cationic protein (ECP; RNase 3) or other membrane destabilization (Notomista *et al.*, 2006; Navarro *et al.*, 2008), protein basicity appears to be solely important. (2) *Enough ribonuclease can reach the cytosol to overwhelm RI* (Leland and Raines, 2001; Naddeo *et al.*, 2005; Leich *et al.*, 2006; Fuchs *et al.*, 2007). This scenario was apparent for the human anti-ErbB-2 scFv-RNase 1 immunotoxin (hERB-RNase 1), which is completely sensitive to RI but displays low-nanomolar toxicity toward cells displaying ErbB-2. Quantitative immunoblotting demonstrated that the anti-ErbB targeting moiety effectively delivers the

conjugate to the cytosol (De Lorenzo *et al.*, 2007). (3) *The ribonuclease enters a sub-cellular compartment (e.g., the nucleus) that is devoid of RI.* The ability to evade RI would not be expected to influence cytotoxicity (Bosch *et al.*, 2004). All three of these scenarios deviate significantly from the mechanism of ribonuclease-mediated cytotoxicity depicted in Figure 1.1 in which the ribonuclease is internalized via non-receptor-mediated endocytosis to deliver ribonucleolytic activity to the cytosol of a target cell. In this mechanism, RI-evasion is essential.

Although its importance is indisputable, RI-evasion is but one of several determinants of cytotoxicity. Equations that correlate multiple biochemical attributes of a ribonuclease with cytotoxic activity have been both useful (Bretscher *et al.*, 2000) and informative (Rutkoski *et al.*, 2005). Nonetheless, a complete mathematical model describing ribonuclease-mediated cytotoxicity remains elusive. Only by thorough and careful consideration and optimization of all relevant factors can the cytotoxic potential of a ribonuclease be realized fully (Futami *et al.*, 2002). As research transitions from the Petri dish to whole animals, techniques for instilling RI-evasion along with increased macromolecular size (*e.g.*, by multimerization, fusion to a targeting protein, or PEGylation) could impart the distinct advantage of enhanced persistence in circulation (Noguchi *et al.*, 1998; Dreher *et al.*, 2006). Further progress is not merely possible, but likely.

The remainder of this thesis describes the implementation of several of these strategies to impair RI-binding with the ultimate goal of producing cytotoxic mammalian ribonucleases.

Table 1.1 Comparison of RI·ribonuclease complexes to other biomolecular interactions

Biomolecular complex[a]	ASA buried[b] ($Å^2$)	S_c[c]	K_d (M)	Reference
RI·ribonuclease	2583–3438	0.67 ± 0.06	$0.3–2.7 \times 10^{-15}$	(Lee *et al.*, 1989; Teufel *et al.*, 2003; Johnson *et al.*, 2007b; Johnson *et al.*, 2007c)
Strength of interaction				
Im9·colicin E9 DNase			9.3×10^{-17}	(Wallis *et al.*, 1995)
PTI·trypsin	1430		6×10^{-15}	(Vincent and Lazdunski, 1972)
biotin·avidin			0.6×10^{-15}	(Green, 1975)
TIMP-2·MMP-2			0.6×10^{-15}	(Hutton *et al.*, 1998)
barstar·barnase	1590	0.70 $(0.82)^d$	1.3×10^{-14}	(Schreiber and Fersht, 1993; Buckle *et al.*, 1994)
Interface area				
G$_{t\beta\gamma}$·Phosducin	4660			(Gaudet *et al.*, 1996; Lo Conte *et al.*, 1999)
EF-Tu·EF-Ts	3660			(Kawashima *et al.*, 1996; Lo Conte *et al.*, 1999)
inhibitor·enzyme	2030 ± 630			(Lo Conte *et al.*, 1999)
antibody·antigen	1680 ± 260	0.64–0.68		(Lo Conte *et al.*, 1999)
inhibitor·protease	1530 ± 170	0.70–0.76		(Lo Conte *et al.*, 1999)
all complexes	1940 ± 760			(Lo Conte *et al.*, 1999)

[a] Im9, immunity protein 9; PTI, protein trypsin inhibitor; TIMP-2, tissue inhibitor of metalloproteinase-2; MMP-2, matrix metalloproteinase-2 (gelatinase A).

[b] Buried accessible surface area (ASA) was calculated with the program NACCESS (Hubbard and Thornton, 1993).

[c] The value of S_c reports on geometrical shape complementarity, where $S_c = 1.0$ for two perfectly complementary surfaces and $S_c = 0$ for two completely dissimilar surfaces (Lawrence and Colman, 1993).

[d] Value of S_c increases when buried solvent is included in the calculation (Buckle *et al.*, 1994).

Table 1.2 RI-affinity and amino-acid sequence identity/similarity[a] of bovine pancreatic ribonuclease superfamily members

K_d (M) for complex with RI		RNase A	RNase 1	EDN	ECP	RNase 4	ANG	RNase 6	RNase 7	RNase 8	BS-RNase	ONC
44×10^{-15} (Lee et al., 1989)	RNase A	100	80.5	44.5	44.9	66.1	51.2	45.5	45.5	43.9	88.7	36.2
0.29×10^{-15} (Johnson et al., 2007c)	RNase 1	68.0	100	42.6	44.3	60.2	52.7	46.3	45.6	41.2	79.7	33.3
2.7×10^{-15} (Teufel et al., 2003)	EDN	29.2	28.4	100	75.4	38.7	35.9	60.4	57.5	58.2	39.4	31.4
Sensitive[b]	ECP	23.5	27.9	64.9	100	37.5	35.5	58.2	52.2	50.0	44.9	25.0
4.0×10^{-15} (Hofsteenge et al., 1998)	RNase 4	41.9	40.6	24.1	22.8	100	49.2	44.7	41.7	39.4	63.7	36.5
0.7×10^{-15} (Lee et al., 1989)	ANG	30.2	33.3	19.7	22.7	35.9	100	38.7	40.9	36.5	50.4	31.2
"Very tight"[c]	RNase 6	33.3	30.9	44.0	41.8	31.1	22.6	100	68.8	66.9	44.7	31.1
Sensitive[d]	RNase 7	35.6	31.6	41.0	37.3	28.8	23.4	55.5	100	82.8	44.7	29.3
Not determined	RNase 8	35.6	32.4	44.0	36.6	27.3	20.4	55.1	76.6	100	41.7	30.3
$>2 \times 10^{-6}$ (Antignani et al., 2001)	BS-RNase[e]	81.5	70.3	27.0	22.8	41.9	31.0	32.6	31.8	31.1	100	33.9
$\geq 10^{-6}$ (Boix et al., 1996)	ONC	20.5	19.4	18.2	14.7	23.8	22.7	19.7	18.8	18.2	20.5	100

The dotted lines separate RI-sensitive and RI-insensitive ribonucleases.

[a] Sequence identities (%) are to the left of the diagonal; sequence similarities (%) are to the right of the diagonal. Both were calculated with the program MacVector v9.5 (MacVector, Inc., Cary, NC). The pairwise matrix was performed with the Gonnet similarity matrix and the default parameters in the "slow" mode. (Open Gap Penalty = 10.0; Extend Gap Penalty = 0.1.) Sequences of the human ribonucleases were obtained by using the accession numbers reported in (Cho et al., 2005). Accession numbers used for RNase A, BS-RNase, and ONC were NM_001014386, NM_181810, and AF332139, respectively.

[b] The ribonucleolytic activity of ECP was shown to be sensitive to a commercial preparation of RI (Domachowske et al., 1998).

[c] The interaction of hRI with RNase 6 was described as being "very tight" (Papageorgiou et al., 1997).

[d] A pyrimidine-specific, ~13-kDa enzyme with endoribonucleolytic activity isolated from human skin was sensitive to hRI (Probst et al., 2006). RNase 7 is expressed primarily in keratinocytes (Harder and Schroder, 2002).

[e] Only the dimeric form of BS-RNase is insensitive to RI. hRI has a K_i value of 9.3×10^{-12} M for monomeric C31K/C32S BS-RNase (Antignani et al., 2001).

33

Table 1.3 Characteristics of RI·ribonuclease complexes with known three-dimensional structure

Complex	$K_d{}^a$ (fM)	Buried ASA^b (Å²)	$S_c{}^c$	No. of contact residues[d]		Character of interface residues[e] [No. (%)]			$H\text{-}bonds^d$	Non-bonded contacts[d]	PDB code
				From RI	From RNase	Non-polar	Uncharged polar	Charged			
pRI·RNase A	67	2583	0.58	26	23	14 (29%)	13 (27%)	22 (45%)	8 (3.01)	90	1djf (Kobe and Deisenhofer, 1995b)
hRI·RNase 1	0.29	2802	0.70	28	23	17 (33%)	14 (27%)	20 (39%)	19 (2.79)	177	1z7x[f] (Johnson et al., 2007c)
hRI·EDN	2.7	3438	0.69	42	31	23 (32%)	26 (36%)	24 (33%)	27 (2.87)	256	2bex[g] (Iyer et al., 2005)
hRI·ANG	0.7	2659	0.70	30	28	16 (28%)	17 (29%)	25 (43%)	14 (2.92)	141	1a4y[h] (Papageorgiou et al., 1997)

[a] Values of K_d are from (Lee et al., 1989; Vicentini et al., 1990; Teufel et al., 2003; Johnson et al., 2007c).

[b] Buried accessible surface area (ASA) was calculated with the program NACCESS (Hubbard and Thornton, 1993).

[c] Shape complementarity values (S_c) for pRI·RNase A, hRI·EDN, and hRI·ANG were from (Kobe and Deisenhofer, 1996), (Iyer et al., 2005), and (Papageorgiou et al., 1997), respectively. S_c for hRI·RNase 1 was calculated with SC v5.0 (Lawrence and Colman, 1993) using the default parameters: dot density = $15.00/Å^2$; interface separation = 8.00 Å; trim width = 1.50 Å; probe radius = 1.70 Å; weight factor = $0.50/Å^2$.

[d] Number of contact residues, H-bonds, and non-bonded contacts were determined with the program PDBsum (Laskowski et al., 2005). These values differ from those reported previously (Kobe and Deisenhofer, 1996; Papageorgiou et al., 1997; Iyer et al., 2005), but this uniform analysis enables more meaningful comparisons between the complexes.

[e] Contact residues were identified by PDBsum as non-polar (A,F,G,I,L,M,P,V,W,Y), uncharged polar (C,N,Q,S,T), or charged (D,E,H,K,R).

[f] Calculations were performed with chain Y (hRI) and chain Z (RNase 1) due to the presence of bound citrate in the active site of RNase 1 in the other complex in the asymmetric unit.

[g] Calculations were performed with chain A (hRI) and chain C (EDN).

[h] Calculations were performed with chain A (hRI) and chain B (ANG).

Table 1.4 Equivalent interactions in RI·ribonuclease complexes with known three-dimensional structure

RI[a]	RNase A	RNase 1	EDN	ANG
Hydrogen bonds				
Asp435	Lys41[b]	Lys41	Lys38	Lys40
Ser460[c]	Gln11	Gln11	Trp10	Gln12
van der Waals contacts				
Tyr434	Lys41	Lys41	Lys38	Lys40
Tyr437	His119	His119	His129	His114

[a] Residue numbers correspond to human RI.

[b] This contact was not observed in the crystal structure (Kobe and Deisenhofer, 1996) due to the presence of a bound sulfate molecule, but its existence has been inferred from site-directed mutagenesis experiments (Chen and Shapiro, 1997; Bretscher *et al.*, 2000).

[c] Although the ribonuclease residues do not correspond in position in the sequence alignment (Figure 1.3B), these residues occupy similar positions in the three-dimensional structure. This hydrogen bond is mediated by the C-terminal carboxyl group of RI with RNase A and RNase 1, but by the side-chain hydroxyl group with ANG and EDN.

Table 1.5 Effect of site-directed mutagenesis on the affinity of ribonucleases for hRI

Ribonuclease	Variant	Ribonucleolytic Activity (%)[a]	K_i or K_d (nM)	IC_{50}[b] (μM)	Reference
ONC	Wild-type	0.01–0.1[c]	>1000[d]	0.3	(Rutkoski et al., 2005)
RNase A	Wild-type	100	44×10^{-6}[e]	>25	(Leland et al., 1998; Bretscher et al., 2000; Haigis et al., 2002; Rutkoski et al., 2005)
	G88D	56	0.052	30	(Leland et al., 1998)
	G88R	51	0.41	7	(Leland et al., 1998)
	K41R/G88R	1.4	3.0	2	(Bretscher et al., 2000)
	K7A/G88R	20	7.2	1	(Haigis et al., 2002)
	D38R/R39D/N67R/G88R	73	510	0.2	(Rutkoski et al., 2005)
	K31A/D38R/R39D/N67R/G88R	92	2500	0.2	(Rutkoski et al., 2005)
RNase 1	Wild-type	100	0.3×10^{-6}[f]	>10	(Leland et al., 2001)
	K7A/N88R/G89D/R91D	115[g]	—[h]	6.7	(Erickson et al., 2006)
	K41R/Q69A/N88R/G89D/R91D	2.2[g]	—[h]	7.4	(Erickson et al., 2006)
	L86E/N88R/G89D/R91D	193	0.21	7	(Leland et al., 2001)
	K7A/N71A/E111A	115	0.5	5.55	(Gaur et al., 2001)
	R4C/L86E/N88R/G89D/R91D/V118C	71	2.6	3	(Leland et al., 2001)
BS-RNase	C31A/C32A	100	9.3×10^{-3}[i]	>50	(Lee and Raines, 2005)
	C31K/C32S/G88R/S89E	103	2.5	1.5[j]	(Antignani et al., 2001)
	C31K/C32S/T87W/G88R/S89E/S90W	100	3.1	1.2[j]	(Antignani et al., 2001)
	C31A/C32A/G88R	121	2.3	0.11	(Lee and Raines, 2005)
	C31A/C32A/G38K/K39G/G88R	89	100	0.046	(Lee and Raines, 2005)

[a] The ribonucleolytic activity of each variant relative to the wild-type enzyme within each study.
[b] Values of IC_{50} for variants of RNase A are for human erythroleukemia cells (K-562).
[c] ONC is a 10^4–10^5-fold less active than RNase A against typical substrates (Boix et al., 1996).
[d] Value of K_d for ONC is from (Boix et al., 1996).
[e] Value of K_d for wild-type RNase A is from (Lee et al., 1989).
[f] Values of K_d for RNase 1 are from (Johnson et al., 2007c).
[g] UpA was used as the substrate for enzymatic activity determinations.
[h] Affinity for RI was determined only qualitatively (K_d <250 nM) but varied inversely with cytotoxicity.
[i] Value of K_d is for C31K/C32S BS-RNase And is from (Antignani et al., 2001).
[j] Values of IC_{50} are SV40-transformed mouse cells (SVT2).

Reproduced with permission of the copyright owner. Further reproduction prohibited without permission.

Table 1.6 Effect of multimerization on the affinity of ribonucleases for RI

Ribonuclease	Preparation	Affinity for RI	Cytotoxicity (IC$_{50}$)[a]	Comments	Reference
BS-RNase dimer	Natural	K_i >2 µM (Antignani et al., 2001)	1.3 µM (K-562) (Lee and Raines, 2005)	2:1 M×M/M=M	(Piccoli et al., 1992)
HHP-RNase	Disulfide linked dimer of Q28L/R31C/R32C/N34K RNase 1	Reduced sensitivity to RI	0.15–6.3 µM (six human tumor cell lines); selective for malignant cell lines		(Piccoli et al., 1999)
HHP2-RNase	Disulfide linked dimer of Q28L/R31C/R32C/N34K/ E111G RNase 1	Reduced sensitivity to RI	1.2 µM (SVT2); twofold more cytotoxic than HHP-RNase; more cytotoxic than BS-RNase		(Di Gaetano et al., 2001)
(RNase A)$_2$	Amino-group cross-linking (Wang et al., 1976)	Reduced (Bartholeyns and Moore, 1974)	Cytotoxic in vitro (Bartholeyns and Baudhuin, 1976; Tarnowski et al., 1976; Bartholeyns and Zenebergh, 1979)	Cleaves dsRNA; enhanced persistence in circulation of mice and rats	(Bartholeyns and Moore, 1974)
(RNase A)$_3$	Amino-group cross-linking (Wang et al., 1976)	Not determined	More cytotoxic than (RNase A)$_2$ (Gotte et al., 1997)	Cleaves dsRNA	(Gotte et al., 1997)
(G89C RNase 1)$_2$	Sulfhydryl-group cross-linking	10^4-fold less affinity than wild-type RNase 1	80 nM (U251) 150 nM (Wehi 7.1; mouse T lymphoma)		(Suzuki et al., 1999)
Lys66–Glu9 RNase A dimers	Lyophilized in vacuo at 85 °C for 96 hours	Insensitive to RI at 1.4 µM	Not determined		(Simons et al., 2007)

[a] IC$_{50}$ values reported are based on the concentration of constituent monomeric active sites.

Table 1.7 Effect of fusion to a cell-targeting moiety on the affinity of ribonucleases for RI

Ribonuclease	Design	Affinity for RI	Cytotoxicity	Comments	Reference
Tf–G89C RNase 1 5E9–G89C RNase 1 Tf–T87C EDN	Site-specific attachment of either transferin (Tf) or anti-human TfR via a thioether bond	10^3-fold lower than bismaleimidohexane–G89C RNase 1; 10^4-fold lower than RNase 1	IC_{50} = 1–2 nM (human glioma cells); 5,000-fold more cytotoxic than wild-type RNase 1	200-fold increase in cytotoxicity attributed to RI-evasion and 25-fold to cellular targeting moiety	(Suzuki et al., 1999)
hERB–RNase 1	C-Terminus of human anti-ErbB-2 receptor scFv fused to N-terminus of RNase 1 with a His$_6$ tag	Very high, but shown to overwhelm cytosolic RI	IC_{50} = 12.5–60 nM (four cell lines displaying ErbB-2)	86% tumor growth inhibition in mice bearing TUBO tumors	(De Lorenzo et al., 2004)
Ber-H2-scFv–RNase 1	C-Terminus of Ber-H2-scFv fused to N-terminus of RNase 1; Ber-H2-scFv binds to CD30	Evasive	Cytotoxic to CD30+ cell lines	Dramatically reduced tumor growth in mice bearing CD30+ TS/A cells	(Braschoss et al., 2007)
des.1–7 RNase 1–hEGF	C-Terminus of Δ1–7 RNase 1 fused to the N-terminus of human EGF	des.1–7 RNase 1 required 3-fold more RI to achieve equivalent inhibition of RNase 1 (Futami et al., 1995)	IC_{50} = 0.35 μM (A431cells) versus 0.55 μM for RNase 1–hEFG (which has 250-fold higher catalytic activity)	Protein was unstable; 0.34% of RNase 1 catalytic activity	(Hoshimoto et al., 2006)
des.1–7 RNase 1–hFGF	C-Terminus of Δ1–7 RNase 1 fused to the N-terminus of human FGF	Not determined	IC_{50} ~2 μM (mouse melanoma B16/BL6 cells)	Comparable cytotoxicity to RNase 1–human FGF, which has 20-fold higher catalytic activity	(Futami et al., 1999)
RNase 1–human bFGF	C-Terminus of human bFGF fused to the N-terminus of RNase 1	Sensitive K_i = 2.1	IC_{50} = 1.6 (mouse melanoma B16/BL6 cells)		(Futami et al., 1999; Tada et al., 2004)
CL-RNase 1	Disulfide bond added at residues 4 and 118	K_i = 1.8 nM	None detected	Additional disulfide bond reduces affinity for RI by 13-fold (Leland et al., 2001)	(Tada et al., 2004)
CL-RNF19	β-trefoil core region (residues 19-146) of bFGF inserted into RNase 1 between Pro19 and Ser20	K_i = 2.1	>3 μM	Negative control, as Pro19 and Ser20 are distal from RI-binding site (Abel et al., 2002)	(Tada et al., 2004)
CL-RFN89	β-trefoil core region (residues 19-146) of bFGF inserted to RNase 1 between Gly89 and Ser90	K_i = 110	0.32 μM	Tumor growth inhibition in mice bearing human A431 SCC tumors (anti-angiogenic effect) (Yagi et al., 2006)	(Tada et al., 2004)
CL-RFN89-2	β-trefoil core region (residues 21-144) of bFGF inserted to RNase 1 between Gly89 and Ser90	K_i = 193 nM	0.23 μM	Removal of linker residues enabled more constrained attachment of FGF moiety	(Tada et al., 2004)

Table 1.8 Effect of chemical modification on the affinity of ribonucleases for RI

Ribonuclease	Modification	Ribonucleolytic activity	K_i or K_d	IC_{50} or phenotype	Reference
C31S BS-RNase or C32S BS-RNase	Sulfhydryl group carboxymethyl-ation	Not quantitated	Reduced affinity for RI	Specifically toxic to spermatogenic layers	(Matoušek et al., 1997)
RNase A	Carboxyl group amidation with ethylenediamine	1.6% of RNase A	Ribonucleo-lytic activity reduced by 10-fold molar excess of RI	0.17 µM (3T3-SV40)	(Futami et al., 2001)
RNase 1	Carboxyl group amidation with ethylenediamine	0.38% of RNase A	Ribonucleo-lytic activity reduced by 10-fold molar excess of RI	0.13 µM for (3T3-SV40)	(Futami et al., 2001)
RNase A	Carboxyl group amidation with ethylenediamine to $Z = +15.6$	5% of RNase A	19 nM	0.085 µM (MCF-7) 0.075 µM (3T3-SV40)	(Futami et al., 2002)
RNase A	Carboxyl group amidation with polyethylenimine (250, 600, 1000, 1800 Da)	Not determined	"Markedly decreased" affinity for RI"	0.33–3.3 µM (3T3-SV40)	(Futami et al., 2005)
RNase A	Amino group amidation with PEG (5, 22 kDa)	Not determined	Not determined	Aspermato-genic and anti-tumoral activity	(Matoušek et al., 2002)
RNase A	Amino group amidation with PHPMA (classic and star-like)	Not determined	Not determined	Tumor growth inhibited in CD-1 nude mice bearing human tumors	(Poučková et al., 2004)

Figure 1.1 Putative mechanism of ribonuclease-based cytotoxicity.

(A) Ribonucleases bind to the cell surface and (B) enter the cell via endocytosis, where (C) a fraction escapes from acidifying endosomes and translocates into the cytosol. (D) In the cytosol, ribonucleases are either (E) bound and inhibited by RI or (F) evade RI, allowing them to degrade cellular RNA, and ultimately cause cell death.
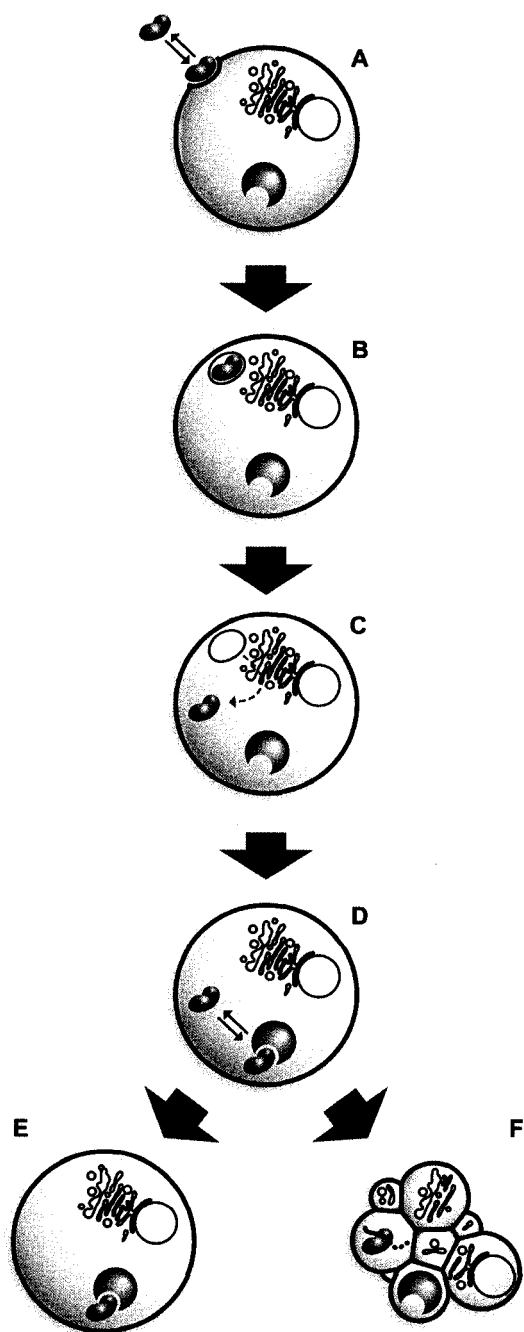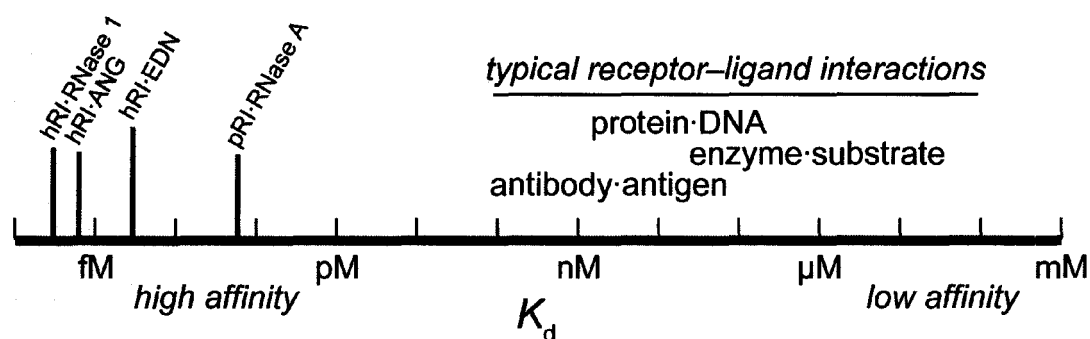
Figure 1.2 Typical values of K_d for common biomolecular complexes and precise

values of K_d for RI·ribonuclease complexes with known three-dimensional

structure (Table 1.3). The lengths of the vertical lines are proportional to

the buried surface areas in the RI·ribonuclease complexes.

Figure 1.3 (A) Overlay of the structures of six ribonucleases bound to hRI. Each

ribonuclease was aligned with RNase 1 in the hRI(gray)·RNase 1(yellow)

complex (chains Y and Z, respectively, of PDB entry 1z7x (Johnson *et al.*,

2007c)). EDN (blue): chain C of 2bex (Iyer *et al.*, 2005); ECP (green):

1qmt (Boix *et al.*, 1999); RNase 4 (teal): 1rnf (Terzyan *et al.*, 1999); ANG

(pink): chain B of 1a4y (Papageorgiou *et al.*, 1997); RNase A (orange):

7rsa (Wlodawer *et al.*, 1988). (B) Amino-acid sequence alignment of the

four ribonucleases whose structure has been solved in a complex with RI

(RNase A, RNase 1, EDN, and ANG) and two RI-evasive homologues

(BS-RNase and ONC) (Beintema *et al.*, 1997). Residue numbers

correspond to RNase A. The assigned secondary structure is above the

sequence (α = α-helix; β = β-sheet) (Kobe and Deisenhofer, 1996).

Residues that contact RI are in the colors of panel (A). Completely

conserved residues are boxed. Enzymic subsites of RNase A are indicated

in italics typeface above the relevant residues (Fisher *et al.*, 1998a; Raines,

1998). The sequences corresponding to the nuclear localization signal and

receptor-binding loop of ANG are underlined (Hallahan *et al.*, 1991;

Moroianu and Riordan, 1994).

A

90°

RNase A
RNase 1
EDN
ANG
ECP
RNase 4

B

1   10   20   30   40   50   60

α1   α2   β1   α3   β2

P2   P2 P1   P1   B1   P0

RNase A   - - - K E T A A A K F E R Q H M D S S T S A A S S S N Y C N Q M M K S R N L T K D - - R C K P V N T F V H E S L A D V Q A V C S Q K N V A C K N G
RNase 1   - - - K E S R A K K F Q R Q H M D S D S S P S S S S T Y C N Q M M R R R N M T Q G - - R C K P V N T F V H E P L V D V Q N V C F Q E K V T C K N G
EDN (RNase 2) K P P Q F T W A Q W F E T Q H I N M T - - - - - - S Q Q C T N A M Q - - V I N N Y Q R R C K N Q N T F L L T T F A N V V N V C G N P N M T C P S N
ANG (RNase 5) - - Q D N S R Y T H F L T Q H Y D A K P Q G R - D D R Y C E S I M R R R G L T S P - - - C K D I N T F I H G N K R S I K A I C E N K N G N P H R E
BS-RNase   K E S A A A K F E R Q H M D S G N S P S S S S N Y C N L M M C C R K M T Q G - - K C K P V N T F V H E S L A D V K A V C S Q K K V T C K N G
ONC   Q D W L T F Q K K H I T N T - - - - - R D V D C D N I M S - T N L F H - - - - C K D K N T F I Y S R P E P V K A I C K G I I A S K N V -

70   80   90   100   110   120   124

β3   β4   β5   β6   β7

B2   B1 P(-1)   B2   P1 P1

RNase A   Q T - - N C Y Q S Y S T M S I T D C R E T G S S K - - Y P N C A Y K T T Q A N K H I I V A C E G N - - - - - - - - - P Y V P V H F D A S V
RNase 1   Q G - - N C Y K S N S S M H I T D C R L T N G S R - - Y P N C A Y R T S P K E R H I I V A C E G S - - - - - - - - - P Y V P V H F D A S V E D S T
EDN (RNase 2) K T R K N C H H S G S Q V P L I H C N L T T F S P Q N I S N C R Y A Q T P A N M F Y I V A C D N R D Q R R D P P Q Y P V V P V H F L D R I I
ANG (RNase 5) - - - - N L R I S K S S F Q V T T C K L H G G S F - W P P C Q Y R A T A G F R N V V V A C E N G - - - - - - - - - - - L P V H L D D S I F R R P
BS-RNase   Q T - - N C Y Q S K S T M R I T D C R E T G S S K - - Y P N C A Y K T T Q V E K H I I V A C G G K - - - - - - - - - - - P S V P V H F D A S V
ONC   - - - - - - - L T T S E F Y L S D C N V T S - - - - - - R P C K Y K L K K S T N K F C V T C E N Q - - - - - - - - - - A P V H F V G V G S C

Figure 1.4   Equivalent interactions among the RI·ribonuclease complexes with known

three-dimensional structure. Alignment of the four RI (dark

gray)·ribonuclease (light gray) complexes for which the three-dimensional

structure is known [pRI·RNase A, PDB entry 1dfj (Kobe and Deisenhofer,

1995b); hRI·RNase 1, chains Y and Z, respectively, from PDB entry 1z7x

(Johnson *et al.*, 2007c); hRI·EDN, chains A and C, respectively, from

PDB entry 2bex (Iyer *et al.*, 2005); hRI·ANG, chains A and B,

respectively, from PDB entry 1a4y (Papageorgiou *et al.*, 1997)].

Numbering for RI and ribonuclease residues is based on the numbering

scheme of hRI and RNase 1. **(A–B)** Ribbon diagrams of the complexes are

shown colored gray with amino acid residues participating in equivalent

contacts explicitly shown as sticks in color. **(B)** Close-up of the equivalent

contacts shown in **A**. **(C–D)** Equivalent hydrogen bonds are represented as

dotted lines with bonding distances given in Ångströms (Å). **(E–F)** The

two equivalent van der Waals interactions among the four complexes are

depicted. Images were created and alignments performed with the program

PyMOL (DeLano Scientific, South San Francisco, CA).
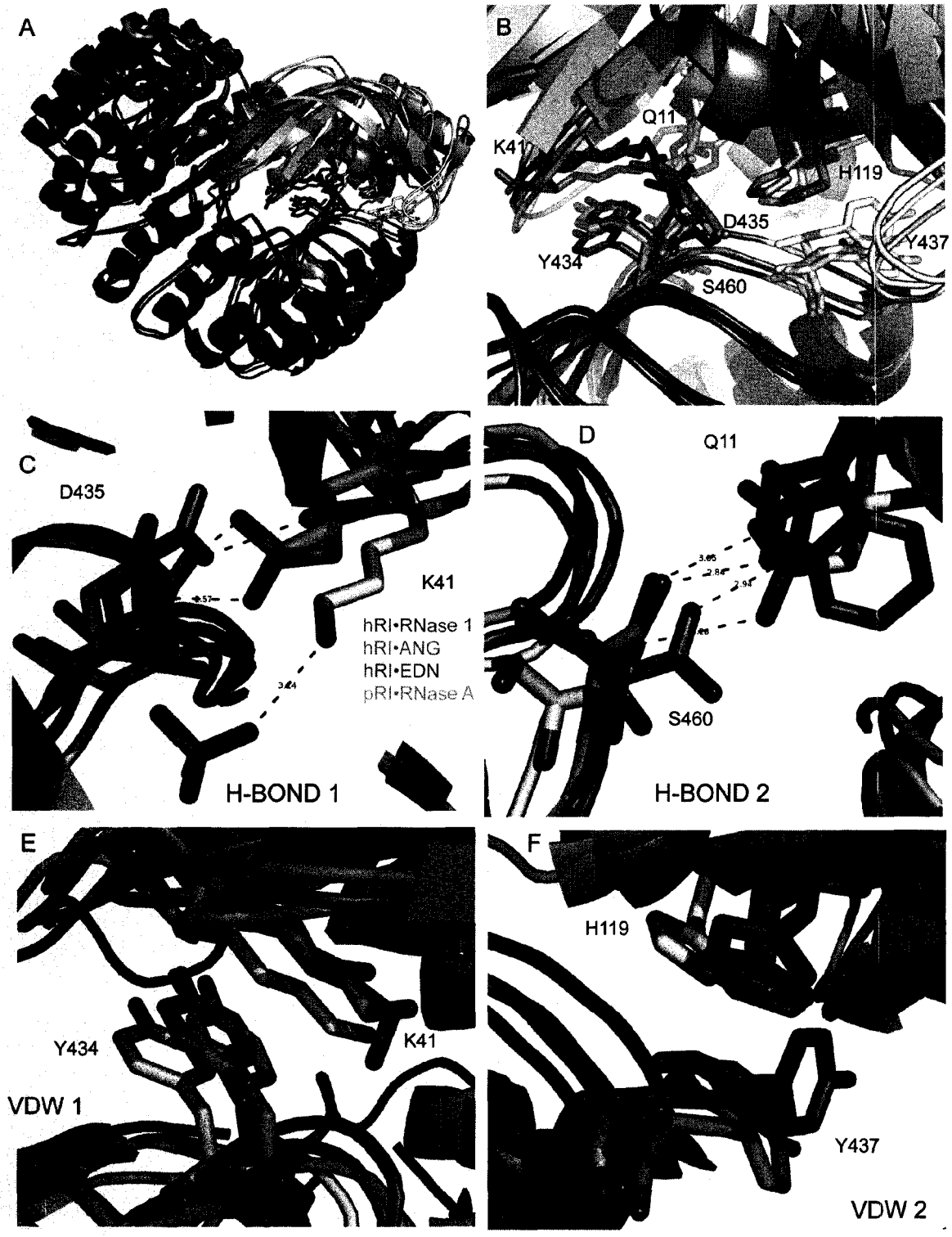
Figure 1.5   Role of ribonuclease surface loops in mediating interactions with RI.

(A) Overlay of the structures of cytotoxic amphibian ribonucleases (ONC:

olive green, 1onc (Mosimann *et al.*, 1994); Amphinase: forest green, 2p7s

(Singh *et al.*, 2007); RC-RNase 3: pea green, 1z5f (Lou *et al.*, 2006))

aligned with RNase A (orange, 7rsa (Wlodawer *et al.*, 1988)).

(B) Structural alignment of RNase A (black) and ONC (gray). The most

prominent surface loops of RNase A are labeled explicitly. The side chains

of the nine residues in these loops for which ONC possesses no analogous

residues are shown explicitly as sticks. (C) Ribbon diagrams of pRI

(green), RNase A (orange), and ONC (gray) are shown along with the

molecular surface of pRI. ONC (PDB entry 1onc) was aligned with

RNase A bound by pRI [chain E from PDB entry 1dfj (Kobe and

Deisenhofer, 1995b)]. The interaction of the β2–β3 loop of RNase A with

RI is shown in greater detail in the right-hand panel (D) to illustrate the

importance of the surface loops of mammalian ribonucleases in mediating

interactions with the inhibitor molecule. Images were created and

alignments were performed with the program PyMOL (DeLano Scientific,

South San Francisco, CA).

A — RNase A / ONC / Amphinase / RC-RNase 3

B — α2–β1, β4–β5, β2–β3, α1–α2

C

D — Y433, C404, N67, D407, RI, K66, Q69, RNase A, ONC β2–β3 loop
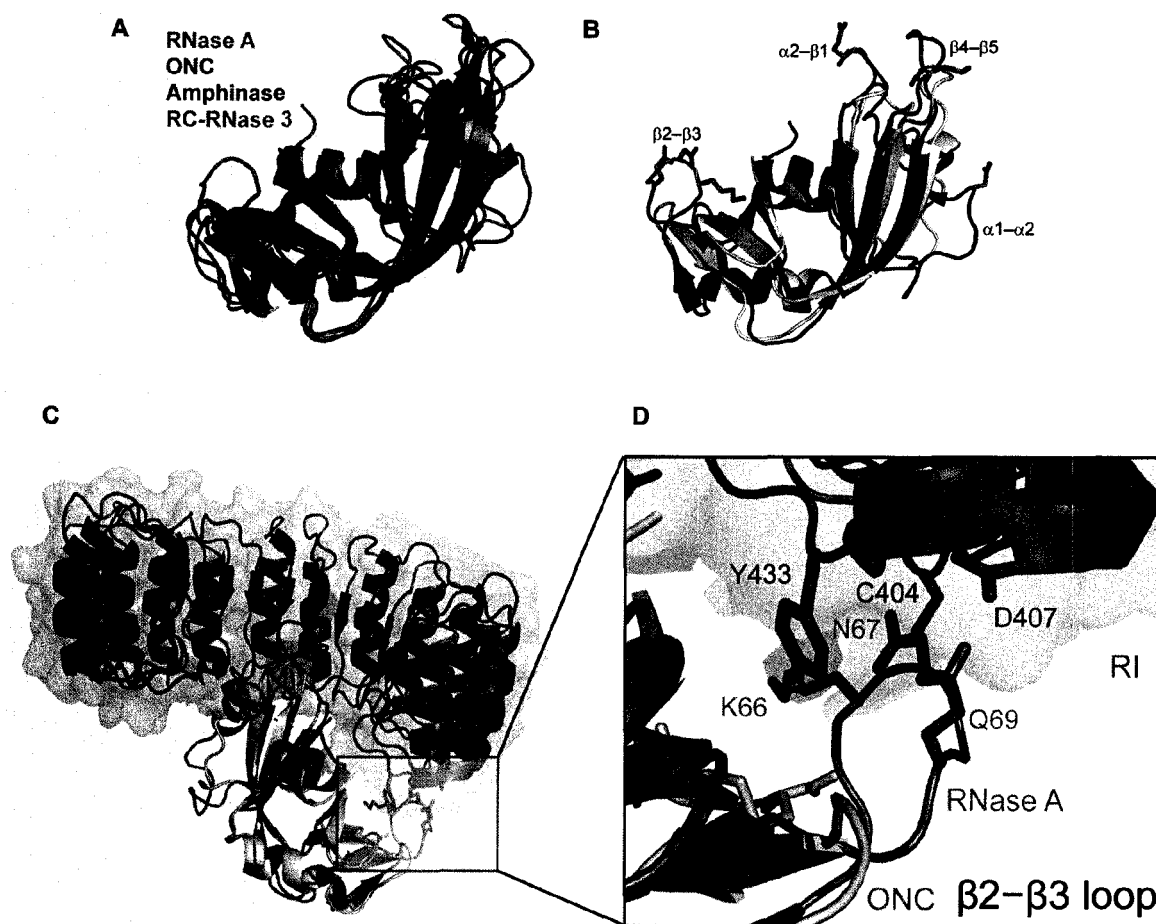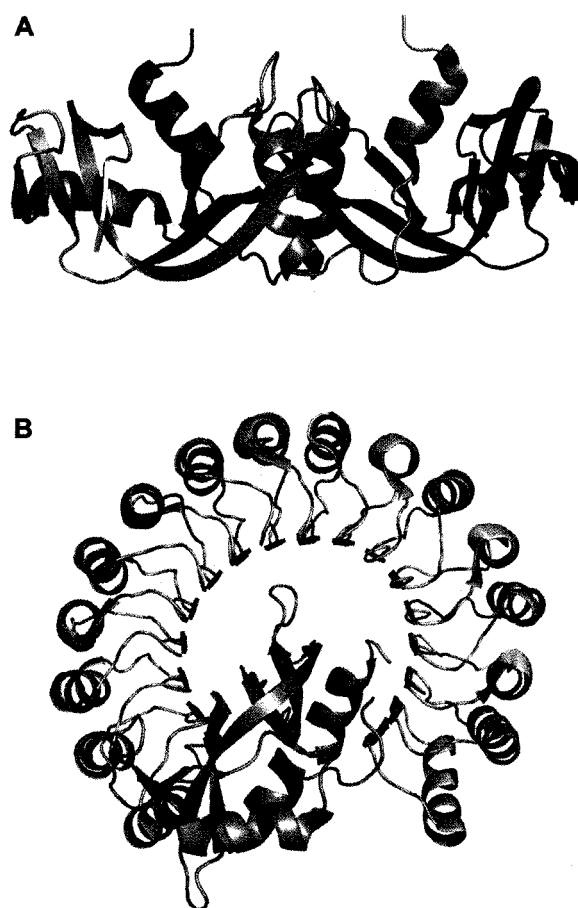
Figure 1.6   The structural origin of RI-evasivity in BS-RNase. (A) Structure of the

M×M form of BS-RNase (Mazzarella *et al.*, 1993). (B) Structure of a

monomeric subunit of the M=M form of BS-RNase (gold: 1r3m (Berisio

et al., 2003)) aligned with RNase 1 (not shown) of the hRI·RNase 1

complex (Johnson *et al.*, 2007c). Alignments were performed and images

created with the program PyMOL (DeLano Scientific, South San

Francisco, CA).

CHAPTER 2

Disruption of Shape-Complementarity Markers

to Create Cytotoxic Variants of Ribonuclease A

Contribution: Expression, purification, and in vitro characterization of ribonucleases, composition of manuscript, and preparation of figure drafts. Preliminary characterization of D38R/R39D RNase A and K7A/D38R/R39D/G88R RNase A was performed by E. L. Kurten. Computational analysis (FADE) of pRI·RNase A complex was performed by J. C. Mitchell.

This chapter was published as:
Rutkoski, T. J., Kurten, E. L., Mitchell, J. C., and Raines, R. T. (2005) Disruption of shape-complementarity markers to create cytotoxic variants of ribonuclease A. *J. Mol. Biol.* **354:** 41–54. (See cover art: Figure A4.1)

2.1 Abstract

Onconase® (ONC), an amphibian member of the bovine pancreatic ribonuclease A (RNase A) superfamily, is in Phase III clinical trials as a treatment for malignant mesothelioma. RNase A is a far more efficient catalyst of RNA cleavage than ONC but is not cytotoxic. The innate ability of ONC to evade the cytosolic ribonuclease inhibitor protein (RI) is likely to be a primary reason for its cytotoxicity. In contrast, the noncovalent interaction between RNase A and RI is one of the strongest known, with the RI·RNase A complex having a K_d value in the femtomolar range. Here, we report on the use of the Fast Atomic Density Evaluation (FADE) algorithm to identify regions in the molecular interface of the RI·RNase A complex that exhibit a high degree of geometric complementarity. Guided by these "knobs" and "holes", we designed variants of RNase A that evade RI. The D38R/R39D/N67R/G88R substitution increased the K_d value of the pRI·RNase A complex by 20-million–fold (to 1.4 µM) with little change to catalytic activity or conformational stability. This and two related variants of RNase A were more toxic to human cancer cells than was ONC. Notably, these cytotoxic variants exerted their toxic activity on cancer cells selectively, and more selectively than did ONC. Substitutions that further diminish affinity for RI (which has a cytosolic concentration of 4 µM) are unlikely to produce a substantial increase in cytotoxic activity. These results demonstrate the utility of the FADE algorithm in the examination of protein–protein interfaces and represent a landmark towards the goal of developing chemotherapeutics based on mammalian ribonucleases.

2.2 Introduction

Bovine pancreatic ribonuclease (RNase A) catalyzes the cleavage of RNA (Raines, 1998). Its putative biological function is to break down the large amounts of RNA that accumulate in the ruminant gut (Barnard, 1969). Other members of the RNase A superfamily possess a variety of interesting biological properties, including antiproliferative, cytotoxic, embryotoxic, aspermatogenic, and antitumoral activities (D'Alessio and Riordan, 1997; Leland and Raines, 2001; Matoušek, 2001; Makarov and Ilinskaya, 2003). Originally isolated from oocytes and early embryos of the Northern leopard frog *Rana pipiens* (Darzynkiewicz *et al.*, 1988; Mikulski *et al.*, 1990), Onconase® (ONC) is an amphibian homolog of RNase A that exhibits anti-tumoral activity both in vitro and in vivo *(Saxena et al., 2003)*. The ability of ONC to hydrolyze RNA is essential to its cytotoxicity (Wu *et al.*, 1993). ONC is currently being evaluated as a treatment for malignant mesothelioma in Phase III clinical trials (Mikulski *et al.*, 2002).

A significant practical limitation on the use of ONC as a chemotherapeutic is its dose-limiting renal toxicity (Mikulski *et al.*, 1993). Pharmacokinetic and biodistribution studies have revealed the renal retention of ONC to be 50- to 100-fold greater than that of mammalian members of the RNase A superfamily (Boix *et al.*, 1996; Vasandani *et al.*, 1996). Additionally, mice produce neutralizing antibodies against ONC but not against RNase A (Matoušek *et al.*, 2003b). ONC shares only 30% amino acid sequence identity with RNase A (Ardelt *et al.*, 1991). Development of cytotoxic *mammalian* ribonucleases could thus provide a more appealing class of cancer therapeutics due to more favorable

tissue distribution and reduced propensity for eliciting an immune response (Leland and Raines, 2001).

Ribonuclease inhibitor (RI) is a 50-kDa protein found in the cytosol of all mammalian cells (Hofsteenge, 1997; Shapiro, 2001; Dickson *et al.*, 2005). RI is a member of the leucine-rich repeat family of proteins and is composed of 15 alternating repeats arranged symmetrically to define a horseshoe shape (Kobe and Deisenhofer, 1993). Having 30 (porcine) or 32 (human) reduced cysteine residues (Kawanomoto *et al.*, 1992), RI can function only in a reducing environment like that of the cytosol (Blázquez *et al.*, 1996). There, RI acts as a sentry against invading ribonucleases (Haigis *et al.*, 2003), binding to members of the RNase A superfamily in a 1:1 stoichiometry (Blackburn *et al.*, 1977) and inhibiting completely their catalytic activity by steric occlusion of the active site (Kobe and Deisenhofer, 1996). The complexes formed between RI and its ligands are among the tightest of known biomolecular associations, with equilibrium dissociation constants in the femtomolar range (Vicentini *et al.*, 1990).

Some RNase A superfamily members, such as ONC and bovine seminal ribonuclease (BS-RNase), possess the ability to evade RI. Evasion is achieved either by virtue of a unique quaternary structure, as in dimeric BS-RNase (Murthy and Sirdeshmukh, 1992; D'Alessio *et al.*, 1997), or by divergent tertiary structure, as in ONC (Wu *et al.*, 1993), which has severe truncations in its surface loops (Boix *et al.*, 1996). The ability to retain ribonucleolytic activity in the presence of RI is a primary determinant of the cytotoxicity of ONC and BS-RNase. We had shown previously that altering RNase A so as to destabilize the RI·RNase A complex can endow RNase A with cytotoxic activity (Leland

et al., 1998). Still, the most cytotoxic variant to date, K7A/G88R RNase A, has nanomolar affinity for porcine RI (pRI) and is nearly 10-fold less cytotoxic than ONC (Haigis *et al.*, 2002). Although the affinity of the K7A/G88R variant for RI is 10^5-fold less than that of wild-type RNase A, its affinity still greatly exceeds that of ONC (estimated $K_d \geq 10^{-6}$ M) (Boix *et al.*, 1996).

Here, we implement a powerful computational tool to guide the design of new RI-evasive variants of RNase A. Specifically, we use the Fast Atomic Density Evaluation (FADE) algorithm (Mitchell *et al.*, 2001) to identify the "knobs" and "holes" in the molecular interface of the pRI·RNase A complex (Crick, 1952). The FADE algorithm approximates the shape of macromolecules by calculating the atomic density at points near the molecular surface. A counting algorithm is used to sum the atomic neighbors as a function of increasing radius from each discrete point. Intuitively, a surface region within a crevice is surrounded by atoms, and so would be expected to have a greater number of atomic neighbors (high atomic density) than would a surface region near a protrusion (low atomic density). To obtain a measure of local shape complementarity for a molecular complex, a three-dimensional grid of points is modeled onto the interface. The atomic density at each point on the grid is calculated with respect to each molecular component comprising the interface and the degree to which the "knobs" of one surface correspond with the "holes" on another is quantified. The descriptor of shape complementarity generated by FADE assigns the greatest significance to regions of the interface possessing adjacent surfaces with the most disparate atomic densities. In several model protein complexes, regions of high shape complementarity identified by FADE

were shown to correlate well with amino acid residues identified in mutational studies as being important for binding affinity (Mitchell *et al.*, 2004). We reasoned that introducing electrostatic and steric incompatibilities in these regions would destabilize the pRI·RNase A complex. We describe the specific amino acid substitutions made to RNase A, the impact of these substitutions on RI affinity as well as catalytic activity and conformational stability, and how this approach ultimately resulted in several RNase A variants that are more toxic than ONC to tumor cells in vitro.

2.3 Experimental Procedures

2.3.1 Materials

Escherichia coli BL21(DE3) cells and pET22b(+) and pET27b(+) plasmids were from Novagen (Madison, WI). K-562 cells were derived from a continuous human chronic myelogenous leukemia line obtained from the American Type Culture Collection (Manassas, VA). Cell culture medium and supplements were from Invitrogen (Carlsbad, CA). [*methyl*-^{3}H]Thymidine (6.7 Ci/mmol) was from Perkin Elmer (Boston, MA). Enzymes were obtained from Promega (Madison, WI) or New England Biolabs (Beverly, MA). Ribonuclease substrates 6-FAM–dArUdAdA–6-TAMRA and 6-FAM–dArUdGdA–6-TAMRA were from Integrated DNA Technologies (Coralville, IA). All other chemicals used were of commercial reagent grade or better, and were used without further purification.

Terrific Broth (TB) contained (in 1.00 L) tryptone (12 g), yeast extract (24 g), glycerol (4 mL), KH_2PO_4 (2.31 g), and K_2HPO_4 (12.54 g). Phosphate-buffered saline

(PBS) contained (in 1.00 L) NaCl (8.0 g), KCl (2.0 g), $Na_2HPO_4 \cdot 7H_2O$ (1.15 g), KH_2PO_4 (2.0 g), and NaN_3 (0.10 g), and had pH 7.4.

2.3.2 Analytical Instruments

[methyl-^{3}H]Thymidine incorporation into K-562 genomic DNA was quantitated by scintillation counting using a Microbeta TriLux liquid scintillation and luminescence counter (Perkin Elmer, Wellesley, MA). The mass of each protein variants was confirmed by MALDI–TOF mass spectrometry using a Voyager-DE-PRO Biospectrometry Workstation (Applied Biosystems, Foster City, CA). Fluorescence measurements were made with a QuantaMaster1 photon-counting fluorometer equipped with sample stirring (Photon Technology International, South Brunswick, NJ). Thermal denaturation data were acquired using a Cary 3 double-beam spectrophotometer equipped with a Cary temperature controller (Varian, Palo Alto, CA).

2.3.3 Design of Ribonuclease A Variants

The Fast Atomic Density Evaluator (FADE) program calculates shape-complementarity markers of proteins at complex interfaces. Atomic density (Kuhn et al., 1992) is measured using fast Fourier transform algorithms based on methods described previously (Mitchell et al., 2001). Using the structure of the crystalline pRI·RNase A complex (PDB entry 1dfj (Kobe and Deisenhofer, 1995b)), critical RNase A residues in close proximity to large clusters of shape-complementarity markers were identified and are listed in Table 2.1. Amino acid substitutions were chosen to create maximal

electrostatic or steric conflict as well as eliminate any favorable Coulombic or short-range interactions.

At the onset of this research, the most cytotoxic variant of RNase A known was K7A/G88R RNase A (Haigis *et al.*, 2002). Subsequent amino acid substitutions inspired by FADE analysis were initially made in the background of these established changes, with the expectation that any additional contributions to evasivity would be additive. As discussed within this chapter, we found that the loss of enzymatic activity accompanying the K7A substitution compromised cytotoxicity, and hence, later substitutions were made in the background of the G88R substitution alone. The G88R background provided a well-characterized benchmark of cytotoxicity and RI-evasion from which we could identify improvements using our established assays (Leland *et al.*, 1998; Abel *et al.*, 2002). Substitutions that were successful in the G88R background were also made alone to assess their individual contribution to evasion of RI and cytotoxicity.

2.3.4 Production of Ribonucleases

cDNA encoding RNase A variants was created by oligonucleotide-mediated site-directed mutagenesis (Kunkel *et al.*, 1987) using a pET22b(+) or pET27b(+) plasmid that contained cDNA encoding wild-type RNase A or its G88R variant, respectively (Leland *et al.*, 1998). ONC, wild-type RNase A, and RNase A variants were produced as described previously (delCardayré *et al.*, 1995; Leland *et al.*, 1998), with the following exceptions. Inclusion bodies from *E. coli* were stirred in 20 mM Tris–HCl buffer at pH 8.0, containing guanidine–HCl (7 M), DTT (0.1 M), and EDTA (10 mM) until

dissolved thoroughly. Ribonucleases were refolded overnight at room temperature following slow dilution into 0.10 M Tris–HCl buffer at pH 8.0, containing NaCl (0.1 M), reduced glutathione (1.0 mM), and oxidized glutathione (0.2 mM). Following purification, proteins were dialyzed against PBS and filtered with a 0.2-µm syringe prior to use in biochemical assays. Protein concentration was determined by UV spectroscopy using an extinction coefficient of $\varepsilon_{278} = 0.72$ mg·ml^{-1}cm^{-1} for RNase A and its variants (Sela et al., 1957) and $\varepsilon_{280} = 0.87$ mg·ml^{-1}cm^{-1} for ONC (Leland et al., 1998).

2.3.5 Production of Ribonuclease Inhibitors

pRI was prepared as described previously (Klink et al., 2001). Freshly prepared pRI was confirmed to be 100% active by its ability to titrate the ribonucleolytic activity of wild-type RNase A.

hRI was produced in E. coli BL21(DE3) cells transformed with a pET22b(+) plasmid that contained cDNA encoding hRI between its NdeI and SalI sites. Cultures (1.0 L) of TB were inoculated to an OD of 0.005 at 600 nm from an overnight culture. The culture was grown at 37 °C to an OD of 1.8–2.0 at 600 nm. IPTG was added to a final concentration of 0.5 mM, and induction was carried out overnight at 18 °C. Subsequent purification of soluble protein and activity determination of hRI was carried out in the same manner as for pRI (Klink et al., 2001).

Following purification, ribonucleases and ribonuclease inhibitor proteins migrated as single bands during SDS–PAGE, confirming their purity and apparent molecular weight.

In addition, the integrity of purified ribonucleases was confirmed by MADLI–TOF mass spectrometry (Table 2.4).

2.3.6 Measurements of Conformational Stability

The conformational stability of the RNase A variants was assessed. Protein was dialyzed exhaustively against PBS and diluted to a concentration of ~25 µM. Assays were performed by incremental heating (0.15 °C/min from 25–75 °C) and measurement of the absorbance at 287 nm (Eberhardt *et al.*, 1996). Data were collected and analyzed with the program THERMAL from Varian Analytical Instruments (Walnut Creek, CA).

2.3.7 Assay of Affinity for Ribonuclease Inhibitor

The affinity of RNase A variants for both pRI and hRI was determined by using a slight modification of a competition assay reported previously (Abel *et al.*, 2002). Briefly, both fluorescein-labeled G88R RNase A (final concentration: 50 nM) and varying concentrations of an unlabeled ribonuclease were added to 2.0 ml of PBS containing DTT (5 mM). Following a 15-min incubation at (23 ± 2) °C, protected from light, the initial fluorescence intensity of the unbound fluorescein-labeled G88R RNase A was monitored for 3 min (excitation at 493 nm, emission at 515 nm). pRI was then added (final concentration: 50 nM, which is sufficient to bind 90% of the fluorescein-labeled G88R RNase A in the absence of unlabeled competitor), and the final fluorescence intensity was measured. The competition assay was carried out identically for hRI. The affinity of hRI for fluorescein-labeled G88R RNase A was determined by titrating 0.8 nM

fluorescein-labeled G88R RNase A with various amounts of hRI (0.026–26 nM) and

recording the decrease in fluorescence upon binding. The value of K_d was found to be

1.4 nM, which is within the standard error of the value determined for unlabeled G88R

RNase A (Table 2.2).

2.3.8 Assay of Catalytic Activity

The ribonucleolytic activities of RNase A and its variants were determined by

assaying their ability to cleave the hypersensitive fluorogenic substrate

6-FAM–dArUdAdA–6-TAMRA (20 nM), which exhibits a 180-fold increase in

fluorescence (excitation at 493 nm, emission at 515 nm) upon cleavage (Kelemen *et al.*,

1999). Assays were carried out at (23 ± 2) °C in 2.0 ml of 0.10 M MES–NaOH (pH 6.0),

containing NaCl (0.10 M). The MES used to prepare the assay buffer was purified by

anion-exchange chromatography to remove trace amounts of oligomeric vinylsulfonic

acid, which is a byproduct of commercial buffer synthesis and has been shown to be a

potent inhibitor of RNase A (Smith *et al.*, 2003). Values of k_{cat}/K_M were obtained with the

equation:

$$k_{cat}/K_M = \left(\frac{\Delta I / \Delta t}{I_{max} - I_0} \right) \frac{1}{[E]} \tag{2.1}$$

where $\Delta I/\Delta t$ represents the initial reaction velocity generated by cleavage of the

6-FAM–dArUdAdA–6-TAMRA substrate upon addition of ribonuclease to the cuvette. I_0 and I_{max} are, respectively, the fluorescence intensities prior to enzyme addition and following the complete cleavage of substrate by excess wild-type RNase A. Activity values for ONC were determined at (23 ± 2) °C in 2.0 ml of OVS-free 20 mM MES–NaOH (pH 6.0), 0.010 M NaCl using 20 nM 6-FAM–dArUdGdA–6-TAMRA (Lee and Raines, 2003).

2.3.9 Assay of Cytotoxicity

IC_{50} values for RNase A, its variants, and ONC were determined by measuring the incorporation of [$methyl$-^{3}H]thymidine into the cellular DNA of K-562 cells in the presence of ribonucleases as described previously (Leland et al., 1998). All cytotoxicity assays were repeated at least three times in triplicate. Each data point represents the mean of three or more experimental values ($\pm$ SE). IC_{50} values were calculated by fitting the curves using nonlinear regression to a sigmoidal dose–response curve with the equation:

$$y = \frac{100\%}{1 + 10^{(\log(IC_{50}) - \log[\text{ribonuclease}])h}}$$ (2.2)

In eq 2.2, y is the total DNA synthesis following a 4-h [$methyl$-^{3}H]thymidine pulse, and h is the slope of the curve.

Cytotoxicity assays other than those carried out using K-562 cells were performed at the Keck–UWCCC Small Molecule Screening Facility. These assays used ten cell lines from a broad spectrum of tissues. Following a 72-h incubation with ribonucleases, IC_{50}

values were determined by measuring the enzymatic conversion of the profluorophore

calcein AM (Molecular Probes, Eugene, OR) to calcein in live cells. Coefficient of

variation and *Z'-factor* (Zhang *et al.*, 1999) were determined for each cell line using

doxorubicin as an internal control. All cytotoxicity assays were performed in triplicate

three times. IC_{50} values were calculated with the equation:

$$IC_{50} = \left(\frac{50\% - \text{low}\%}{\text{high}\% - \text{low}\%}\right)\left([\text{ribonuclease}]_{\text{high}} - [\text{ribonuclease}]_{\text{low}}\right) + [\text{ribonuclease}]_{\text{low}} \quad (2.3)$$

where low% and high% refer to inhibition by the two concentrations, $[\text{ribonuclease}]_{\text{low}}$

and $[\text{ribonuclease}]_{\text{high}}$, that bracket 50% inhibition.

2.4 Results

2.4.1 FADE Analysis

The results of the FADE analysis on the pRI·RNase A complex (PDB entry 1dfj

(Kobe and Deisenhofer, 1995b)) are depicted in Figures 2.1 and 2.2. In these figures,

FADE geometric-complementarity markers are displayed as solid spheres. These spheres

do not represent atoms. Instead, the spheres represent points in the molecular interface

near which local complementarity is most significant. Complementarity markers within

2 Å of any atom within a particular residue were summed to determine the cluster sizes

listed in Table 2.1. The residues in RNase A that are proximal to the largest number of

complementarity markers and distal from the enzymic active site (Raines, 2004) were

targeted for disruption. We refrained from changing residues in RI because a goal of our work was to develop new cytotoxic ribonucleases.

We reasoned that disruption could, in general, be achieved best by replacing small neutral or anionic residues in RNase A with arginine. We suspected that arginine, as the most polar and second largest amino acid (Radzicka and Wolfenden, 1988), could generate electrostatic repulsion and steric strain while increasing the net positive charge, which is known to enhance cell internalization (Futami *et al.*, 2001; Fuchs and Raines, 2005; Fuchs *et al.*, 2007; Johnson *et al.*, 2007a). In addition, we replaced lysine residues in RNase A with alanine to create truncated neutral side chains and thereby eliminate favorable interactions within the complex.

D38R/R39D Swap. (Figure 2.2C). Arg39 was identified by the FADE algorithm as being proximal to the greatest number of complementarity markers of any residue in RNase A (Table 2.1). With 14 atom–atom contacts to pRI, Arg39 also makes more contacts with RI than any residue in RNase A with the exception of Glu111, which also makes 14 contacts (Kobe and Deisenhofer, 1996). Together, Asp38 and Arg39 of RNase A form three hydrogen bonds with Arg453 and Glu397 from pRI, respectively, with Arg39 interacting with Glu397 in a bidentate manner. Additionally, these two RNase A residues make van der Waals contacts with Gln426, Val428, Tyr430, and Ile455 of RI. Although Asp38 was not identified explicitly by the FADE analysis, we reasoned that by interchanging this residue with Arg39, we could disrupt three favorable interactions at the pRI·RNase A interface simultaneously. Moreover, the D38R/R39D swap was conservative in that it preserved the local amino acid content.

β4–β5 loop. (Figure 2.2D) Four surface loops of RNase A contribute 16 of the 24 residues that contact RI . The β4–β5 loop of RNase A, containing residues 87–96, packs against an especially hydrophobic region of pRI defined by three tryptophan residues: Trp257, Trp259, and Trp314. Three RNase A residues within this loop, Gly88, Ser89, and Lys91, were identified by FADE as being important for mediating shape complementarity with RI. Earlier attempts to create an RI-evasive RNase A showed the replacement of Gly88 (FADE cluster size 5) with an arginine residue to be extremely effective at introducing steric and electrostatic strain, increasing the K_d value of the pRI·RNase A complex by nearly four orders of magnitude (Leland *et al.*, 1998). Therefore, although residues Ser89 and Lys91 were identified by the FADE algorithm as being near large complementarity clusters, we assumed this region of the complex to be disrupted maximally by the G88R substitution and hence did not pursue further alteration of this loop.

N67R substitution. (Figure 2.2A) Asn67 was proximal to the third largest cluster of complementarity markers, following Arg39 and residues of the β4–β5 loop of RNase A. Asn67 makes six contacts with pRI residues Cys404, Val405, Gly406, and Tyr433, including a hydrogen bond with the main-chain oxygen of Val405. It is noteworthy that Tyr433 of pRI, which makes contacts with Asn67 of RNase A, was identified as being proximal to the largest number of complementarity markers of any residue in either protein. In accordance, Camacho and coworkers identified Tyr433 of RI and Asn67 of RNase A as the "anchor residues" in the pRI·RNase A complex (Rajamani *et al.*, 2004).

Other FADE-identified residues. Lys7 (Figure 2.2B) was the lowest scoring of the RNase A residues listed in Table 2.1, with a complementarity cluster size of 2. Nonetheless, Lys7 makes seven atom–atom contacts with Ser456 of pRI, including several hydrogen bonds. Previous studies had shown this residue to contribute significantly to complex stability (Neumann and Hofsteenge, 1994; Haigis et al., 2002). We also examined Asn24 and Lys31, which make seven and four atom–atom contacts and are located near cluster sizes of 5 and 2, respectively. Asn24 makes seven van der Waals contacts and two hydrogen bonds with Asp89 and Asp117 of RI; Lys31 makes three atom–atom contacts with His6 of pRI and one contact with Asp31.

2.4.2 Catalytic Activity

A ribonuclease must retain its catalytic activity to be cytotoxic (Kim et al., 1995a). Accordingly, the catalytic activity of each ribonuclease was assayed to determine if any of the amino acid substitutions compromised cytotoxicity by reducing the ability of the enzyme to degrade RNA. Values of k_{cat}/K_M for wild-type RNase A, its variants, and ONC are listed in Table 2.2. The k_{cat}/K_M values of wild-type RNase A, G88R RNase A, K7A/G88R RNase A, and ONC were 5.2×10^7, 7.4×10^7, 5.3×10^6, and 2.2×10^5 $M^{-1}s^{-1}$, respectively, which are in good agreement with values reported previously (Haigis et al., 2002; Lee and Raines, 2003). Swapping residues 38 and 39 of RNase A had a minor effect on catalysis by the enzyme. The value of k_{cat}/K_M for D38R/R39D RNase A was 1.8×10^7 $M^{-1}s^{-1}$, which represents only a 3-fold loss in ribonucleolytic activity. A similarly small effect was seen in the D38R/R39D/G88R

variant; its k_{cat}/K_M value of $3.1 \times 10^7 \, M^{-1} s^{-1}$ was 2.5-fold less than that of G88R

RNase A. Interestingly, when the single R39D substitution was made in the context of the

G88R substitution, the effect on ribonucleolytic activity was more pronounced, reducing

the k_{cat}/K_M value of G88R RNase A by 17-fold to $4.3 \times 10^6 \, M^{-1} s^{-1}$. This decrease could

result from enhanced negative charge in this region, possibly reducing the number of

productive collisions between the enzyme and its anionic substrate.

The P2 substrate binding site of RNase A, which contains Lys7, plays an important

role in catalysis by RNase A (Boix *et al.*, 1994; Nogués *et al.*, 1995; Fisher *et al.*, 1998b).

Consistent with previous results (Haigis *et al.*, 2002), K7A/G88R RNase A displayed an

almost 10-fold decrease in ribonucleolytic activity, having a k_{cat}/K_M value of

$5.3 \times 10^6 \, M^{-1} s^{-1}$. This deleterious contribution to catalysis was additive when combined

with other amino acid substitutions that diminished activity; the D38R/R39D swap

(3-fold decrease in k_{cat}/K_M) when combined with the K7A substitution (10-fold decrease

in k_{cat}/K_M) resulted in a K7A/D38R/R39D variant with an activity of $1.6 \times 10^6 \, M^{-1} s^{-1}$,

which is 30-fold less than that of wild-type RNase A. Additionally, the K7A substitution

was responsible for a 15-fold reduction in the activity of D38R/R39D/G88R RNase A,

reducing the activity of the quadruple variant K7A/D38R/R39D/G88R RNase A to

$1.6 \times 10^6 \, M^{-1} s^{-1}$.

The majority of the FADE-inspired substitutions had no significant effect on

ribonucleolytic activity. The N67R, K31A, and N24R substitutions, when combined

individually with the G88R substitution, produced enzymes with catalytic activity

roughly comparable to that of G88R RNase A itself. Values of k_{cat}/K_M for these three

variants were 9.2×10^7, 5.2×10^7, and $7.8 \times 10^7\,\mathrm{M^{-1}s^{-1}}$, respectively. Therefore,

RNase A variants combining many of these substitutions (such as

K31A/D38R/R39D/N67R/G88R RNase A and D38R/R39D/N67R/G88R RNase A)

possessed nearly the k_{cat}/K_M value of the wild-type enzyme (4.8×10^7 and

$3.8 \times 10^7\,\mathrm{M^{-1}s^{-1}}$, respectively).

2.4.3 Affinity for Ribonuclease Inhibitor

The amino acid sequences of pRI and hRI are quite similar (77% identity). Moreover,

of the 28 residues in pRI that contact RNase A (Kobe and Deisenhofer, 1995a), only two

are replaced by dissimilar residues in hRI. Despite the assumption that the two inhibitor

proteins would possess similar affinities for the RNase A variants, we determined the K_d

values of complexes with both pRI and hRI. These K_d values are listed in Table 2.2.

As a rigorous test of the utility of the FADE algorithm for identifying residues

important for protein–protein interactions, we determined the K_d values of the FADE-

inspired variants in complexes with pRI. The K_d values of 0.57 and 17 nM obtained for

G88R RNase A and K7A/G88R RNase A in complexes with pRI, were in good

agreement with those determined previously (Haigis et al., 2002). The N24R substitution

was the only change that did not diminish the affinity of pRI for RNase A. Indeed, with a

K_d value of 0.27 nM, N24R/G88R RNase A actually appeared to form a slightly tighter

complex with pRI than did G88R RNase A. The most significant increases in values of

K_d were observed for the D38R/R39D swap and the N67R substitution, whose complexes

exhibited K_d values of 0.30 and 0.36 nM, respectively. These amino acid changes were

responsible for 4,500- and 5,400-fold increases in K_d value, respectively. The K7A/D38R/R39D, N67R/G88R, and D38R/R39D/G88R variants formed complexes with pRI that have K_d values of 3.5, 45, and 8.0 nM, respectively.

The combination of multiple substitutions produced the most RI-evasive variants of RNase A. Of note are the K7A/D38R/R39D/G88R and D38R/R39D/N67R/G88R variants, which formed complexes with pRI having K_d values of 0.12 and 1.4 μM, respectively. Notably, D38R/R39D/N67R/G88R RNase A is the first RNase A variant observed to form a complex with pRI that has a micromolar K_d value. By changing only four out of 124 residues in RNase A, the K_d value of the pRI·RNase A complex was increased by 20-million fold with the D38R/R39D/N67R/G88R variant.

Values of K_d for the complexes of pRI with RNase A variants are ideal for assessing the ability of the FADE algorithm to identify shape-complementarity markers. As a chemotherapeutic, however, cytotoxic ribonucleases must be capable of eluding human RI. For this reason, values of K_d were also determined for the hRI complexes with RNase A variants. With the exception of N67R/G88R RNase A (K_d = 44 nM), K_d values for the hRI complexes were greater than those obtained for pRI, with the magnitude of the differences ranged from 2- to 230-fold. The highest K_d value observed for a complex with hRI was that of K7A/D38R/R39D/G88R RNase A at 27 μM, which represents a 400 million-fold decrease in affinity for hRI.

Importantly, the destabilizing effects of these substitutions on the complex were not entirely additive, indicating that the pRI·RNase A interface is plastic. The accommodating nature of the binding interface can be seen upon comparison of $\Delta\Delta G$

values (Table 2.2). For example, the G88R and N67R substitutions destabilize the complex by approximately 5 kcal/mol each. Yet, the N67R/G88R double variant exhibits an 8 kcal/mol loss in binding free energy, despite the spatial separation of these two substitutions. Chen and Shapiro had previously described multiple changes made in hRI as having sub-additive effects on complex destabilization (Chen and Shapiro, 1999). They explained this negative cooperativity as a result of a broad distribution of binding energy over a large interface (Chen and Shapiro, 1999). Our results support this observation.

2.4.4 Conformational Stability

The conformational stability of a ribonuclease is necessary for biological function, including cytotoxicity (Klink and Raines, 2000). Hence, the T_m value of each RNase A variant was determined and is listed in Table 2.2. The N67R substitution was the most destabilizing, decreasing the T_m value of wild-type RNase A by 7 °C to a value of 57 °C. This loss in conformational stability was not recovered by additional substitutions, being observed in all variants containing the N67R substitution. The N67R/G88R and D38R/R39D/N67R/G88R variants had T_m values of 58 and 56 °C, respectively. K31A/D38R/R39D/N67R/G88R RNase A had the lowest T_m value of 54 °C, which is nearly 10 °C lower than that of the wild-type enzyme. Still, this T_m value is significantly greater than physiological temperature. None of the other amino acid substitutions reduced the T_m value by more than a few °C.

2.4.5 Cytotoxicity

The toxicity of each ribonuclease was measured with the K-562 human leukemia cell line. Ribonucleases are listed in order of increasing cytotoxicity in Table 2.2, using IC_{50} values derived by applying equation 2.2 to the data in Figure 2.3 ($h = 1.43 \pm 0.02$ for the 12 cytotoxic ribonucleases). ONC, G88R RNase A, and K7A/G88R RNase A displayed IC_{50} values similar to those reported previously (Leland *et al.*, 1998; Bretscher *et al.*, 2000; Haigis *et al.*, 2002). D38R/R39D RNase A (Figure 2.3A) and N67R RNase A (Figure 2.3C) exhibited no cytotoxic activity, even at concentrations of 25 μM. The lack of cytotoxicity for the latter two variants is interesting, considering the large increase in cytotoxicity they exhibited in the context of the G88R substitution.

Upon incorporation of the K7A substitution into the D38R/R39D/G88R variant, its affinity for hRI decreased 40-fold, consistent with the loss of favorable interactions between the lysine side chain and C-terminal serine residue of hRI. This larger K_d value was accompanied by a loss in catalytic activity, leading to an IC_{50} value nearly twice that of D38R/R39D/G88R RNase A. Although Asp38 was not identified explicitly by the FADE analysis, its importance in the conservative D38R/R39D swap is apparent when the IC_{50} value of R39D/G88R RNase A ($IC_{50} = 0.69$ μM) is compared with that of D38R/R39D/G88R RNase A ($IC_{50} = 0.22$ μM).

Two of the most cytotoxic variants of RNase A discovered in this work, D38R/R39D/G88R and D38R/R39D/N67R/G88R, as well as ONC, wild-type RNase A, and G88R RNase A, were screened for cytotoxic activity against ten different cell lines. The resulting IC_{50} values of these ribonucleases are listed in Table 2.3. All of the cell

lines are of human origin except for NmuMG, which is a mouse mammary normal epithelial cell line. With the exception of the Hep3B cell line, all of the human cancer cell lines, like the human leukemia K-562 line, are among the 60 cell lines screened by the National Cancer Institute in search of novel cancer chemotherapeutics.

The cell lines are listed in Table 2.3 according to increasing doubling times. There did not appear to be any direct correlation between doubling time and sensitivity to the ribonucleases as had been reported previously (Haigis et al., 2003). In general, the trend of cytotoxicity among the RNase A variants reflected that seen in the K-562 cell line, namely D38R/R39D/N67R/G88R > D38R/R39D/G88R > G88R > wild-type RNase A, with the D38R/R39D/N67R/G88R variant consistently having the lowest IC_{50} value. The HCT-116, A549, and SF268 cell lines were exceptions to this general trend, as all were more sensitive to wild-type RNase A than was G88R RNase A. Batra and coworkers have reported that wild-type human pancreatic ribonuclease (RNase 1) is toxic to some cell lines (Gaur et al., 2001), just as we found several cell lines susceptible to wild-type RNase A. These three cell lines derive from three different tissue types: colon, lung, and CNS, respectively.

A goal of this research was to develop RNase A variants possessing cytotoxicity equal to or greater than that of ONC. This goal was achieved with the D38R/R39D/N67R/G88R variant in the K-562, Du145, Hep-3B, and SF268 cell lines. In the remaining six cell lines, ONC exhibited 3- to 30-fold greater cytotoxicity than did the RNase A variants. Interestingly, none of the RNase A-derived variants tested in this screen were toxic to the normal cell line NmuMG at the maximum concentrations tested.

This discrimination was not observed with ONC, which had an IC_{50} of 1.62 μM for the normal mouse cell line.

2.5 Discussion

ONC and BS-RNase exhibit natural cytotoxic activity, an attribute due in part to their ability to evade RI (Youle and D'Alessio, 1997; Leland and Raines, 2001; Matoušek, 2001; Makarov and Ilinskaya, 2003). RNase A is bound tightly by RI and lacks cytotoxicity. We showed previously that diminishing the affinity of RNase A for RI enables the enzyme to degrade cellular RNA and elicit cell death (Leland *et al.*, 1998; Haigis *et al.*, 2002; Dickson *et al.*, 2003). Encouraged by these results, we set out to unleash the full cytotoxic potential of RNase A by more thoroughly disrupting its interaction with RI.

2.5.1 An Atypical Interface

Proper biological function requires macromolecules to interact with specific recognition and appropriate affinity. There are many properties of a protein–protein interface that can endow the complex with stability, including total surface area, nonpolar surface area, packing density, and polar interactions (Lo Conte *et al.*, 1999). The 2,550 Å² of solvent-accessible surface area buried upon formation of the pRI·RNase A complex is relatively large for an enzyme·inhibitor complex, and is considerably larger than the 1600 Å² that is typical for protease·inhibitor complexes (Janin, 1995). In general, protein interfaces resemble the chemical character of solvent-exposed protein surfaces,

which are comprised of approximately 57% nonpolar, 24% neutral polar, and 19% charged amino acid residues (Miller *et al.*, 1987). Typical protein–protein interfaces do, however, contain fewer charged residues and more neutral polar residues than do solvent-exposed protein surfaces. Deviating from this trend, the pRI–RNase A interface is significantly more charged, with 49% nonpolar, 27% neutral polar, and 24% charged residues (Kobe and Deisenhofer, 1996). Indeed, electrostatics seem to play an important role in the complex formed between the basic RNase A (p*I* 9.3 (Ui, 1971)) and the acidic RI protein (p*I* 4.7 (Kobe and Deisenhofer, 1996)) at cytosolic pH.

In contrast to the larger role of charge–charge interactions within the pRI·RNase A complex, the degree of shape complementarity between the two surfaces is lower than average. The shape correlation statistic, S_c, describes how well two surfaces mesh, with a value of 1.0 describing a perfect match and 0.0 describing two unrelated surfaces (Lawrence and Colman, 1993). The pRI·RNase A interface has a relatively low S_c value of 0.58 (Kobe and Deisenhofer, 1995b), as compared to values of 0.70–0.76 for typical protease·inhibitor complexes and 0.64–0.68 for typical antibody·antigen complexes (Lawrence and Colman, 1993). The packing of atoms at the pRI–RNase A interface is also less dense than a typical protein interior or protein–protein interface (Lo Conte *et al.*, 1999). The large amount of buried surface area could compensate for the relatively low degree of shape complementarity, to yield a highly stable interaction between RI and RNase A.

2.5.2 Disrupting the RI·RNase A Complex

Prior to this work, K7A/K41R/G88R RNase A was the most RI-evasive of known variants (Haigis et al., 2002). This variant formed a complex with pRI that had a K_d value of 47 nM, nearly 10^2-fold greater than that of G88R RNase A. Still, K7A/K41R/G88R RNase A is not a potent cytotoxin, owing largely to the 10^2-fold decrease in ribonucleolytic activity caused by the replacement of its active-site lysine residue with arginine (Messmore et al., 1995; Bretscher et al., 2000; Dickson et al., 2003).

The FADE algorithm revealed new "knobs" and "holes" in the pRI·RNase A complex for disruption by site-directed mutagenesis (Figures 2.1 and 2.2, Table 2.1). In the RNase A variants created in this work, the D38R/R39D swap and N67R substitution produced the largest decrease in affinity for RI. Alone, each of these substitutions effected a destabilization of the pRI·RNase A complex nearly equal to that of the G88R substitution (Leland et al., 1998). Combining the most disruptive FADE-inspired substitutions resulted in ribonucleases that were not only 30-fold more RI-evasive than K7A/K41R/G88R RNase A, but also retained nearly wild-type catalytic activity (Table 2.2). Moreover, the D38R/R39D/G88R, D38R/R39D/N67R/G88R, and K31A/D38R/R39D/N67R/G88R variants were all more cytotoxic to K-562 cells than was ONC (Figure 2.3).

One interesting finding is the difference in affinity of the porcine and human homologs of RI observed for some of the RNase A variants. In general, RNase A variants were bound more tightly by pRI than hRI (Table 2.2). This higher affinity of pRI for RNase A was not observed when the equilibrium dissociation constants were measured

originally for complexes of wild-type RNase A with pRI (K_d = 6.7 × 10^{-14} M (Vicentini *et al.*, 1990)) and hRI (K_d = 4.4 × 10^{-14} M (Lee *et al.*, 1989)). Of the 28 pRI residues that contact RNase A, 25 are identical in hRI. The three differences among the RNase A binding residues are the replacements of His6 in pRI with a glutamine residue in pRI, Asp228 with alanine, and Val405 with leucine (Chen and Shapiro, 1997). All three of these pRI residues make atom–atom contacts exclusively with FADE-identified RNase A residues. His6 makes three contacts with Lys31 of RNase A, Asp228 makes two contacts with Ser89, and Val405 makes three contacts with Asn67. These three changes are likely to contribute to the differential affinity of pRI and hRI for the RNase A variants.

2.5.3 RI Evasion as a Molecular Determinant of Cytotoxicity

Several factors have been shown to be important molecular determinants for ribonuclease cytotoxicity, including catalytic activity (Kim *et al.*, 1995a) and evasion of RI (Haigis *et al.*, 2003). We unified the impact of these two parameters with the equation:

$$\left(k_{cat}/K_M\right)_{cyto} = \frac{k_{cat}/K_M}{1 + [RI]/K_d} \qquad (2.4)$$

In eq 2.4, the parameter $\left(k_{cat}/K_M\right)_{cyto}$ reports on the activity of a ribonuclease in the cytosol , which contains RI at an invariant concentration of ~4 μM (Nadano *et al.*, 1994; Blázquez *et al.*, 1996; Leland *et al.*, 1998; Haigis *et al.*, 2003). Although eq 2.4 does not take into account important properties such as cationic charge and conformational stability, we and others have found that eq 2.4 is a useful forecaster of ribonuclease

cytotoxicity (Raines, 1999; Bretscher *et al.*, 2000; Futami *et al.*, 2002; Haigis *et al.*, 2002; Dickson *et al.*, 2003).

In general, the cytotoxic activities of the RNase A variants in Table 2.2 correlate well with their $(k_{cat}/K_M)_{cyto}$ values. One exception to the predictive ability of eq 2.4 is R39D/G88R RNase A. With a $(k_{cat}/K_M)_{cyto}$ value of 2.6×10^6, we expected this variant to be more toxic to K-562 cells than was observed herein. Molecular charge is likely responsible for the anomaly. Replacing Arg39 with an aspartate residue not only decreases catalytic activity by 10-fold, but also reduces the net charge by two. The lower charge could diminish endocytosis of the protein and thus account for its lowered cytotoxicity, as has been observed for other ribonuclease variants (Futami *et al.*, 2001; Futami *et al.*, 2002; Ilinskaya *et al.*, 2002; Makarov and Ilinskaya, 2003).

The relationship between IC_{50} and $(k_{cat}/K_M)_{cyto}$ is depicted in Figure 2.4. The value of $(k_{cat}/K_M)_{cyto}$ is constrained by eq 2.4 to be less than $k_{cat}/K_M = 5 \times 10^7 \ M^{-1}s^{-1}$, which refers to the ribonucleolytic activity of wild-type RNase A. The vertical dashed line in Figure 2.4 depicts this uppermost value. The horizontal dotted line reflects what appears to be the lowest IC_{50} value that could be achieved by improving RI evasion alone. The variants in the upper left quadrant of the plot show a distinct decrease in IC_{50} value with increasing $(k_{cat}/K_M)_{cyto}$ value. The only outlier to this trend is R39D/G88R, which has a lower molecular charge (*vide supra*). As the $(k_{cat}/K_M)_{cyto}$ value reaches $\sim 5 \times 10^6 \ M^{-1}s^{-1}$, the trend levels off with little further increases in cytotoxicity. Thus, we believe we have exhausted the improvements in cytotoxicity that can be achieved via RI evasion alone. A

further reduction in IC_{50} value is likely to be achievable, but only by altering other features of the pathway leading to cell death.

2.5.4 Utility of the FADE Algorithm

We used the FADE algorithm to identify quickly and objectively RNase A residues within the pRI·RNase A complex that exhibit a high degree of shape complementarity. Several of the residues identified by the FADE algorithm were previously shown experimentally to contribute a significant amount of binding energy to the pRI·RNase A complex (Neumann and Hofsteenge, 1994; Chen and Shapiro, 1997) or to be excellent targets for disruption by mutagenesis (Leland *et al.*, 1998; Haigis *et al.*, 2002). The success of the FADE algorithm in predicting the importance of these regions gave credence to its utility and justified our subsequent analysis of additional RNase A residues identified by FADE. Although a similar list of residues could have been identified by careful examination of the three-dimensional structure, the evident advantage of FADE is the extreme speed at which it identifies regions of high complementarity. Additionally, the computational algorithm is objective, eliminating possible human error or bias.

2.5.5 Therapeutic Index

An important characteristic of any drug is its therapeutic index, which is the ratio of its toxic dose to its effective dose. In humans, ONC exhibits a highly favorable therapeutic index as a cancer chemotherapeutic, enabling its progress to Phase III clinical

trials (Mikulski *et al.*, 2002). Mammalian ribonucleases could exhibit an even greater therapeutic index than does ONC. For example, the Hep-3B liver carcinoma cell line is the most vulnerable to all of the ribonucleases tested herein (Table 2.3). ONC has a therapeutic index (TI), here defined as $IC_{50}^{NmuMG}/IC_{50}^{Hep-3B}$, of 31. In contrast, the D38R/R39D/N67R/G88R, D38R/R39D/G88R, and G88R variants of RNase A have TI values of >323, >500, and >118, respectively. A biochemical explanation for the therapeutic index of ribonucleases (amphibian or mammalian) awaits further experimentation.

2.6 Conclusions

Based on the results presented herein, we conclude that the FADE algorithm is an effective tool for identifying residues at the interface of a protein–protein complex that can be altered to disrupt the complex. Such alterations to RNase A reduce its affinity for RI, and thus increase its cytotoxicity. Some of these variants of RNase A are more toxic to cancer cells than is its amphibian homolog ONC, and thus represent a landmark on the path to the development of chemotherapeutics based on mammalian ribonucleases.

Research Fellowship, University Bookstore Academic Excellence Award, and Trewartha Senior Thesis Grant. The University of Wisconsin–Madison Biophysics Instrumentation Facility was established with Grants BIR-9512577 (NSF) and RR13790 (NIH). The Keck–UWCCC Small Molecule Screening Facility was established with grants from the W.M. Keck Foundation and University of Wisconsin Comprehensive Cancer Center.

Table 2.1 Residues of highest shape complementarity in the pRI·RNase A complex (PDB code: 1dfj) as identified with the FADE algorithm

Chain	Residue	Cluster size[a]
RNase A	Lys7	2
	Asn24	5
	Gln28	3
	Lys31	2
	Arg39	31
	Asn67	6
	Gly88	5
	Ser89	14
	Lys91	9
RI	Tyr430	22
	Asp431	10
	Tyr433	38

[a] Number of FADE complementarity markers within 2 Å of an atom in the indicated residue.

Table 2.2 Biochemical parameters and cytotoxic activities of RNase A, its variants, and ONC

Ribonuclease	T_m^a (°C)	k_{cat}/K_M^b (10⁶ M⁻¹s⁻¹)	K_d (pRI)^c (nM)	$\Delta\Delta G^d$ (pRI) (kcal/mol)	K_d^e (hRI) (nM)	$(k_{cat}/K_M)_{cyto}^f$ (10⁶ M⁻¹s⁻¹)	IC_{50}^g (μM)
wild-type RNase A	64	52 ± 4	67 × 10⁻⁶ ᵸ	–	ND	–	>25
D38R/R39D RNase A	60	18 ± 3	0.30 ± 0.01	5.0	–	–	>25
N67R RNase A	57	73 ± 19	0.36 ± 0.01	5.1	ND	–	>25
K7A/D38R/R39D RNase A	62	1.6 ± 0.1	3.5	6.4	ND	–	17 ± 5
N24R/G88R RNase A	60	78 ± 5	0.27	4.9	ND	–	8.4 ± 0.7
G88R RNase A	60 ⁱ	74 ± 4	0.57 ± 0.05 ʲ	5.3	7.8 ᵏ	–	4.6 ± 0.4
K31A/G88R RNase A	ND	52 ± 2	ND	ND	58 ± 6	0.74	1.5 ± 0.2
K7A/G88R RNase A	62 ˡ	5.3 ± 0.4	17 ± 1	7.4	510 ± 20	0.60	1.1 ± 0.1
R39D/G88R RNase A	61	4.3 ± 1	ND	ND	(6.4 ± 0.3) × 10³	2.6	0.69 ± 0.07
N67R/G88R RNase A	58	92 ± 4	45 ± 2	8.0	44 ± 7	1.0	0.51 ± 0.05
K7A/D38R/R39D/G88R RNase A	60	1.6 ± 0.2	120 ± 10	8.5	(27 ± 3) × 10³	1.4	0.41 ± 0.05
ONC	90 ᵐ	0.22 ± 0.01	≥10³	–	≥10³	–	0.27 ± 0.02
D38R/R39D/G88R RNase A	60	31 ± 3	8.0 ± 0.4	6.9	670 ± 40	4.4	0.22 ± 0.04
K31A/D38R/R39D/N67R/G88R RNase A	54	48 ± 7	ND	–	(19 ± 1) × 10³	40	0.21 ± 0.06
D38R/R39D/N67R/G88R RNase A	56	38 ± 6	(1.4 ± 0.1) × 10³	10.0	(3.4 ± 0.1) × 10³	17	0.19 ± 0.02

ND, not determined.

^{a} Values of T_m (± 2 °C) for RNase A and its variants were determined in PBS by UV spectroscopy.

^{b} Values of k_{cat}/K_M (± SE) for RNase A and its variants are for catalysis of 6-FAM–dArU(dA)₂–6-TAMRA cleavage at (23 ± 2) °C in 0.10 M MES–NaOH buffer (OVS-free) at pH 6.0, containing NaCl (0.10 M). The value of k_{cat}/K_M (± SE) for ONC is for catalysis of 6-FAM–dArUdGdA–6-TAMRA cleavage at (23 ± 2) °C in 0.020 M MES–NaOH buffer (OVS-free) at pH 6.0, containing NaCl (0.010 M).

^{c} Values of K_d (± SE) are for the complex with pRI at (23 ± 2) °C. The K_d value for ONC is an estimate from (Wu et al., 1993).

^{d} Values of $\Delta\Delta G$ were calculated with the equation: $\Delta\Delta G = -RT\ln(K_d^{wild-type}/K_d^{variant})$.

^{e} Values of K_d (± SE) are for the complex with hRI at (23 ± 2) °C.

^{f} Values of $(k_{cat}/K_M)_{cyto}$ were calculated with eq 2.1 and values of K_d for the complex with hRI.

^{g} Values of IC₅₀(±SE) are for incorporation of [methyl-³H]thymidine into the DNA of ribonuclease-treated K-562 cells, and were calculated with eq 2.3.

^{h} From (Vicentini et al., 1990); ^{i} From (Leland et al., 1998); ^{j} From (Abel et al., 2002).

^{k} For fluorescein-labeled G88R RNase A; ^{l} From (Haigis et al., 2002).

^{m} From (Leland et al., 1998) and determined by circular dichroism spectroscopy.

Table 2.3 IC$_{50}$ values of RNase A, its variants, and ONC for ten cell lines

Cell line	Description	Doubling time (h)	IC$_{50}$ (μM)[a]				
			wild-type	DRNG[b]	DRG[b]	G88R	ONC
HCT-116	colon carcinoma	17.4	4.7	0.49	1.4	10.4	0.14
NCI-H460	lung carcinoma	17.8	39	0.71	0.60	11.0	0.13
A549	lung adenocarcinoma	22.9	15.5	4.8	13.7	27.0	0.15
MCF-7	breast adenocarcinoma	25.4	21.7	0.27	0.42	4.4	0.086
Du145	prostate carcinoma	32.3	5.5	0.085	0.45	2.0	0.11
SF-268	CNS glioblastoma	33.1	3.8	0.18	0.64	4.6	0.088
NCI/ADR-RES	breast adenocarcinoma	34.0	19	1.00	2.3	5.8	0.06
SK-OV-3	ovary adenocarcinoma	48.7	3.2	0.76	1.5	2.8	0.13
Hep-3B	liver carcinoma	ND	2.8	0.031	0.040	0.34	0.051
NmuMG	mammary normal epithelial (mouse)	ND	>40	>10	>20	>40	1.6

[a] Values of IC$_{50}$ are for the conversion of calcein AM to calcein in cells exposed to a ribonuclease, and were calculated with eq 2.3.
[b] DRNG and DRG refer to the D38R/R39D/N67R/G88R and D38R/R39D/G88R variants of RNase A, respectively.

Table 2.4 Mass analysis of RNase A, its variants, and ONC

Ribonuclease	m/z [a] (Da) expected	observed
wild-type RNase A	13,682	13,682
D38R/R39D RNase A	13,682	13,692
N67R RNase A	13,724	13,711
K7A/D38R/R39D RNase A	13,625	13,630
N24R/G88R RNase A	13,824	13,833
G88R RNase A	13,781	13,785
K31A/G88R RNase A	13,724	13,723
K7A/G88R RNase A	13,724	13,726
R39D/G88R RNase A	13,740	13,741
N67R/G88R RNase A	13,824	13,829
K7A/D38R/R39D/G88R RNase A	13,724	13,735
ONC	11,820	11,825
D38R/R39D/G88R RNase A	13,781	13,793
K31A/D38R/R39D/N67R/G88R RNase A	13,766	13,765
D38R/R39D/N67R/G88R RNase A	13,824	13,825

[a] Values of m/z were determined by MALDI–TOF mass spectrometry.

Figure 2.1   pRI·RNase A complex with FADE-identified shape-complementarity

markers. Ribbon diagrams of pRI (green) and RNase A (blue) are shown

along with their molecular surfaces. Complementarity markers identified

by the FADE algorithm are represented as spheres colored on a

temperature scale based on the degree of local complementarity. Red

markers indicate the regions with optimal shape complementarity, and

orange and yellow markers indicate regions in which the geometric match

is significant, but to a lesser extent. FADE calculations and modeling were

performed using the atomic coordinates from PDB entry 1dfj (Kobe and

Deisenhofer, 1995b). The conventional view of the pRI·RNase A complex

is shown in panel (**A**), and is rotated 90° into the plane of the page in panel

(**B**). Images were created with the program PyMOL (DeLano Scientific,

South San Francisco, CA).

A

B
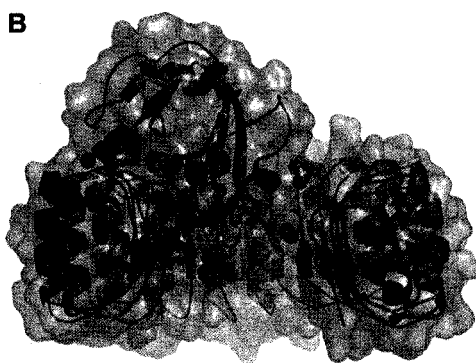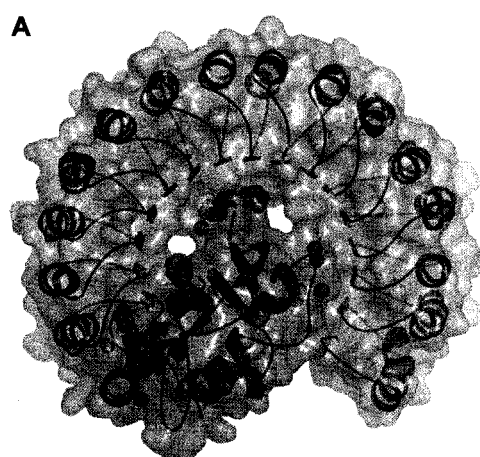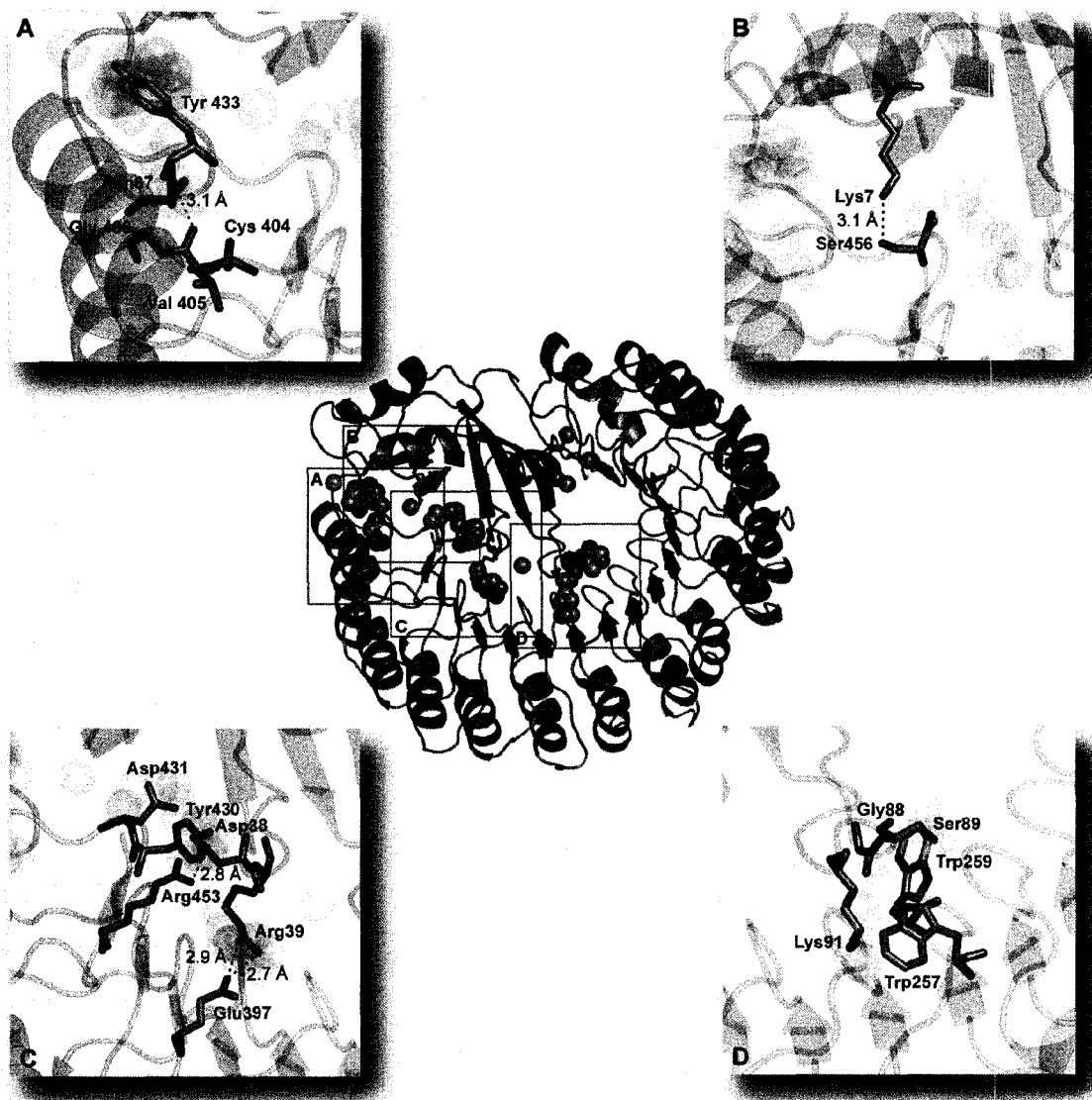
Figure 2.2   Regions of the pRI·RNase A interface targeted for disruption. Depictions

were created as in Figure 2.1. The side chains of residues proximal to

shape-complementarity clusters (Table 2.1) are shown as sticks in the

color of their protein. Interface regions of interest are shown in greater

detail in panels (**A–D**), along with relevant interprotein hydrogen bonds.

Figure 2.3   Effect of ribonucleases on the proliferation of K-562 cells. The

incorporation of [$methyl$-^{3}H]thymidine into cellular DNA was used to

monitor the proliferation of K-562 cells in the presence of ribonucleases.

Data points indicate the mean (± SE) of at least three separate experiments

carried out in triplicate. In each panel, data for wild-type RNase A, G88R

RNase A, and ONC, are shown as open symbols with curves fitted as

dashed lines. (A) Effect of the D38R/R39D swap. (B) Effect of the K7A

substitution. (C) Effect of additional FADE-inspired substitutions in the

context of G88R, including N24R, K31A, and N67R. (D) Compilation of

data for variants with cytotoxicity greater than that of ONC.
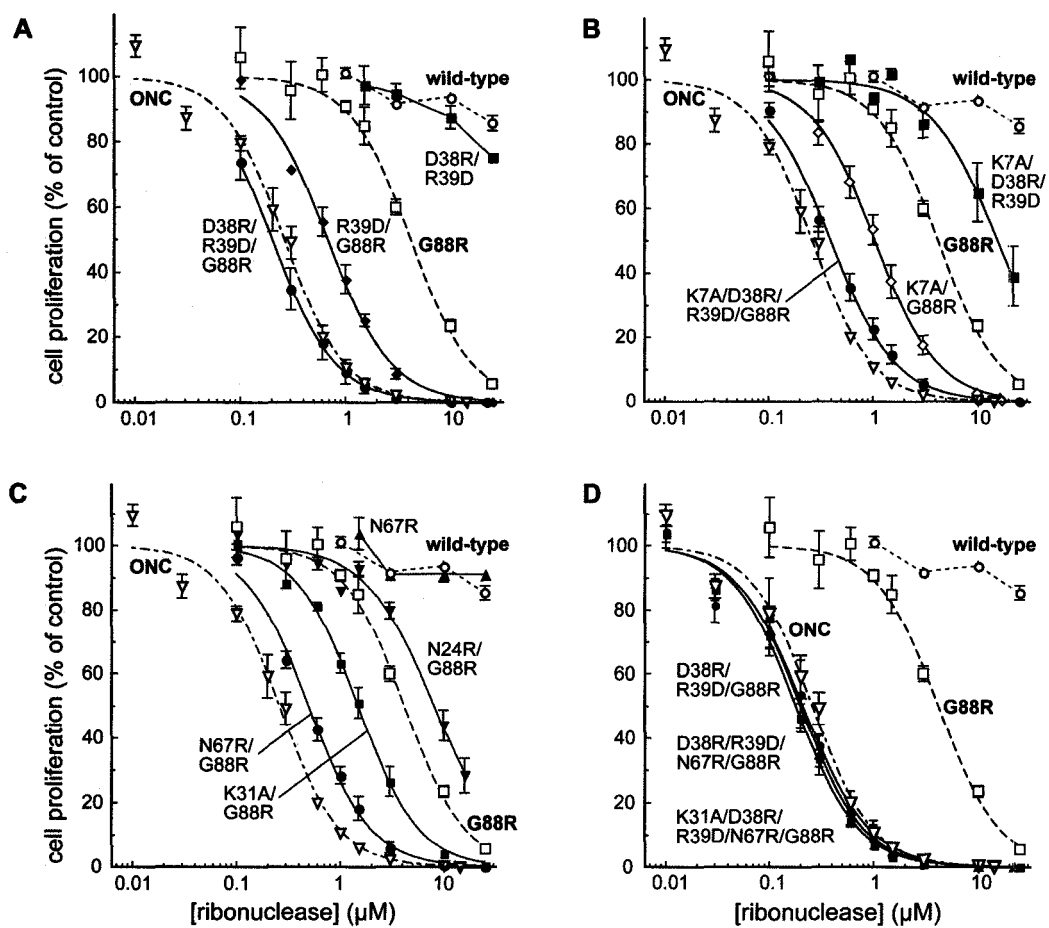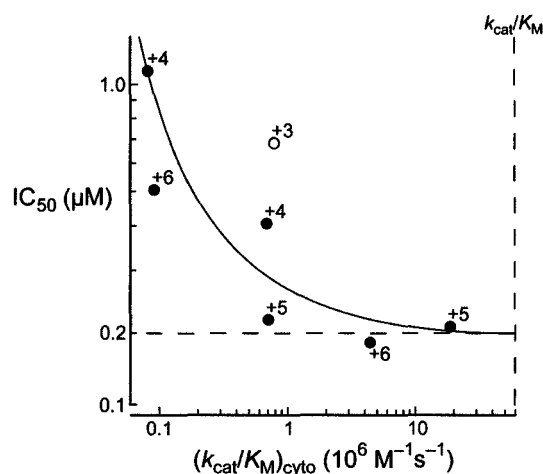
Figure 2.4 Relationship of $(k_{cat}/K_M)_{cyto}$ and cytotoxicity. IC_{50} values of RNase A

variants for K-562 cells are plotted against their $(k_{cat}/K_M)_{cyto}$ values

(Table 2.2). Each point represents an individual RNase A variant. Both

axes have a log scale. Dashed line at 0.2 μM indicates the apparent upper

limit of the cytotoxicity attainable against this cell line by enhancing RI

evasion.

CHAPTER 3

Cytotoxic Dimers and Trimers of Mammalian Ribonucleases Generated via Site-Specific Chemical Tethering

Contribution: Protein purification, chemical conjugation, characterization, in vitro analysis, preparation of ribonucleases and ribonuclease conjugates for animal studies, composition of the manuscript, and preparation of figure drafts. Animal studies were designed by J. A. Kink and L. E. Strong and executed by J. A. Kink. Synthesis of N,N',N''-(1,3,5-phenylene)trimaleimide (PTM) was performed by C. I. Schilling under the supervision of L. D. Lavis.

3.1 Abstract

Noncovalent multimeric aggregates or covalent conjugates of pancreatic-type ribonucleases exhibit biochemical activities that are directly attributable to their quaternary structure. Examples of these ribonuclease multimers include bovine seminal ribonuclease (which is a dimer), aggregates of RNase A formed upon lyophilization from acetic acid solutions, and ribonuclease conjugates that have been cross-linked by chemical reagents. Site-specific chemical tethering is a particularly desirable means for generating multimeric ribonucleases because this method yields a homogeneous product, eliminates the risk of active-site residue modification, and provides precise control of the spatial linkage of the constituent monomers. Here, variants of mammalian ribonucleases, engineered to possess a solvent-exposed, free thiol group, are coupled using eight different di- and tri-functional sulfhydryl-reactive cross-linking reagents to produce dimeric and trimeric ribonuclease conjugates with varying degrees of freedom between the constituent monomers. Both the site of conjugation and the restrictiveness of tethering afforded by a particular linker are found to modulate sensitivity to the ribonuclease inhibitor protein (RI), and therefore cytotoxicity. Additionally, multimerization increases both the net charge and effective radius of the ribonuclease conjugates relative to monomers, which have opposite effects on the amount of ribonucleolytic activity delivered to the cytosol. Finally, trimeric ribonuclease conjugates are shown to inhibit tumor growth in mice bearing solid human tumors both at a lower dose and with a less frequent administration schedule than cytotoxic monomers. This observation, which is

attributable to an enhanced persistence of the trimers in circulation, suggests a means to maximize the clinical efficacy of ribonucleases.

3.2 Introduction

Bovine seminal ribonuclease (BS-RNase) and several amphibian ribonucleases, including Onconase® (ONC), exhibit innate antitumoral activity (Leland and Raines, 2001). In fact, ONC is currently in Phase IIIb confirmatory trials for the treatment of malignant mesothelioma (Pavlakis and Vogelzang, 2006), and was designated an orphan-drug by the U.S. Food and Drug Administration in January 2007. The key commonality between these two homologues of bovine pancreatic ribonuclease (RNase A), which differ dramatically in both primary (Ardelt et al., 1991) and quaternary structure (Mosimann et al., 1994), is their ability to evade the potent inhibition of the cytosolic ribonuclease inhibitor protein (RI), thus endowing them with cytotoxicity (Murthy and Sirdeshmukh, 1992; D'Alessio et al., 1997; Saxena et al., 2003). The ability to retain ribonucleolytic activity in the presence of RI is a primary determinant of the cytotoxicity of ONC, BS-RNase, and other engineered ribonucleases (Rutkoski et al., 2005). The divergent tertiary structure of ONC, which possesses severely truncated surface loops compared to those of RNase A, is responsible for its extremely low affinity for RI (Boix et al., 1996), whereas the dimeric nature of BS-RNase is responsible for its ability to evade RI by sterically precluding RI-binding (Murthy and Sirdeshmukh, 1992).

The constituent RI-sensitive monomers of the BS-RNase homodimer are linked covalently through two intermolecular disulfide bonds at Cys31 and Cys32. Additionally,

at equilibrium, two-thirds of the BS-RNase dimers are further stabilized by the swapping of N-terminal domains ("M×M"). This additional degree of quaternary association affords greater protection against dissociation upon internalization into the reducing environment of the cytosol as compared to the non-domain swapped form ("M=M") (Piccoli et al., 1992; Kim et al., 1995b). The insensitivity of dimeric BS-RNase to inhibition by RI allows it to exert unique biological effects, including toxicity towards tumor cells as well as aspermatogenic, embryotoxic, and immunosuppressive activities (Vescia et al., 1980; Murthy et al., 1996).

The naturally dimeric nature of BS-RNase is unique among the members of the RNase A superfamily. Prior to the discovery and characterization of BS-RNase (D'Alessio et al., 1972b), however, it was reported that lyophilization of solutions of RNase A in 50% (v/v) acetic acid yielded dimers and higher order oligomers of RNase A (Crestfield et al., 1962). These oligomers of RNase A—as large as nonameric species have been reported (Gotte et al., 2006)—were formed as a result of the three-dimensional domain swapping of either the N- and/or C-termini to yield catalytically active composite active sites (Libonati and Gotte, 2004). Unlike naturally monomeric RNase A, which lacks any biological activities other than its prodigious ribonucleolytic activity which presumably serves a digestive function in the ruminant gut (Barnard, 1969), these oligomers demonstrated antitumoral activity as well as a dramatically enhanced ribonucleolytic activity against double-stranded RNA (dsRNA). Both of these properties, which are a result of their higher order quaternary structure, are concomitant with their degree of oligomerization: tetramers > trimers > dimers (Libonati, 2004).

Subsequent to the discovery of the antitumoral activity of BS-RNase, a variety of creative strategies were applied toward mimicking the dimeric nature of BS-RNase in order to recapitulate some of its unique biological activities (See Section 1.6.2 and Table 1.6). For example, interest grew in generating chemically-linked dimers of RNase A in an attempt to reproduce these activities by semisynthesis (Hartman and Wold, 1967; Wang et al., 1976). In contrast to BS-RNase or the noncovalent, domain-swapped oligomers of RNase A, dimers produced by chemical coupling are not able to dissociate under biologically relevant conditions (Wang et al., 1976). Dimers of RNase A that were cross-linked using bifunctional amine-reactive imido esters, inhibited tumor cell proliferation in vitro (Bartholeyns and Baudhuin, 1976), exhibited antitumoral activity in mice (Tarnowski et al., 1976; Bartholeyns and Zenebergh, 1979), possessed both a newly acquired enzymatic activity against dsRNA, and had an enhanced persistence in the circulation of rats (Bartholeyns and Moore, 1974). Interestingly, it was observed that chemically-dimerized RNase A exhibited selectivity to tumor cells over normal fibroblast cell lines (Bartholeyns and Baudhuin, 1976; Bartholeyns and Zenebergh, 1979)—an important property for a cancer therapeutic. More recently, cross-linked trimers of RNase A generated with a dimethyl suberimidate linker displayed higher cytotoxic activity against a cervical carcinoma cell line than did cross-linked dimers of RNase A. The cross-linked trimers also possessed enhanced activity against dsRNA, compared to that of cross-linked dimers (Gotte et al., 1997), conforming to the trend observed with the noncovalent domain-swapped oligomers of RNase A discussed above.

A disadvantage of utilizing amine-reactive linkers such as dimethyl suberimidate for chemically cross-linking RNase A, however, is the resultant heterogeneous mixture of products due to the presence of 11 free amino groups in RNase A. This heterogeneous mixture of products confounds biochemical characterization of the conjugates, making this methodology undesirable for the development of human therapeutics. Furthermore, modification of active site amines, such as Lys41 in RNase A, can reduce catalytic efficiency by up to 10^5-fold (Messmore et al., 1995).

In our group, bBBr **3.8** (Figure 3.1) had been used to prepare site-specifically cross-linked dimers of C31S BS-RNase that were inert to dissociation in the highly reducing environment of the mammalian cytosol (Kim and Raines, 1995). We did not, however, determine either the affinity for RI or toxicity toward tumor cell lines. Youle and coworkers generated homogeneous homodimeric conjugates of both human pancreatic ribonuclease (RNase 1) and eosinophil-derived neurotoxin (EDN; RNase 2) by introducing a cysteine residue via site-directed mutagenesis and reacting its thiol with 1,6-bis(maleimido)hexane (BMH; **3.1**; Figure 3.1) to generate a thioether (Suzuki et al., 1999). These cysteine residues were introduced at positions that were predicted to be the most disruptive to RI-binding. This site-specific tethering resulted in covalently-linked, non-reducible, dimeric conjugates that were up to four orders of magnitude less sensitive to inhibition by RI, and effectively transformed these two non-toxic, RI-sensitive, monomeric ribonucleases into cytotoxic dimers (Suzuki et al., 1999).

The thiol-reactive linker used by Youle and coworkers was, however, relatively long and flexible, containing 12 atoms and 9 rotatable bonds between the sulfur atoms of the

two engineered cysteine residues. We reasoned that superior RI-evasion, and thus superior cytotoxicity, could be achieved by utilizing linkers that installed few atoms and/or rotatable bonds between the ribonucleases, thus introducing fewer degrees of freedom between the ribonuclease moieties. Additionally, inspired by the increased cytotoxicity of both non-specifically cross-linked trimers of RNase A (Gotte *et al.*, 1997) and noncovalent, domain-swapped trimers of RNase A (Libonati, 2004), we set out to produce, what is to our knowledge, the first example of site-specifically tethered trimers of mammalian ribonucleases. This goal was achieved using both a commercially available homotrifunctional, thiol-reactive linker, tris(2-maleimidoethyl)amine (TMEA; **3.7**; Figure 3.1), as well as a novel linker, *N,N',N''*-(1,3,5-phenylene)trimaleimide (PTM; **3.6**; Figure 3.1). Here, we describe the synthesis and biochemical characterization of these conjugates. We show both the choice of coupling reagent as well the site of attachment are important considerations for the production of site-specific, restrictively-tethered, dimeric and trimeric ribonuclease conjugates that are cytotoxic both in vitro and in vivo.

3.3 Experimental Procedures

3.3.1 Materials

Protein expression, purification and characterization. *E. coli* BL21(DE3) cells, pET22b(+) and pET27b(+) plasmids were from Novagen (Madison, WI). K-562 (derived from a continuous human chronic myelogenous leukemia line), DU 145 (human prostate carcinoma), and A549 (human non-small cell lung carcinoma) cells were obtained from

the American Type Culture Collection (ATCC; Manassas, VA). Cell culture medium,

Dulbecco's phosphate-buffered saline (DPBS), antibiotics, trypsin, and fetal bovine

serum (FBS) were from Invitrogen (Carlsbad, CA). RPMI 1640 medium was also

obtained from Mediatech (Herndon, VA). [$methyl$-^{3}H]Thymidine (6.7 Ci/mmol) was

from PerkinElmer (Boston, MA). CellTiter-Blue cell viability assay was from Promega

(Madison, WI). Oligonucleotides for site-directed mutagenesis and sequencing, as well as

the ribonuclease substrates, and 6-FAM–dArUdGdA–6-TAMRA, were from Integrated

DNA Technologies (Coralville, IA). 1,6-Bis(maleimido)hexane (BMH; **3.1**; Figure 3.1),

1,2-bis(maleimido)ethane (BMOE; **3.2**; Figure 3.1), tris(2-maleimidoethyl)amine

(TMEA; **3.7**; Figure 3.1), N-ethylmaleimide, and BCA protein assay kit were from Pierce

(Rockford, IL). Dibromobimane (bBBr; **3.8**; Figure 3.1) was from Molecular Probes Inc.

(Eugene, OR). N,N'-(1,2-phenylene)dimaleimide (o-PDM; **3.3**; Figure 3.1),

N,N'-(1,3-phenylene)dimaleimide (m-PDM; **3.4**; Figure 3.1), and

N,N'-(1,4-phenylene)dimaleimide (p-PDM; **3.5**; Figure 3.1) were from Aldrich Chemical

(Milwaukee, WI). FPLC HiLoad 26/60 Superdex G75 and G200 gel-filtration columns,

HiTrap Desalting, SP, and Q columns were from GE Healthcare (Uppsala, Sweden).

Gel-filtration standards, SDS–PAGE molecular-weight standards, and pre-cast gels for

poly(acrylamide) gel electrophoresis were from BioRad (Hercules, CA). Flat-bottom,

black polystyrene (PS), Costar assay plates (96-well) with non-binding surface (NBS)

were from Corning Life Sciences (Acton, MA). Molecular biology-grade bovine serum

albumin (BSA) was obtained as a 20 mg/mL solution from Sigma Chemical (St. Louis,

MO). Fluorometric enzymatic activity measurements were made using 4.5-mL

methacrylate cuvettes from VWR (West Chester, PA). All other chemicals used were of commercial reagent grade or better, and were used without further purification.

Terrific Broth (TB) contained (in 1.00 L) tryptone (12 g), yeast extract (24 g), glycerol (4 mL), KH_2PO_4 (2.31 g), and K_2HPO_4 (12.54 g). Phosphate-buffered saline (PBS) used for dialysis of purified proteins and conjugates contained (in 1.00 L) NaCl (8.0 g), KCl (2.0 g), $Na_2HPO_4 \cdot 7H_2O$ (1.15 g), KH_2PO_4 (2.0 g), and NaN_3 (0.10 g), and had pH 7.4.

Synthesis of N,N',N''-(1,3,5-phenylene)trimaleimide. Dimethylformamide (DMF), tetrahydrofuran (THF), and dichloromethane (CH_2Cl_2) were drawn from a Baker CYCLE-TAINER solvent delivery system. All other reagents were obtained from Aldrich Chemical (Milwaukee, WI) or Fisher Scientific (Hanover Park, IL) and used without further purification. 1,3,5-Triaminobenzene **3.9** (Scheme 3.1) was prepared via hydrogenation of phloroglucinol trioxime with Raney Ni as described previously (Arai *et al.*, 1981). Thin-layer chromatography was performed using aluminum-backed plates coated with silica gel containing F_{254} phosphor and visualized by UV illumination or staining with I_2, ceric ammonium molybdate, or phosphomolybdic acid. The term "high vacuum" refers to a vacuum (≤ 1 mm Hg) achieved by a mechanical belt-drive oil pump. NMR spectra were obtained with a Bruker DMX-400 Avance spectrometer at the NMR Facility at Madison (NMRFAM).

Xenograft studies. Homozygous (*nu/nu*) Balb/c (−/−) mice were obtained from Harlan Sprague Dawley (Indianapolis, IN).

3.3.2 Instrumentation

[methyl-^{3}H]Thymidine incorporation into K-562 and A549 genomic DNA was quantitated by scintillation counting using a Microbeta TriLux liquid scintillation and luminescence counter (PerkinElmer, Wellesley, MA). The molecular mass of ribonuclease variants and multimeric conjugates was confirmed by MALDI–TOF mass spectrometry using 3,5-dimethoxy-4-hydroxycinnamic acid as a matrix and a Voyager-DE-PRO Biospectrometry Workstation (Applied Biosystems, Foster City, CA) in the Biophysics Instrumentation Facility (BIF) at the University of Wisconsin–Madison. Cuvette-scale fluorescence measurements were made with a QuantaMaster1 photon-counting fluorometer equipped with sample stirring (Photon Technology International, South Brunswick, NJ). Fluorescence-based activity inhibition assays, competition binding assays performed in 96-well plate format, and cell viability assays utilizing CellTiter-Blue were read with an EnVison 2100 Plate Reader (Perkin–Elmer, Waltham, MA) in the Keck Center for Chemical Genomics at the University of Wisconsin–Madison. Thermal denaturation data were acquired using a Cary 400 Bio double-beam spectrophotometer equipped with a Cary temperature controller (Varian, Palo Alto, CA) in the Biophysics Instrumentation Facility at the University of Wisconsin–Madison. BCA protein quantitation was determined by measuring the absorbance at 570 nm in a 96-well plate using a Bio-Tek ELx800 plate reader (Bio-Tek Instruments, Inc., Winooski, VT). Graphs were manipulated and parameters were calculated with the programs Microsoft Excel 2003 and GraphPad Prism 4.

3.3.3 Synthesis of N,N',N''-(1,3,5-phenylene)trimaleimide **3.6**

Maleic anhydride (271 mg, 2.76 mmol) was dissolved in DMF (0.6 mL) under Ar(g).

1,3,5-Triaminobenzene (**3.9**, 98 mg, 0.78 mmol) in DMF (0.5 mL) was added dropwise,

giving rise to a white precipitate. A catalytic amount of $Co(OAc)_2$, triethylamine (40 µL,

0.29 mmol), and acetic anhydride (0.7 mL, 7.41 mmol) were added, and the resulting

brown solution was stirred for 20 h at 50 °C, protected from light. The reaction mixture

was poured into ice water, and the resulting dark brown precipitate was collected by

filtration. The solid was washed with water and Et_2O, and dried under high vacuum.

Compound **3.6** was isolated as a dark brown powder and used without further purification

(286 mg, 98% yield). ^{1}H NMR (400 MHz, DMSO-d_6) δ (ppm): 7.43 (s, 3H), 7.21 (s, 6H).

^{13}C NMR (100 MHz, DMSO-d_6) δ (ppm): 169.50, 134.82, 132.26, 124.12.

3.3.4 Production of Ribonucleases and Ribonuclease Inhibitor

cDNA encoding ribonuclease variants was generated by Quickchange site-directed

mutagenesis (Stratagene, La Jolla, CA) using plasmid pSR1 (BS-RNase) (Kim and

Raines, 1993), pONC (ONC) (Leland et al., 1998), pHP-RNase (RNase 1) (Leland et al.,

2001), pBXR (RNase A) (delCardayré et al., 1995), or pET27b(+) containing cDNA

encoding D38R/R39D/N67R/G88R RNase A (Rutkoski et al., 2005). The plasmid

containing cDNA for RNase 1 (pHP-RNase) was modified to include the codon for the

C-terminal threonine residue (Thr128), which establishes the native full-length protein

(Seno et al., 1994). Wild-type RNase A, RNase 1, ONC, and G88R RNase A were

produced as described previously (delCardayré et al., 1995; Leland et al., 1998; Leland et

al., 2001). Free cysteine-containing variants of RNase A (A19C, G88C, and

D38R/R39D/N67R/G88C), ONC (S72C), BS-RNase (C31A/C32A/G88C), and RNase 1

(G89C) were prepared in a similar fashion, but with several alterations. The protein

solution containing dissolved inclusion bodies was diluted by 10-fold with a thoroughly

degassed acetic acid solution (20 mM), subjected to centrifugation to remove precipitate,

and dialyzed overnight against aqueous acetic acid (20 mM) that had been purged with

$N_2(g)$ or Ar(g). Ribonucleases were allowed to refold for ≥ 3 days at 4 °C following slow

dilution into 0.10 M Tris–HCl buffer at pH 8.0, containing NaCl (0.10 M), L-arginine

(0.5 M), EDTA (10 mM), reduced glutathione (GSH; 1.0 mM), and oxidized glutathione

(GSSG; 0.2 mM). For free-cysteine containing variants of RNase 1, the concentrations of

GSH and GSSG used were 3.0 mM and 0.6 mM, respectively. The refolding solution was

purged with $N_2(g)$ or Ar(g) prior to the addition of denatured protein to prevent the

oxidation of the engineered free cysteines. Following purification by gel-filtration, the

free thiol groups of the engineered, unpaired cysteine residues were protected from

inadvertent air oxidation with 5,5'-dithiobis(2-nitrobenzoic acid) (DTNB) as described

previously (Messmore *et al.*, 1995). Finally, the TNB-protected ribonucleases were

applied to a HiTrap SP cation-exchange column, eluted with a linear gradient of NaCl

(0.15–0.40 M) in 50 mM NaOAc buffer at pH 5.0, and stored at 4 °C until subsequent

modification with sulfhydryl-reactive compounds. Protein concentration (excluding

TNB-protected ribonucleases) was determined either by BCA assay (Smith *et al.*, 1985)

or by UV spectroscopy using an extinction coefficient of $\varepsilon_{278} = 0.72$ mg·ml^{-1}cm^{-1} for

RNase A and its variants (Sela *et al.*, 1957), $\varepsilon_{278} = 0.465$ mg·ml^{-1}cm^{-1} for

C31A/C32A/G88C BS-RNase (D'Alessio *et al.*, 1972a), $\varepsilon_{280} = 0.53$ mg·ml^{-1}cm^{-1} for

RNase 1 and its variants (Leland *et al.*, 2001), and $\varepsilon_{280} = 0.87$ mg·ml^{-1}cm^{-1} for ONC and

its variants (Leland *et al.*, 1998).

hRI was produced and purified as described previously (Rutkoski *et al.*, 2005; Smith,

2006) and stored in PBS containing DTT (10 mM). Freshly prepared hRI was assumed to

be 100% active (*i.e.*, fully reduced) for up to one month following purification and was

not used beyond this time without re-purification.

Following purification, ribonucleases and ribonuclease inhibitor proteins migrated as

single bands during SDS–PAGE, confirming their purity and apparent molecular weight.

In addition, the identity and integrity of purified ribonuclease variants was confirmed by

MADLI–TOF mass spectrometry.

3.3.5 Semisynthesis of Ribonuclease Dimers and Trimers

The pH of the protein solution containing TNB-protected ribonucleases in the HiTrap

SP elution buffer was adjusted from 5.0 to ~8.0 by addition of either 10% (v/v) 10× PBS

and/or 8–10% (v/v) Tris–HCl buffer (1.0 M) at pH 8.0. TNB^{2-} was released by the

addition of DTT (5–10-fold molar excess) and allowing the reaction to proceed at room

temperature for ≥ 5 min, resulting in the immediate generation of the yellow

2-nitro-5-thiobenzoate anion (TNB^{2-}) (Ellman, 1958). DTT, salt, and TNB^{2-} were

removed from the ribonucleases using a HiTrap desalting column equilibrated with PBS

containing EDTA (1 mM).

Semisynthetic dimers. Stock solutions (20–100 mM) of dibromobimane (bBBr **3.8**)

or bismaleimide-derivatized linker (BMOE **3.2**, o-PDM **3.3**, m-PDM **3.4**, or p-PDM **3.5**)

were prepared in DMF, and 0.6 molar equivalents were added to a solution containing a

deprotected ribonuclease (50–250 µM) so that the total organic content in the conjugation

reaction was <1% (v/v). The sub-stoichiometric amounts of linker were found to produce

the desired dimeric (or trimeric) conjugates in the highest yield, as reported previously

for the dimerization of C31S BS-RNase (Kim and Raines, 1995). A 0.6–5.0-fold larger

molar excess of linker favored the production of bismaleimide-derivatized monomeric

ribonuclease, and a >10-fold molar excess of linker resulted in the undesirable

nonspecific modification of the ε-amino group of lysine residues, despite maleimides

being >10^3-fold more reactive toward thiols than primary amines groups at pH 7 (Ji,

1983). Conjugation reactions were protected from light and allowed to proceed at room

temperature for 2 h or overnight at 4 °C. Reactions were terminated by the addition of

DTT (5-fold molar excess over ribonuclease). The resulting crude reaction mixture was

applied to a HiLoad 26/60 G75 Superdex gel-filtration column, and eluted with 50 mM

NaOAc buffer at pH 5.0 containing NaCl (0.10 M) and NaN_3 (0.05% w/v). Fractions

were analyzed by SDS–PAGE to distinguish monomeric and multimeric species, and

then combined to yield the final desired conjugate at ≥95% homogeneity (Figure 3.7).

Typical yields for the production of homodimers and homotrimers were 70% and 50%,

respectively. Semisynthetic variants were dialyzed exhaustively against PBS prior to

further biochemical characterization.

Semisynthetic trimers. Trimeric ribonuclease conjugates were synthesized in the same manner as described above for the dimeric conjugates, except that the trismaleimide-containing linkers in DMF were added to PBS containing ribonucleases (50–250 μM) at 0.4 molar equivalents (TMEA **3.7**) or 2.0 molar equivalents (PTM **3.6**). The larger molar excess of the linker **3.6** was required due to the presence of impurities.

3.3.6 N-Ethylmaleimide Modification of Ribonucleases

G88C RNase A and G89C RNase 1 were modified with N-ethylmaleimide (NEM) under conditions similar to those used to perform the thiol-specific semisynthesis of the dimers and trimers with the following exceptions: NEM (5-fold molar excess from a 100 mM stock in DMF) was added to the deprotected protein that had been desalted into PBS. The reaction was protected from light and allowed to proceed overnight at 4 °C. It was subsequently quenched by the addition of DTT (final concentration of 1 mM). The reaction was then diluted 10-fold with NaOAc buffer (50 mM) at pH 5.0, applied to a HiTrap SP cation-exchange column, and eluted with a linear gradient of NaCl (0–0.4 M). The masses of the resulting ribonuclease–NEM conjugates were confirmed by MALDI–TOF mass spectrometry.

3.3.7 Biochemical Characterization of Ribonuclease Dimers and Trimers

Assays of catalytic activity. The enzymatic activity of each of the ribonucleases or ribonuclease conjugates in the present study (with the exception of ONC) was determined by assaying their ability to cleave the hypersensitive fluorogenic substrate

6-FAM–dArUdAdA–6-TAMRA (20 nM) (λ_{ex} = 493 nm; λ_{em} = 515 nm) (Kelemen *et al.*,

1999). Assays were carried out at ambient temperature in DPBS (2.0 mL) containing

BSA (0.1 mg/mL) to prevent the non-specific binding of ribonuclease to the cuvette.

Values of k_{cat}/K_M were obtained with the equation:

$$k_{cat}/K_M = \left(\frac{\Delta I / \Delta t}{I_{max} - I_0}\right)\frac{1}{[E]} \tag{3.1}$$

where $\Delta I/\Delta t$ represents the initial reaction velocity generated by cleavage of the

6-FAM–dArUdAdA–6-TAMRA substrate upon addition of ribonuclease (E) to the

cuvette. I_0 and I_{max} are, respectively, the fluorescence intensities prior to enzyme addition

and following the complete cleavage of substrate by addition of excess wild-type

RNase A. Activity values for ONC and its conjugates were determined at room

temperature in DPBS (2.0 mL) containing BSA (0.1 mg/mL) using the substrate

6-FAM–dArUdGdA–6-TAMRA (50 nM) (Lee and Raines, 2003).

K_i' determinations of ribonucleases and ribonuclease conjugates. Twofold serial

dilutions of hRI (2 μM–1 pM) were prepared in 10 mM MOPS buffer at pH 7.1

containing NaCl (0.138 M), BSA (0.1 mg/mL), and DTT (5 mM) using Eppendorf

Protein LoBind tubes. These hRI-containing serial dilutions were delivered (50 μL/well)

to a 96-well plate. Ribonucleases and their conjugates were diluted in the same buffer

described above and added to the hRI-containing wells (50 μL/well; typical final working

concentration: 15 pM active site). Plates were incubated for at least 30 min at ambient

temperature prior to the addition of fluorogenic substrate (6-FAM–dArUdAdA–

6-TAMRA; final concentration: 50 nM) to initiate the assay. The plate was shaken briefly

(30 s), and the fluorescence intensity was then measured at 30-s intervals for 5 min on a plate reader using a FITC filter set (excitation at 485 nm with a 14-nm bandwidth; emission at 535 nm with a 25-nm bandwidth; dichroic mirror cutoff at 505 nm). An identical quantity of 6-FAM–dArUdAdA–6-TAMRA was cleaved with an excess amount of ribonuclease (>10 nM) and the final fluorescence was measured to ensure that over the course of the activity assays <10 % of the total substrate was degraded. Additionally, an aliquot of the untreated substrate was assayed at the end of the experiment to confirm that it had not been appreciably degraded during the course of the experiment—indicating ribonuclease contamination. Initial slope values were obtained from the data points by linear regression. Relative activities were determined by comparison to a control containing no hRI. Relative activity plots were fitted by nonlinear regression to a sigmoidal variable-slope curve using the equation:

$$y = F_B + \frac{(F_T - F_B)}{1 + 10^{(\log(K_i) - \log[hRI])h}} \tag{3.2}$$

In eq 3.2, h is the slope of the curve. Data points represent the mean of triplicate values ($\pm$ SE). F_T and F_B correspond to the maximum relative activities at both low and high concentrations of hRI, respectively.

Gel-filtration analysis. Ribonucleases and ribonuclease conjugates (1 mL of a 1 mg/mL solution in gel-filtration buffer) were applied to a HiLoad 26/60 Superdex G200 gel-filtration column and eluted with NaOAc buffer (50 mM) at pH 5.0 containing NaCl (0.10 M) and NaN$_3$ (0.05%; w/v) at a flow rate of 4 mL/min. Gel-filtration standards were prepared and separated using the same column according to the guidelines of the manufacturer.

Measurements of conformational stability. The conformational stability of several of the dimers and trimers of RNase A was determined by T_m measurement. Protein was dialyzed exhaustively against DPBS, and diluted to a concentration of ~25 μM in DPBS. Assays were performed by slow incremental heating (0.15 °C/min from 25–80 °C), and monitoring of the absorbance at 287 nm, which decreases as RNase A is denatured (Hermans and Scheraga, 1961; Eberhardt *et al.*, 1996). Data were collected and analyzed with the program THERMAL from Varian Analytical Instruments (Walnut Creek, CA), which fits the data to a two-state process, and enables the determination of the value of T_m (Pace *et al.*, 1998)—the temperature at the midpoint of the transition between the folded and unfolded states.

Assays of ribonuclease inhibitor binding. The affinity of ribonucleases and ribonuclease conjugates for hRI was determined by using a fluorescence-based competition assay, as described previously (Lavis *et al.*, 2007). For the unlabeled competing multimeric ribonuclease conjugates, the molar concentration used was that of the constituent active sites and not that of the entire conjugate.

Assays of cytotoxicity. IC_{50} values for ribonucleases and ribonuclease conjugates were determined by measuring the incorporation of [*methyl*-^{3}H]thymidine into the cellular DNA of either A549 or K-562 cells in the presence of ribonucleases, as described previously (Leland *et al.*, 1998). All cytotoxicity assays were performed at least three times in triplicate. Each data point represents the mean of three or more experimental values (± SE). The proliferation of DU 145 cells in the presence of ribonucleases was monitored by quantitating the ability of a cell culture to reduce resazurin to resorufin.

Briefly, 2,500 cells per well were incubated for 44 h in the presence of ribonucleases.

Cell proliferation relative to PBS control was determined by addition of 10 μL

CellTiter-Blue and incubation for 1 h at 37 °C after which time the plate was read on a

fluorescence plate reader (λ_{ex} = 544 nM; λ_{em} = 590 nM). IC$_{50}$ values were calculated by

fitting the curves using nonlinear regression to a sigmoidal dose–response curve with

eq 3.3. In this instance, y represents the total DNA synthesis following a 4-h

[*methyl*-^{3}H]thymidine pulse or 1 h incubation with CellTiter-Blue, and h is the slope of

the curve.

$$y = \frac{100\%}{1 + 10^{(\log(IC_{50}) - \log[\text{ribonuclease}])h}}$$ (3.3)

3.3.8 Xenograft Mouse Studies

Ribonucleases and trimeric conjugates were tested for their ability to suppress the

growth of human tumors implanted into the flanks of nude mice. The tumor cell lines

were selected for both their ability to proliferate in mice and their low rate of spontaneous

regression. Importantly, each tumor chosen represents a clinically relevant target and is

used frequently in the testing of new chemotherapeutic agents. The lines used were A549

(non-small cell lung cancer) and DU 145 (prostate cancer). The cell lines were implanted

into the right rear flank of 5–6 week old male homozygous (*nu/nu*) nude mice. Tumors

were allowed to grow to an average size of ≥75 mm^3 before treatment was initiated.

Xenograft animals of each tumor type, with the properly-sized tumors, were divided into

treatment groups. All the test compounds were diluted in PBS (drug vehicle) and, to serve

as a negative control, one set of animals was treated with vehicle alone on the dosing

schedule with greatest frequency. All treatments were administered by intraperitoneal (i.p.) injection, and the volume of drug/vehicle injected was based upon the body weight of the animal (10 μL/g). Treatment with all agents was ongoing throughout the entire experiment. Tumor size was measured twice weekly using calipers, and tumor volume (mm^3) was determined by using the formula for an ellipsoid sphere (eq 3.4):

$$\text{tumor volume} = \frac{l \times w^2}{2} \tag{3.4}$$

The percent tumor growth inhibition (% TGI) was calculated by using eq 3.5:

$$\%\text{TGI} = 1 - \left(\frac{(\text{volume}_{final} - \text{volume}_{inital})_{treated}}{(\text{volume}_{final} - \text{volume}_{inital})_{control}} \right) \times 100 \tag{3.5}$$

(G88C RNase A)$_3$–**3.7** was used to treat both A549 and DU 145 xenograft mice. A549 xenograft mice were each implanted with 4×10^6 cells that had been grown in F12K media containing 10% FBS. Treatment was administered at a dose of 25 mg/kg (i.p.; 1 × wk). DU 145 xenograft mice each received 2.89×10^6 cells that had been grown in DMEM media containing 10% v/v FBS. Treatment was administered at a dose of 25 mg/kg (i.p.; 1 × wk). A549 xenograft mice were also treated with (G89C RNase 1)$_3$–**3.7**, and each received 3.98×10^6 cells that had been grown in F12K media containing 10% v/v FBS. Treatment was administered at a dose of either 7.5 or 75 mg/kg (1 × wk).

3.4 Results

3.4.1 Design of Free Cysteine-containing Ribonuclease Variants

RNase A. For the purposes of enhancing the ability of these ribonucleases to evade the ribonuclease inhibitor, we wanted to test the hypothesis that greater evasion (and thus

greater antitumoral activity) would be observed if the residue utilized for tethering multiple ribonuclease monomers was within the RI–RNase A interface (Kobe and Deisenhofer, 1996). Position 88 on RNase A was chosen as the point of attachment within the complex interface (Figure 3.2A–B), as single amino acid substitutions at this residue have been found to be the most destabilizing to the RI·RNase A complex (Leland *et al.*, 1998; Rutkoski *et al.*, 2005). Position 19 of RNase A, on the other hand, was chosen as a representative site outside of the RI–RNase A interface (Figure 3.2A–B) because non-proteinaceous appendages, *e.g.*, fluorescein, have been attached at this location (A19C RNase A) without any detectable reduction in the affinity of the ribonuclease for RI (Kothandaraman *et al.*, 1998; Abel *et al.*, 2002).

BS-RNase. Because of the high sequence identity between BS-RNase And RNase A (83%), and the high structural similarity (Sica *et al.*, 2003) of the two proteins, amino-acid substitutions in BS-RNase analogous to those that were effective in mediating the evasion of RI in RNase A were also effective in endowing monomeric (C31A/C32A) variants with the ability to evade RI (Lee and Raines, 2005). Based on these results, we reasoned that position 88 would also be the most effective position to tether monomeric variants of BS-RNase with the aim of maximizing the ability to evade RI.

RNase 1. Although no single amino acid substitution in the β4–β5 loop of RNase 1 has been shown to be as effective as the G88R substitution in RNase A in effecting RI-evasion, the importance of this loop in mediating contacts with RI is well established (Gaur *et al.*, 2001; Leland *et al.*, 2001; Johnson *et al.*, 2007c). Furthermore, Youle and coworkers demonstrated the effectiveness of the G89C substitution for engineering

dimeric conjugates involving RNase 1 capable of evading hRI (Suzuki *et al.*, 1999). However, in the recent structure determination of RNase 1 bound by hRI, Arg91 was found to exert the greatest influence on the stability of the complex and may therefore have been an even more desirable residue through which to tether RNase 1 into dimeric and trimeric conjugates (Johnson *et al.*, 2007c).

The RI-insensitive frog ribonuclease ONC was also tethered into trimers through a residue (S72C) that is also in the β4–β5 loop (albeit truncated with respect to the mammalian homologues) and analogous to Gly88 in RNase A (Mosimann *et al.*, 1994). The ONC trimer served as a control for the effect of increased size, which could modulate internalization and effect differences in cytotoxicity independent of any gains in the ability of the constituent monomers to evade hRI. To the same end of investigating the effect of trimerization on an already RI-evasive mammalian ribonuclease, trimeric conjugates were also prepared with D38R/R39D/N67R/G88C RNase A using the TMEA linker **3.7**. Except for the fact that position 88 was used as the site of conjugation to two other RNases, this conjugate approximates a trimer of monomeric D38R/R39D/N67R/G88R RNase A, which was demonstrated previously to possess cytotoxic activity in vitro comparable to that of ONC (Rutkoski *et al.*, 2005).

3.4.2 *Conformational Stability of Ribonuclease Dimer and Trimers*

To maintain its ribonucleolytic activity and thus its biological activity, a ribonuclease must maintain its native tertiary structure (Klink and Raines, 2000). To determine whether the act of chemical tethering of ribonucleases into dimers of trimers

compromises their conformational stability, the T_m values of G88C RNase A–NEM,

(G88C RNase A)₂–3.2 and (G88C RNase A)₃–3.7 were determined and are listed in

Table 3.1. Thermal denaturation curves are shown in Figure 3.9. The dimeric and trimeric

conjugates of G88C RNase A, as well as the N-ethylmaleimide-derivatized protein

(G88C RNase A–NEM), all possessed T_m values nearly indistinguishable from that of

wild-type RNase A. Thus, multimerization did not appear to be in any way deleterious to

the conformational stability of these conjugates. Furthermore, no evidence of cooperative

unfolding was observed for dimeric or trimeric conjugates.

3.4.3 Assay of Ribonucleolytic Activity

Site-specific covalent tethering of mammalian ribonucleases had a negligible effect

on their ribonucleolytic activity per active site as can be seen from the values reported in

Table 3.1. Nearly all multimeric conjugates as well as N-ethylmaleimide-derivatized

G88C RNase A exhibited k_{cat}/K_M values (per active site) that were within error of

wild-type RNase A. Exceptions were (G88C RNase A)₂–3.1, (G88C RNase A)₂–3.8, and

trimeric conjugates of G88C RNase A prepared with either of the homotrifunctional

linkers (3.6 or 3.7), which displayed ~twofold increased activity per active site toward the

6-FAM–dArUdAdA–6-TAMRA substrate. The S72C ONC trimer, however, displayed

the largest change in activity upon trimerization. Its k_{cat}/K_M value of $0.012 \times 10^6 \, M^{-1}s^{-1}$

per active site was nearly 7-fold higher than that of wild-type ONC.

3.4.4 Affinity for Ribonuclease Inhibitor

Competition binding assay/K_d' determinations. Dimeric and trimeric ribonuclease conjugates could conceivably be bound by more than one RI molecule. Furthermore, the initial binding of one RI molecule to the conjugate is likely to influence the likelihood of subsequent binding events or preclude subsequent RI-binding entirely. Therefore, there could be multiple binding sites for RI that vary in their affinity for RI based upon the occupancy of the other sites. The fluorescence-based competition assay used here does not report on the stoichiometry of RI-binding or determine microscopic values of K_d. Apparent K_d values (K_d') were determined for the various conjugates. The K_d' values listed in Table 3.1 are based on the concentration of the constituent active sites.

The K_d value of 1.8 nM obtained for G88R RNase A was in gratifying agreement with values obtained previously (Rutkoski *et al.*, 2005; Lavis *et al.*, 2007). G88C RNase A–NEM exhibited a nearly equivalent affinity for RI, having a K_d value of 1.4 nM. Among the dimeric conjugates, (G88C RNase A)$_2$–**3.3** possessed the lowest affinity for RI, having a K_d' value of 18 nM. With the exception of (G88C RNase A)$_2$–**3.1** (K_d' = 2.6 nM), the remaining dimeric conjugates of G88C RNase A all had similar affinity for RI with K_d' = 8.2–14 nM. Compared to each other, the two trimeric conjugates of G88C RNase A displayed significantly different affinities for RI. Those prepared with the novel trimaleimide linker **3.6** were substantially more evasive than those prepared with TMEA **3.7**, with K_d' values being 39 and 17 nM, respectively. In general, after correcting for the molar concentration of ribonuclease moieties and when comparing between conjugates prepared from linkers of similar structure (*i.e.*, BMOE **3.2**

vs. TMEA **3.7**; *o*-PDM **3.3** vs. PTM **3.6**), trimeric conjugates of G88C RNase A had a

lower affinity for RI than did dimers of G88C RNase A. Trimers of A19C RNase A,

which are tethered at a position outside of the RI interface, possessed an affinity for RI

that was sufficiently high to preclude quantitation in our assay and is therefore reported

as having a K_d' value <1.4 nM. (BS-RNase)$_3$–**3.7** trimeric conjugates were the most RI-

evasive of the conjugates assayed, having a K_d' value of 84 nM.

***K$_i'$* Determinations.** A novel assay was developed to determine the stoichiometry of

RI-binding. The ability of the ribonuclease conjugates to cleave a fluorogenic substrate

following pre-incubation with varying concentrations of RI was assayed. Apparent K_i'

values were obtained by applying eq 3.2 to the data in Figure 3.3.

The apparent K_i' values of G88R and K31A/D38R/R39D/N67R/G88R RNase A were

41.4 pM and 103 nM respectively. (G88C RNase A)$_3$–**3.7** exhibited an apparent K_i' value

of 0.94 nM which was 23-fold higher than that of G88R RNase A. Furthermore, near

physiological concentrations of RI, the fractional relative activity of the trimeric

conjugate plateaus at ~0.31. This is consistent with one active site of the trimer remaining

inaccessible to RI even at 1 µM concentrations of the inhibitor protein.

(G88C RNase A)$_3$–**3.6** behaved in a nearly identical manner to (G88C RNase A)$_3$–**3.7**

(data not shown). Conversely, (A19C RNase A)$_3$–**3.7**, which differs from

(G88C RNase A)$_3$–**3.7** only in that it is restrictively tethered through a residue outside of

the interface with RI, is inhibited tightly and completely by RI with an apparent K_i' value

of 17 pM. This value is close to the concentration of enzymic active sites present in the

assay solution (15 pM), and thus merely represents an upper limit for the apparent K_i'

value (Henderson, 1972).

(G88C RNase A)$_2$–**3.2** was more readily inhibited by RI than was (G88C RNase A)$_3$–

3.7, though only slightly, with a K_i' value of 0.40 nM. Interestingly, the relative activity

of these dimers also asymptotically approach a non-zero value as did (G88C RNase A)$_3$–

3.7, however the significance of stabilizing at a relative activity value of 0.11 is not as

readily interpretable as in the former case with (G88C RNase A)$_3$–**3.6** and (G88C

RNase A)$_3$–**3.7**. Nonetheless, at physiological RI concentrations, trimers that reach the

cytosol would be expected to retain a larger amount of unfettered ribonuclease activity

than would dimers.

3.4.5 In Vitro Cytotoxicity

The toxicity of each ribonuclease was measured toward the K-562 human leukemia

cell line. IC$_{50}$ values are given in Table 3.1 on both a conjugate and an active-site basis

and were derived by applying eq 3.3 to the data in Figure 3.4. The results and fitted

curves in Figure 3.4 are based upon the concentration of the entire conjugate, not just the

active sites, and those will be the IC$_{50}$ values discussed herein unless indicated otherwise.

ONC and G88R RNase A displayed IC$_{50}$ values similar to those reported previously

(Leland *et al.*, 1998; Rutkoski *et al.*, 2005). (A19C RNase)$_3$–**3.7** (Figure 3.4A) exhibited

no cytotoxic activity, even at concentrations of 20 μM. This lack of cytotoxicity is

consistent with its preserved sensitivity to RI, which was demonstrated in the previous

inhibition and RI-binding assays, and underscores the importance of constraining the

ribonucleases through a position that is found within the RI–RNase A interface. G88C

RNase A–NEM (IC_{50} = 28 μM; Figure 3.4A) was nearly 10-fold less cytotoxic than

G88R RNase A. This substantial decrease in cytotoxic activity was surprising because of

their nearly identical affinities for RI, as determined in the competition binding assay.

(G88C RNase A)$_2$–3.2 (IC_{50} = 11 μM) was 3-fold less toxic to K-562 cells than was

G88R RNase A (Figure 3.4A) despite its substantially greater resistance to inhibition by

RI in vitro (Figure 3.3).

The differential effects on cytotoxicity of linking two molecules of G88C RNase A

either *ortho-*, *meta-*, or *para-* to each other about a phenyl ring is demonstrated in

Figure 3.4B. Surprisingly, the relatively subtle chemical differences between the three

linkers were manifested on a macroscopic (*i.e.*, cellular) level as detectable and

reproducible differences in the cytotoxic effects they exerted on K-562 cells. The IC_{50}

values exhibited by (G88C RNase A)$_2$–3.3, (G88C RNase A)$_2$–3.4, and

(G88C RNase A)$_2$–3.5 were 10, 14, and 27 μM, respectively, consistent with our

hypothesis that more restrictively tethered conjugates of ribonucleases should possess

greater cytotoxicity. The triply-substituted (G88C RNase A)$_3$–3.6 (IC_{50} = 16 μM;

Figure 3.4D) displayed cytotoxicity similar to that of (G88C RNase A)$_2$–3.4, despite

possessing an additional active site that was inaccessible to RI at physiological

concentrations of RI in our K_i' determination experiments.

Using the same TMEA linker 3.7, trimers of three different homologous mammalian

ribonucleases, G88C RNase A, G89C RNase 1, and C31A/C32A/G88C BS-RNase, were

tethered through structurally analogous positions within the β4–β5 surface loop and

tested for toxicity towards K-562 cells (Figure 3.4C). As reported previously (Leland *et al.*, 2001), wild-type RNase 1 had no effect on the proliferation of K-562 cells. Per conjugate molecule, the (G88C RNase A)$_3$–**3.7** conjugate (IC$_{50}$ = 8.6 μM; Z = +13) was more toxic toward K-562 cells than any of the dimeric conjugates of RNase A linked through the same position. (G89C RNase 1)$_3$–**3.7** (IC$_{50}$ = 1.5 μM; Z = +19) and (G88C BS-RNase)$_3$–**3.7** (IC$_{50}$ = 0.78 μM; Z = +28) were 6- and 11-fold more fold more cytotoxic when compared to semisynthetic TMEA trimers of their homologue RNase A.

ONC and D38R/R39D/N67R/G88R RNase A both represent monomeric ribonucleases that are highly cytotoxic (IC$_{50;\ (K-562)}$ = 0.27 and 0.19 μM, respectively) because they are either naturally insensitive to RI (ONC) or have been engineered to be RI-evasive (D38R/R39D/N67R/G88R RNase A) (Rutkoski *et al.*, 2005). The cytotoxic activities of homotrimeric conjugates of these two ribonucleases are shown in Figure 3.4D. Trimerization significantly impairs the cytotoxic activities of both (S72C ONC)$_3$–**3.7** (IC$_{50}$ = 0.79 μM) and (D38R/R39D/N67R/G88C RNase A)$_3$–**3.7** (IC$_{50}$ = 1.0 μM). On a per active-site basis, the cytotoxicity of ONC and D38R/R39D/N67R/G88R RNase A is reduced by 10- and 17-fold upon trimerization.

3.4.6 Xenograft Mouse Studies

Mice bearing DU 145 prostate carcinoma tumors were used for initial animal studies, as the DU 145 cell line had previously been shown to be sensitive to variants of RNase A (Rutkoski *et al.*, 2005). *(Proliferation assays were again carried out in vitro to again demonstrate the sensitivity of the DU 145 cell line to evasive ribonuclease variants;*

Figure 3.11.) Dose–response experiments were first carried out with a monomeric

evasive variant of RNase A (K7A/D38R/R39D/G88R RNase A; $K_{d; (hRI)}$ = 2.9 μM

(Rutkoski *et al.*, 2005)) to establish an effective dose and administration schedule to

which trimeric conjugates could be compared. A dose of 15 mg/kg (qd×5; i.p.) was

identified as being optimal for eliciting the maximum inhibition of tumor growth

(TGI = 83%) while displaying only minor toxic side effects as monitored by change in

body weight (+2%) (Figure 3.5A). In fact, this dose of K7A/D38R/R39D/G88R RNase A

inhibits the growth of DU 145 tumors in mice as effectively as does ONC (5 mg/kg; i.p.,

1×wk) (Figure 3.5B). In this experiment, the mice in the K7A/D38R/R39D/G88R

RNase A treatment group received 15-fold more ribonuclease (by mass) on a weekly

basis than did mice in the ONC treatment group. Yet, this greater amount of mammalian

RNase seems to be better tolerated as indicated by the loss in body weight of the animals

in the ONC treatment group (–25%) during the course of the experiment (Figure 3.5B

inset).

The importance of frequent administration (qd×5) for monomeric

K7A/D38R/R39D/G88R RNase A to achieve maximal tumor growth inhibition is

illustrated in Figure 5C, where mice received 75 mg/kg 1×wk instead of the previous

15 mg/kg qd×5. While equivalent on a mass/week basis, the once-weekly administration

of K7A/D38R/R39D/G88R RNase A was dramatically less effective at inhibiting tumor

growth (TGI = 15%). Docetaxel (15 mg/kg 1×wk) was much more effective at inhibiting

tumor growth (TGI = 80%).

Having established and characterized the response of mice bearing DU 145 tumors to known cytotoxic RNase treatments, mice were treated with (G88C RNase A)$_3$-**3.7**. Because chemically coupled dimers of RNase A using dimethyl suberimidate exhibited an enhanced circulation time in both mice and rats when compared to that of wild-type monomeric RNase A (2–12-fold retention enhancement) (Bartholeyns and Moore, 1974; Tarnowski *et al.*, 1976), we anticipated that trimeric conjugates would exhibit an even greater persistence in circulation. Preliminary pharmacokinetic analysis confirmed the enhanced retention time in circulation of (G88C RNase A)$_3$-**3.7** compared to that of monomeric G88R RNase A (J.A.K. and L.E.S., unpublished results; data not shown). A dose of 25 mg/kg (1×wk) of (G88C RNase A)$_3$-**3.7**, which is a third of the ribonuclease by mass that was used in Figure 3.5C, was administered to mice bearing DU 145 tumors. This dose inhibited the growth of tumors, which grew to only 25% the size of the vehicle control without any indication of systemic toxicity in the animals (Figure 3.5D).

Encouraged by the success in the DU 145 tumor-bearing mouse models, xenograft studies were continued using a lung adenocarcinoma cell line (A549; Figure 3.6), which had been shown previously to be the least sensitive to cytotoxic ribonucleases in a panel of ten different cell lines tested in vitro (Rutkoski *et al.*, 2005). *(Proliferation assays were carried out in vitro to demonstrate that the A549 cell line was not anomalously sensitive to the multimeric conjugates; Figure 3.10.)* (G88C RNase A)$_3$-**3.7** also inhibited the growth of these tumors substantially (Figure 3.6A; TGI = 68%), though not as completely as did cisplatin (TGI = 89%), which, however, was toxic to the mice as evidenced by a significant reduction in body weight (27%). Photographs of A549 tumor-bearing mice

from both the treatment (Figure 3.6C) and vehicle control (Figure 3.6D) groups upon completion of the experiment are shown in Figure 3.6A, showing obvious reduction of tumor size in animals receiving the (G88C RNase A)$_3$–**3.7** conjugate.

Towards the goal of developing human ribonuclease-based cancer therapeutics, (G89C RNase 1)$_3$–**3.7** was administered to mice bearing A549 human tumors (Figure 3.6B). Although at a dose of 7.5 mg/kg, 1×wk tumor volume was only slightly reduced over the course of the experiment (TGI = 30%), a 10-fold higher dose (75 mg/kg; 1×wk) inhibited the growth of these tumors in a manner comparable to that of erlotinib hydrochloride (Tarceva®) (100 mg/kg; 2×wk), which both achieved an ~80% reduction in tumor growth. Though the human trimer performed comparably to Tarceva®, we note that on a molar basis, ~300 molecules of Tarceva® were required to for every one trimeric ribonuclease conjugate to achieve a similar therapeutic effect.

3.5 Discussion

3.5.1 Molecular Rulers

A host of bis-maleimide (and other sulfhydryl-reactive) cross-linking reagents are commercially available because bifunctional cross-linking reagents, in general, have found broad utility in a range of applications (Ji, 1983; Pierce, 2006). Specifically, these cross-linking reagents have been used as "molecular rulers" or tools to probe both conformational changes and quaternary structural organization of large macromolecular complexes (Fasold *et al.*, 1971; Chang and Flaks, 1972; Peters and Richards, 1977; Swaney, 1986; Kwaw *et al.*, 2000; Rappsilber *et al.*, 2000). When bis-maleimide

cross-linking reagents are used as molecular rulers, their length refers to the span (in Å)

between the intervening sulfur atoms of the two cysteine residues involved in the cross-

link. Recently, stochastic molecular dynamics analysis was applied to 32 commonly used

homobifunctional cross-linking reagents and revealed dramatic deviations from the

distances commonly cited for these reagents which are generally based on the fully

extended conformations of these structures (Green et al., 2001). Therefore, guided by the

more realistic lengths put forth by Green et al., we selected five alternative

homobifunctional linkers that were anticipated to yield more restrictively tethered

linkages (compared to BMH **3.1**) due to their shorter S-S span and/or increased rigidity

(inferred from the range of S-S distances) (Table 3.2; Figure 3.1). Similar quantitative

modeling was not available for the commercially available tris-maleimide cross-linker

(TMEA; **3.7**), however, inspired by the PDM series (**3.3–3.5**) the novel linker **3.6** was

synthesized (Scheme 3.1). Owing to the rigid benzyl scaffold, we expected **3.6** to afford a

more constrained linkage of the three ribonuclease substituents.

3.5.2 Preservation (and perhaps enhancement?) of Ribonucleolytic Activity

Importantly, site-specific multimerization did not have any deleterious effects on the

catalytic activity of any of the ribonucleases as evidenced by the ability of the conjugates

to degrade the small fluorogenic substrate 6-FAM–dArUdAdA–6-TAMRA. In contrast,

the enzymatic activity of RNase A cross-linked with diimido esters is negatively

correlated to length of exposure to these reagents (Wang et al., 1976). The source of the

enhanced ribonucleolytic activity of (S72C ONC)$_3$–**3.7** was not investigated, however it

is interesting to speculate that perhaps the increased charge density of this conjugate accelerates the rate of substrate association. The low catalytic activity of ONC is thought to originate in the low affinity of this enzyme for its substrate (Lee and Raines, 2003). It is perhaps not surprising that a similar enhancement was not observed for the mammalian enzymes as they possess a much higher basal activity (10^4–10^5-fold greater (Boix *et al.*, 1996)) and operate near the diffusion limit (Park and Raines, 2003). Thus, it might be more feasible to observe a modest improvement in the comparatively poorer catalyst.

Enhanced activity against dsRNA compared to that of monomeric ribonucleases, especially RNase A, has been described for BS-RNase (Libonati and Floridi, 1969), noncovalent aggregates of RNase A (Libonati, 1971), and for ribonuclease conjugates produced via semisynthesis both non-specifically (Bartholeyns and Moore, 1974) and site-specifically (Suzuki *et al.*, 1999). It should be noted that RNase A has virtually no activity against duplex RNA at physiological salt concentrations (Billeter *et al.*, 1966). Although the ability to degrade other substrates such as viral dsRNA or homopolymeric dsRNA was not tested, the multimeric conjugates described in this work would be expected to exert greater ribonucleolytic activity toward duplex RNA than their monomeric counterparts similar to that observed for dimeric (Bartholeyns and Moore, 1974; Wang *et al.*, 1976) and trimeric (Gotte *et al.*, 1997) conjugates of RNase A prepared with dimethyl suberimidate. These chemically prepared dimers of RNase A were reported to possess between 8.5- (Wang *et al.*, 1976) and 78-fold (Bartholeyns and Moore, 1974) enhanced ability to hydrolyze poly(A)·poly(U) duplex RNA over that of monomeric RNase A. Furthermore, activity toward duplex RNA correlated to the order of

oligomerization: trimers > dimers >> monomers (Gotte *et al.*, 1997). This same trend was observed in the ability of multimeric aggregates of RNase A prepared upon lyophilization from 40% acetic acid to degrade dsRNA (Libonati, 2004) which are also capable of degrading DNA·RNA hybrids (Libonati *et al.*, 1975).

This enhanced activity against dsRNA has been explained to be a result of increased ability of these ribonucleases to bind to and melt duplex nucleic acids whose A-type double helix (RNA) is otherwise not susceptible to hydrolysis due to the geometrical constraints of the reaction mechanism of pancreatic ribonucleases (Opitz *et al.*, 1998). Therefore, although activity against dsRNA has not been directly correlated with cytotoxicity (Gotte *et al.*, 1997), it is tempting to speculate that this propensity to bind to and melt higher order RNA structure would be a boon to cytotoxic ribonucleases whose mechanism of action it is to render cytosolic RNA indecipherable (Leland and Raines, 2001). Trimers of RNase 1, (*e.g.*, G89C RNase 1)$_3$–**3.7**), might be particularly active against duplex RNA owing to the fact the basic RNase 1 monomer is already 300-fold more active against dsRNA than is RNase A (Sorrentino *et al.*, 2003).

3.5.3 Importance of Linkage Position

A distinct advantage of site-specific generation of multimers (over non-specific cross-linking or techniques such as tandemization) is that it enables the experimenter to select one (or more) discrete site(s) of attachment in order to preserve or maximize a particular biological function. For example, to effect multivalent binding of HIV glycoprotein gp120, multimeric forms of CD4 have been prepared using BMH **3.1** to

ensure that the gp120-binding surface was not compromised (Chen *et al.*, 1991).

Similarly, Youle and co-workers chose to link ribonucleases through regions of their

surfaces that were both distal to the active site and would be expected to maximally

disrupt RI-binding (Suzuki *et al.*, 1999). To demonstrate that the site of linkage is a

determinant of RI-evasion we prepared two trimeric conjugates of RNase A,

(A19C RNase A)$_3$–**3.7** and (G88C RNase A)$_3$–**3.7**, that differ only at their site of linkage

(Figure 3.2).

Position 19 lies within the α1– α2 loop of RNase A (Figure 3.2). Previously, the

attachment of small molecule fluorophores (*e.g.*, 5-IAF, DEFIA) at this position was

shown to have no effect on the ability to bind RI (Kothandaraman *et al.*, 1998; Abel *et*

al., 2002; Lavis *et al.*, 2007). The geometrical organization of the three ribonuclease

moieties of (A19C RNase A)$_3$–**3.7** can readily accommodate the binding of three

molecules of RI with high affinity ($K_i' \leq 17$ pM; Figure 3.3). This preservation of

sensitivity to RI is corroborated by the results of the competition binding assay

($K_d' \leq 1.4$ nM) and translates to a ribonuclease conjugate that is completely non-toxic to

K-562 cells. On the other hand, (G88C RNase A)$_3$–**3.7** is toxic to K-562 with an IC$_{50}$

value of 8.6 μM. The of this conjugate toxicity stems from its dramatically reduced

susceptibility to RI. Most strikingly, under in vitro conditions which approximate

cytosolic RI concentration, one active site remains entirely inaccessible to RI—free to

degrade cellular RNA (Figure 3.3). Therefore, we have definitively shown that the choice

of position through which the ribonucleases are linked can be the difference between a

toxic and non-toxic multimeric conjugate. This conclusion is supported by the results of

Yamada and co-workers who spliced human basic fibroblast growth factor (bFGF) into

human pancreatic ribonuclease (RNase 1) as a separate domain through insertional fusion

(Tada *et al.*, 2004). RI-evasion, and thus efficacy as a immunotoxin, was significantly

greater when the bFGF graft was made between residues 89 and 90, as opposed to

residues 19 and 20, which are structurally analogous to the positions of linkage explored

in this work (Tada, H., personal communication; See also section 1.6.3 and Table 1.3).

3.5.4 Importance of the Number of Degrees of Freedom in the Linker

A primary motivation of this work was to design and characterize site-specifically

conjugated ribonuclease multimers that were tethered more restrictively than those

prepared previously using BMH **3.1**. The physical constraints imposed by the

bifunctional linkers used in this study (determined by computational modeling (Green *et

al.*, 2001)) have been compared to the directly measured biochemical properties of RI

affinity and cytotoxicity of dimers prepared from G88C RNase A (Table 3.2). The

cross-linking reagents are listed in the order of increasing maximum length. The

ribonuclease moieties would be most susceptible to RI in this most-extended linker

conformation. With the exception of **3.5** and **3.8**, the reagents conform to the general

trend of greater RI-evasion and cytotoxic activity observed as the length of the

cross-linking span is reduced. All of the bifunctional reagents tested yielded dimeric

ribonuclease conjugates that were more RI-evasive than those prepared with BMH **3.1**

(K^r_d = 2.6 nM). Furthermore, all but one of the reagents (**3.5**) produced ribonuclease

dimers that were more effective at inhibiting the proliferation of K-562 cells than was

(G88C RNase A)$_2$–**3.1**. The more rigid scaffold of the novel phenylenetrimaleimide linker **3.6** likewise resulted in more RI-evasive trimers (~2-fold) than those prepared with the comparatively more flexible TMEA **3.7**. Surprisingly, the superior RI-evasivity of (G88C RNase A)$_3$–**3.6** did not translate to superior cytotoxicity. The triethyl tertiary amine of TMEA **3.7** would be expected to possess a pK_a of ~11 (McMurry, 1996) and would therefore be protonated at physiological pH values, giving this trimeric conjugate a net charge of +13 compared to +12 for (G88C RNase A)$_3$–**3.6**. Cationicity of ribonucleases has been correlated with their efficiency of internalization and therefore cytotoxicity (Futami *et al.*, 2001; Fuchs *et al.*, 2007; Johnson *et al.*, 2007a) and might be partially responsible for the greater than expected cytotoxicity of (G88C RNase A)$_3$–**3.7** relative to (G88C RNase A)$_3$–**3.6**. Because trimers of G88C RNase A prepared with **3.7** displayed greater cytotoxic activity in vitro, this linker was utilized for subsequent in vivo studies.

3.5.5 Correlation Between Net Charge and Cytotoxicity

All of the ribonucleases used in this study possess a net positive charge. RNase A (Z = +4), RNase 1 (Z = +6), and BS-RNase (Z = +9) share a high degree of sequence similarity (80.5 and 88.7% similarity to RNase A for RNase 1 and BS-RNase, respectively; Table 1.2; Figure 1.3) and display similar catalytic activities. Despite these similarities, these three homologues and their resulting trimeric conjugates, (G88C RNase A)$_3$–**3.7**, (G89C RNase 1)$_3$–**3.7**, and (G88C BS-RNase)$_3$–**3.7**, possess significantly different net charges—Z = +13, +19, and +28, respectively for the trimers.

As mentioned above, cationicity has been correlated with cytotoxicity (Futami *et al.*, 2001; Fuchs *et al.*, 2007; Johnson *et al.*, 2007a). This relationship also appears to hold true for trimeric ribonuclease conjugates as the IC_{50} values were observed to decrease with increasing net charge from 8.6 μM [(G88C RNase A)$_3$-**3.7**], to 1.5 μM [(G89C RNase 1)$_3$-**3.7**], to 0.78 μM [(G88C BS-RNase)$_3$-**3.7**] (Table 3.1; Figure 3.4C). However, cytotoxicity is influenced by a host of variables (Futami *et al.*, 2002) and therefore the impact of other factors, such as their differential affinities for RI, cannot be excluded.

3.5.6 Size as a Liability to Internalization

Per active-site, the cytotoxicity of ONC and D38R/R39D/N67R/G88R RNase A is reduced by 10- and 17-fold, respectively upon trimerization. These two ribonucleases remove the variable of RI-evasion and from this we conclude that the process of multimerization itself is deleterious to the deliverance of ribonucleolytic activity to the cytosol. Similarly, the quaternary structure of BS-RNase was concluded to be a liability to its cytotoxic activity as monomeric variants of BS-RNase designed to be RI-evasive were more cytotoxic than dimeric versions of the same variants (Lee and Raines, 2005). In the present work we suggest that the trimeric conjugates: 1) are endocytosed less efficiently, 2) undergo an altered trafficking pattern which reduces cytosolic access, and/or 3) translocate less efficiently across the lipid bilayer to the cytosol (*i.e.*, reduced endosomal/lysosomal escape). Bartholeyns and Baudhuin found that chemically-dimerized RNase A associated to a greater extent with the cell membrane (at 0 °C) and

was taken up 20 times more rapidly than monomeric RNase A by HTC cells (hepatoma

tissue cells) (Bartholeyns and Baudhuin, 1976)—seemingly ruling out the first

possibility. However, their results should be taken *cum grano salis* as they also concluded

that enzymatic activity of the dimer was not necessary for its cytotoxic effect. In contrast,

the uptake efficiency by non-phagocytic cells of fluorescent latex beads of discrete size

ranging from 50–500 nm in diameter was quantitated by FACS and was found to

correlate negatively with size (*i.e.*, larger beads were taken up more slowly) (Rejman *et*

al., 2004). Though this trend is interesting we note that the molecular diameters of

monomeric and trimeric ribonucleases are ~10-fold smaller (5 nm; 50 Å) than those of

the smallest beads used and therefore might not be applicable. Though the source of the

negative impact is unclear, trimerization reduces the deliverance of ribonucleolytic

activity to the cytosol.

3.5.7 Size as an Asset for Persistence in Circulation

Members of the RNase A superfamily are efficiently and rapidly removed from

plasma circulation by the kidneys (Rabinovitch and Dohi, 1956; Dohi *et al.*, 1959;

Lázníček *et al.*, 1993; Vasandani *et al.*, 1996). In both mice and rats the rate of clearance

of these enzymes approaches that of the glomerular filtration rate (GFR) itself (Lázníček

et al., 1993; Vasandani *et al.*, 1996). The half-life of intravenously administered

monomeric ribonucleases in the circulation of both rats and mice is on the order of

minutes (2–5 min) (Bartholeyns and Moore, 1974; Tarnowski *et al.*, 1976; Vasandani *et*

al., 1996). This rapid disappearance from circulation is consistent with what is known about the renal filtration of proteins.

The glomerular capillary wall (GCW) essentially acts as a molecular sieve, removing low molecular weight proteins (*e.g.*, proteohormones and secretory proteins), while efficiently retaining abundant larger plasma proteins such as albumin and IgG (Maack, 2000). The low molecular weight proteins in the filtrate are then re-absorbed from the primary urine by the proximal tubule cells of the kidney, where they are primarily endocytosed and degraded into their constituent amino acids (Dohi *et al.*, 1959; Cortney *et al.*, 1970). The glomerular sieving coefficient (GSC; θ) of macromolecules, which is the ratio of their filtrate-to-plasma concentrations, can be calculated empirically using surrogate polymers such as Ficoll or dextran and used to construct descriptive mathematical models of how the GCW functions and to diagnose various nephropathies. Although the complexity of these models varies, the simplest model entails a multitude of equivalent, albumin-restrictive, negatively-charged pores. The necessity for the albumin-restrictive radius of these pores stems from the extremely low sieving coefficient ($\theta = 6.4 \times 10^{-4}$) determined experimentally for albumin (Tojo and Endou, 1992; Lund *et al.*, 2003; Haraldsson and Sorensson, 2004) in conjunction with the fact that this important carrier protein constitutes 55% of plasma protein and possesses a lifetime of about 21 days in circulation (Anderson and Anderson, 2002). Typically, modeling of restricted diffusion through a porous membrane treats the solutes as hard-spheres (Venturoli and Rippe, 2005). Further modifications (*e.g.*, inclusion of a hydration sphere for these hard spheres) improve the model (Rippe and Stelin, 1989; Chalikian *et al.*,

1996; Venturoli and Rippe, 2005). To accommodate albumin retention, which has a Stokes–Einstein radius of ~35Å (Table 3.3), as well as a host of empirical data for the clearance of numerous other endogenous proteins (Lund *et al.*, 2003), ultimately necessitates a pore radius of only 37–38 Å (Venturoli and Rippe, 2005). In addition to size, extensive studies implicate other characteristics as being important determinants of molecular sieving efficiency including shape and charge of the macromolecule, though to a lesser extent than size (Maack *et al.*, 1992; Maddox *et al.*, 1992; Maack, 2000; Venturoli and Rippe, 2005). Indeed, for small proteins (<20 Å), size is the dominating (nearly exclusive) determinant of GSC. Only when molecular size begins to approach that of the filtration pore (~30 Å) do other factors such as charge have an appreciable influence (Maack, 2000).

In light of this functional model of renal protein filtration, it is perhaps not surprising that pancreatic-type ribonucleases (radius$_{SE}$ ~19 Å; Table 3.3; Figure 3.8) are so rapidly cleared from circulation in the same manner as other low molecular weight proteins (Maack, 1975; Maack *et al.*, 1979). Dimeric ribonucleases, either naturally occurring in the case of BS-RNase or chemically dimerized, were found to exhibit a longer half-life in circulation (Bartholeyns and Moore, 1974; Tarnowski *et al.*, 1976; Vasandani *et al.*, 1996). Though measureable, the extended persistence in circulation was modest (~2-fold compared to that of monomers) and still the half-life was on the scale of several minutes. We expect that trimeric ribonuclease conjugates such as (G88C RNase A)$_3$–**3.7** would display a much more dramatically increased persistence in circulation as these trimers are similar in size to and more asymmetrical than HSA (Figure 3.8 and Table 3.3). Though

further pharmacokinetic analyses are required, greater plasma retention would largely explain the high efficacy of the trimeric ribonuclease conjugates to reduce tumor growth in vivo.

Previously, the importance of net molecular charge for ribonuclease cytotoxicity was described as "dichotomous" as a result of the opposing influence of charge on two separate aspects of ribonuclease-mediated cytotoxicity—cellular internalization and RI-evasion (Johnson et al., 2007a). Assuming that the cationicity of ribonucleases accelerates their removal from circulation as has been seen for numerous other proteins (Brenner et al., 1978; Rennke et al., 1978; Takakura et al., 1990), then perhaps glomerular filtration adds yet another dimension to the importance of Coulombic interactions for ribonuclease cytotoxicity.

3.6 Conclusions

Using eight different sulfhydryl-reactive homobifunctional linkers (six dimeric and two trimeric), we have demonstrated that the cytotoxic activity of ribonuclease multimers correlates with how well they evade RI. Importantly, the catalytic activity and conformational stability are preserved in all of the tethered ribonucleases. Finally, trimeric conjugates of G88C RNase A and G89C RNase 1 prepared with TMEA were as effective as highly evasive monomeric variants of RNase A at inhibiting tumor growth in tumor-bearing mouse models—but could be administered less frequently and at a higher dose. This enhanced activity in vivo is likely to arise from an increased persistence circulation as a result of a reduced rate of glomerular filtration. Inspired by the uniquely

dimeric BS-RNase, this work demonstrates the potential of non-reducible, covalent conjugates of mammalian ribonucleases as human cancer therapeutics.

Table 3.1 Biochemical parameters and cytotoxic activities of ribonucleases and their semi-synthetic dimeric and trimeric conjugates

Ribonuclease	T_m^a (°C)	k_{cat}/K_M^b (10^6 M⁻¹s⁻¹ A.S.⁻¹)	K_d' (hRI)^c (nM)	$(k_{cat}/K_M)_{cyto}^d$ (10^4 M⁻¹s⁻¹)	IC_{50}^e (µM)	IC_{50}^f (A.S.⁻¹) (µM)	Z
wild-type RNase A	64	6.4 ± 0.3	4.4×10^{-5} [g]	1.1×10^{-5}	>25	>25	+4
G88R RNase A	63	8.2 ± 0.2	1.8 ± 0.3	0.29	3.3 ± 0.1	3.4	+5
G88C RNase A–NEM	64	6.8 ± 0.1	1.4 ± 0.4	0.29	28 ± 2	28	+4
(G88C RNase A)₂–3.1	ND	11 ± 1	2.6 ± 0.2	0.72	25 ± 1	50	+8
(G88C RNase A)₂–3.2	64	6.6 ± 0.6	9.6 ± 0.4	1.6	11 ± 1	21	+8
(G88C RNase A)₂–3.8	ND	12 ± 1	8.2 ± 0.2	2.5	22 ± 3	44	+8
(G88C RNase A)₂–3.3	ND	7.4 ± 0.5	18 ± 2	3.2	10 ± 1	20	+8
(G88C RNase A)₂–3.4	ND	8.6 ± 0.1	8.6 ± 1.6	1.8	14 ± 1	27	+8
(G88C RNase A)₂–3.5	ND	5.5 ± 0.03	14 ± 3	1.6	27 ± 2	55	+8
(A19C RNase A)₃–3.7	ND	7.5 ± 0.4	<1.4	–	>25	>25	+13
(G88C RNase A)₃–3.7	64	16 ± 0.4	17 ± 1	6.6	8.6 ± 0.5	27	+13
(G88C RNase A)₃–3.6	ND	12 ± 1	39 ± 3	12	16 ± 1	48	+12
(D38R/R39D/N67R/G88C RNase A)₃–3.7	ND	8.4 ± 0.3	–	–	1.0 ± 0.1	3.3	+16
RNase 1	58	29 ± 1	2.9×10^{-7} [h]	–	>25	>25	+6
(G89C RNase 1)₃–3.7	ND	16 ± 3	<1.4	–	1.5 ± 0.1	4.6	+19
(G88C BS-RNase)₃–3.7	ND	5.8 ± 0.3	84 ± 12	12	0.78 ± 0.05	2.1	+28
ONC	90 [i]	0.0018 ± 0.00005	$\geq 10^3$ [j]	–	0.22 ± 0.01	0.22	+5
(S72C ONC)–3.7	ND	0.012 ± 0.0005	ND	–	0.79 ± 0.05	2.8	+16

ND, not determined. A.S., active site.

[a] Values of T_m (± 2 °C) for RNase A and its variants were determined in 1×DPBS by UV spectroscopy.

[b] Values of k_{cat}/K_M per active site ($\pm$ SE) for ribonucleases and their multimeric conjugates are for catalysis of 6-FAM–dArU(dA)₂–6-TAMRA cleavage at (20 ± 2) °C in 1×DPBS containing 0.1 mg/mL BSA. For ONC and its trimeric conjugate, 6-FAM–dArUdGdA–6-TAMRA was used.

[c] Values of K_d ($\pm$ SE) are for the complex with hRI at (20 ± 2) °C. Concentrations were based on that of the constituent active sites.

[d] Values of $(k_{cat}/K_M)_{cyto}$ were calculated with eq 2.4, total values of k_{cat}/K_M (including all active sites), and the values of K_d for the complex with hRI.

[e] Values of IC_{50} ($\pm$ SE) are for incorporation of [methyl-³H]thymidine into the DNA of K-562 cells exposed to a ribonuclease, calculated with eq 3.3.

[f] Values of IC_{50} per active site were calculated by multiplying the IC_{50} value by the number of monomers in the conjugate.

[g] From Lee et al. (Lee et al., 1989).

[h] From Johnson et al. (Johnson et al., 2007c).

[i] From Leland et al. (Leland et al., 1998) and determined by circular dichroism spectroscopy.

[j] The K_d value for ONC is an estimate of its equilibrium dissociation from porcine RI from (Wu et al., 1993).

Table 3.2 Stochastic MD measurements of homo-bifunctional cross-linking reagents and the in vitro biochemical parameters of (G88C RNase A)$_2$ prepared with each linker

Cross-linking reagent	Average distance[a] (Å)	Standard deviation[a] (Å)	Range of distances[a] (Å)	K'_d[b] (nM)	IC_{50}[b] (µM)
bBBr **3.8**	4.88	0.57	3.17–6.61	8.2	22
oPDM **3.3**	9.39	0.47	7.67–10.47	18	10
BMOE **3.2**	8.18	0.75	6.27–10.52	9.6	11
mPDM **3.4**	10.65	0.55	8.84–11.87	8.6	14
pPDM **3.5**	11.13	0.52	9.20–12.29	14	27
BMH **3.1**	10.16	2.41	3.47–15.64	2.6	25

[a] Average distance, SD, and range of distances are from (Green et al., 2001).
[b] Same values as those reported in Table 3.1.

Table 3.3 Relationship between molecular weight and effective molecular size for globular proteins[a]

Protein	MW (Da)	Stokes–Einstein Radius (in Å)		
		Hard sphere (HS)	Hydrated HS	Globular protein
RNase A	13, 682	16	17.6	19.1
(G88C RNase A)–3.2	27, 676	20.2	22.3	25.0
(G88C RNase A)–3.7	41, 570	23.1	25.5	29.3
(G89C RNase 1)–3.7	44, 617	23.7	26.2	30.1
HSA	66, 450	27	29.9	35.1
IgG	146, 000	35.1	38.8	47.6

[a] Equations for S–E radius (HS, hydrated HS, and globular protein) were from (Venturoli and Rippe, 2005)
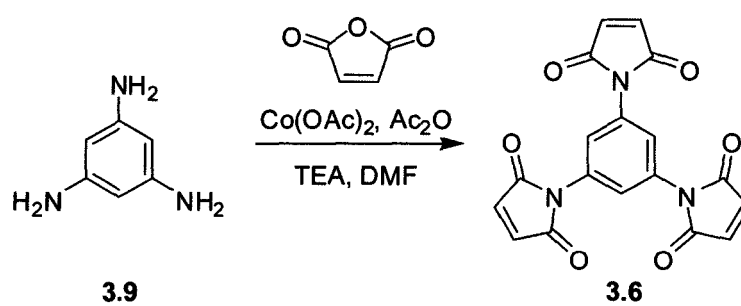
Scheme 3.1 Synthesis of *N,N',N''*-(1,3,5-phenylene)trimaleimide **3.6** from

1,3,5-triaminobenzene **3.9**.
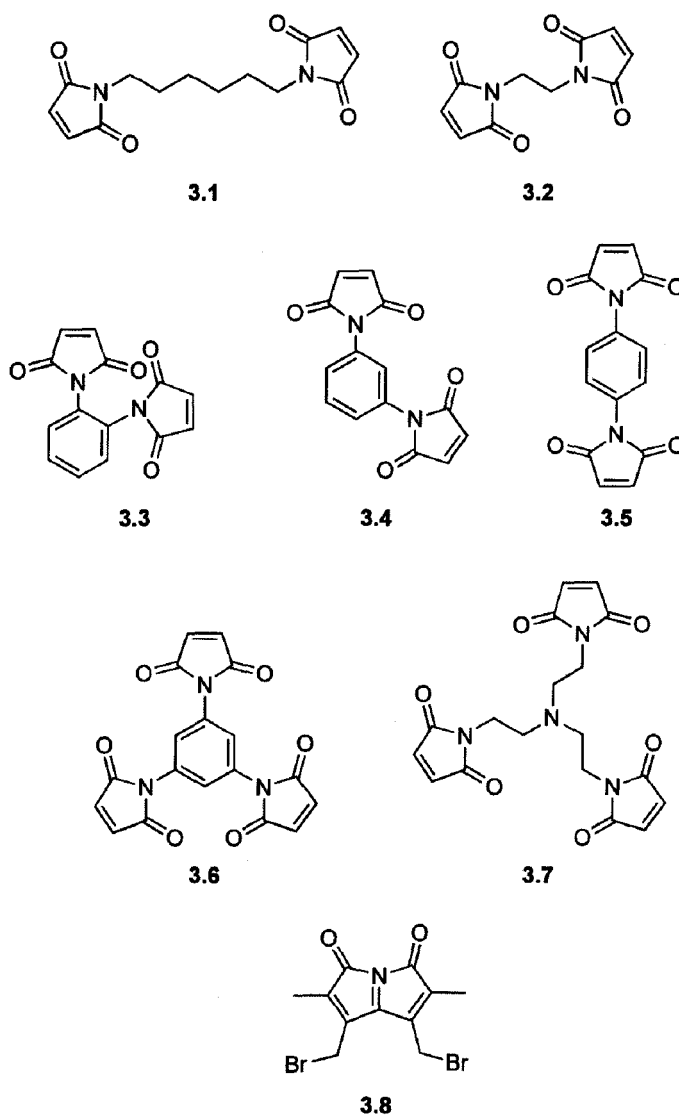
Figure 3.1   Thiol-reactive bi- and tri-functional linkers used to tether restrictively free

thiol-containing ribonuclease variants into dimers and trimers.
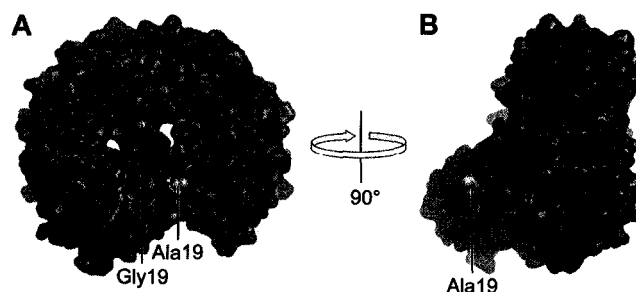
Figure 3.2   pRI·RNase A complex indicating the locations on RNase A at which

unpaired cysteine residues were introduced. Ribbon diagrams of RNase A

(blue) and pRI (red) are shown along with their molecular surfaces. Gly88

(within the protein–protein interface) and Ala19 (outside of the contact

region) of RNase A have been replaced by cysteine residues whose atoms

are shown explicitly as spheres (yellow). (A) "Front" view. (B) Complex

rotated 90° to the left about the vertical axis. Images were created and

modeling was performed using the program PyMOL (DeLano Scientific,

South San Francisco, CA) and the atomic coordinates from PDB entry 1dfj

(Kobe and Deisenhofer, 1995b).
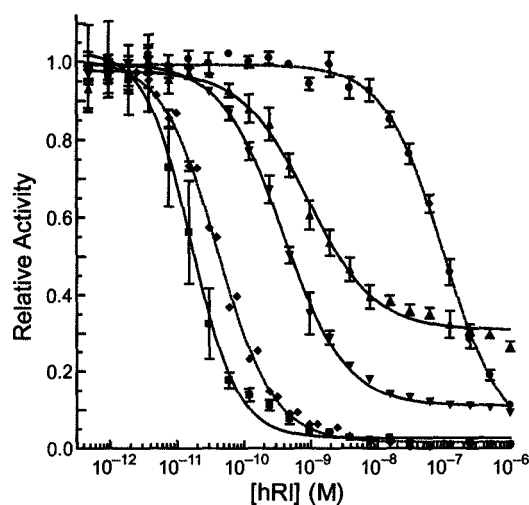
Figure 3.3   Relative ribonucleolytic activity of variants of RNase A and their

multimeric conjugates following pre-incubation with increasing

concentrations of hRI. Data points indicate the mean (± SE) of three

separate experiments. Data for G88R RNase A (diamonds) and

K31A/D38R/R39D/N67R/G88R RNase A (circles) were curve-fitted with

dotted and dashed lines, respectively. Data for (A19C RNase A)$_3$–**3.7**

(squares), (G88C RNase A)$_2$–**3.2** (upside-down triangles), and

(G88C RNase A)$_3$–**3.7** (right side-up triangles) were curve-fitted with

solid lines.

Figure 3.4   Effect of ribonucleases on the proliferation of K-562 cells. The

incorporation of [methyl-^{3}H]thymidine into cellular DNA was used to

monitor the proliferation of K-562 cells in the presence of ribonucleases.

Data points indicate the mean (± SE) of at least three separate experiments

carried out in triplicate. In each panel, data for wild-type RNase A, G88R

RNase A, and ONC are shown as open symbols with curves fitted as

broken lines. For dimeric and trimeric conjugates, the concentration is that

of the entire conjugate, not that of the constitutive active sites.

(A) Importance of tethering ribonucleases through the RI-interface.

(B) Differential cytotoxicity of *ortho-*, *meta-*, and *para-* ribonuclease-

substituted phenylenedimaleimide. (C) Trimeric conjugates of mammalian

ribonuclease homologues with net charges spanning the range of +13 to

+28. (D) Trimeric conjugates of evasive monomeric ribonucleases and a

trimeric conjugate of RNase A prepared with the novel cross-linking

reagent phenylenetrimaleimide.

A

(A19C RNase A)₃–3.7

wild-type RNase A

(G88C RNase A)₂–3.1

G88R RNase A

G88C RNase A–NEM

(G88C RNase A)₂–3.2

ONC

B

(G88C RNase A)₂–3.5

(G88C RNase A)₂–3.3

(G88C RNase A)₂–3.4

C

wild-type RNase 1

(G88C RNase A)₂–3.8

(C31A/C32A/G88C BS-RNase)₃–3.7

(G89C RNase 1)₃–3.7

(G88C RNase A)₃–3.7

D

(G88C RNase A)₃–3.6

(D38R/R39D/N67R/G88C RNase A)₃–3.7

(S72C ONC)₃–3.7

cell proliferation (% of control)

[ribonuclease] (µM)
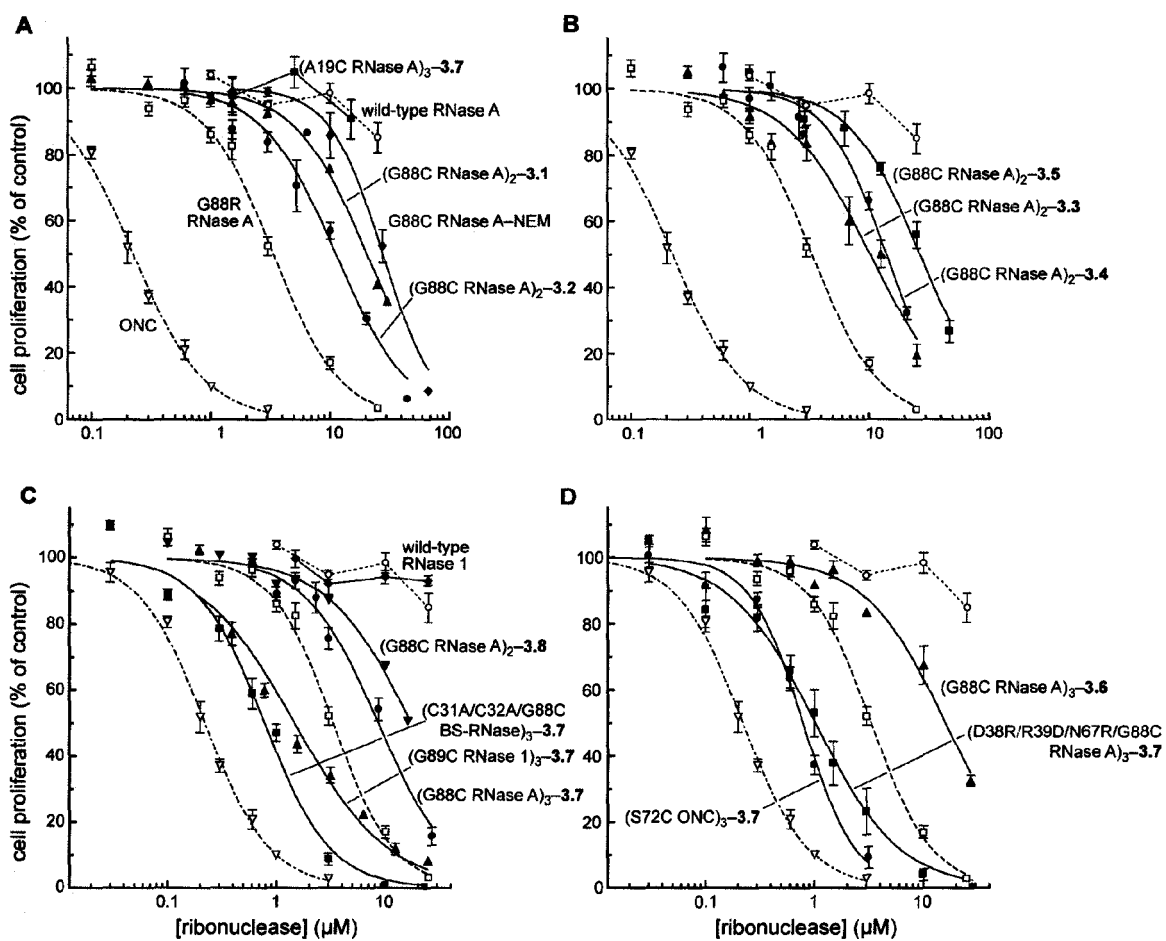
Figure 3.5   Effect of K7A/D38R/R39D/G88R RNase A and (G88C RNase A)$_3$–**3.7** on

the tumor volume and body weight (insets) of Balb c(–/–) mouse

xenografts bearing human DU 145 prostate tumors. Data plotted represent

the mean (± SE) for the number animals indicated in panel descriptions.

Values in parentheses are percentage tumor growth inhibition (% tumor

volume compared to that of the vehicle control on the last day of the

experiment). Vehicle control (open circles; n = 7–8). (**A**) Dose–response

using K7A/D38R/R39D/G88R RNase A (i.p., qd×5; n = 7; closed squares,

5 mg/kg; closed triangles, 15 mg/kg; closed diamonds, 45 mg/kg).

(**B**) K7A/D38R/R39D/G88R RNase A (closed circles, 15 mg/kg; i.p.,

qd×5; n = 7), ONC (open squares, 5 mg/kg; i.p., 1×wk; n = 7).

(**C**) Infrequent dosing schedule of K7A/D38R/R39D/G88R RNase A

(closed circles, 75 mg/kg; i.p., 1×wk; n = 7) compared to docetaxel control

(open squares, 15 mg/kg; i.p., 1×wk, n = 7*). (**D**) (G88C RNase A)$_3$–**3.7**

(closed triangles, 25 mg/kg; i.p., 1×wk, n = 7).

*In the docetaxel group four animals died during the course of the
experiment. Therefore the size of this group changed throughout the
duration of the study: day 28 (n = 6); day 35 (n = 5); day 49 (n = 4); day
63 (n = 3). In the ribonuclease and ribonuclease conjugate treatment
groups, all animals survived. (*i.e.*, death is not an endpoint in these
studies).
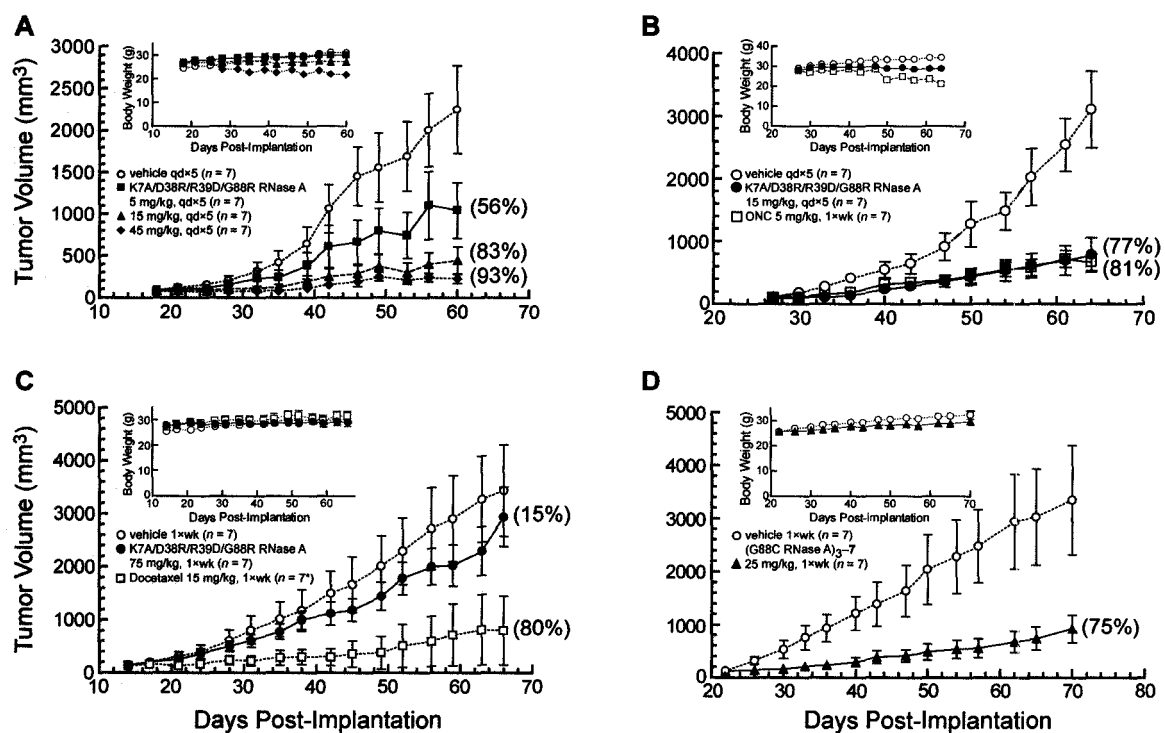
Figure 3.6   Effect of trimeric ribonuclease conjugates on tumor volume and body

weight (insets) of Balb c(–/–) mouse xenografts bearing human A549 lung

tumors. Data plotted represent the mean ± SE for the number animals

indicated in panel descriptions. Values in parentheses are percentage

tumor growth inhibition (% tumor volume compared to that of the vehicle

control on the last day of the experiment). Vehicle control (open circles;

$n = 7$–8). (**A**) (G88C RNase A)$_3$–**3.7** (closed triangles, 25 mg/kg; i.p.,

1×wk, $n = 7$) and cisplatin (open squares, 6 mg/kg; i.p., 1×wk, $n = 7$).

(**B**) (G89C RNase 1)$_3$–**3.7** (closed down triangles, 7.5 mg/kg; closed up

triangles, 75 mg/kg; i.p., 1×wk, $n = 7$) and Tarceva® (open squares,

100 mg/kg, i.p., 2×wk, $n = 7$). (**C–D**) Photographs of A549 tumor-bearing

mice from both the treatment (**C**) and control (**D**) groups upon completion

of the experiment are shown in (**A**).

A

B

C

D
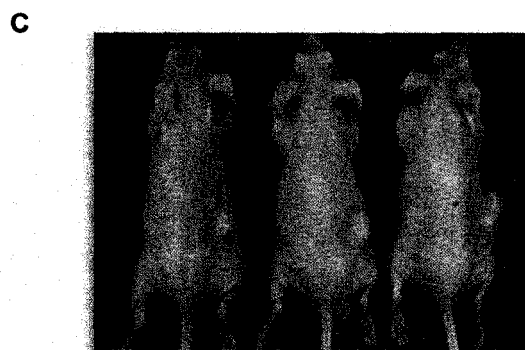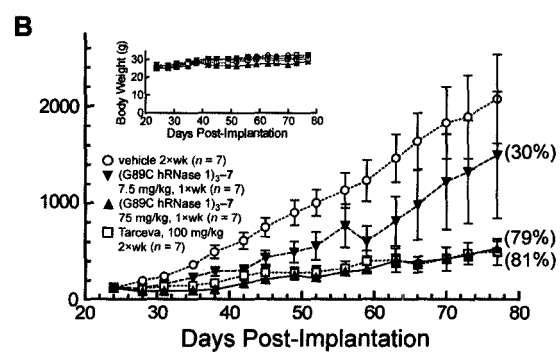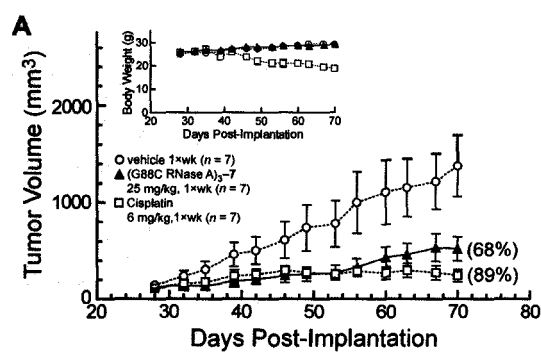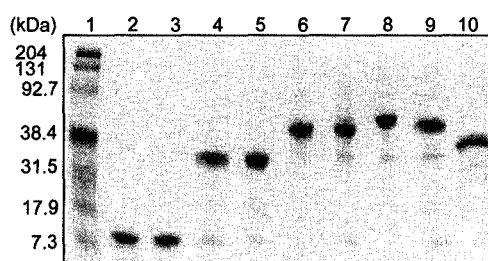
Figure 3.7   SDS–PAGE (12% w/v acrylamide; Tris–HCl) analysis of ribonuclease

monomers and multimeric conjugates (2 μg each). Lane 1: Pre-stained

molecular weight markers. Lane 2: G88R RNase A.

Lane 3: G88C RNase A–NEM. Lanes 4: (G88C RNase A)₂-3.2.

Lane 5: (G88C RNase A)₂-3.3. Lane 6: (G88C RNase A)₂-3.6.

Lane 7: (G88C RNase A)₂-3.7. Lane 8: (G89C RNase 1)₃-3.7.

Lane 9: (G88C BS-RNase)₃-3.7. Lane 10: (S72C ONC)₃-3.7. Molecular

weights shown for standards (myosin, β-galactosidase, bovine serum

albumin, carbonic anhydrase, soybean trypsin inhibitor, lysozyme, and

aprotinin) are calibrated molecular weights (in kDa) for a Tris–HCl gel.

The gel was stained with Coomassie Brilliant Blue R-250 and

subsequently destained.

Figure 3.8   (A) Molecular size of RNase A and (G88C RNase A)₃–**3.7** in comparison

to that of predominant and highly retained plasma proteins. Molecular

structures of immunoglobulin gamma (IgG; yellow and brown; PDB code:

1igt (Harris *et al.*, 1997)), human serum albumin (HSA; green; PDB code:

1bm0 (Sugio *et al.*, 1999)), and RNase A (blue; PDB code: 7rsa

(Wlodawer *et al.*, 1988)) were modeled to the same scale relative to each

other using the program PyMOL (South San Francisco, CA). In the

absence of a three-dimensional structure for (G88C RNase A)₃–**3.7**, three

RNase A molecules were tethered virtually with linker **3.7** (bonds shown

explicitly) to convey the approximate molecular size of these trimeric

conjugates. Stokes–Einstein radii (radius$_{SE}$) were calculated using the

equation for globular proteins from (Venturoli and Rippe, 2005). [a]The

values of p*I* for IgG, HSA, and RNase A are from (Tracy *et al.*, 1982),

(Evenson and Deutsch, 1978), and (Ui, 1971), respectively. (B) The

potential impact of increased size on the rate of renal clearance. [b]The pore

radius (37–38 Å) for the glomerular filter is from (Renkin and Gilmore,

1973; Venturoli and Rippe, 2005). (C) SEC analysis (see methods for

conditions). Brown (IgG) and green (HSA) arrows represent elution

positions for IgG and HSA calculated from molecular weight standards.

Dotted vertical lines demark the approximate glomerular filtration MW

exclusion limit (range 40–60 kDa) (Maack, 2000; Anderson and

Anderson, 2002; Venturoli and Rippe, 2005).

A

RNase A
MW = 13,682
radius$_{SE}$ = 19 Å
p*I* = 9.3 [a]

IgG
MW = 146,000
radius$_{SE}$ = 47.6 Å
p*I* = 6.4–9.0 [a]

Human Serum Albumin
MW = 66,450
radius$_{SE}$ = 35.1 Å
p*I* = 4.8–5.6 [a]

(G88C RNase A)$_3$–3.7
MW = 41,570
radius$_{SE}$ = 29.3–30.1 Å
p*I* = 9.3 [a]

B

Plasma proteins

Sieve (37–38 Å)[b]
for neutral proteins

Large molecules are
returned to circulation

Small proteins
(*e.g.*, RNase A) are
eliminated rapidly

C

— wild-type RNase A
······ G88C RNase A–NEM
— (G88C RNase A)$_2$–3.5
— (G88C RNase A)$_2$–3.4
— (G88C RNase A)$_3$–3.6

Figure 3.9   Thermal denaturation of (G88C RNase A)₃–**3.7** (black),

(G88C RNase A)₂–**3.2** (blue), and G88C RNase A–NEM (red).
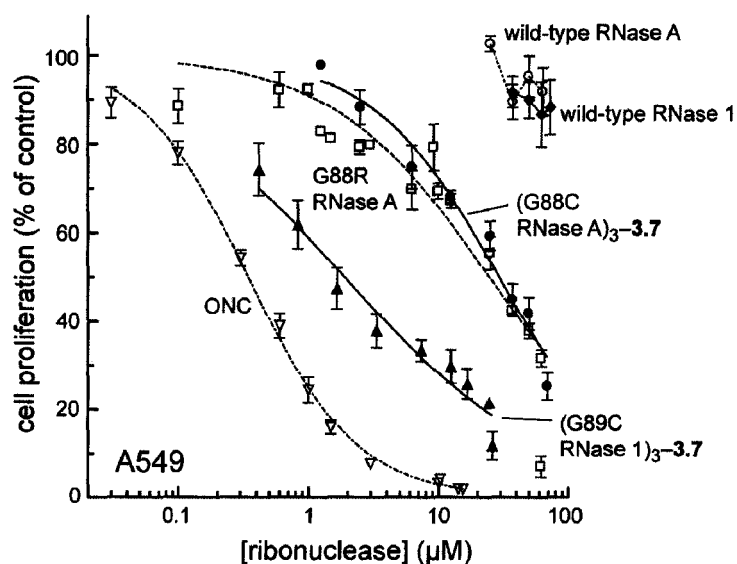
Figure 3.10   Effect of ribonucleases and trimeric ribonuclease conjugates on the

proliferation of A549 cells. The incorporation of [methyl-^{3}H]thymidine

into cellular DNA was used to monitor the proliferation of A549 cells in

the presence of ribonucleases. Data points indicate the mean (± SE) of at

least three separate experiments carried out in triplicate. Data for wild-

type RNase A (open circles), G88R RNase A (open squares), and ONC

(open triangles) are shown as open symbols with curves fitted as broken

lines. For (G88C RNase A)$_3$-3.7 (closed circles) and (G89C RNase 1)$_3$-

3.7 (closed triangles), the concentration is that of the entire conjugate, not

that of the constitutive active sites.
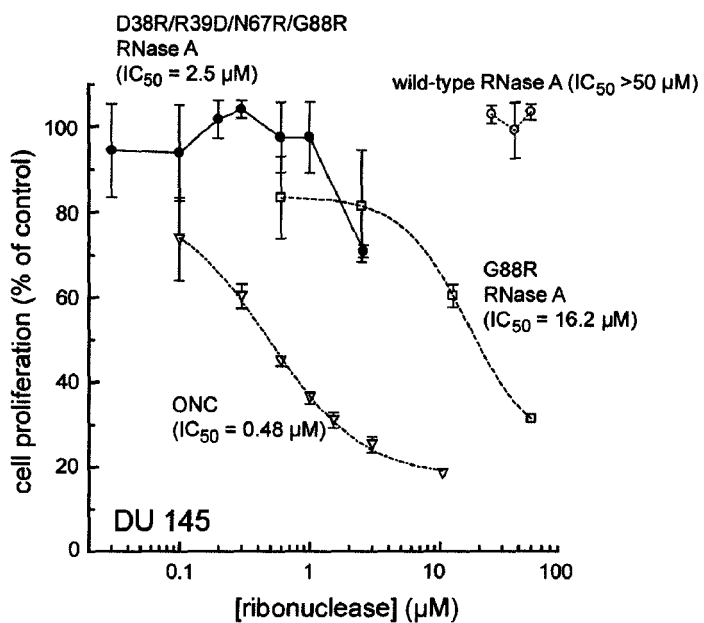
Figure 3.11   Effect of ribonucleases on the proliferation of DU 145 cells. The ability of

cells to reduce resazurin to resorufin was used to monitor their

proliferation in the presence of ribonucleases. Data points indicate the

mean (± SE) of at least three separate experiments carried out in triplicate.

CHAPTER 4

Site-Specific PEGylation of Ribonuclease A to Evade
Ribonuclease Inhibitor and Improve Pharmacokinetics

4.1 Abstract

Onconase® (ONC), an amphibian member of the bovine pancreatic ribonuclease

(RNase A) superfamily, possesses innate antitumoral activity. Now in Phase IIIb clinical

trials for the treatment of malignant mesothelioma, ONC is the forerunner of a promising

new class of ribonuclease-based chemotherapeutics. Compared to ONC, mammalian

ribonucleases, such as RNase A, have the potential to be superior therapeutics owing to

their greater catalytic activity, more favorable tissue distribution, and lower immunogenic

potential. The cytotoxic potential of RNase A is, however, obscured by its sensitivity to

the cytosolic ribonuclease inhibitor (RI), which binds and inactivates its ligands with

femtomolar affinity. When administered intravenously in mice or rats, ribonucleases are

efficiently removed from circulation by the kidneys and therefore exhibit a low residence

time in serum ($t_{1/2}$ ~5 min), owing to their small size (12–14 kDa). Site-specific

PEGylation of RNase A provides a means to reduce sensitivity to RI and to extend serum

half-life. Free thiol-containing variants of RNase A, when reacted with maleimide-

functionalized monomethoxypoly(ethylene glycol) (MAL–mPEG) were found to retain

full ribonucleolytic activity (against both large and small substrates) and conformational

stability. The site of PEGylation, PEG size, and order of PEG branching all influenced

the degree of RI-evasion and hence the cytotoxicity. Diminished in vitro biological

activity (*i.e.*, cytotoxicity) is attributed to reduced efficiency of internalization due to the

shielding of positive charge by the PEG polymer. The resulting enhanced persistence in

circulation more than compensates for the reduced in vitro efficacy, and is manifested by

dramatic tumor growth inhibition in mice. Site-specific PEGylation further expands the

promise of mammalian ribonuclease therapeutics by more suitably tailoring their selective cytotoxicity for use in whole animals.

4.2 Introduction

Some bovine pancreatic ribonuclease (RNase A) superfamily members, including bovine seminal ribonuclease (BS-RNase) and amphibian homologues such as Onconase® (ONC), exhibit innate anti-tumoral activity both in vitro and in vivo (D'Alessio *et al.*, 1997; Saxena *et al.*, 2003). Additionally, the cytotoxic activity of these enzymes is selective for cancer cells, stimulating interest in their development as a novel class of cancer therapeutics (Leland and Raines, 2001; Benito *et al.*, 2005; Arnold and Ulbrich-Hofmann, 2006; Lee and Raines, 2008; Rutkoski and Raines, 2008). The promise of ribonuclease-based chemotherapeutics is exemplified by ONC, which is currently in a Phase IIIb confirmatory clinical trial for the treatment of malignant mesothelioma (Mikulski *et al.*, 2002) and is poised to become the first FDA-approved ribonuclease drug (Pavlakis and Vogelzang, 2006).

Mammalian ribonucleases such as RNase A or human pancreatic ribonuclease (RNase 1) are potentially more desirable as biologic therapeutics than ONC, owing to their superior catalytic activity, more favorable tissue distribution, lower immunogenic potential, and greater therapeutic index but are limited by their susceptibility to inhibition by the ubiquitous cytosolic ribonuclease inhibitor protein (RI) (Rutkoski *et al.*, 2005; Rutkoski and Raines, 2008). RI is found exclusively in the reducing environment of the cytosol. There, RI serves as a intracellular sentry, preserving the integrity of cytosolic

RNA by binding to and inactivating adventitiously expressed ribonuclease ligands with

femtomolar affinity (Haigis *et al.*, 2003). Neither BS-RNase nor ONC are inhibited by

RI, and this ability to evade inhibition by RI is a primary determinant of their cytotoxicity

(Murthy and Sirdeshmukh, 1992; Boix *et al.*, 1996; Rutkoski and Raines, 2008). Indeed,

variants of RNase A that have been engineered to evade RI are more potent cytotoxins

in vitro than is ONC (Rutkoski *et al.*, 2005).

As small (12–14 kDa), parenterally administered enzymes, ribonucleases are subject

to many of the same obstacles that generally plague biotherapeutic development such as

rapid renal clearance and exposure to proteases (Gad, 2007). Surface modification of

RNase A with poly(ethylene glycol) (PEG) could allow these barriers to be overcome

while simultaneously reducing sensitivity to RI. PEGylation enshrouds the molecule to

which it is attached with an immunogenically inert polymer, endowing it with greater

resistance to proteolysis, improved solubility, and reduced immunogenicity, as well as

dramatically enhanced persistence in circulation (Delgado *et al.*, 1992; Harris and

Zalipsky, 1997; Harris *et al.*, 2001; Greenwald *et al.*, 2003a; Harris and Chess, 2003;

Veronese and Harris, 2008). The utility of PEGylation as a strategy to enhance the

in vivo efficacy of macromolecular drugs is evidenced by more than half a dozen

clinically-approved PEG–protein conjugates on the market, including PEG–asparaginase

(Oncaspar®), PEG–adenosine deaminase (Adagen®), PEG–granulocyte colony-

stimulating factor (Neulasta®), and PEG–interferon-α (PEG-Intron® and Pegasys®), as

well as by more than a dozen PEG–protein conjugates in late-stage clinical trials (Pasut

and Veronese, 2007).

In general, first-generation PEG conjugates were characterized by the attachment of several relatively short (generally <12-kDa), linear, amine-reactive monomethoxy-PEG (mPEG) moieties, often containing significant concentrations of PEG-diol contaminants, that occasionally employed unstable linkage chemistries (Harris and Chess, 2003). This "first-generation" technology was utilized by several groups to generate PEGylated RNase A using either 2-kDa (Veronese *et al.*, 1985), 5-kDa (Caliceti *et al.*, 1990; Schiavon *et al.*, 1991; Matoušek *et al.*, 2002; Matoušek *et al.*, 2004), or 20-kDa mPEG (Matoušek *et al.*, 2002) as well as PEGylated BS-RNase (Matoušek *et al.*, 2002; Michaelis *et al.*, 2002). Although these PEG–RNase A conjugates did exhibit markedly increased stability to proteolytic degradation (Schiavon *et al.*, 1991; Monfardini *et al.*, 1995), a 40- to 50-fold enhanced persistence in circulation (Schiavon *et al.*, 1991; Lázníček *et al.*, 1993), and a reduced affinity for anti-RNase A antibodies (Caliceti *et al.*, 1990) compared to unmodified RNase A, there are shortcomings to this method of PEGylation. Derivatization of a protein such as RNase A with amine-reactive PEG, which possesses 11 primary amines, generates a heterogeneous population of conjugates—varying both in the number and position of PEG-modified amines. This extent of heterogeneity is undesirable from both a regulatory and practical perspective, as it confounds purification and characterization. In the case of interferon-α, laborious chromatographic separation, in conjunction with peptide mapping, permitted the homogeneous purification of seven positional PEGylation isomers that displayed vastly differing biological activities (Monkarsh *et al.*, 1997; Grace *et al.*, 2005). Additionally, PEGylation of active-site lysine residues, such as Lys41 of RNase A, can be deleterious

to the ribonucleolytic activity (Messmore *et al.*, 1995), which is essential for cytotoxicity (Kim *et al.*, 1995a). Indeed, extensive modification of RNase A with amine-reactive PEG reduced catalytic activity to 3% (Caliceti *et al.*, 1990). Furthermore, PEGylation of surface amines reduces net positive charge (*Z*), which adversely affects cellular internalization, reducing cytotoxicity (Futami *et al.*, 2001; Chapman, 2002; Johnson *et al.*, 2007a).

To address these shortcomings, subsequent generations of PEGylated conjugates have utilized large (20–60-kDa or more), and in some instances, branched, PEG groups at one or two specific sites on the protein (Harris and Chess, 2003). Site-specific PEGylation has been achieved using a variety of strategies. One method of site-specific PEGylation involved the removal of all lysine residues from TNF-α, thereby allowing site-specific, amine-reactive PEGylation at its N-terminus (Yamamoto *et al.*, 2003). Recently, Brocchini and co-workers reported the site-specific bis-alkylation of the two Cys sulfur atoms of a native disulfide bond to form a three-carbon PEGylated bridge (Shaunak *et al.*, 2006). Both of these methods were precluded in the present work, as RNase A possesses both a catalytically essential lysine residue at position 41 as well as four intramolecular disulfide bonds (Raines, 1998). A more general approach entails the installation of a free cysteine residue at the protein surface via site-directed mutagenesis and subsequent reaction with a thiol-reactive PEG moiety to achieve site-specific PEGylation (Goodson and Katre, 1990; Morpurgo *et al.*, 1996; Veronese, 2001; Yang *et al.*, 2003).

Here, we have employed this final strategy and have prepared homogeneous, site-specifically PEGylated RNase A using maleimide-functionalized PEGs and variants of

RNase A engineered to display a free thiol group at a discrete location on the surface. The influence of PEG chain length, branching order, and position of conjugation on RI-evasion and hence, cytotoxicity, were explored. Additionally, the effect of PEGylation on conformational stability as well as catalytic activity against both large and small substrates was determined.

Protein PEGylation is routinely observed to cause a significant decrease in the biological activity of the conjugate in vitro (Chapman, 2002; Harris and Chess, 2003; Grace et al., 2005). Nevertheless, the dramatically enhanced pharmacokinetics of the protein–polymer conjugate generally more than compensates for this loss, resulting in an overall increase in potency in vivo (Harris and Chess, 2003; Fishburn, 2008). We find this to be the case for site-specifically PEGylated variants of RNase A, as they were much less cytotoxic in vitro than expected based on their complete preservation of catalytic activity and ability to evade RI. Yet, these same conjugates exerted dramatic tumor growth inhibition at low doses in xenograft mice bearing solid human tumors. Site-specific PEGylation therefore represents a means to simultaneously effect RI-evasion while extending serum half-life—increasing the practicality of exploiting mammalian ribonucleases as chemotherapeutics.

4.3 Experimental Procedures

4.3.1 Materials

Escherichia coli BL21(DE3) cells, pET22b(+) and pET27b(+) plasmids were from Novagen (Madison, WI). K-562 (derived from a continuous human chronic myelogenous

leukemia line) and DU 145 (human prostate carcinoma) cell lines were obtained from the

American Type Culture Collection (Manassas, VA). Homozygous (*nu/nu*) nude mice

(male) were from Harlan (Indianapolis, IN). Cell culture medium and supplements

(including Dulbecco's phosphate-buffered saline, DPBS) were from Invitrogen

(Carlsbad, CA). [*methyl*-^{3}H]Thymidine (6.7 Ci/mmol) was from PerkinElmer (Boston,

MA). Enzymes were obtained from Promega (Madison, WI). Ribonuclease substrates

6-FAM–dArUdAdA–6-TAMRA and 6-FAM–dArUdGdA–6-TAMRA were from

Integrated DNA Technologies (Coralville, IA). Poly(C) was from Midland Certified

Reagents (Midland, TX). mPEG–maleimide (2-kDa; **4.1**; Figure 4.2) was from SunBio

(Anyang City, South Korea). mPEG–maleimide (20-kDa; **4.2**; Figure 4.2),

mPEG$_2$–maleimide (20-kDa; **4.3**; Figure 4.2), mPEG–succinimidyl propionate (5-kDa;

4.4; Figure 4.2), and mPEG$_2$–*N*-hydroxysuccinimide (20-kDa; **4.5**; Figure 4.2) were from

Nektar Therapeutics (Huntsville, AL). FPLC HiLoad 26/60 Superdex G75 and G200

gel-filtration columns, HiTrap Desalting, SP, and Q columns (5 mL) were from

GE Healthcare (Uppsala, Sweden). BCA Protein Assay Kit and *N*-ethylmaleimide were

from Pierce (Rockford, IL). Gel-filtration standards, SDS–PAGE molecular weight

standards, and pre-cast gels for poly(acrylamide) electrophoresis were from BioRad

(Hercules, CA). Flat-bottom, black polystyrene, assay plates (96-well) with non-binding

surface were from Corning Life Sciences (Acton, MA). Acetylated-BSA

(pharmacokinetic assays) was from Sigma Chemical (St. Louis, MO). Black non-treated

96-well plates (pharmacokinetic assays) were from NUNC (Rochester, NY). All other

chemicals used were of commercial reagent grade or better, and were used without further purification.

Terrific Broth (TB) contained (in 1.00 L) tryptone (12 g), yeast extract (24 g), glycerol (4 mL), KH_2PO_4 (2.31 g), and K_2HPO_4 (12.54 g). Phosphate-buffered saline (PBS) used for dialysis of purified proteins and conjugates contained (in 1.00 L) NaCl (8.0 g), KCl (2.0 g), $Na_2HPO_4 \cdot 7H_2O$ (1.15 g), KH_2PO_4 (2.0 g), and NaN_3 (0.10 g), and had pH 7.4.

4.3.2 Analytical Instruments

[*methyl*-^{3}H]Thymidine incorporation into K-562 and DU 145 genomic DNA was quantitated by scintillation counting using a Microbeta TriLux liquid scintillation and luminescence counter (PerkinElmer, Wellesley, MA). The mass of protein variants and PEGylated conjugates was confirmed by MALDI–TOF mass spectrometry using a Voyager-DE-PRO Biospectrometry Workstation (Applied Biosystems, Foster City, CA) in the campus Biophysics Instrumentation Facility. Cuvette-scale fluorescence measurements were made using a QuantaMaster1 photon-counting fluorometer equipped with sample stirring (Photon Technology International, South Brunswick, NJ). Fluorescence-based competition assays performed in 96-well plate format were read using a Perkin–Elmer EnVison 2100 Plate Reader in the Keck Center for Chemical Genomics at the University of Wisconsin–Madison. Thermal denaturation data were acquired using a Cary 400 Bio double-beam spectrophotometer equipped with a Cary

temperature controller (Varian, Palo Alto, CA) in the campus Biophysics Instrumentation Facility.

4.3.3 Production of Ribonucleases and Ribonuclease Inhibitor

cDNA encoding RNase A variants was created by oligonucleotide-mediated site-directed mutagenesis using a pET22b(+) or pET27b(+) plasmid that contained cDNA encoding wild-type RNase A or D38R/R39D/N67R/G88R variants, respectively (Leland *et al.*, 1998; Rutkoski *et al.*, 2005). ONC, wild-type RNase A, G88R and D38R/R39D/N67R/G88R RNase A variants were produced as described previously (delCardayré *et al.*, 1995; Leland *et al.*, 1998; Rutkoski *et al.*, 2005). Free cysteine-containing variants of RNase A (A19C, G88C, and D38R/R39D/N67R/G88C) were prepared in a similar fashion, but with the following exceptions: the protein solution containing dissolved inclusion bodies was diluted 10-fold with a thoroughly degassed acetic acid solution (20 mM), centrifuged to remove precipitant, and dialyzed overnight against aqueous acetic acid (20 mM) that had been purged with $N_2(g)$ or $Ar(g)$. Ribonucleases were refolded ≥3 days at 4 °C following slow dilution into 0.10 M Tris–HCl buffer at pH 8.0, containing NaCl (0.10 M), L-arginine (0.5 M), EDTA (10 mM), reduced glutathione (1.0 mM), and oxidized glutathione (0.2 mM). The refolding solution was purged with $N_2(g)$ or $Ar(g)$ prior to the addition of denatured protein to prevent oxidation of the free cysteine residues. Following gel-filtration purification, the thiol groups of the engineered, unpaired cysteine residues introduced at positions 19 or 88 were protected from inadvertent air oxidation with 5,5'-dithiobis(2-nitrobenzoic acid) as

previously described (Messmore *et al.*, 1995). Finally, the 2-nitro-5-thiobenzoic acid-protected ribonuclease was applied to a HiTrap SP cation-exchange column and eluted with a linear gradient of NaCl (0.15–0.40 M) in 50 mM sodium acetate buffer at pH 5.0 and stored at 4 °C until subsequent modification with maleimide-derivatized monomethoxypoly(ethylene glycol) (mPEG or mPEG$_2$). Protein concentration (excluding 2-nitro-5-thiobenzoic acid -protected ribonuclease) was determined either by bicinchoninic acid method (Smith *et al.*, 1985) or by UV spectroscopy using an extinction coefficient of $\varepsilon_{278} = 0.72$ mg·ml^{-1}cm^{-1} for RNase A and its variants (Sela *et al.*, 1957) and $\varepsilon_{280} = 0.87$ mg·ml^{-1}cm^{-1} for ONC (Leland *et al.*, 1998).

Human RI (hRI) was prepared as described previously (Klink *et al.*, 2001; Rutkoski *et al.*, 2005; Smith, 2006). Freshly prepared RI was confirmed to be 100% active by its ability to titrate the ribonucleolytic activity of wild-type RNase A.

Following purification, each ribonuclease and hRI migrated in a single band during SDS–PAGE, confirming their purity and apparent molecular weight. In addition, the identity of each purified ribonuclease and PEGylated variant was confirmed by MALDI–TOF mass spectrometry (Table 4.1; Figure 4.4).

4.3.4 Design of PEGylated Variants of RNase A

To enhance the ability of RNase A to evade hRI, we sought to address three aspects of PEG attachment: the site on the protein where the PEG is coupled, the size of the PEG moiety, and the branching order of the PEG moiety. Specifically, we wanted to test the hypothesis that greater evasion would be observed if the locus of attachment for the PEG

prosthesis on RNase A was within the RI·RNase A interface. Position 88 on RNase A was chosen as the point of attachment within the complex interface (Figure 4.1), as single amino-acid substitutions at this residue have been found to destabilize greatly the RI·RNase A complex (Leland *et al.*, 1998; Rutkoski *et al.*, 2005). Position 19 of RNase A, on the other hand, was chosen as a representative site outside of the RI–RNase A interface because non-proteinaceous appendages, *e.g.*, fluorescein, have been attached at this location previously without any detectable reduction in the affinity of the ribonuclease for RI (Kothandaraman *et al.*, 1998; Abel *et al.*, 2002).

We selected three different PEG chains (**4.1–4.3**; Figure 4.2) for conjugation as size (Harris and Chess, 2003) and branching (Monfardini *et al.*, 1995) have both been reported to impact the biochemical properties of conjugates in vitro (Monfardini *et al.*, 1995) and the behavior of conjugates in whole organisms (Yamaoka *et al.*, 1994). We chose two different masses of PEG, 2-kDa (**4.1**) and 20-kDa (**4.2** and **4.3**). For the 20-kDa mPEG, both linear **4.2** and bifurcated structures, consisting of two 10-kDa arms **4.3**, were explored.

4.3.5 Thiol-specific PEGylation of RNase A Variants

The pH of the protein solution containing 2-nitro-5-thiobenzoic acid-protected ribonucleases in HiTrap SP elution buffer was adjusted from 5 to 7.4–8.0 by the addition of either 10% (v/v) 10× PBS and/or 1.0 M Tris–HCl buffer at pH 8.0. The protecting group was removed by the addition of DTT (5-fold molar excess) and allowing the reaction to proceed at room temperature for ≥5 min, resulting in the immediate generation

of the yellow 2-nitro-5-thiobenzoic acid (Ellman, 1958). DTT and salt were removed

from the ribonucleases using a HiTrap desalting column equilibrated with 0.1 M sodium

phosphate buffer at pH 6.0 containing EDTA (2 mM). A 10-fold molar excess of **4.1**, **4.2**

or **4.3** was dissolved in a small volume of 0.1 M sodium phosphate buffer at pH 6.0

containing EDTA (2 mM) and added to the solution containing a deprotected

ribonuclease (50–250 μM). PEGylation reactions were protected from light and allowed

to proceed at room temperature for 2 h or overnight at 4 °C. Reactions were terminated

by ~6-fold dilution with 50 mM sodium acetate buffer at pH 5.0 and application to a

column of HiTrap SPHP cation-exchange resin equilibrated with the same buffer.

PEGylated and unmodified RNase A variants were differentially eluted from the column

with a linear gradient of NaCl (0–0.4 M) in 50 mM sodium acetate buffer at pH 5.0

(Figure 4.3). For 2-kDa mPEG-modified A19C RNase A, the smaller PEG moiety did not

sufficiently reduce the interaction with the ion-exchange resin to achieve baseline

separation from unmodified ribonuclease. Hence, this conjugate was instead purified by

chromatography using a HiLoad 26/60 G75 Superdex gel-filtration column. All

PEGylated variants of RNase A were assayed by SDS–PAGE and found to be ≥98%

homogeneous, containing only trace amounts of unmodified ribonuclease and no free

PEG (Figure 4.5). Proteins were concentrated and dialyzed extensively against 1× PBS.

Protein concentrations of PEGylated RNase A variants were determined in the same

manner as described above for the unmodified ribonucleases. The presence of the PEG

moieties was found not to interfere with either method of quantitation.

A second batch of 20-kDa mPEG$_2$–G88C RNase A was prepared in a slightly different fashion than the first (Scheme 4.1). Briefly, ~66 mg of 20-kDa mPEG$_2$–N-hydroxysuccinimide **4.5** was dissolved in 2 mL of 0.20 M NaHCO$_3$ buffer at pH 8.1 containing NaCl (0.10 M) and reacted with a 20-fold molar excess of N-(2-aminoethyl)maleimide trifluoroacetic acid salt **4.6**, which was synthesized in house as described previously (Antczak *et al.*, 2001), at room temperature for 30 min, protected from light. Maleimide-derivatized mPEG$_2$ **4.7** was then separated from excess N-(2-aminoethyl)maleimide by applying the crude reaction mixture to a HiTrap desalting column equilibrated with 1× DPBS (Invitrogen) and collecting the salt-free, PEG-containing fractions that eluted rapidly. This 20-kDa mPEG$_2$–maleimide was reacted subsequently with G88C RNase A as described above for **4.3**. 20-kDa mPEG$_2$–G88C RNase A prepared in this manner behaved identically to the conjugate prepared with commercially obtained 20-kDa mPEG$_2$–maleimide **4.3** (*i.e.*, SDS–PAGE migration, enzymatic activity assays; data not shown).

4.3.6 Amine-Specific PEGylation of Wild-type RNase A

Wild-type RNase A was desalted into 0.1 M sodium phosphate buffer at pH 7.4 using a HiTrap desalting column. One molar equivalent of 5-kDa mPEG–succinimidyl propionate (SPA) **4.4** was reacted with RNase A (238 µM) at room temperature for 1 h. Unreacted SPA groups were then quenched by the addition of ethanolamine to a final concentration of 0.5 M. The result was a mixture of 5-kDa mPEG–RNase A conjugates modified with 0–2 PEG groups as evidenced by SDS–PAGE analysis (data not shown).

These differentially PEGylated proteins were separated by applying the quenched reaction to a HiLoad 26/60 Superdex G200 equilibrated with 0.10 M sodium acetate buffer at pH 5.0 containing NaCl (0.10 mM) and sodium azide (0.05%).

4.3.7 N-Ethylmaleimide Modification of G88C RNase A

G88C RNase A was modified with N-ethylmaleimide under conditions similar to those used to perform the thiol-specific PEGylation of RNase A variants with the following exceptions: deprotected G88C RNase A was applied to a HiTrap desalting column equilibrated with 1×PBS containing EDTA (2 mM). Sufficient N-ethylmaleimide (0.1 M in dimethyl formamide; DMF) was added to the protein to achieve a 5-fold molar excess. The reaction was allowed to proceed in the dark at 4 °C overnight, and subsequently quenched by the addition of DTT to a final concentration of 1 mM. The reaction mixture was then diluted 10-fold with 50 mM sodium acetate buffer at pH 5.0, applied to a HiTrap SP HP cation-exchange column, and eluted from the column with a linear gradient of NaCl (0–0.4 M). The mass of the resulting N-ethylmaleimide–G88C RNase A conjugate was confirmed by MALDI–TOF mass spectrometry $(m/z_{obs} = 13,857.32; m/z_{calc} = 13,853.13)$.

4.3.8 Analysis and Characterization of PEGylated RNase A Variants

Analytical size-exclusion chromatography. One mg of protein in one mL of gel-filtration buffer was applied to a HiLoad 26/60 Superdex G200 gel-filtration column and eluted with 50 mM sodium acetate buffer at pH 5.0 containing NaCl (0.10 M) and NaN$_3$

(0.05%) at a flow rate of 4 mL/min. Gel-filtration standards were prepared and separated using the same column according to the guidelines of the manufacturer.

Measurements of conformational stability. PEGylated variants of RNase A were dialyzed exhaustively against 1×PBS and diluted to a concentration of ~25 μM in PBS. Assays were performed by incremental heating (0.15 °C/min from 25–80 °C) and measurement of the absorbance at 287 nm, which decreases as RNase A is denatured and its six tyrosine residues become more exposed to solvent (Hermans and Scheraga, 1961; Eberhardt *et al.*, 1996). Data were collected and analyzed with the program THERMAL from Varian Analytical Instruments (Walnut Creek, CA), which fits the data to a two-state process and enables the determination of the value of T_m —the temperature at the midpoint of the transition between the folded and unfolded states (Pace *et al.*, 1998).

Assays of ribonuclease inhibitor binding. The affinity of PEGylated RNase A variants for hRI was determined by using a variation of a fluorescence-based competition assay (Abel *et al.*, 2002) that was modified as recently reported (Lavis *et al.*, 2007). The basis for this assay is a 38% reduction in fluorescence intensity of 2′,7′-diethylfluorescein-labeled A19C/G88R RNase A upon binding to RI—the K_d value for this interaction being 1.4 nM. Values of K_d for new variants of RNase A were obtained by the addition of varying concentrations of unlabeled competitor (Lavis *et al.*, 2007).

Assays of catalytic activity. *6-FAM–dArUdAdA–6-TAMRA*. The ribonucleolytic activities of RNase A and its PEGylated variants were determined by assaying their ability to cleave the hypersensitive fluorogenic substrate 6-FAM–dArUdAdA–6-TAMRA

(20 nM), which exhibits a ~180-fold increase in fluorescence (λ_{ex} = 493 nm and

λ_{em} = 515 nm) upon cleavage (Kelemen *et al.*, 1999). Assays were carried out at ambient

temperature in 2.0 mL of 0.10 M MES–NaOH buffer at pH 6.0, containing NaCl

(0.10 M). The MES used to prepare the assay buffer was purified by anion-exchange

chromatography to remove trace amounts of oligomeric vinylsulfonic acid, which is a

byproduct of commercial buffer synthesis and has been shown to be a potent inhibitor of

RNase A (Smith *et al.*, 2003). Values of k_{cat}/K_M were obtained as reported previously

(Kelemen *et al.*, 1999). Activity values for ONC were determined at room temperature in

2.0 mL of OVS-free 20 mM MES–NaOH buffer at pH 6.0, containing NaCl (0.010 M)

using the substrate 6-FAM–dArUdGdA–6-TAMRA (50 nM) (Lee and Raines, 2003).

Poly(C). Poly(C) (ε = 6,200 $M^{-1}cm^{-1}$ per nucleotide at 268 nm) is hyperchromic

which allows the ribonuclease-catalyzed cleavage of this substrate to be monitored by the

increase in UV absorption ($\Delta\varepsilon$ = 2,380 $M^{-1}cm^{-1}$ at 250 nm) (delCardayré and Raines,

1994). Assays were performed at room temperature in 0.10 M MES–NaOH buffer at

pH 6.0, containing NaCl (0.10 M), poly(C) (0.010–1.5 mM), and enzyme (2 nM for

RNase A and its PEGylated variants). Values of k_{cat} and K_M were obtained after fitting

initial velocity data to the Michaelis–Menten equation with GraphPad Prism (GraphPad

Software Inc., San Diego, CA).

Assays of cytotoxicity. The cytotoxic activities of RNase A, its variants, PEGylated

variants, and ONC were determined by measuring the incorporation of

[*methyl*-^{3}H]thymidine into the cellular DNA of K-562 cells in the presence of

ribonucleases as described previously (Leland *et al.*, 1998). All cytotoxicity assays were

repeated at least three times and done in triplicate. Each data point represents the mean of three or more experimental values ($\pm$ SE). IC_{50} values were calculated by fitting the curves using nonlinear regression to a sigmoidal dose–response curve as reported previously (Rutkoski *et al.*, 2005).

4.3.9 Xenograft Mouse Studies

Variants and PEGylated conjugates of RNase A were tested for their ability to suppress the growth of human tumors implanted into the flanks of nude mice. The DU 145 tumor cell line was selected both for its ability to proliferate in mice and its low rate of spontaneous regression. Importantly, the DU 145 tumor line represents a clinically relevant target and is used frequently in the testing of new chemotherapeutic agents. The cell lines were implanted into the right rear flank of 5–6 week old male homozygous (*nu/nu*) nude mice. Tumors were allowed to grow to an average size of ≥ 75 mm^3 before initiation of treatment. Xenograft animals, with the properly-sized tumors, were divided into treatment groups. All test ribonucleases were diluted in PBS (drug vehicle) and, to serve as a negative control, one set of animals was treated with vehicle alone on the dosing schedule with greatest frequency. All treatments were administered by intraperitoneal (i.p.) injection, and the volume of drug/vehicle injected was based upon the body weight of the animal (10 μL/g). Treatment with all agents was ongoing throughout the entire experiment. Tumor size was measured twice weekly using calipers, and tumor volume (mm^3) was determined by using the formula for an ellipsoid sphere (eq 4.1):

$$\text{tumor volume} = \frac{l \times w^2}{2} \qquad (4.1)$$

The percent tumor growth inhibition (% TGI) was calculated by using eq 4.2:

$$\%\text{TGI} = 1 - \left(\frac{(\text{volume}_{\text{final}} - \text{volume}_{\text{inital}})_{\text{treated}}}{(\text{volume}_{\text{final}} - \text{volume}_{\text{inital}})_{\text{control}}} \right) \times 100 \qquad (4.2)$$

2-kDa mPEG–G88C RNase A and 20-kDa mPEG$_2$–G88C RNase A were both used to treat DU 145 xenograft mice. 2-kDa mPEG–G88C RNase A treatment was administered at a dose of 11.2 or 15 mg/kg (i.p.; 2 × wk); 20-kDa mPEG$_2$–G88C RNase A treatment was administered at a dose of 75 mg/kg (i.p.; 1 × wk). DU 145 xenograft mice each received 2.89×10^6 cells that had been grown in DMEM media containing FBS (10% v/v).

4.3.10 Pharmacokinetic Studies

Ribonucleolytic activity remaining in the serum of mice was used to monitor the amount of injected ribonuclease remaining in circulation over time. The method was similar to one reported previously (Tarnowski *et al.*, 1976), except for the assay used to quantify ribonuclease activity. Blood was collected from two or three mice by nicking the tail vein at various time intervals after dosing. The blood was allowed to clot for 30 min at 2–8 °C and then subjected to centrifugation (~1500×g) for 5–10 min. Serum samples were stored frozen in the dark at –80 °C, and thawed on ice prior to analysis. Ribonucleolytic activity in the serum samples was assayed in a 96-well plate using the fluorogenic substrate 6-FAM–dArUdAdA–6-TAMRA. Pre-diluted serum (10 µL of a 1:10,000 dilution) was added to wells (160 µL/well) containing 0.1 M Tris–HCl buffer at

pH 7.0, containing NaCl (0.10 M) and acetylated BSA (0.1 mg/mL). The assay was initiated by the addition of substrate (30 μL of a 1.33 μM stock solution). Fluorescence was monitored using a Tecan Safire plate reader with excitation and emission wavelengths of 490 and 525 nm, respectively.

4.4 Results

4.4.1 Specificity of Maleimide-derivatized mPEG

Near pH 7, maleimides are at least 10^3-fold more reactive toward thiols than primary amines (Ji, 1983). To ascertain whether the variants of RNase A were being modified at residues other than cysteine, wild-type RNase A was subjected to a sham PEGylation with a 10-fold excess of 20-kDa mPEG–maleimide. The procedure reproduced exactly the conditions used to prepare the other PEGylated conjugates described above, including exposure to 5-fold molar excess of DTT and desalting into 0.1 M sodium phosphate buffer at pH 6.0 containing EDTA (2 mM). All proteinaceous material from the PEGylation reaction eluted from a HiTrap cation-exchange column as a single peak at a salt concentration (0.32 M) consistent with the material being unmodified RNase A (data not shown). This assignment was confirmed by both MALDI–TOF mass spectrometry (m/z_{obs} = 13,683.14; m/z_{calc} = 13,682) and SDS–PAGE, during which its retention was identical to that of unmodified RNase A (data not shown). Therefore, we were confident that in all of the subsequently prepared PEGylated variants of RNase A, the mPEG is attached through the added free cysteine residue, as designed.

4.4.2 Biophysical Analysis of PEGylated RNase A Variants

Proteins derivatized with PEG or other large linear hydrophilic polymers tend to behave as larger species than would be expected for globular proteins of the same mass (Kurfürst, 1992; Harris and Chess, 2003). We were interested in determining both the actual mass of the conjugates (for the purpose of confirming our site-specific mono-PEGylation) and how these conjugates behave during molecular sieving techniques for the purpose of correlating apparent mass (i.e., effective molecular size) with enhanced persistence in circulation in vivo. For this reason we characterized the mass of the PEGylated variants of RNase A by MALDI–TOF mass spectrometry, SDS–PAGE, and size-exclusion chromatography.

The observed masses for the PEGylated conjugates were consistent with the attachment of only one PEG moiety of the expected mass to the free cysteine-containing variants of RNase A (Table 4.1). The larger discrepancies between calculated and observed m/z values for the PEGylated variants of RNase A reflect the broad ion peaks that were observed and are a result of the polydispersity of the PEG moiety (Figure 4.4).

The apparent molecular weights of the PEGylated variants of RNase A determined by using SDS–PAGE (Figure 4.5) were significantly higher than those observed by MALDI–TOF mass spectrometry as exemplified by the 20-kDa mPEG–A19C RNase A conjugate (m/z_{obs} = 35,872 Da) whose observed $MW_{app,SDS–PAGE}$ was 61.1 kDa—nearly twice the actual mass of this conjugate. This phenomenon has been routinely observed for PEGylated proteins and has been attributed to both the extensively hydrated and extended nature of the PEG polymer as well as the ability of the PEG to shield the charge of the

protein, thus reducing the electrophoretic force experienced by the protein (Kurfürst, 1992). It is also worth noting that the apparent mass of the bifurcated mPEG$_2$ conjugates is roughly 10% greater than that of the linear mPEG conjugates of nearly equivalent mass, presumably due to the greater hydrodynamic volume of the branched polymer (Veronese *et al.*, 1997), although this assumption has recently been challenged (Fee, 2007).

Size-exclusion chromatography (SEC) was performed as an additional method of characterizing the size and shape of these PEGylated variants of RNase A (Figure 4.6). The apparent molecular weights observed by SEC are reported in Table 4.1. The PEGylated variants of RNase A were found to behave as much larger species by SEC than by either MALDI–TOF mass spectrometry or SDS–PAGE analysis. Interestingly, and in contrast to the SDS–PAGE results, there was no significant difference in the apparent masses of the linear and branched 20-kDa mPEG conjugates, suggesting that they possess the same viscosity radii (Fee and Van Alstine, 2004; Fee, 2007). Of particular note is the heterogeneity observed for the 2-kDa mPEG–G88C RNase A as evidenced by the broad leading shoulder with two conspicuous peaks at ~189 mL (54.2 kDa) and ~168 mL (97.3 kDa) which were presumed to result from a greater degree of polydispersity in the original PEG reagent, despite the low polydispersity reported by the manufacturer (1.02). Without further testing we could not rule out the possibility that these leading shoulders are due to the presence of aggregates of PEGylated proteins, although the local maxima of these shoulders are not consistent with an integer number of associated conjugates.

4.4.3 Assays of Ribonucleolytic Activity

Activity against 6-FAM–dArUdAdA–6-TAMRA. Preservation of ribonucleolytic

activity is essential to the cytotoxic activity of pancreatic-type ribonucleases (Kim *et al.*,

1995a). For this reason, the catalytic activity of each PEGylated ribonuclease was

assayed to ascertain if the attachment of the PEG moiety at either position had a

deleterious effect on the ability of the enzyme to degrade RNA. Values of k_{cat}/K_M for

wild-type RNase A, G88R RNase A, PEGylated variants of RNase A, and ONC are listed

in Table 4.2. The k_{cat}/K_M values of wild-type RNase A, G88R RNase A, and ONC were

6.7×10^7, 7.4×10^7, and 2.2×10^5 $M^{-1}s^{-1}$, respectively, which are in good agreement with

values reported previously (Haigis *et al.*, 2002; Lee and Raines, 2003). Modification of

the A19C or G88C variant with PEG had no measurable influence on its ability to cleave

the relatively small 6-FAM–dArUdAdA–6-TAMRA substrate, regardless of the size or

branching of the polymeric substituent. The 20-kDa mPEG–D38R/R39D/N67R/G88C

RNase A showed a modest, 2.3-fold decrease in catalytic activity, in agreement with the

slightly reduced value of k_{cat}/K_M observed for the unmodified D38R/R39D/N67R/G88R

variant (Rutkoski *et al.*, 2005). Therefore, the presence of PEG at either position 19 or 88

was found to have a benign effect on the catalytic activity of RNase A as determined by

its ability to degrade the 6-FAM–dArUdAdA–6-TAMRA substrate.

Catalysis of Poly(C) cleavage. The catalytic activity of RNase A and its PEGylated

variants toward polymeric RNA was also determined, as its greater length (compared to

that of 6-FAM–dArUdAdA–6-TAMRA) is probably more similar to actual physiological

substrates and possibly more sensitive to the presence of PEG appendages. The poly(C)

used in these assays had >250 bases with an average size of 300–800 bases, according to the manufacturer. All PEGylated conjugates of G88C RNase A were active catalysts of poly(C) cleavage (Table 4.3). The catalytic efficiency of the PEGylated RNase A conjugates were only slightly reduced (<2-fold) and exhibited k_{cat}/K_M values that ranged from 66% (20-kDa mPEG$_2$–G88C RNase A) to 79% (2-kDa mPEG–G88C RNase A) of the native unmodified enzyme. It is interesting to note that the observed slightly diminished catalytic efficiency was a result of larger K_M values for these PEG-modified enzymes. The K_M values increased with both the size and the branching order of the attached PEG possibly indicative of a slightly less accessible enzymic active site for these PEGylated conjugates.

4.4.4 Preparation of Amine-PEGylated Ribonucleases

Wild-type RNase A was PEGylated with mPEG-succinimidyl propionate, which is specific for primary amines. Unmodified, mono-, and di-PEGylated forms of RNase A were isolable by gel-filtration chromatography. To determine the effect of differential PEG modification on the enzymatic activity of RNase A, the k_{cat}/K_M values of these three species were determined using 6-FAM–dArUdAdA–6-TAMRA as a substrate and found to be 8.34×10^7, 6.26×10^7, and 3.63×10^7 $M^{-1}s^{-1}$, respectively, which represent 75% and 43 % wild-type activity for the mono- and di-PEGylated conjugates. This reduction in catalytic activity is in agreement with results from previous amine-reactive PEGylation of RNase A (Monfardini *et al.*, 1995).

4.4.5 Assay of Conformational Stability

Pancreatic-type ribonucleases must maintain their conformational stability in order to exert their cytotoxic effects within a cell (Klink and Raines, 2000). Furthermore, several groups have reported the presence of PEG moieties having altered the thermal stability of the protein to which it was attached (Monfardini *et al.*, 1995; Ramon *et al.*, 2005; Lee *et al.*, 2007). For these reasons the conformational stability of each of the PEGylated variants of RNase A was determined (Figure 4.7) and is reported in Table 4.2. Wild-type RNase A and G88R RNase A were found to have T_m values of 63.7 and 63.2 °C, consistent with previous results (Leland *et al.*, 1998). Interestingly, all three PEGylated forms of G88C RNase A were found to exhibit slightly increased conformational stability with T_m values ranging from 64.2–64.4 °C. The degree of stabilization was essentially independent of the size or branching order of the PEG attached. The presence of the PEG was thought unlikely to be the source of the modest stabilization because when these same polymers were attached to A19C RNase A, these conjugates all possessed nearly identical, slightly diminished values of T_m (61.2–61.4 °C). We thus attributed the slight deviations in conformational stability (increased or decreased for G88C and A19C RNase A, respectively) not to the presence of the PEG but to the cysteine amino acid substitution in the amino acid sequence.

As a control, *N*-ethylmaleimide-derivatized G88C RNase A was prepared and its conformational stability was determined. With the exception of the methoxy-PEG moiety, this conjugate possesses an identical atomic composition to that of the

mPEG–G88C RNase A conjugates (linear), including the presence of the thiol-linked maleimide (1-ethyl-pyrolidine-2,5-dione). The N-ethylmaleimide–G88C RNase A conjugate was found to have a T_m value of 64.0 °C which is 0.3 °C higher than of wild-type RNase A, but also 0.3 °C less than the mean T_m value of the mPEG–G88C RNase A conjugates. We conclude from these results that although the amino-acid substitutions in RNase A may not account entirely for the modest deviations in conformational stability for these PEGylated conjugates, the PEG appendage alters the T_m value by <0.5 °C. Finally, the T_m value for 20-kDa mPEG–D38R/R39D/N67R/G88C RNase A was 55.4 °C, which is nearly identical to the T_m value of 56 °C reported for D38R/R39D/N67R/G88R RNase A (Rutkoski et al., 2005) and is consistent with the negligible effect of PEG attachment at the Cys88 position.

4.4.6 Affinity for Ribonuclease Inhibitor

We determined the K_d values for the PEGylated variants of RNase A in complex with hRI. Indeed, the site of PEG attachment was an important determinant of the ability of the ribonuclease to evade RI. The PEGylated A19C RNase A conjugates all possessed K_d values less than 1.2 nM (0.11–0.18 nM) with no obvious correlation with either PEG length or branching. This high affinity for RI is makes it impossible to determine a precise K_d value for these conjugates (which are listed in Table 4.1 as <1.2 nM), as our competition assay has a lower limit in the nanomolar range (Abel et al., 2002) due to the extremely long time periods required to reach equilibrium in these instances.

Attachment of the different PEG groups through Cys88, on the other hand, proved to be much more disruptive to the formation of the RI·RNase A complex. With a K_d value of 8.0 nM, the 2-kDa mPEG–G88C RNase A conjugate was almost 7-fold more evasive than the G88R RNase A variant. Attachment of a much larger linear PEG chain (20-kDa) further reduced the affinity for RI only slightly—to 8.9 nM. Finally, the ability of PEG–G88C RNase A conjugates to evade RI was enhanced more dramatically by utilizing a 20-kDa PEG chain consisting of two 10-kDa arms. This conjugate possessed the largest K_d value of those investigated—37.0 nM (with the exception of 20-kDa mPEG–D38R/R39D/N67R/G88C RNase A, which contains additional amino-acid substitutions for the purpose of enhancing RI evasion). The presence of a 20-kDa mPEG$_2$ moiety at this position is more than 30-fold more effective at precluding the binding of RI than an arginine side chain.

Attachment of a PEG group at position 88 in the context of other amino acids substitutions (D38R/R39D/N67R) that were known to disrupt the RI·RNase A complex (Rutkoski *et al.*, 2005) resulted in the most evasive conjugate, which exhibited a K_d value of 3.31 μM. This conjugate is not only 75 million-fold more RI-evasive than the native enzyme but also more evasive than the most highly evasive variant reported previously, K7A/D38R/R39/G88R RNase A (K_d = 2.9 μM) (Rutkoski *et al.*, 2005).

4.4.7 Cytotoxicity

The toxicity of wild-type RNase A, G88R RNase A, D38R/R39D/N67R/G88R RNase A and the PEGylated variants of RNase A was measured with the K-562 human

leukemia cell line. IC_{50} values were derived from the data in Figure 4.8 as reported

previously (Rutkoski *et al.*, 2005) and are reported in Table 4.2. The IC_{50} values for the

G88R and D38R/R39D/N67R/G88R variants were in gratifying agreement with those

determined previously (Rutkoski *et al.*, 2005). None of the PEGylated variants of

RNase A exhibited any toxicity toward the K-562 cells even at concentrations of 25 μM,

with the exception of the 2-kDa mPEG–G88C RNase A and 20-kDa mPEG–

D38R/R39D/N67R/G88C RNase A conjugates, which had IC_{50} values of 10.4 and

1.9 μM, respectively.

4.4.8 Animal Studies

Xenograft studies. Nude mice bearing DU 145 prostate carcinoma tumors were used

for initial animal studies, as the DU 145 cell line had been shown previously to be

sensitive to variants of RNase A (Rutkoski *et al.*, 2005). 2-kDa mPEG–G88C RNase A

(K_d = 8.0 nM) was selected for initial in vivo studies as this variant of RNase A had

demonstrated in vitro cytotoxicity (Figure 4.8; IC_{50} = 1.9 μM). In a preliminary

experiment, 2-kDa mPEG–G88C RNase A (15 mg/kg; 2×wk; i.p.) significantly inhibited

tumor growth (TGI = 73%) while displaying only minor toxic side effects as monitored

by change in body weight (–2%; inset) (Figure 4.9A). Even at a slightly reduced dose

(11.2 mg/kg; 2×wk; i.p.), 2-kDa mPEG–G88C RNase A effected comparable tumor

growth inhibition (TGI = 73%) to that of much more evasive unPEGylated variants

(D38R/R39D/N67R/G88R RNase A, DRNG, TGI = 62%, K_d = 510 nM;

K7A/D38R/R39D/G88R RNase A, KDRG, TGI = 86%, K_d = 2.9 μM) that were

administered both more frequently and at a higher dose (15 mg/kg; $qd \times 5$; i.p.)

(Figure 4.9B). Also noteworthy is that among the three treatment groups in Figure 4.9B, 2-kDa mPEG–G88C RNase A was better tolerated than the DRNG or KDRG variants, as indicated by change in body weight over the duration of the experiment (–2% versus –16 and –6%, respectively). Finally, the significantly larger and more RI-evasive 20-kDa mPEG$_2$–G88C RNase A (K_d = 37.0 nM) was tested for its ability to inhibit tumor growth in vivo despite its lack of in vitro efficacy. A once-weekly dose of 20-kDa mPEG$_2$–G88C RNase A (75 mg/kg; 1×wk; i.p.) inhibited tumor growth nearly completely (TGI = 93%) and was, in fact, comparable in efficacy to Docetaxel (TGI = 103%; 8 mg/kg; 1×wk; i.p.), an FDA-approved anti-mitotic chemotherapeutic (Figure 4.9C). The weekly dose of 20-kDa mPEG$_2$–G88C RNase A is 2.5-fold greater (by mass) than that of the 2-kDa mPEG–G88C RNase A. Importantly, it should be noted, that because of the much larger PEG moiety in 20-kDa conjugate, the number of ribonuclease molecules administered each week is quite comparable in panels 4.9A and 4.9C (1.9 μmol/kg/wk and 2.2 μmol /kg/wk, respectively). The 20-kDa mPEG$_2$–G88C RNase A was well-tolerated as indicated by the 2% increase in body weight over the duration of the study.

To control for any physiological differences between the DU 145 and K-562 cell lines that might alter their response to the PEGylated variants of RNase A, in vitro cytotoxicity assays were performed using the DU 145 cell line using the same [*methyl*-^{3}H]thymidine incorporation assay described for the K-562 cell line. In fact, the DU 145 cell line was even *less* sensitive to PEG–G88C RNase A than was the K-562 cell line. 2-kDa mPEG–

G88C RNase A, 20-kDa mPEG–G88C RNase A, and 20-kDa mPEG$_2$–G88C RNase A

each had an IC$_{50}$ value of >25 μM (data not shown). ONC was used as a cytotoxic control

and had an IC$_{50}$ ~0.2 μM (data not shown) which is comparable to the value reported

previously for ONC against DU 145 cells (Rutkoski et al., 2005). Hence, the efficacy of

2-kDa mPEG–G88C RNase A and 20-kDa mPEG$_2$–G88C RNase A in DU 145 xenograft

mice cannot be attributed to a greater in vitro sensitivity of this cell line.

Pharmacokinetic analysis. RNase A clears rapidly ($t_{1/2}$ = 5 and 3.5 min from rats and

mice, respectively) from the bloodstream of organisms (Tarnowski et al., 1976),

consistent with what is known about the renal clearance of small proteins

(Venkatachalam and Rennke, 1978; Maack et al., 1979). 5-kDa PEGylated RNase A had

been shown to exhibit a 40- to 50-fold increase in circulation half-life in rats injected IV,

SC, and IM (Schiavon et al., 1991; Láznìček et al., 1993). A similarly large enhancement

was seen for 20-kDa mPEG$_2$–G88C RNase A compared to that of G88R RNase A

(Figure 4.10).

4.5 Discussion

Mammalian ribonucleases have great potential as chemotherapeutics but are limited

by their sensitivity to RI. Previously, we showed that RNase A variants, engineered to

evade RI are potent cytotoxins in vitro (Leland et al., 1998; Haigis et al., 2002; Rutkoski

et al., 2005). In vivo, the relatively small size of pancreatic-type ribonucleases allow for

their rapid clearance via glomerular filtration (Maack et al., 1979; Vasandani et al., 1996;

Maack, 2000). PEGylation has been shown to be a robust strategy for improving the

efficacy of biologic pharmaceutics (Pasut and Veronese, 2007). Here, we set out to address simultaneously both the sub-optimal pharmacokinetic properties of RNase A and its sensitivity to RI by attaching maleimide-PEG to cysteine residues installed by site-directed mutagenesis. The thiol-reactive PEGylation chemistry was chosen to preserve both ribonucleolytic activity and conformational stability, both of which were indeed affected negligibly by PEGylation.

4.5.1 PEGylation Mediates RI-Evasion

The influence of PEGylation on RI-binding had never been examined previously. Based on our results, we can conclude that (1) the site of PEGylation, (2) the length of the attached PEG moiety, and (3) the branching order of the PEG group all influence the affinity for RI. Because mPEG$_2$ functionalization afforded RNase A greater protection against protease degradation (Monfardini et al., 1995), it is perhaps not surprising that the this same effect would extend to inhibitor binding. Furthermore, PEG–RNase A conjugates have also been reported to display a reduced affinity for anti-RNase A antibodies as well as reduced activity towards large RNA substrates (Caliceti et al., 1990), indicating that PEGylation appears to impede association with macromolecules of all kinds. The highly evasive 20-kDa mPEG–D38R/R39D/N67R/G88C RNase A (K_d = 3.3 μM) demonstrates that gains in RI-evasion through PEGylation can be augmented with other amino-acid substitutions. The impressive in vitro cytotoxicity of this conjugate (IC$_{50}$ = 1.9 μM) intimates that this conjugate would exert substantial tumor growth inhibition in vivo. These experiments are on-going in our laboratory.

4.5.2 PEGylation as a Liability for Internalization

Previously (Raines, 1999), the effects of two important determinants of cytotoxicity, catalytic activity and RI-evasion, were integrated with the equation:

$$(k_{cat}/K_M)_{cyto} = \frac{k_{cat}/K_M}{1+[RI]/K_d}$$ (4.3)

where [RI] = 4 µM. The resulting term $(k_{cat}/K_M)_{cyto}$ has been useful both in understanding the relationship between these two properties and as a reliable predictor of cytotoxicity in vitro (Bretscher *et al.*, 2000; Haigis *et al.*, 2003; Rutkoski *et al.*, 2005). Based on its $(k_{cat}/K_M)_{cyto}$ value alone (0.56×10^6 $M^{-1}s^{-1}$), 20-kDa mPEG$_2$–G88C RNase A would be expected to be a relatively potent cytotoxin in vitro with an IC$_{50}$ value (K-562) of ~0.3 µM. Instead, this conjugate demonstrated no measureable cytotoxicity (IC$_{50}$ >25 µM). What is the basis for the failure of otherwise useful eq 4.3? It was shown previously that for variants whose net charge (Z) deviated substantially from that of the wild-type protein (Z = +4), eq 4.1 began to break down. Indeed, the importance of electrostatic interactions for ribonuclease binding and internalization have been well-established (Futami *et al.*, 2001; Fuchs and Raines, 2005; Fuchs *et al.*, 2007; Johnson *et al.*, 2007a). However, 20-kDa mPEG$_2$–G88C RNase A has a net charge of +4. We attribute the lack of in vitro cytotoxicity to inefficient cellular association and internalization as a result of charge-shielding by the PEG group. This hypothesis is supported by the reduced affinity of PEGylated RNase A for cation-exchange resin, which facilitates its separation from unmodified variants of RNase A (Figure 4.3). Diminished binding to this resin could mimic diminished binding to heparan sulfate

proteoglycans (HSPGs), which play an important role in ribonuclease internalization (Soncin *et al.*, 1997; Fuchs and Raines, 2006).

4.5.3 Next Generation of Site-specifically PEGylated RNase A Variants

It is possible that presence of the PEG chain not only impedes cellular association and internalization but also subsequent translocation into the cytosol—about which little is known. It could therefore be advantageous to link the PEG chain via a disulfide bond that would be cleaved in the slightly reducing environment of the endosome (Harris and Chess, 2003). Alternatively, a pH-sensitive linker could accomplish the same goal (Pasut and Veronese, 2007). Secondly, the 20-kDa mPEG$_2$ moieties displayed the greatest bioactivity in vivo. The correlation between PEG size and half-life in circulation has been studied thoroughly, and the glomerular permeability limit for PEG is known to occur at a MW of ~30,000 Da (Yamaoka *et al.*, 1994). Thus, even longer PEG chains could increase the half-life in circulation. Coupling of PEG >20-kDa would also be expected to enhance RI-evasion further. A thorough examination of in vivo bioactivity over a broader mass range of PEG–RNase A conjugates would be required to determine what size PEG enables maximum tumor-growth inhibition. Many competing processes are influenced by PEGylation of mammalian ribonucleases, and each factor must be considered with the overall goal of in vivo efficacy, similar to the approach that was taken to optimize in vitro cytotoxicity (Futami *et al.*, 2002).

4.6 Conclusions

We report for the first time the site-specific PEGylation of RNase A with the aim of reducing sensitivity to RI while simultaneously extending serum half-life. We found that the greatest improvements in RI-evasion are achieved when large, branched PEG groups are attached at positions/locations on the surface of RNase A that make intimate contact with RI at the interface of the RI·RNase A complex. Indeed, for 20-kDa mPEG$_2$–G88C RNase A, the affinity of RNase A for RI was reduced by 8.4×10^5-fold. The ribonucleolytic activity and thermal stability of this conjugate were nearly indistinguishable from wild-type RNase A. The lower cytotoxic activity of the PEGylated conjugates in vitro is attributed to a reduced association of the ribonuclease with the cell membrane due to a charge-shielding effect of the PEG group. This hypothesis is supported by the reduced affinity of PEGylated RNase A for a cation-exchange resin, which permits its facile separation from unmodified variants of RNase A using ion exchange chromatography. Despite the attenuated (in some cases nonexistent) bioactivity of mPEG–G88C RNase A in vitro, these conjugates are as effective at inhibiting tumor growth in xenograft mice as are larger doses of highly-evasive non-PEGylated variants of RNase A administered more frequently. Site-specific PEGylation further expands the promise of mammalian ribonuclease therapeutics by increasing the practicality of their use in whole animals.

Table 4.1 Mass determination of RNase A, its PEGylated variants, and ONC

Ribonuclease	Mass[a] (m/z)		Apparent MW (kDa)	
	Expected	Observed	SDS–PAGE	Gel-filtration
Wild-type RNase A	13 682	13 682	ND	14.0
G88R RNase A	13 781	13 785	18.2	ND
2-kDa mPEG–G88C RNase A	15 810	15 928	21.5	37.9
20-kDa mPEG–G88C RNase A	35 397	35 581	59.5	ND
20-kDa mPEG$_2$–G88C RNase A	34 746	35 702	66.4	ND
2-kDa mPEG–A19C RNase A	15 803	15 927	21.5	ND
20-kDa mPEG–A19C RNase A	35 390	35 872	61.1	268
20-kDa mPEG$_2$–A19C RNase A	34 739	35 372	66.4	260
20-kDa mPEG–D38R/R39D/N67R/G88C RNase A	35 446	35 637	62.8	ND
ONC	11 820	11 825	ND	ND

[a] Values of m/z were determined by MALDI–TOF mass spectrometry.

Table 4.2 Biochemical parameters of RNase A, its PEGylated variants, and ONC

Ribonuclease	$T_m{}^a$ (°C)	$k_{cat}/K_M{}^b$ (10^7 $M^{-1}s^{-1}$)	$K_d{}^c$ (nM)	$(k_{cat}/K_M)_{cyto}$ (10^6 $M^{-1}s^{-1}$)	$IC_{50}{}^d$ (μM)
wild-type RNase A	63.7	6.7 ± 0.3	44×10^{-6}	0.0000009	>25
G88R RNase A	63.3	7.4 ± 0.2	1.2 ± 0.2	0.022	4.6 ± 0.4
2-kDa mPEG–G88C RNase A	64.4	4.0 ± 0.3	8.0 ± 1.3	0.080	10.4
20-kDa mPEG–G88C RNase A	64.2	6.8 ± 0.6	8.9 ± 0.1	0.15	>25
20-kDa mPEG$_2$–G88C RNase A	64.3	6.1 ± 0.4	37.0 ± 2.4	0.56	>25
2-kDa mPEG–A19C RNase A	61.2	5.0 ± 0.4	<1.2	$-.^e$	>25
20-kDa mPEG–A19C RNase A	61.4	7.5 ± 0.2	<1.2	$-.^e$	>25
20-kDa mPEG$_2$–A19C RNase A	61.4	6.9 ± 0.3	<1.2	$-.^e$	>25
20-kDa mPEG–D38R/R39D/N67R/G88C RNase A	55.4	2.9 ± 0.04	$3.3 \pm 0.2 \times 10^3$	13	1.9
ONC	90.0	0.022 ± 0.002	$\geq 10^3$	0.044	0.19

[a] Values of T_m (± 2 °C) were determined in PBS by UV spectroscopy. The T_m values for G88R RNase A and ONC in PBS are from (Leland *et al.*, 1998).

[b] Values of k_{cat}/K_M ($\pm$ SE) are for the catalysis of 6-FAM–dArU(dA)$_2$–6-TAMRA cleavage at room temperature in MES–NaOH buffer (0.10 M) at pH 6.0 containing NaCl (0.10 M) except for the k_{cat}/K_M ($\pm$ SE) of ONC. The k_{cat}/K_M value for ONC is for the catalysis of 6-FAM–dArUdGdA–6-TAMRA cleavage at room temperature in MES–NaOH buffer (0.020 M) at pH 6.0 containing NaCl (0.010 M).

[c] Values of K_d ($\pm$ SE) are for the complex with human RI at room temperature. The K_d value for RNase A is from (Lee *et al.*, 1989). The K_d value for G88R RNase A is from (Lavis *et al.*, 2007). The K_d value for ONC is an estimate from (Wu *et al.*, 1993).

[d] Values of IC_{50} ($\pm$ SE) are for incorporation of [methyl-^{3}H]thymidine into the DNA of K-562 cells.

[e] Values of $(k_{cat}/K_M)_{cyto}$ could not be determined for these conjugates due to the relative uncertainly of their low K_d values (<1.2 nM).

Table 4.3 Steady-state kinetic parameters for catalysis of poly(C) cleavage[a]

Ribonuclease	k_{cat} (s^{-1})	K_M (μM)	k_{cat}/K_M $(\times 10^6 \, M^{-1} s^{-1})$
Wild-type RNase A	368.0 ± 11.0	33.1 ± 2.6	11.2 ± 0.6
2-kDa mPEG–G88C RNase A	422.5 ± 11.5	48.6 ± 5.5	8.8 ± 0.8
20-kDa mPEG–G88C RNase A	428.0 ± 21.0	53.5 ± 4.0	8.0 ± 0.2
20-kDa mPEG$_2$–G88C RNase A	401.5 ± 15.5	54.8 ± 2.4	7.4 ± 0.6

[a] The ribonuclease-catalyzed cleavage of poly(C) was monitored by the increase in UV absorption ($\Delta\varepsilon = 2{,}380 \, M^{-1} cm^{-1}$ at 250 nm). Assays were performed at room temperature in 0.10 M MES–NaOH buffer at pH 6.0, containing NaCl (0.10 M), poly(C) (0.010–1.5 mM), and enzyme (2 nM for RNase A and its PEGylated variants). Kinetic parameters ($\pm$ SE) were obtained after fitting initial velocity data to the Michaelis–Menten equation.

Table 4.4 Relative activity of amine-PEGylated wild-type RNase A

No. of PEG chains[a]	k_{cat}/K_M [b] $(10^7 \text{ M}^{-1}\text{s}^{-1})$	Relative Activity (%)
0	8.35 ± 0.11	100
1	6.26 ± 0.80	75
2	3.63 ± 0.29	43

[a] PEG-mers were separated by gel-filtration chromatography and stoichiometry was confirmed by SDS–PAGE and MALDI–TOF mass spectrometry.

[b] Values of k_{cat}/K_M (± SE) are for the catalysis of 6-FAM–dArU(dA)$_2$–6-TAMRA cleavage at room temperature in 0.10 M MES–NaOH buffer (pH 6.0) containing NaCl (0.10 M).
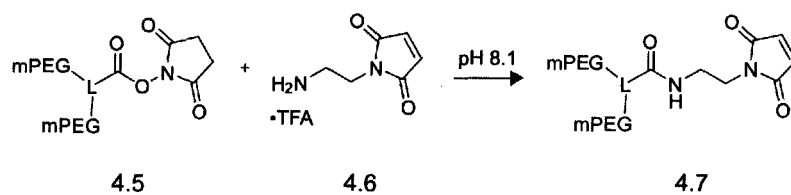
Scheme 4.1 Derivatization of 20-kDa mPEG$_2$-N-hydroxysuccinimide with

N-(2-aminoethyl)maleimide to yield a thiol-reactive branched mPEG$_2$.
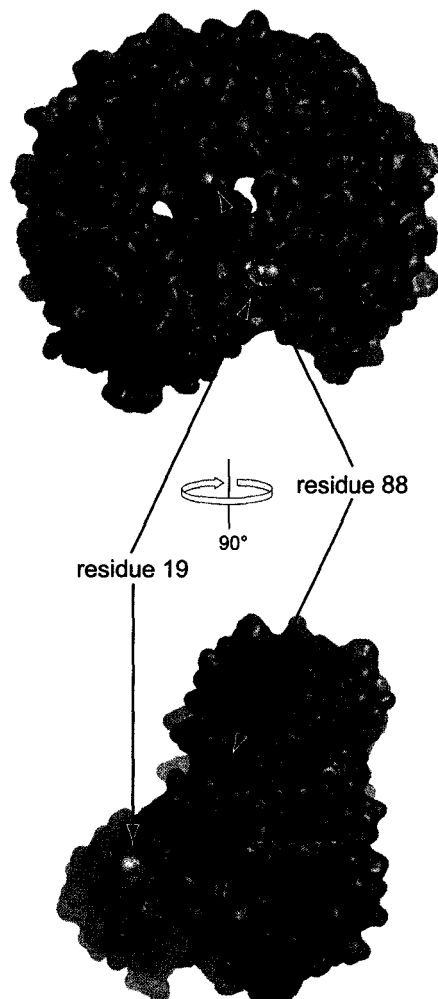
Figure 4.1   Ribbon diagram of RI·RNase A complex depicting the locations where

cysteine residues were installed for thiol-specific PEGylation. The *virtual*

amino acid substitutions of A19C and G88C were made in RNase A (blue)

and the atoms of these new residues are shown explicitly as spheres

(yellow). RI is shown in red. Images and models were made using PyMol

(Delano Scientific) and the atomic coordinates from PDB entry 1dfj (Kobe

and Deisenhofer, 1996).
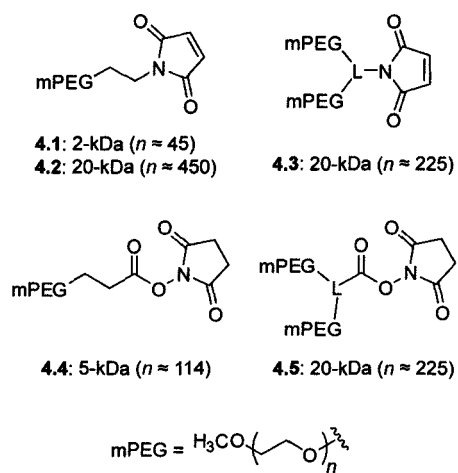
Figure 4.2 Chemical structures of the reactive mPEG molecules utilized for the site-specific PEGylation of RNase A and its variants. L = linker and is used when the explicit chemical structure was not provided or available from the manufacturer.
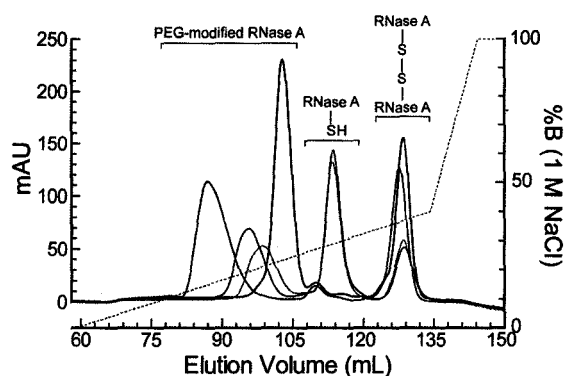
Figure 4.3   Purification of PEGylated RNase A variants using HiTrap SPHP cation-

exchange column chromatography. The chromatograms from multiple

purifications (20-kDa mPEG$_2$–G88C RNase A, (red line);

20-kDa mPEG$_2$–A19C RNase A, (blue line); 20-kDa mPEG–A19C

RNase A, (green line); and 2-kDa mPEG–G88C RNase A, (black line))

were superimposed to simplify graphical representation. Right y-axis

depicts the concentration of NaCl (2 linear gradients: 0–0.40 M and 0.40–

1.0 M; dotted line). Unmodified monomeric (SH-RNase) and dimeric

(RNase–S–S–RNase) protein consistently eluted at ~0.29 and ~0.37 M

NaCl, respectively. PEGylated variants of RNase A all eluted at lower

concentrations of salt. The concentration of salt needed to elute the

modified protein was dependent on the attachment site, size, and

branching order of the attached PEG moiety.
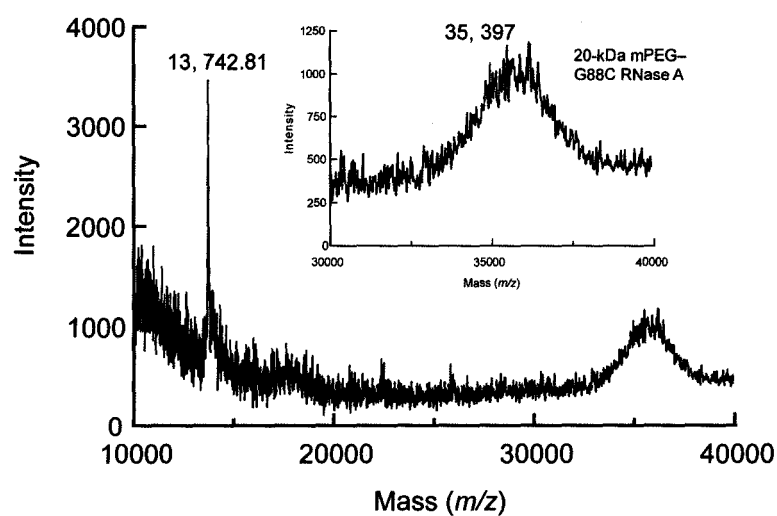
Figure 4.4   MALDI–TOF mass spectrometry analysis of PEGylated RNase A

variants. This mass spectrum of 20-kDa mPEG G88C RNase A is

representative of the other PEG–RNase A conjugates. The breadth of the

peak at m/z = 35, 397 (inset) is a result of the polydispersity (though low)

of the PEG reagent.
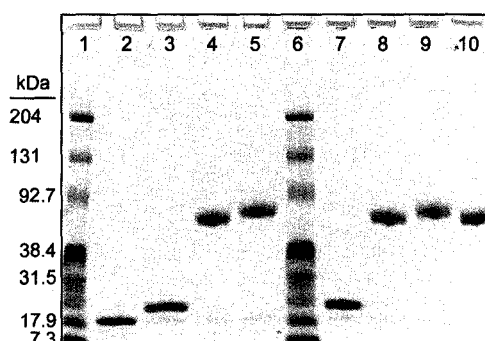
Figure 4.5   SDS–PAGE (Tris–HCl; 4–15% w/v poly(acrylamide) gradient) analysis of

RNase A and PEGylated variants of RNase A (1 μg each). Lane 1 and 6:

Kaleidoscope Pre-stained Standards (BioRad). Lane 2: G88R RNase A.

Lanes 3–5: G88C RNase A modified with (respectively), 2-kDa mPEG–

maleimide 1, 20-kDa mPEG–maleimide (linear) 2-, and 20-kDa mPEG$_2$–

maleimide (branched) 3. Lanes 7–9: A19C RNase A modified with the

same PEG reagents as previously described for A19C RNase A. Lane 10:

20-kDa mPEG–D38R/R39D/N67R/G88C RNase A. Molecular weights

shown for Kaleidoscope Pre-stained Standards (myosin, β-galactosidase,

bovine serum albumin, carbonic anhydrase, soybean trypsin inhibitor,

lysozyme, and aprotinin) are calibrated molecular weights (in kDa) for a

Tris–HCl gel. The gel was first stained with Coomassie Brilliant Blue

R-250, destained, and then stained for PEG using barium iodide (Skoog,

1979; Kurfürst, 1992).
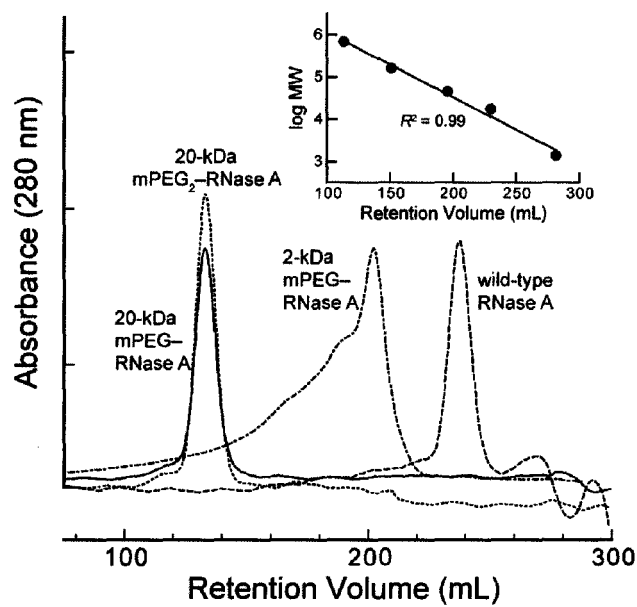
Figure 4.6   Size exclusion chromatographic analysis RNase A and PEGylated variants

of RNase A. Calibration curve (inset) was generated from gel-filtration

standards which included (in order of elution) bovine thyroglobulin

(670 kDa), bovine γ-globulin (158 kDa), chicken ovalbumin (44 kDa),

horse myoglobin (17 kDa), and vitamin B-12 (1.35 kDa).
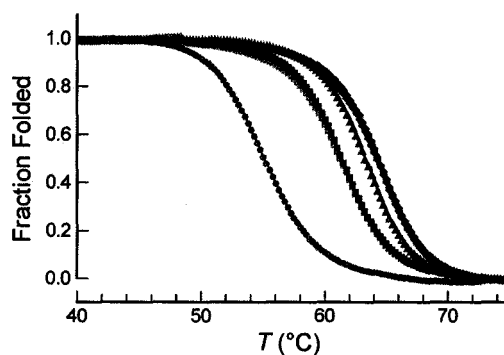
Figure 4.7   Thermal denaturation of G88R RNase A (gray triangles) and PEGylated

variants of RNase A. The data corresponding to the conformational

stability of A19C (blue) and G88C (red) RNase A derivatized with either

2-kDa mPEG (dotted line), 20-kDa mPEG (dashed line), or 20-kDa

$mPEG_2$ (solid line) as well as that of 20-kDa mPEG

D38R/R39D/N67R/G88C RNase A (green) are shown with curves fitted

to a two-state model for thermal denaturation. For a particular variant of

RNase A (A19C or G88C), the stability among the different PEG-

substituted conjugates is nearly indistinguishable.
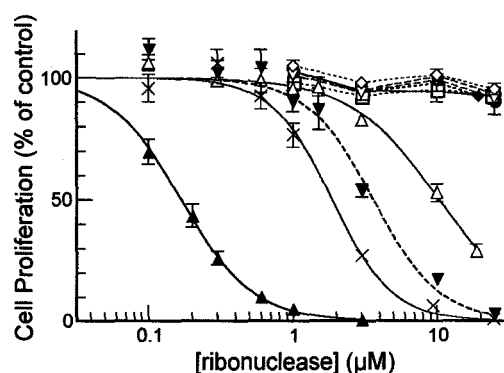
Figure 4.8   Effect of site-specifically PEGylated variants of RNase A on the

proliferation of K-562 cells. The incorporation of [*methyl*-^{3}H]thymidine

into cellular DNA was used to monitor the proliferation of K-562 cells in

the presence of ribonucleases. Data points indicate the mean (± SE) of at

least three separate experiments carried out in triplicate. Data for A19C

(blue) and G88C (red) PEGylated ribonucleases are shown with curves

fitted as either solid lines (2-kDa mPEG), dashed lines (20-kDa mPEG), or

dotted lines (20-kDa mPEG$_2$). Data for 20-kDa mPEG–

D38R/R39D/N67R/G88C RNase A (green) is curve fitted as a solid line.

Data for wild-type RNase A (dotted black line), G88R RNase A (dashed

black line), and D38R/R39D/N67R/G88R RNase A (solid black line) are

shown as closed black symbols.

Figure 4.9   Effect of PEGylated or unmodified variants of RNase A on the tumor

volume and body weight (insets) of Balb c(–/–) mouse xenografts bearing

human DU 145 prostate tumors. Data plotted represent the mean (± SE)

for the number animals indicated in panel descriptions. Values in

parentheses are percentage tumor growth inhibition (% tumor volume

compared to that of the vehicle control on the last day of the experiment).

Vehicle control (open circles; $n = 7$). (**A**) 2-kDa mPEG–G88C RNase A

(closed squares, 15 mg/kg; i.p., 2×wk; $n = 3$) versus vehicle control.

(**B**) Comparison of 2-kDa mPEG–G88C RNase A (closed squares,

11.2 mg/kg; i.p., 2×wk; $n = 3$) to D38R/R39D/N67R/G88R RNase A

(open triangles, 15 mg/kg; i.p., $qd×5$; $n = 7$) and K7A/D38R/R39D/G88R

RNase A (open diamonds, 15 mg/kg; i.p., $qd×5$; $n = 7$). (**C**) Once weekly

administration of 20-kDa mPEG$_2$–G88C RNase A (closed diamonds,

75 mg/kg; i.p., 1×wk; $n = 5$) versus docetaxel control (open triangles,

8 mg/kg; i.p., 1×wk, $n = 7$). In the docetaxel treatment group one mouse

died on day 42 and another on day 68.
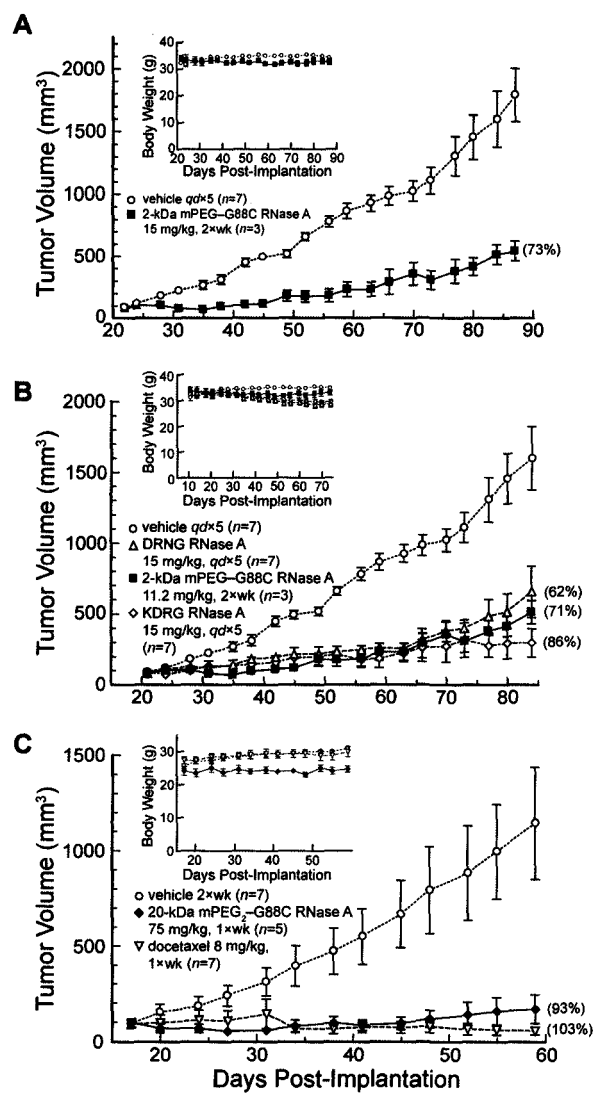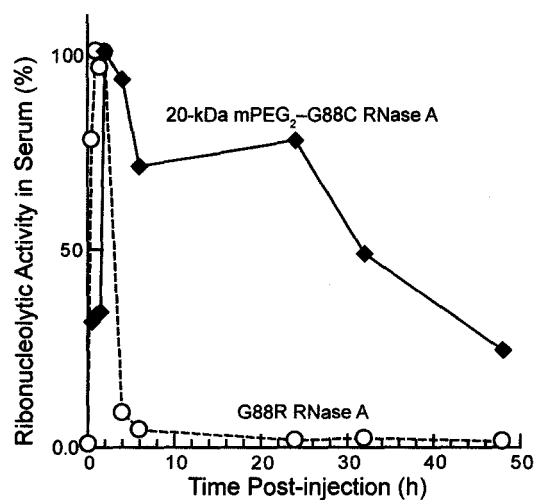
Figure 4.10   Effect of site-specific PEGylation of RNase A on its persistence in the

circulation of mice. Blood was drawn at various times after ribonuclease

administration, treated as described in the Experimental Procedures

section *4.3.10* and subsequently assayed for ribonucleolytic activity.

CHAPTER 5

Site-Specific PEGylation of Recombinant Human Pancreatic

Ribonuclease to Evade Ribonuclease Inhibitor and Improve In Vivo Efficacy

5.1 Abstract

Onconase® (ONC) is poised to become the first ribonuclease-based therapeutic. Although the harbinger of a promising new class of biotherapeutics with antitumoral activity, mammalian homologues of ONC are potentially superior for this application because of their higher ribonucleolytic activity, more favorable tissue distribution, and reduced immunogenic potential. They are limited, however, by their sensitivity to the cytosolic ribonuclease inhibitor protein. The small size of ribonucleases presents a liability for their use as an intravenously/parenterally administered drug because they are rapidly removed from circulation by glomerular filtration. Previously (CHAPTER 4), site-specific PEGylation was shown to be an effective strategy to enhance the ability of RNase A both to evade RI and persist in circulation. Here, we extend this strategy to the human homologue of RNase A—human pancreatic ribonuclease (RNase 1). Attachment of thiol-reactive PEG (5–60-kDa) to free cysteine-containing variants of RNase 1 (G89C) negligibly affects their ribonucleolytic activity but dramatically increases the effective volume of these conjugates. Despite their lack of cytotoxic activity in vitro, the PEGylated conjugates exert dramatic tumor growth inhibition in xenograft mice as a result of their extended half-life in circulation. Additionally, we show that site-specific di-PEGylation of RNase 1 is more effective than mono-PEGylation for reducing sensitivity to RI. Finally, we describe a method for derivatizing amine–PEG to iodoacetamide–PEG *in situ* as an alternative method of thiol-specific PEGylation, circumventing the use of hydrolytically susceptible maleimide linkage chemistry.

5.2 Introduction

Mammalian members of the RNase A superfamily represent a potentially powerful new class of cancer therapeutics (Leland and Raines, 2001; Makarov and Ilinskaya, 2003). However, their potency is limited by both their susceptibility to the ribonuclease inhibitor protein (RI) and their rapid clearance from circulation via glomerular filtration (Rutkoski and Raines, 2008). In the previous chapter, site-specific PEGylation was demonstrated to be a viable means to overcome simultaneously both of these hurdles for RNase A. The motivation for this work was to extend the site-specific PEGylation technology developed in CHAPTER 4 toward the development of a fully-human ribonuclease therapeutic. The primary advantage of using a human protein is to eliminate any concerns about the potential immunogenicity of non-human proteins. Over the last two decades, monoclonal antibody technology has evolved from the use of wholly murine proteins, to murine/human chimeras, to "humanized", and finally to fully human therapeutics to address immune response (Presta, 2006). Elicitation of anti-drug antibodies poses not only immediate safety/health concerns but can also reduce the efficacy of the drug through neutralization or enhanced clearance (Rojas *et al.*, 2005; De Groot and Scott, 2007). Due to the necessity of many repeated injections over an extended period of time, the concern of therapeutic ribonucleases eliciting an immune response is real. Utilization of an endogenous human protein would eliminate the need for any subsequent downstream engineering such as "humanization" or "de-immunization". Indeed, the variants of RNase 1 used here for PEGylation are >99% identical in amino acid sequence to the protein already circulating in the plasma of

normal healthy individuals.

Additionally, inspired by the efficacy of the largest mPEG–RNase A conjugate (20-kDa mPEG$_2$–RNase A) to inhibit tumor growth in xenograft mouse models (See section 4.4.8 and Figure 4.8) and the established correlation between PEG size and persistence in circulation (Yamaoka *et al.*, 1994), we wanted to explore derivatization with larger PEGs (>30 kDa) in pursuit of the next generation of site-specifically PEGylated ribonucleases (See section 4.5.3) (Harris and Chess, 2003). As illustrated in the previous chapter, increased PEG size appears to be a "double-edged sword" in that it enhances the half-life in circulation while at the same time hindering deliverance to its ultimate functional destination—the cytosol (Fishburn, 2008). But what size PEG moiety will optimize the efficacy of PEG–ribonuclease conjugates in animals? Might PEGs larger than 20 kDa completely abrogate cellular internalization?

Herein, we report on the biochemical and physical properties of site-specifically PEGylated variants of RNase 1. Designed with the goal of maximizing antitumoral activity by simultaneously enhancing RI-evasion and reducing renal clearance we explored the efficacy of these conjugates in tumor-bearing xenograft mouse models. This works represents, what is to our knowledge, the first example of PEGylation of a human pancreatic-type ribonuclease.

5.3 Experimental Procedures

5.3.1 Materials

Escherichia coli BL21(DE3) cells and pET22b(+) plasmid were from Novagen (Madison, WI). K-562 (derived from a continuous human chronic myelogenous leukemia line), DU 145 (human prostate carcinoma), and A549 (human lung carcinoma) cell lines were obtained from the American Type Culture Collection (Manassas, VA). Homozygous (*nu/nu*) nude mice (male) were from Harlan (Indianapolis, IN). Cell culture medium and supplements (including Dulbecco's phosphate-buffered saline, 1×DPBS) were from Invitrogen (Carlsbad, CA). [*methyl*-^{3}H]Thymidine (6.7 Ci/mmol) was from PerkinElmer (Boston, MA). Enzymes were obtained from Promega (Madison, WI). Ribonuclease substrate 6-FAM–dArUdAdA–6-TAMRA was from Integrated DNA Technologies (Coralville, IA). Both linear mPEG–maleimide (5-, 20-kDa; **5.1–5.2**; Figure 5.1) and branched mPEG$_2$–maleimide (60-kDa; **5.3**; Figure 5.1), as well as mPEG–amine (20-, 30-kDa; **5.4–5.5**; Scheme 5.1) were from Nektar Therapeutics (Huntsville, AL). Iodoacetic acid *N*-hydroxysuccinimide ester (IAA; **5.6**; Scheme 5.1) and acetylated-BSA were from Sigma Chemical (St. Louis, MO). Iodine solution was from EM Science (Titrisol 9910; Gibbstown, OH). All chromatography columns and resins were from GE Healthcare (Uppsala, Sweden). BCA protein assay kit was from Pierce (Rockford, IL). Gel-filtration standards, SDS–PAGE molecular weight standards, and pre-cast gels for poly(acrylamide) electrophoresis were from BioRad (Hercules, CA). Black non-treated 96-well plates for pharmacokinetic assays were from NUNC

(Rochester, NY). All other chemicals used were of commercial reagent grade or better, and were used without further purification.

Terrific Broth (TB) contained (in 1.00 L) tryptone (12 g), yeast extract (24 g), glycerol (4 mL), KH_2PO_4 (2.31 g), and K_2HPO_4 (12.54 g). Phosphate-buffered saline (PBS) used for dialysis of purified proteins and conjugates contained (in 1.00 L) NaCl (8.0 g), KCl (2.0 g), $Na_2HPO_4 \cdot 7H_2O$ (1.15 g), KH_2PO_4 (2.0 g), and NaN_3 (0.10 g), and had pH 7.4.

5.3.2 Analytical Instruments

[methyl-^{3}H]Thymidine incorporation into K-562 and A549 genomic DNA was quantitated by scintillation counting using a Microbeta TriLux liquid scintillation and luminescence counter (PerkinElmer, Wellesley, MA). The mass of protein variants was confirmed by MALDI–TOF mass spectrometry using a Voyager-DE-PRO Biospectrometry Workstation (Applied Biosystems, Foster City, CA) in the campus Biophysics Instrumentation Facility. Cuvette-scale fluorescence measurements were made using a QuantaMaster1 photon-counting fluorometer equipped with sample stirring (Photon Technology International, South Brunswick, NJ).

5.3.3 Production of Ribonucleases and hRI

cDNA encoding RNase 1 variants was created by oligonucleotide-mediated site-directed mutagenesis using a pET22b(+) plasmid that contained cDNA encoding wild-type human RNase 1 (pHP-RNase) (Leland et al., 2001). The pHP-RNase plasmid

was modified to include the codon for the C-terminal threonine residue (Thr128), which

establishes the native full-length protein (Seno *et al.*, 1994). ONC, wild-type RNase A,

G88R RNase A, and wild-type RNase 1 were produced as described previously

(delCardayré *et al.*, 1995; Leland *et al.*, 2001). Free cysteine-containing variants of

RNase 1 were prepared in a similar fashion, but with the following exceptions: the

protein solution containing dissolved inclusion bodies was diluted 10-fold with a

thoroughly degassed acetic acid solution (20 mM), centrifuged to remove precipitant, and

dialyzed overnight against aqueous acetic acid (20 mM) that had been purged with $N_2(g)$

or $Ar(g)$. Ribonucleases were refolded ≥ 3 days at 4 °C following slow dilution into

0.10 M Tris–HCl buffer at pH 8.0, containing NaCl (0.10 M), L-arginine (0.5 M), EDTA

(10 mM), reduced glutathione (3.0 mM), and oxidized glutathione (0.6 mM). The

refolding solution was purged with $N_2(g)$ or $Ar(g)$ prior to the addition of denatured

protein to prevent oxidation of the free cysteine residues. Variants of RNase 1 containing

two free cysteine residues (G38C/G89C and N67C/G89C) were refolded for ≥ 8 days.

Following gel-filtration purification, the thiol groups of the engineered, unpaired cysteine

residues were protected from inadvertent air oxidation with 5,5'-dithiobis(2-nitrobenzoic

acid) as described previously (Messmore *et al.*, 1995). Finally, the 2-nitro-5-thiobenzoic

acid (TNB)-protected ribonuclease was applied to a HiTrap SP cation-exchange column

and eluted with a linear gradient of NaCl (0.35–0.65 M) in 50 mM sodium acetate buffer

at pH 5.0 and stored at 4 °C until subsequent modification with sulfhydryl-reactive

monomethoxypoly(ethylene glycol) (mPEG or mPEG$_2$). Protein concentration (excluding

TNB-protected ribonuclease) was determined either by bicinchoninic acid method (Smith et al., 1985) or by UV spectroscopy using an extinction coefficient of

$\varepsilon_{280} = 0.53$ mg·ml^{-1}cm^{-1} for RNase 1 and its variants (Leland et al., 2001),

$\varepsilon_{278} = 0.72$ mg·ml^{-1}cm^{-1} for RNase A and its variants (Sela et al., 1957) and

$\varepsilon_{280} = 0.87$ mg·ml^{-1}cm^{-1} for ONC (Leland et al., 1998).

Human RI (hRI) was prepared as described previously (Klink et al., 2001; Rutkoski et al., 2005; Smith, 2006). Freshly prepared RI was confirmed to be 100% active by its ability to titrate the ribonucleolytic activity of wild-type RNase A.

Following purification, each ribonuclease and hRI migrated in a single band during SDS–PAGE, confirming its purity and apparent molecular weight.

5.3.4 PEGylation of RNase 1 Variants Using mPEG–Maleimide

The pH of the protein solution containing TNB-protected ribonucleases in cation-exchange elution buffer was adjusted from 5 to 7.4–8.0 by the addition of 20% (v/v) 1.0 M Tris–HCl buffer at pH 7.8–8.0. The protecting group was removed by the addition of DTT to a final concentration of 5 mM and allowing the reaction to proceed at room temperature for ≥ 5 min, resulting in the immediate generation of the yellow 2-nitro-5-thiobenzoate (TNB^{2-}) (Ellman, 1958). DTT, TNB^{2-}, and salt were removed from the ribonucleases using a HiTrap desalting column equilibrated with 1×DPBS. A 10-fold molar excess of **5.1**, **5.2** or **5.3** was dissolved in an equivalent volume of 1×DPBS (relative to the volume of ribonuclease-containing solution) and added to the solution containing the deprotected ribonuclease (final concentration ribonuclease: ~200 μM).

PEGylation reactions were protected from light and allowed to proceed at room temperature for ~2 h or overnight at 4 °C. Any remaining maleimide groups were quenched by the addition of DTT to a final concentration of 2 mM. To lessen the concentration of residual salt, reactions were diluted to 50 mL with 50 mM sodium acetate buffer at pH 5.0 and dialyzed overnight against 4 L of 50 mM sodium acetate buffer at pH 5.0. The dialyzed crude PEGylation reactions were applied to a column of HiTrap SPHP cation-exchange resin equilibrated with the same buffer. PEGylated and unmodified RNase 1 variants were differentially eluted from the column with a linear gradient of NaCl (0–0.65 M) in 50 mM sodium acetate buffer at pH 5.0. For the 20-kDa mPEG–maleimide PEGylation, the peak corresponding to the 20-kDa mPEG–G89C RNase 1 was sufficiently broad to preclude baseline separation from the unmodified ribonuclease. Complete separation of the PEGylated and non-PEGylated species was achieved using a HiLoad 26/60 G200 Superdex gel-filtration column equilibrated with 50 mM sodium acetate buffer at pH 5.0 containing NaCl (0.10 M) and NaN$_3$ (0.05%).

Our general purification scheme for PEGylated ribonucleases exploits the differential affinity of the PEG–ribonuclease and free ribonuclease for the ion-exchange media (Figure 4.3). The excess unreacted PEG does not interact with the column at all and is removed during the sample loading and subsequent column washing. Initial attempts to purify 60-kDa mPEG$_2$-modified RNase 1 demonstrated that a significant amount of the desired conjugate was not interacting with the cation exchange resin but was co-eluting with the excess of unreacted mPEG in the flow thru fractions. This observation was attributed to the charge-shielding effect of this large PEG moiety. To overcome this weak

affinity for the ion exchange resin the concentration of residual salt was further reduced by concentrating the flow thru fractions by 3-fold and then diluting this material 10-fold with 50 mM sodium acetate buffer at pH 5.0. This additional dilution permitted sufficient affinity of 60-kDa mPEG$_2$-modified RNase 1 for the cation exchange media to allow its purification to homogeneity. Additionally, it was observed that the large PEG moiety reduced the binding capacity of the resin (milligrams of ribonuclease–PEG per milliliter of resin) and necessitated numerous smaller injections of the crude reaction.

5.3.5 PEGylation of RNase 1 Variants Using mPEG–iodoacetamide

Amine-derivatized mPEG (5.4 or 5.5) was dissolved in 0.20 M sodium bicarbonate buffer at pH 8.06 containing NaCl (0.10 M) (final [mPEG–amine] = ~2.1 μmol/mL). To the mPEG–amine solution, a sub-stoichiometric amount (0.9 molar equivalents) of iodoacetic acid N-hydroxysuccinimidyl ester (IAA-NHS; 5.6; Scheme 5.1) was added from a 10 mg/mL stock in DMF. The reaction was protected from light and allowed to proceed for ~45 min at room temperature. The reaction was quenched by addition of ethanolamine to a final concentration of 10 mM. The TNB group was removed from the ribonuclease in same manner as above and subsequently desalted into 0.10 M sodium phosphate buffer at pH 7.4. The deprotected protein was added directly to the iodoacetamide-derivatized mPEG reaction (containing 5.7 or 5.8), protected from light, and reacted overnight at 4 °C. The crude reaction was diluted to 50 mL with 50 mM sodium acetate buffer at pH 5.0 and purified as described above. Yields of PEGylated protein using this procedure were typically 27–38% compared to 54–61% yields for

20-kDa mPEG–maleimide PEGylation. PEGylated variants of RNase 1 were assayed by SDS–PAGE and found to be ≥98% homogeneous, containing only trace amounts of unmodified ribonuclease and no free PEG (lane 6, Figure 5.2). Proteins and PEGylated conjugates were concentrated and dialyzed extensively against 1× PBS. Protein concentrations of PEGylated RNase 1 variants were determined in the same manner as described above for the unmodified ribonucleases. The presence of the PEG moieties was found not to interfere with either method of quantitation.

5.3.6 Multi-PEGylation of RNase 1 Variants Using mPEG–iodoacetamide

Variants of RNase 1 containing two unpaired cysteine residues were PEGylated using the mPEG–amine/IAA procedure described in Section 5.3.5 with several modifications. 30-kDa mPEG–amine **5.5** was reacted with 3-molar equivalents of IAA-NHS **5.6**. Remaining N-hydroxysuccinimide ester groups were quenched by addition of excess ethanolamine as before, but the excess **5.6** necessitated the desalting of the mPEG–iodoacetamide into 0.10 M sodium phosphate buffer at pH 7.4 using a HiTrap desalting column prior to the addition of the deprotected ribonuclease to remove any N-(2-hydroxyethyl)-2-iodoacetamide. Application of the crude PEGylation reactions to a HiLoad 26/60 G200 Superdex gel-filtration column afforded poor resolution of the mono- and di- PEGylated ribonucleases as ascertained by SDS–PAGE. (This gel-filtration step was therefore omitted from subsequent purifications.) Di-PEGylated ribonuclease-containing fractions were pooled and dialyzed exhaustively against 16 L 50 mM sodium acetate buffer at pH 5.0. Dialysate was loaded onto a column of HiTrap

SPHP cation-exchange resin equilibrated with the same buffer. Mono- and di-PEGylated

RNase 1 were differentially eluted from the column with a linear gradient of NaCl

(0–0.40 M) over 20 column volumes in 50 mM sodium acetate buffer at pH 5.0. The

homogeneity of (2)30-kDa mPEG–RNase 1 was confirmed by SDS–PAGE.

5.3.7 Analysis and Characterization of PEGylated RNase 1 Variants

Analytical size-exclusion chromatography. One mg of protein in one mL of

gel-filtration buffer was applied to a HiLoad 26/60 Superdex G200 gel-filtration column

and eluted with 50 mM sodium acetate buffer at pH 5.0 containing NaCl (0.10 M) and

NaN_3 (0.05%) at a flow rate of 4 mL/min. The resulting chromatograms are shown in

Figure 5.3. Gel-filtration standards were prepared and separated using the same column

according to the guidelines of the manufacturer.

Assays of ribonuclease inhibitor binding. The affinity of PEGylated RNase 1

variants for hRI was determined by using a variation of a fluorescence-based competition

assay (Abel et al., 2002) as described previously (Rutkoski et al., 2005).

Assay of catalytic activity. The ribonucleolytic activities PEGylated variants of

RNase 1 were determined by assaying their ability to cleave the hypersensitive

fluorogenic substrate 6-FAM–dArUdAdA–6-TAMRA (20 nM), which exhibits a

~180-fold increase in fluorescence (λ_{ex} = 493 nm and λ_{em} = 515 nm) upon cleavage

(Kelemen et al., 1999). Assays were carried out at ambient temperature in 2.0 mL of

0.10 M MES–NaOH buffer at pH 6.0, containing NaCl (0.10 M). The MES used to

prepare the assay buffer was purified by anion-exchange chromatography to remove trace

amounts of oligomeric vinylsulfonic acid, which is a byproduct of commercial buffer synthesis and has been shown to be a potent inhibitor of RNase A (Smith *et al.*, 2003). Values of k_{cat}/K_M were obtained as reported previously (Kelemen *et al.*, 1999).

Assays of cytotoxicity. The cytotoxic activities of RNase 1 and PEGylated variants were determined by measuring the incorporation of [*methyl*-^{3}H]thymidine into the cellular DNA of K-562 cells in the presence of ribonucleases as described previously (Leland *et al.*, 1998). All cytotoxicity assays were repeated at least three times and done in triplicate. Each data point represents the mean of three or more experimental values (± SE). IC_{50} values were calculated by fitting the curves using nonlinear regression to a sigmoidal dose–response curve as reported previously (Rutkoski *et al.*, 2005).

5.3.8 Xenograft Studies

PEGylated conjugates of RNase 1 were tested for their ability to suppress the growth of human tumors implanted into the flanks of nude mice. The A549 and DU 145 tumor cell lines were selected both for its ability to proliferate in mice and its low rate of spontaneous regression. Importantly, these tumor lines represents clinically relevant targets and are used frequently in the testing of new chemotherapeutic agents. The cell lines were implanted into the right rear flank of 5–6 week old male homozygous (*nu/nu*) nude mice. Each xenograft mouse received 3.27×10^6 A549 cells that had been grown in DMEM media containing FBS (10% v/v). Tumors were allowed to grow to an average size of ≥75 mm^3 before initiation of treatment. Xenograft animals, with the properly-sized tumors, were divided into treatment groups. All test ribonucleases were diluted in

PBS (drug vehicle) and, to serve as a negative control, one set of animals was treated with vehicle alone on the dosing schedule with greatest frequency. All treatments were administered by intraperitoneal (i.p.) injection, and the volume of drug/vehicle injected was based upon the body weight of the animal ($10 \ \mu L/g$). Treatment with all agents was ongoing throughout the entire experiment. Tumor size was measured twice weekly using calipers, and tumor volume (mm^3) was determined by using the formula for an ellipsoid sphere (eq 5.1):

$$\text{tumor volume} = \frac{l \times w^2}{2} \tag{5.1}$$

The percent tumor growth inhibition (% TGI) was calculated by using eq 5.2:

$$\%\text{TGI} = 1 - \left(\frac{(\text{volume}_{\text{final}} - \text{volume}_{\text{inital}})_{\text{treated}}}{(\text{volume}_{\text{final}} - \text{volume}_{\text{inital}})_{\text{control}}} \right) \times 100 \tag{5.2}$$

5-kDa mPEG–G89C RNase 1, 20-kDa mPEG–G89C RNase 1 and 60-kDa mPEG$_2$–G89C RNase 1 were all used to treat A549 xenograft mice. All three PEGylated variants of RNase 1 were administered at a dose of either 7.5 or 75 mg/kg (i.p.; 1 × wk). It is important to note that the mass used to calculate the administered dose included that of both the mPEG and the ribonuclease (See Table 5.2). 60-kDa mPEG$_2$–G89C RNase 1 was used to treat A549 xenograft mice and was administered at a dose of either 7.5 or 75 mg/kg (i.p.; 1 × wk).

5.3.9 Pharmacokinetic Studies

Ribonucleolytic activity remaining in the serum of mice was used to monitor the amount of injected PEGylated ribonuclease remaining in circulation over time. The

method was similar to one reported previously (Tarnowski *et al.*, 1976), except for the assay used to quantify ribonuclease activity. Blood was collected from two or three mice by nicking the tail vein at various time intervals after dosing. The blood was allowed to clot for 30 min at 2–8 °C and then subjected to centrifugation (~1500×g) for 5–10 min. Serum samples were stored frozen in the dark at –80 °C, and thawed on ice prior to analysis. Ribonucleolytic activity in the serum samples was assayed in a 96-well plate using the fluorogenic substrate 6-FAM–dArUdAdA–6-TAMRA. Pre-diluted serum (10 μL of a 1:10,000 dilution) was added to wells (160 μL/well) containing 0.1 M Tris–HCl buffer at pH 7.0, containing NaCl (0.10 M) and acetylated BSA (0.1 mg/mL). The assay was initiated by the addition of substrate (30 μL of a 1.33 μM stock solution). Fluorescence was monitored using a Tecan Safire plate reader with excitation and emission wavelengths of 490 and 525 nm, respectively.

5.4 Results and Discussion

5.4.1 A sulfhydryl-reactive alternative to maleimides

Site-specifically PEGylated variants of RNase 1 were prepared using commercially-available maleimide-activated mPEGs (Figure 5.1; **5.1–5.3**) in a manner analogous to that used previously to produce PEG–RNase A conjugates (See CHAPTER 4). In addition, we sought to achieve thiol-specific PEGylation without the use of the maleimide functional group for two reasons. (1) A consistent supply of inexpensive and high quality (low polydispersity) mPEG–maleimide is not always readily available. (The 2-kDa mPEG–RNase A in Figure 4.5 demonstrates the result of using a sub-optimal PEGylation

reagent). (2) Perhaps more importantly is the underappreciated susceptibility of the intervening imido groups of the resulting succinimidyl thioether linkage to undergo spontaneous hydrolysis. Although the PEG moiety would remain covalently attached to the protein, such hydrolysis introduces significant chemical heterogeneity as well as carboxylic acid groups that are capable of ionizing near neutral pH (Kalia and Raines, 2007). The resulting reduction in net charge of the PEGylated conjugate might impart a further detriment to internalization as cationicity is an important determinant of cytotoxicity (Futami *et al.*, 2001; Fuchs *et al.*, 2007; Johnson *et al.*, 2007a). For these reasons, we developed a method to elaborate amine-functionalized mPEG to a thiol-specific iodoacetamido–mPEG (Scheme 5.1). We demonstrated the utility of this chemistry in a "one-pot" reaction to PEGylate variants of RNase 1 in high yield which could subsequently be purified to homogeneity (Figure 5.2). The chemistry also proved to be scalable and was used to produce >135 mg of 20-kDa mPEG–G89C RNase 1 for use in animal studies (this animal study data not shown).

5.4.2 Biochemical Characterization

Similar to what was observed for RNase A (See section 4.4.3), PEGylation of variants of RNase 1 had only a negligible effect on the ability of these conjugates to cleave 6-FAM–dArUdAdA–6-TAMRA, regardless of the size of the PEG prosthesis. In all cases, mPEG–RNase 1 demonstrated catalytic efficiency against this small substrate that was within ~twofold of the unmodified enzyme (Table 5.1). Ribonucleolytic activity against larger substrates was not examined.

Position 89 of RNase 1, which is within the RI-RNase 1 binding interface (Johnson *et al.*, 2007c), was selected as the site of attachment of the PEG moiety in an effort to reduce the sensitivity of RNase 1 to hRI while simultaneously enhancing its persistence in circulation. The rationale for making chemical modifications at position 89 was more fully discussed in Section 3.4.1. Additionally, Gly89 has been proposed to be the structurally analogous residue to Gly88 of RNase A (Pous *et al.*, 2000; Pous *et al.*, 2001). Contrary to what was observed for the PEGylated variants of RNase A (Table 4.2), all mono-PEGylated variants of RNase 1 (5-, 20-, and 60-kDa mPEG–RNase 1) retained sufficiently high affinity for hRI to preclude precise quantitation using our competition assay (Abel *et al.*, 2002; Rutkoski *et al.*, 2005). The value of K_d for all of these conjugates is therefore reported as <1.4 nM (Table 5.1). This retention of sensitivity to RI is presumably a result not only of the higher basal affinity of the hRI·RNase 1 complex compared to the that of hRI·RNase A complex (150-fold higher; Table 1.2), but also the less ideal orientation of residue 89 within the β4–β5 for effecting RI-evasion through elaboration of its side chain (Johnson *et al.*, 2007c). As anticipated, due to both the high affinity of these conjugates for RI (though likely significantly less than unmodified wild-type enzyme) and the detrimental effect of PEGylation on the cellular binding/internalization of ribonucleases (See section 4.5.2), these conjugates had no effect on the proliferation of K-562 cells, with values of IC_{50} >50 μM (Table 5.1 and Figure 5.4).

5.4.3 Pharmacokinetics and in vivo Efficacy

Nonetheless, we tested the ability of these three PEGylated conjugates to inhibit the growth of solid human tumors implanted in mice, as the reduced in vitro bioactivities of PEGylated proteins is often more than compensated for in vivo by their enhanced persistence in circulation (Harris and Chess, 2003; Fishburn, 2008). Indeed, this was observed for 20-kDa mPEG$_2$–G88C RNase A, which, like the PEGylated RNase 1 conjugates, had no effect on the proliferation of K-562 cells (Figure 4.7), but dramatically inhibited the growth of human prostate tumors (DU 145) in xenograft mice models (Figure 4.8). For the current study, mice bearing human lung carcinomas (A549) were utilized which had previously been shown to be much more refractory to ribonuclease treatment in vitro than other cell lines such as DU 145(Rutkoski et al., 2005). Indeed, we confirmed that 5-kDa mPEG–G89C RNase 1, 20-kDa mPEG–G89C RNase 1 and 60-kDa mPEG$_2$–G89C RNase 1 all had no effect on the proliferation of A549 cells in vitro (data not shown).

Despite their innocuous effect on K-562, all three conjugates significantly inhibited the growth of A549 tumors when administered to mice weekly at either a "high" (75 mg/kg; TGI: 63–91%; Figure 5.5A, top) or "low" dose (7.5 mg/kg; TGI: 45–75%; Figure 5.5A, bottom). In general, the effect was more pronounced in the higher dosing group and for conjugates with larger PEG moieties achieved more substantial tumor growth inhibition (Table 5.2 and Figure 5.6). This result is attributed to the enhanced persistence of these conjugates in circulation which has been correlated with PEG molecular weight (60-kDa $_{t½}$ > 20-kDa $_{t½}$ > 5-kDa $_{t½}$)—the most dramatic effects being

observed for PEG in excess of 30 kDa (Yamaoka *et al.*, 1994). Our preliminary

pharmacokinetic analysis (Figure 5.7) supports this hypothesis with elevated levels of

ribonucleolytic activity in the serum following the same trend: 60-kDa > 20-kDa >

5-kDa. The increased half-life in circulation is attributed to the reduced glomerular

filtration of these conjugates which have much larger effective volumes (from calculated

viscosity radii) than does the unmodified enzyme (Figure 5.3 and Table 5.2) (Maack,

2000; Fee and Van Alstine, 2004). The superior ability of the larger conjugates to effect

tumor growth inhibition is, in fact, even greater than is suggested by the data depicted in

Figure 5.5, if one considers the relative molar amount of ribonuclease administered in

each treatment group because the reported dose (*e.g.*, 75 mg/kg) includes the mass of the

polymer. For example, in the "low" dose treatment group (7.5 mg/kg/wk conjugate), the

60-kDa mPEG$_2$–RNase 1 conjugate was more effective than the 5-kDa mPEG–RNase 1

conjugate at inhibiting the growth of A549 tumors (TGI = 75 and 45%, respectively)

even though nearly four times as many molecules of the smaller conjugate were

administered to the mice in that particular treatment group (Table 5.2 and Figure 5.6).

5.4.4 The EPR Effect and Cancer Cell Selectivity

The reduced plasma clearance of larger molecules in combination with a number of

dramatic architectural differences between normal and neoplastic tissues (Jain, 1994)

have been observed to mediate the passive accumulation of macromolecules at the site of

a tumor—the so-called EPR (enhanced permeability and retention) effect, which is a

universal characteristic of solid tumors (Maeda *et al.*, 1992; Maeda *et al.*, 2000). Some of

the unique aspects of tumor physiology that contribute to the EPR effect are the increased permeability of tumor vasculature as well as the poor lymphatic drainage of tumor tissues (Maeda *et al.*, 1992). The extremely large size of the 60-kDa $mPEG_2$–RNase 1 conjugate may permit it to both remain in circulation for many hours and gradually leach into tumor tissue from which it cannot escape back into the bloodstream due to its large size (Noguchi *et al.*, 1998).

None of the PEGylated variants of RNase 1 exhibited any systemic toxicity to the animals as evidenced by their maintenance of body weight throughout the duration of the studies (Figure 5.5, insets). On the contrary, the anti-mitotic chemotherapeutic drug, cisplatin (6 mg/kg/wk), caused pronounced toxicity (Figure 5.5B, inset) when administered at a dose comparable to the dose of 60-kDa $mPEG_2$–RNase 1 (75 mg/kg/wk) that inhibited A549 tumor growth (TGI $\approx$ 66%, through Day 50). These data support the notion that ribonuclease exert their cytotoxicity selectively towards neoplastic cells (Rutkoski *et al.*, 2005).

5.4.5 Comparison to PEG–RNase A

It is difficult to draw many conclusions regarding the relative efficacy of PEG–RNase A versus PEG–RNase 1 conjugates as they were never compared directly side-by-side in any of our in vivo experiments. However, considering the superior ability of the PEGylated RNase A conjugates to evade RI (K_d = 8–37 nM) as opposed to the sub-nanomolar affinity of PEG–RNase 1 (K_d <1.4 nM), the former conjugates would be expected to exert greater tumor growth inhibition in vivo. The effect of 60-kDa $mPEG_2$–

RNase 1 on the growth DU 145 tumors supports this conjecture (Figure 5.8).

60-kDa mPEG$_2$-RNase 1 administered once weekly to mice at either 7.5 of 75 mg/kg substantially inhibited the growth of these human prostate tumors (TGI = 29 and 50%, respectively). Nonetheless, 20-kDa mPEG$_2$-RNase A (K_d = 37 nM; 75 mg/kg; i.p.; 1×wk) inhibited, almost completely (TGI = 93%; Figure 4.8C), tumors in mice derived from the same cell line. Extension on the trend observed for PEG–RNase 1 in Figure 5.6 to PEGylated conjugates of RNase A, 60-kDa mPEG$_2$-RNase A (which was not prepared) would be expected to be even *more* efficacious than the 20-kDa mPEG$_2$– RNase A. The results in Figure 5.8, therefore, support the conclusion that PEG–G88C RNase A would be expected to outperform (in xenograft mouse models) the equivalently PEGylated G89C RNase 1, and that this enhanced efficacy is a result of a superior ability of PEG–G88C RNase A to evade RI.

5.4.6 Multi-site PEGylation of RNase 1

Finally, we tested whether PEGylation of RNase 1 at multiple sites within the RI-RNase 1 interface might be more effective at mediating RI-evasion than at a single position. In addition to G89C, two other positions were selected for replacement by cysteine (Gly38 and Asn67) based on the previous identification of these regions as "hot-spots" within the RI·RNase 1 complex (Rutkoski *et al.*, 2005; Johnson *et al.*, 2007c). Although residue 38 itself does not mediate any contacts with RI, the neighboring Arg39 residue was identified as an "electrostatic targeting residue" (Johnson *et al.*, 2007c). We chose to spare residue 39 to preserve the overall net charge of the ribonuclease and

instead anchored one of two 30-kDa mPEG chains through a cysteine residue installed at

residue 38. The analogous residue in RNase A was shown to be important for RI binding

(Rutkoski *et al.*, 2005). In fact, for effecting RI-evasion, there appears to be an advantage

to distributing 60 kDa of mPEG at two distal positions within the RI-interface, as the

(2)30-kDa mPEG–G38C/G89C RNase 1 conjugate exhibited a K_d value for the inhibitor

protein of 2.6 nM (Table 5.1) The di-PEGylated conjugate employing the N67C/G89C

RNase1 variant maintained affinity for RI that was below the limits of detection of our

assay. Nonetheless, the (2)30-kDa mPEG–G38C/G89C RNase 1 conjugate demonstrates

that it is feasible to site-specifically PEGylate ribonucleases at multiple points within the

inhibitor binding interface to eke out additional RI-evasion from PEGylation. This

conjugate represents a promising candidate for further animal studies and would be

expected to outperform the 60-kDa mPEG$_2$–RNase 1 conjugate at inhibiting the growth

of human tumors borne on mice.

5.5 Conclusions

Site-specific PEGylation is a promising strategy for further development of human

pancreatic ribonuclease as a cancer therapeutic. Attachment of the PEG moiety to

RNase 1 through a G89C substitution results in PEGylated conjugates with preserved

catalytic activity as was observed for PEGylated variants of RNase A. The PEG–RNase 1

conjugates were not as evasive as PEG–RNase A conjugates even when variants of

RNase 1 were PEGylated at two discrete positions within the RI-ribonuclease interface.

Despite their lack of cytotoxic activity against K-562 cells in vitro, PEGylated conjugates

of RNase 1 displayed marked activity for inhibiting the growth of tumors in xenograft mouse models without causing any measureable systemic toxicity. The antitumoral activity of these conjugates in vivo was found to increase with increasing size of the attached polymer, which is consistent our preliminary pharmacokinetic analysis. We conclude that the size of the largest conjugates enables them to persist in circulation and to accumulate passively in solid tumors through the EPR effect—perhaps extending the already selective nature of ribonuclease-mediated cytotoxicity. This works lends credence to the practical potential of PEGylated conjugates of human pancreatic ribonuclease as cancer therapeutics.

Table 5.1 Biochemical parameters and cytotoxic activity of RNase 1 and its PEGylated variants

Ribonuclease	$k_{cat}/K_M{}^a$ $(10^7\ M^{-1}s^{-1})$	$K_d{}^b$ (nM)	$IC_{50}{}^c$ (μM)
wild-type RNase 1	2.9 ± 0.1	2.9×10^{-7}	>25
G88R RNase A	ND	1.3 ± 0.2	3.3 ± 0.1
5-kDa mPEG–G89C RNase 1	2.6 ± 0.3	$<1.4\ (0.20)$	>50
20-kDa mPEG–G89C RNase 1	6.8 ± 0.1	$<1.4\ (0.81)$	>50
60-kDa mPEG$_2$–G89C RNase 1	6.1 ± 0.3	$<1.4\ (0.13)$	>50
ONC	0.00018 ± 0.000005	$>10^3$	0.22 ± 0.1
(2)30-kDa mPEG–G38C/G89C RNase 1	0.59 ± 0.03^d	2.6 ± 0.7	ND
(2)30-kDa mPEG–N67C/G89C RNase 1	0.16 ± 0.01^d	$<1.4\ (0.68)$	ND

ND, not determined.

[a] Values of k_{cat}/K_M ($\pm$ SE) are for the catalysis of 6-FAM–dArU(dA)$_2$–6-TAMRA cleavage at room temperature in 0.10 M MES–NaOH buffer at pH 6.0 containing NaCl (0.10 M). The values of k_{cat}/K_M for RNase 1 and ONC are from Table 3.1.

[b] Values of K_d ($\pm$ SE) are for the complex with human RI at room temperature. The K_d value for RNase 1 is from (Johnson *et al.*, 2007c). The K_d value for G88R RNase A is from (Lavis *et al.*, 2007). The K_d value for ONC is an estimate from (Wu *et al.*, 1993).

[c] Values of IC_{50} ($\pm$ SE) are for incorporation of [methyl-^{3}H]thymidine into the DNA of K-562 cells. The values of IC_{50} for RNase 1, G88R RNase A, and ONC are from Table 3.1.

[d] Values of k_{cat}/K_M ($\pm$ SE) were determined in 0.10 M MES–NaOH buffer at pH 6.0 containing NaCl (0.50 M) and are comparable to the value for wild-type RNase 1 under the same condition: $0.57 \times 10^7\ M^{-1}s^{-1}$.

Table 5.2 Effect of PEGylated variants of RNase 1 on tumor growth inhibition in vivo

PEG–ribonuclease	Dose (mg/kg/wk)	(μmol/kg/wk)[a]	TGI (%)	$r_{viscosity}$[b] (Å)
5-kDa mPEG–RNase 1	75	3.6	69	32.4
20-kDa mPEG–RNase 1	75	2.1	63	52.5
60-kDa mPEG$_2$–RNase 1	75	0.96	91	93.1
5-kDa mPEG–RNase 1	7.5	0.36	45	32.4
20-kDa mPEG–RNase 1	7.5	0.21	61	52.5
60-kDa mPEG$_2$–RNase 1	7.5	0.096	75	93.1

[a]Values were calculated using masses of 20, 707.61 Da; 35, 563.61 Da; and 77, 810.61 Da for 5-kDa, 20-kDa, and 60-kDa mPEG–RNase 1, respectively. PEG masses were from the manufacturer specifications and were determined by MALDI–TOF mass spectrometry.
[b]Viscosity radii were calculated from equation 11 in (Fee and Van Alstine, 2004).
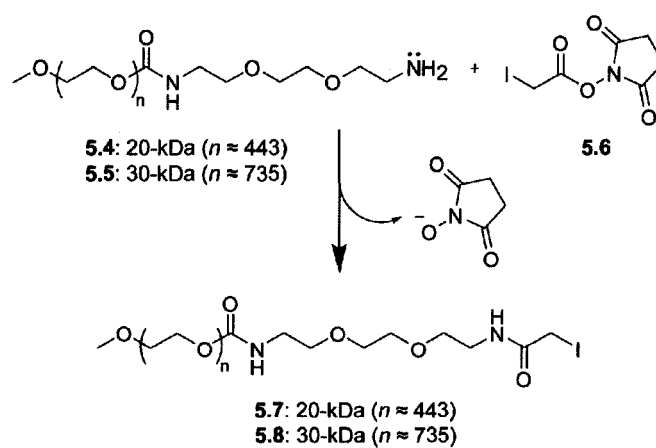
Scheme 5.1 Derivatization of mPEG–amine (**5.4, 5.5**) with iodoacetic acid

N-hydroxysuccinimide ester (**5.6**) to yield mPEG–iodoacetamide (**5.7,**

5.8).

5.1: 5-kDa ($n \approx 127$)
5.2: 20-kDa ($n \approx 465$)

5.3: 60-kDa ($n \approx 711$)
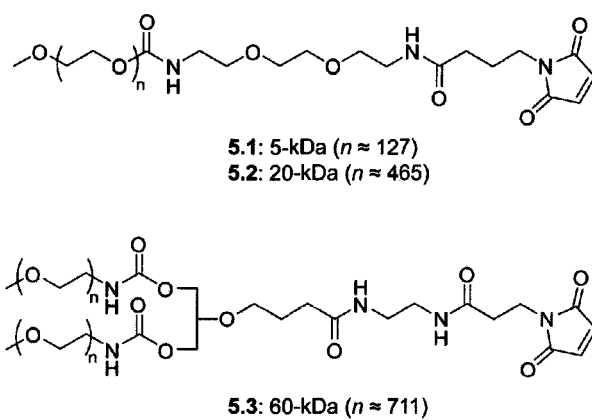
Figure 5.1   Chemical structures of the maleimide-functionalized reactive mPEG

molecules utilized for the site-specific PEGylation of variants of RNase 1.
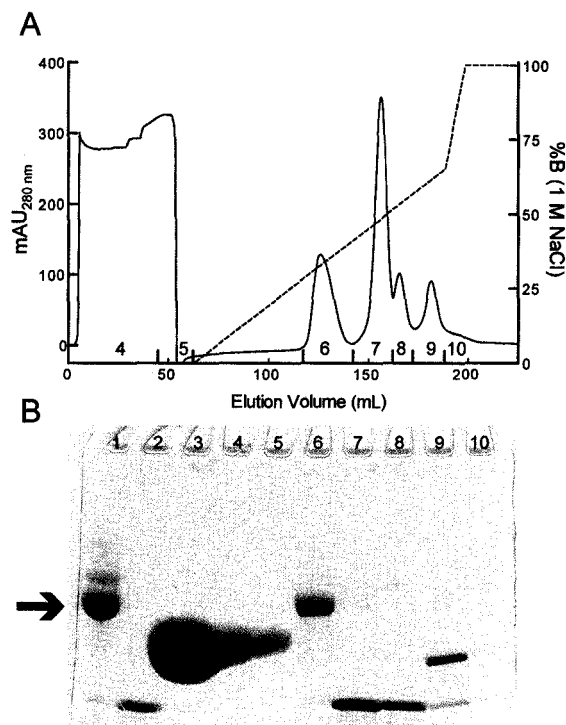
Figure 5.2 (A) Purification of 20-kDa mPEG–G89C RNase 1 (prepared using 5.7 as

in Scheme 5.1) from crude PEGylation reaction by cation-exchange

column chromatography. Right y-axis depicts the concentration of NaCl

(two linear gradients: 0–0.65 M and 0.65–1.0 M; dotted line). Numbers

correspond to pools that were analyzed by SDS–PAGE in (B). SDS–

PAGE analysis (Tris–HCl; 4–15% poly(acrylamide) gradient gel). Lane 1:

20-kDa mPEG(MAL)–RNase 1, Lane 2: G89C RNase 1 (unmodified),

Lane 3: 20-kDa mPEG–amine **5.4**. The gel was first stained with

Coomassie Brilliant Blue R-250, destained, and then stained for PEG

using barium iodide (Skoog, 1979; Kurfürst, 1992).
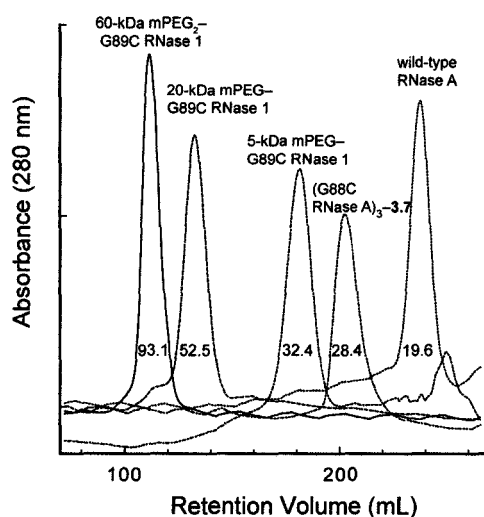
Figure 5.3   Size exclusion chromatographic analysis of PEGylated variants of

RNase 1. Wild-type RNase A and a trimeric conjugate of RNase A, (G88C

RNase A)$_3$–3.7, are included for comparison. The numbers within the base

of each peak are the calculated values of viscosity radii for each species

(Fee and Van Alstine, 2004).
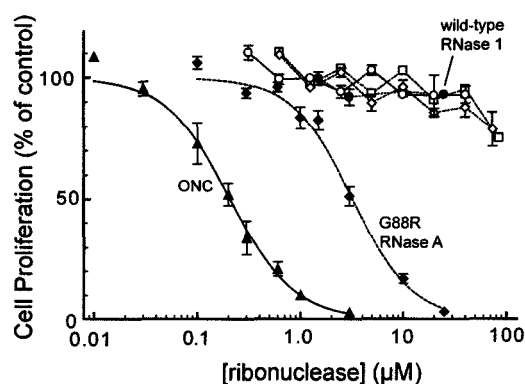
Figure 5.4   Effect of site-specifically PEGylated variants of RNase 1 on the

proliferation of K-562 cells. The incorporation of [*methyl*-³H]thymidine

into cellular DNA was used to monitor the proliferation of K-562 cells in

the presence of ribonucleases. Data points indicate the mean (± SE) of at

least three separate experiments carried out in triplicate. Data for wild-

type RNase 1, G88R RNase A, and ONC are shown as closed symbols.

Data for 5-kDa mPEG–G89C RNase 1 (squares), 20-kDa mPEG–G89C

RNase 1 (diamonds), and 60-kDa mPEG₂–G89C RNase 1 (circles) are

shown as open symbols.

Figure 5.5   Effect of PEGylated variants of RNase 1 on the tumor volume and body

weight (insets) of Balb c(–/–) mouse xenografts bearing human A549 lung

tumors. Data plotted represent the mean (± SE) for the number animals

indicated in panel descriptions. Values in parentheses are percentage

tumor growth inhibition (% tumor volume compared to that of the vehicle

control on the last day of the experiment). Vehicle control (open circles).

(**A**) Effect of mPEG size (5-, 20-, or 60-kDa) on tumor growth inhibition

of PEGylated ribonucleases administered weekly at either a "HIGH"

(75 mg/kg; i.p., 1×wk; n = 5) or a "LOW" (7.5 mg/kg; i.p., 1×wk; n = 5)

dose versus vehicle control. (**B**) Comparison of 60-kDa mPEG$_2$–G89C

RNase 1 (closed squares, 75 mg/kg; i.p., 1×wk; n = 7) versus cisplatin

control (open triangles, 6 mg/kg; i.p., 1×wk; n=7).

A

HIGH

o vehicle 1×wk (*n*=6)
△ 20-kDa mPEG–G89C RNase 1
◆ 5-kDa mPEG–G89C RNase 1
■ 60-kDa mPEG$_2$–G89C RNase 1
All: 75 mg/kg, 1×wk (*n*=5)

(63%)
(69%)
(91%)

LOW

o vehicle 1×wk (*n*=6)
◆ 5-kDa mPEG–G89C RNase 1
△ 20-kDa mPEG–G89C RNase 1
■ 60-kDa mPEG$_2$–G89C RNase 1
All: 7.5 mg/kg, 1×wk (*n*=5)

(45%)
(61%)
(75%)

B

o vehicle 1×wk (*n*=7)
◆ 60-kDa mPEG$_2$–G89C RNase 1
  75 mg/kg, 1×wk (*n*=7)
▽ cisplatin 6 mg/kg,
  1×wk (*n*=7)

(68%)
(84%)

Days Post-Implantation
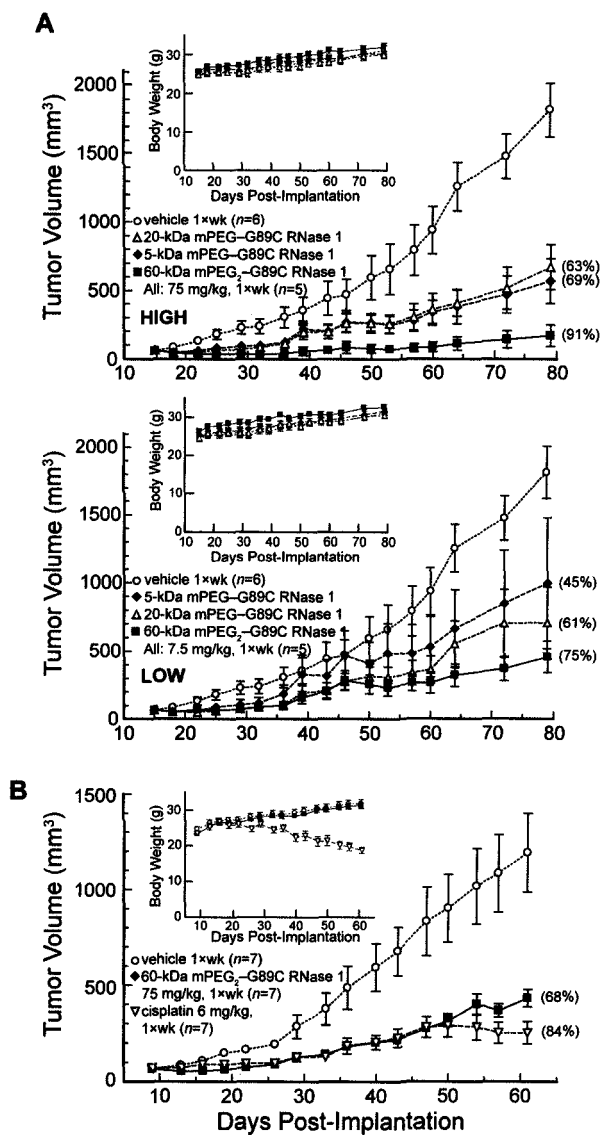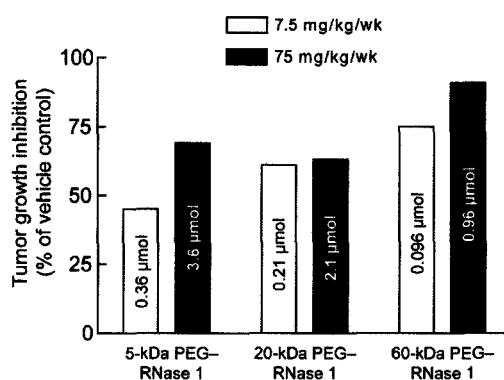
Figure 5.6   Effect of PEGylated variants of RNase 1 on A549 tumor growth inhibition

(TGI %) in vivo. Bar height corresponds to the TGI values shown in

parentheses in Figure 5.5A. The low and high dosing groups are shown as

white and black bars, respectively. The molar amount of ribonuclease (in

μmol) administered per kilogram per week is given within each bar.
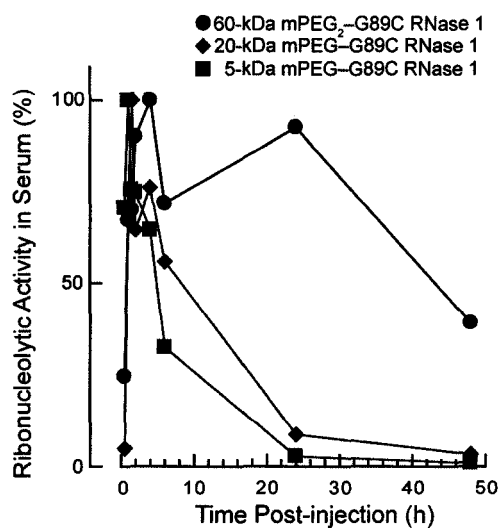
Figure 5.7   Pharmacokinetic analysis of mPEG–G89C RNase 1. Effect of site-specific

PEGylation of RNase 1 on its persistence in the circulation of mice. Blood

was drawn at various times after ribonuclease administration, treated as

described in the Experimental Procedures (Section 5.3.9) and subsequently

assayed for ribonucleolytic activity.
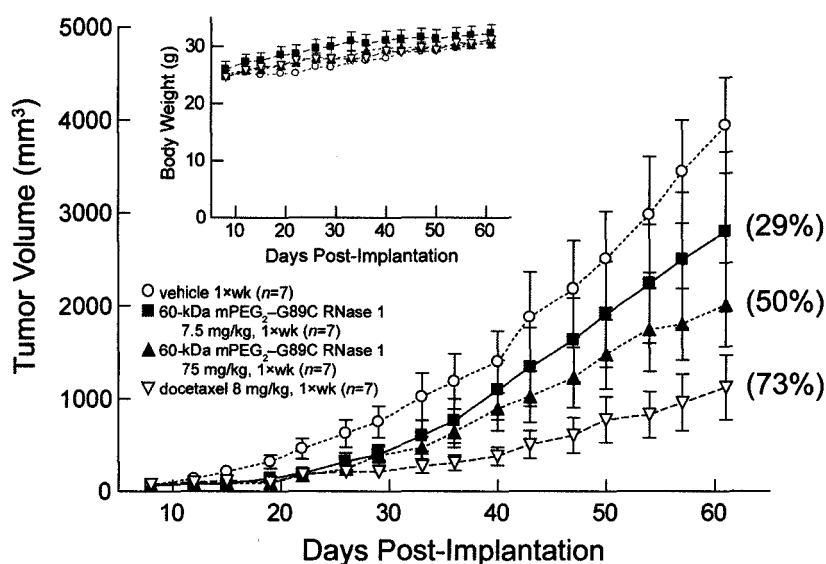
Figure 5.8   Effect of 60-kDa mPEG$_2$-G89C RNase 1 (7.5 mg/kg, i.p., 1×wk, ■; or

75 mg/kg, i.p., 1×wk, ▲) on the tumor volume and body weight (inset) of

Balb c(–/–) mouse xenografts bearing human DU 145 prostate tumors

compared to vehicle (open circles, i.p., 1×wk) or docetaxel controls (open

triangles, 8 mg/kg; i.p., 1×wk). Data plotted represent the mean (± SE) for

the number animals in each treatment group (n = 7). Values in parentheses

are percentage tumor growth inhibition (% tumor volume compared to that

of the vehicle control on the last day of the experiment).

CHAPTER 6

Future Directions

6.1 Enzymes as Therapeutics

The concept of using purified enzymes for human therapeutic applications is more than 40 years old (De Duve, 1966). In fact, in 1931, Avery and Dubos described the protective effects of a bacterial glycosidase, administered intraperitoneally, against pneumococcal infection in mice (Avery and Dubos, 1931). Furthermore, enzymes likely comprised some of the active ingredients in topical preparations that have been used for medicinal purposes by humans for centuries (Holcenberg and Roberts, 1977). It was not until 1987, however, that the first FDA-approved therapeutic enzyme, tissue plasminogen activator (rt-PA), appeared on the market (the second recombinant protein therapeutic after insulin). Since then, due to their exquisite specificity, coupled with their catalytic nature, therapeutic enzymes have been developed for a host of diseases and disorders including genetic metabolic syndromes, infectious diseases, clotting disorders, and cancer (Vellard, 2003).

It is a truly exciting time in the area of therapeutic cytotoxic ribonucleases with ONC poised to become the first FDA-approved ribonuclease therapeutic (Pavlakis and Vogelzang, 2006) and a phase I clinical trial of a cytotoxic variant of human pancreatic ribonuclease slated to begin within the year (Newman, 2007). A number of intriguing avenues of research have been inspired by the work described in the preceding five chapters. Several future research aims are outlined below that might represent the next step forward in the burgeoning field of ribonuclease therapeutics.

6.2 Beyond Highly-Evasive Cytotoxic Ribonucleases

The impetus for this thesis work was to increase the toxicity of ribonucleases toward cancer cells by reducing their susceptibility to RI. Indeed, this goal was successfully achieved using a number of strategies. As discussed in CHAPTER 2, it appears that gains in RNase A cytotoxicity through modulation of RI-evasion via site-directed mutagenesis have been exhausted (Rutkoski *et al.*, 2005). Enhancement of RNase A cytotoxicity has also been accomplished without modulating affinity for RI by appending the protein with an R_9-tag (Fuchs and Raines, 2005) or by installing an arginine "graft" (Fuchs *et al.*, 2007).

Attempts to synthesize several of these cytotoxic activity-promoting strategies with the goal of producing "hyper-cytotoxic" variants of RNase A ($IC_{50,K-562} < 0.2$ μM) have been on-going in our laboratory. Preliminary results indicate that the resultant low conformational stability of these variants remains a barrier to the utility of this approach. For example, the arginine "graft" described in APPENDIX 2 was installed onto the highly evasive and cytotoxic D38R/R39D/N67R/G88R RNase A variant described in CHAPTER 2. The moderately destabilizing effects of the E49R/D53R amino-acid substitutions ($\Delta T_m = -10$ °C) further reduced the conformational stability of D38R/R39D/N67R/G88R RNase A ($T_m = 56$ °C), resulting in a variant with a T_m value of ~47 °C. As conformational stability is also intimately tied to cytotoxic activity (Klink and Raines, 2000), we concluded that the disappointing cytotoxic activity of this variant ($IC_{50} \approx 0.3$ μM; Figure 6.1) was a result of this additive destabilization. Similar conclusions were drawn from experiments in which evasive variants of RNase A were

either appended with an R₉-tag, which is also moderately destabilizing ($\Delta T_m = -8$ °C

(Fuchs and Raines, 2005)) or whose acid functional groups were derivatized chemically

using recently reported methodologies (Krusemark *et al.*, 2008). Nonetheless, by

bolstering the conformational stability of these ribonuclease variants by any number of

means (Pace, 1990; Futami *et al.*, 2000), these shortcomings in conformational stability

should be surmountable.

6.3 The Next Generation of PEGylated Ribonucleases

The site-specific PEGylation of mammalian ribonucleases for parenteral

administration was described in CHAPTERS 4–5. For all of its merits in enhancing the

persistence in circulation of its ribonuclease cargo, PEG was also shown, albeit

indirectly, to reduce the delivery of ribonucleolytic activity to the cytosol. These

dichotomous effects of PEGylation on the pharmacokinetics (PK) and

pharmacodistribution (PD) of its payloads are well-documented (Fishburn, 2008).

More thorough and direct characterization of the effects of PEGylation on the cellular

internalization of ribonucleases is warranted. Fluorogenic labels developed in the Raines

Laboratory (Chandran *et al.*, 2005; Lavis *et al.*, 2006b; Lavis *et al.*, 2006a) have already

been exploited to study directly the cellular internalization of ribonucleases (Johnson *et

al.*, 2007a). Attachment of these or other more conventional fluorophores could be used

to label either the protein or the PEG moiety (the latter requiring the use of a

bifunctionally-activated PEG molecule), to quantitatively map-out by FACS analysis the

differences in how PEG–RNase A conjugates interact with and are trafficked through cells.

Though PEGylation was shown to effect RI-evasion, additional gains in cytotoxicity were observed in vitro when the FADE-identified amino-acid substitutions of CHAPTER 2 were combined with site-specific PEGylation. Thus, 20-kDa mPEG–D38R/R39D/N67R/G88C RNase A (K_d = 3.3 μM) was nearly 400-fold more evasive than 20-kDa mPEG–G88C RNase A and was a potent cytotoxin (IC_{50} = 1.9 μM) in vitro. Further xenograft mouse studies need to be conducted to establish the in vivo potency of this and other dually evasive/PEGylated ribonuclease variants, such as the multi-PEGylated variants of RNase 1 that exhibited enhanced RI-evasion.

Finally, pro-drug strategies could be applied to PEGylated ribonucleases to promote deliverance of the ribonuclease to its cytosolic site of action. Two distinct approaches are envisioned: (1) the PEG and the ribonuclease moieties are joined through a hydrolytically susceptible or pH-sensitive linkage, or (2) the protein and polymer are separated by an intervening sequence that is preferentially cleaved at the site of the tumor. Enabling the first strategy, Greenwald and co-workers have developed a number of linkage chemistries permitting the PEG group to be jettisoned, allowing controlled release of the enzyme (Greenwald *et al.*, 2000; Lee *et al.*, 2001; Greenwald *et al.*, 2003b). Alternatively, if internalization studies indicate that the efficiency of endosomal escape is significantly perturbed by PEGylation, pH-sensitive linkages (Oishi *et al.*, 2005) could take advantage of the acidic nature of this sub-cellular compartment. The second strategy might exploit extracellular proteases such as matrix metalloprotease family members (MMPs) whose

high expression allows the degradation of the extracellular matrix and subsequent

metastasis of many cancers (Lopez-Otin and Matrisian, 2007). The expectation of this

approach is that unmasked, efficiently internalized ribonucleases would be preferentially

available at the site of the tumor.

6.4 What is the Basis for the Cancer Cell Selectivity of Ribonucleases?

Cytotoxic ribonucleases were shown to exert their toxicity selectively against tumor

cells both in vitro (CHAPTER 2) and in vivo (CHAPTERS 3–5), yet little is known about the

basis of this selectivity. This discrimination could be a result of macroscopic

physiological differences between tumors and normal tissues (e.g., aberrant, leaky

vasculature or altered interstitial pressures) or a result of more cellular/molecular

deviations (e.g., altered phospholipid composition of the plasma membrane, glycoprotein

expression, or mechanism of intracellular vesicular trafficking). The contrast agent–

ribonuclease studies described in APPENDIX 3 could clarify the basis of the therapeutic

index of cytotoxic ribonucleases (Rutkoski et al., 2005). If further analyses (such as

gadolinium content of the mouse tissues from the experiment in Figure A3.6) confirm the

lack of detectable tumor accumulation, it is likely that the differential response of normal

and cancerous tissues to ribonucleases stems from their intracellular fate following

internalization. Research into the intracellular trafficking of ribonucleases is on-going in

the Raines Laboratory.
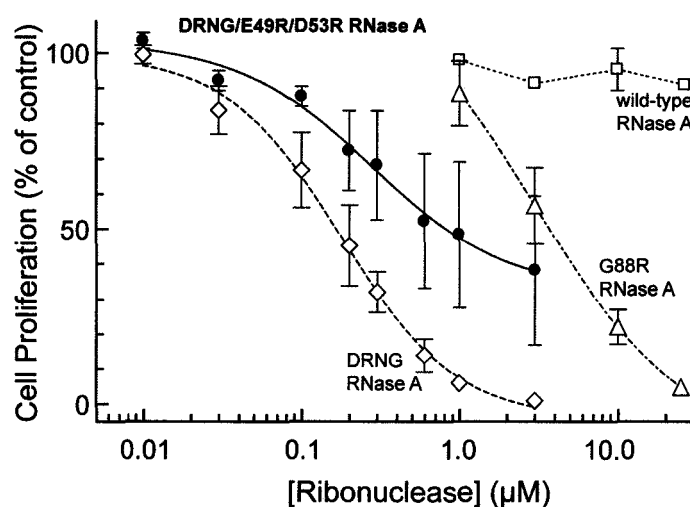
Figure 6.1   Effect of appending a highly evasive cytotoxic variant of RNase A

(DRNG RNase A) with an "arginine graft" (E49R/D53R; APPENDIX 2) on

its ability to inhibit the proliferation of K-562 cells. The incorporation of

[*methyl*-^{3}H]thymidine into cellular DNA was used to monitor the

proliferation of K-562 cells in the presence of ribonucleases. Data points

indicate the mean (± SE) of two separate experiments carried out in

triplicate. Data for wild-type RNase A, G88R RNase A, and

D38R/R39D/N67R/G88R (DRNG) RNase A are shown as open symbols

and are curve-fitted with broken lines. Data for DRNG/E49R/D53R

RNase A are shown as closed circles, curve-fitted with a solid line.

APPENDIX 1

Tuning the pK_a of Fluorescein to Optimize Binding Assays

A1.1 Abstract

The phenolic pK_a of fluorescein varies depending on its environment. The fluorescence of the dye varies likewise. Accordingly, a change in fluorescence can report on the association of a fluorescein-conjugate to another molecule. Here, we demonstrate how to optimize this process with chemical synthesis. The fluorescence of a fluorescein-labeled model protein, bovine pancreatic ribonuclease (RNase A), decreases upon binding to its cognate inhibitor protein (RI). Free and RI-bound fluorescein–RNase A have pK_a values of 6.35 and 6.70, respectively, leaving the fluorescein moiety largely unprotonated at physiological pH and thus limiting the sensitivity of the assay. To increase the fluorescein pK_a and, hence, the assay sensitivity, we installed an electron-donating alkyl group *ortho* to each phenol group. 2′,7′-Diethylfluorescein (DEF) has spectral properties similar to those of fluorescein but a higher phenolic pK_a. Most importantly, free and RI-bound DEF–RNase A have pK_a values of 6.68 and 7.29, respectively, resulting in a substantial increase in the sensitivity of the assay. Using DEF–RNase A rather than fluorescein–RNase A in a microplate assay at pH 7.12 increased the *Z′-factor* from –0.17 to 0.69. We propose that synthetic "tuning" of the pK_a of fluorescein and other pH-sensitive fluorophores provides a general means to optimize binding assays.

A1.2 Introduction

The xanthene dye fluorescein (A1.1) was first synthesized by Baeyer in 1871(Baeyer, 1871). Despite its antiquity, fluorescein remains one of the most widely utilized fluorophores in modern biochemical, biological, and medicinal research. This persistence can be attributed to the excellent spectral properties of fluorescein and the established synthetic chemistry of the dye. Fluorescein serves as a modular scaffold that is well-suited for elaboration to create various molecular tools, including ion indicators, fluorogenic enzyme substrates, and fluorescent labels for biomolecules (Haugland *et al.*, 2005; Urano *et al.*, 2005).

An important (and underappreciated) property of fluorescein is its complex acid–base equilibria in aqueous solution. Fluorescein can exist in seven prototropic forms. The determination of the distinct properties of each of these molecular forms has been the subject of numerous studies (Zanker and Peter, 1958; Lindqvist, 1960; Martin and Lindqvist, 1975; Chen *et al.*, 1979; Mchedlov-Petrosyan, 1979; Diehl, 1989; Diehl and Markuszewski, 1989; Sjoback *et al.*, 1995; Klonis and Sawyer, 1996; Lakowicz, 1999; Magde *et al.*, 2002; Smith and Pretorius, 2002; Krol *et al.*, 2006). The monoanion **A1.2** and dianion **A1.3** are the principal ground-state species under biologically-relevant conditions. Scheme A1.1 shows these two forms of fluorescein with the ranges of reported phenolic pK_a values and other spectral properties in aqueous solution. The dianionic form **A1.3** is responsible for the characteristic strong visible absorption band and potent fluorescence emission. The absorbance of the monoionic form **A1.2** is less intense, and the maxima are blue-shifted relative to **A1.3**. The quantum yield of the

monoanion is also significantly lower than that of the dianion. Because of the dissimilar optical properties of **A1.2** and **A1.3** and the proximity of the pK_a value to physiological pH, special care must be taken when using fluorescein and fluorescein-labeled conjugates in biological experiments. To circumvent this pH-sensitivity problem, fluorescein derivatives have been developed that employ the electron-withdrawing nature of chlorine (Mchedlov-Petrossyan *et al.*, 1992; Sparano *et al.*, 2004) or fluorine (Sun *et al.*, 1997) substituents to shift this phenolic pK_a to a lower value, thereby suppressing the heterogeneity of the protonation state of this phenolic group at physiologically relevant pH values.

The sensitivity of the fluorescence of fluorescein to its chemical environment has been exploited in assays of biological processes. Because of the proximity of the phenolic pK_a to biologically relevant pH values, small-molecule fluorescein derivatives have been employed as pH sensors (Thomas *et al.*, 1979; Paradiso *et al.*, 1984; Graber *et al.*, 1986; Nedergaard *et al.*, 1990; Liu *et al.*, 1997; Wu *et al.*, 2000; Schroder *et al.*, 2005). In addition, the pK_a value itself is sensitive to the electrostatic environment around the fluorescein molecule (Stanton *et al.*, 1984; Thelen *et al.*, 1984; Omelyanenko *et al.*, 1993; Griep and Mesman, 1995; Agi and Walt, 1997). Thus, the phenolic pK_a of a fluorescein label attached to a protein, for example, can be perturbed depending on the status of the biomolecule. The difference in pK_a value translates to an alteration in fluorescent intensity at constant pH. This environmentally-sensitive fluorescence variation has been used as an index to monitor changes in proteins (Garel, 1976; Labhardt *et al.*, 1983; Griep and Mchenry, 1990; Goldberg and Baldwin, 1998b; Goldberg and Baldwin, 1998a;

Goldberg and Baldwin, 1999) and nucleic acids (Friedrich and Woolley, 1988; Friedrich *et al.*, 1988; Sjoback *et al.*, 1998; Liu *et al.*, 2006). Studies of protein–protein interactions, in particular, can benefit from assays relying on the pK_a shift of a fluorescein label. Such assays circumvent the double-label requirement of Förster resonance energy transfer (FRET) (Sapsford *et al.*, 2006), and the size limitations of fluorescence polarization (FP) (Owicki, 2000).

Although binding assays relying on the pK_a shift of fluorescein are prevalent, the development of such assays is largely empirical. The effects of minor modifications to the fluorescein label remain unexplored. We were especially interested in discerning whether altering the pK_a of the dye would have a significant effect on assay performance. Our interest stems from a fluorescence-based assay developed in our laboratory (Abel *et al.*, 2002; Rutkoski *et al.*, 2005) for the determination of equilibrium dissociation constants for variants of bovine pancreatic ribonuclease (RNase A (Raines, 1998)) and its homologues in complex with the ribonuclease inhibitor protein (RI (Dickson *et al.*, 2005)). The ability of these pancreatic-type ribonucleases to evade RI is a prerequisite for their toxic activity toward cancer cells (Rutkoski *et al.*, 2005). Our assay is based on the decrease in fluorescence (~10–20%) of a fluorescein-labeled ribonuclease variant once bound by RI (Abel *et al.*, 2002). Competitive binding of RI by unlabeled ribonuclease variants restores fluorescence intensity, allowing accurate determination of equilibrium dissociation constants. Although the assay has proven to be useful, the low dynamic range requires a laborious, cuvette-based assay using sensitive instrumentation and large assay volumes. Expansion of the utility of this assay to a miniaturized, high-throughput

system (*e.g.*, microplate format) requires an increase in the fluorescence change without severe modification of other assay parameters.

Here, we describe a general means to improve binding assays through the synthesis and use of a "tuned" fluorescein derivative. As a model system, we use the RI–RNase A interaction, which allows for assays to be performed over a wide range of pH. First, we determine the pK_a values of the original fluorescein-labeled RNase A variant in the absence and presence of excess RI. From this analysis, we confirm a shift in the pK_a value of the fluorescein label upon complex formation, and surmise that tuning the pK_a to a higher value could lead to an improved dynamic range in our assay. Then, we synthesize and evaluate 2',7'-diethylfluorescein (DEF), which contains an electron-donating ethyl group proximal to each hydroxyl group. We find that DEF displays a higher phenolic pK_a than does fluorescein, making it a more useful probe. Next, we synthesize a novel thiol-reactive derivative of DEF for bioconjugation, 2',7'-diethylfluorescein-5-iodoacetamide (DEFIA), and determine pK_a values of a DEF-labeled RNase A in the absence and presence of RI. We observe a substantial increase in assay dynamic range near neutral pH, and show that the diethylfluorescein derivative is a near-optimal probe for this binding assay at our target pH. Lastly, we adapt this improved assay to a microplate format and use this simple, robust system to measure the dissociation constants of several complexes containing RI and variants of RNase A. These findings herald a new and comprehensive strategy for facilitating the analysis of biomolecular interactions.

A1.3 Experimental Procedures

A1.3.1 General Information

Fluorescein (reference standard grade) and 5-iodoacetamidofluorescein (5-IAF) were from Molecular Probes (Eugene, OR). Dulbecco's phosphate-buffered saline (Dulbecco and Vogt, 1954) (DPBS; Gibco) was from Invitrogen (Carlsbad, CA). Dithiothreitol (DTT) and *tris*-(hydroxymethyl)-aminomethane (TRIS) were from Research Products International (Mount Prospect, IL). All other chemicals were from Fisher Scientific (Hanover Park, IL) or Sigma–Aldrich (Milwaukee, WI). Bovine serum albumin (BSA) was obtained as a 20 mg/mL solution (Sigma; Product B8667). 2-(N-Morpholino)-ethanesulfonic acid (MES) was purified as described previously (Smith *et al.*, 2003) to eliminate oligo(vinylsulfonic acid) contamination. MALDI–TOF mass spectra were obtained with a Perkin–Elmer Voyager mass spectrometer in the Biophysics Instrumentation Facility (BIF) at the University of Wisconsin–Madison.

A1.3.2 Preparation of RI and Fluorophore-labeled Ribonucleases

Human ribonuclease inhibitor (RI), K7A/G88R RNase A, D38R/R39D/N67R/G88R RNase A, and K7A/D38R/R39D/G88R RNase A were prepared as described previously (Rutkoski *et al.*, 2005). The G88R and A19C/G88R variants of RNase A and the fluorescein-labeled conjugate (fluorescein–RNase A) were prepared as described previously (Abel *et al.*, 2002) with the following change: the proteins were refolded for ≥ 4 days under an inert atmosphere of $N_2(g)$. The DEFIA–protein conjugate (DEF–RNase A) was prepared by reaction of A19C/G88R RNase A with ten-fold excess of

DEFIA (**A1.14**) for 2.5 h at ambient temperature and then 16 h at 4 °C. Purification using a HiTrap SP HP cation-exchange column (GE Healthcare, Uppsala, Sweden) afforded the desired conjugate; MS (MALDI): *m/z* 14,261.00 (expected = 14,258.46). Protein concentration was determined by UV absorption or a bicinchoninic acid (BCA) assay kit from Pierce (Rockford, IL) using wild-type RNase A as a standard.

A1.3.3 UV–Visible and Fluorescence Spectroscopy

Absorption spectra were recorded in methacrylate cuvettes having 1-cm path length and 1.5-mL volume from Fisher Scientific on a Cary Model 50 spectrometer from Varian (Sugar Land, TX). Fluorometric measurements were made by using 4.5-mL methacrylate cuvettes from VWR or 4.5-mL glass cuvettes from Starna Cells (Atascadero, CA) and a QuantaMaster1 photon-counting spectrofluorometer from Photon Technology International (South Brunswick, NJ) equipped with sample stirring. All measurements were recorded at ambient temperature (23 ± 2 °C) and buffers were not degassed prior to measurements. Compounds were prepared as stock solutions in DMSO and diluted such that the DMSO concentration did not exceed 1% v/v. The pH was measured with a Beckman glass electrode that was calibrated prior to each use. Microplate-based experiments were performed in Costar 96-well NBS microplates (Product #3650) from Corning Life Sciences (Acton, MA). The fluorescence intensity was recorded using a Perkin–Elmer EnVison 2100 Plate Reader and an FITC filter set (excitation at 485 nm with 14-nm bandwidth; emission at 535 nm with 25-nm bandwidth; dichroic mirror cutoff at 505 nm) in the Keck Center for Chemical Genomics at the University of

Wisconsin–Madison. Graphs were manipulated and parameters were calculated with the programs Microsoft Excel 2003 and GraphPad Prism 4.

A1.3.4 Determination of pK$_a$ Values

The fluorescein acid–base equilibrium between phenol **A1.2** and phenolate **A1.3** is shown in eq A1.1:

$$\textbf{A1.2} \leftrightarrows \textbf{A1.3} + \text{H}^+ \qquad (A1.1)$$

The observed fluorescence intensity (I) at a given excitation and emission wavelength is given by eq A1.2:

$$I = f_2 I_2 + f_3 I_3 \qquad (A1.2)$$

where f_2 and f_3 are the fractions of the phenol and phenolate form of fluorescein, respectively, and I_2 and I_3 are the phenol and phenolate fluorescence intensities (Stanton *et al.*, 1984). The pK$_a$ of this acid–base equilibrium can be estimated by measuring the fluorescence intensity as a function of pH and fitting the data to eq A1.3:

$$I = I_2 + \frac{I_3 - I_2}{1 + 10^{pK_a - pH}} \qquad (A1.3)$$

which is derived from eq A1.2 and the Henderson–Hasselbalch equation.

Buffers contained NaCl (138 mM), DTT (1 mM), and NaOAc, MES, NaH_2PO_4,

TRIS, and $NaHCO_3$ (10 mM each). The pH of the buffered solutions was adjusted with

1.0 M NaOH or 1.0 M HCl. All experiments were performed in cuvettes using λ_{ex} = 493

nm and λ_{em} = 515 nm. The pK_a values of the free dyes were determined at a final dye

concentration of 50 nM. For determination of the pK_a of the protein labels, fluorescein–

RNase A or DEF–RNase A was added to the buffer solution at a final concentration of

50 nM, and the initial fluorescence was measured. RI was then added to a final

concentration of 350 nM, and the resulting fluorescence intensity was measured. The

average pK_a values were determined from triplicate experiments involving separate

buffer preparations.

A1.3.5 Spectral Properties

The extinction coefficient (ε) of fluorescein and 2',7'-diethylfluorescein was

determined with solutions in 0.1 M NaOH (A < 1.0). The absorbance of a series of

fluorescein and DEF concentrations were plotted against concentration, and the

extinction coefficient was calculated by linear regression using Beer's Law. The quantum

yield of DEF was determined by using dilute samples (A < 0.1) in 0.1 M NaOH. These

values were obtained by the comparison of the integrated area of the emission spectrum

of the samples with that of fluorescein in 0.1 M NaOH, which has a quantum efficiency

of 0.95 ± 0.03 (Lakowicz, 1999). The concentration of the fluorescein reference was

adjusted to match the absorbance of the test sample at the excitation wavelength. Under

these conditions, the quantum yield (Φ) was calculated with eq A1.4.

$$\Phi_{sample} = \Phi_{standard}(\int F_{em,sample} / \int F_{em,standard}) \tag{A1.4}$$

A1.3.6 Assay Comparison and Z'-factor Determination

Comparison of the gross dynamic range of the two protein conjugates was made using a cuvette format in DPBS containing BSA (2 µg/mL). The fluorescent protein conjugate (fluorescein–RNase A or DEF–RNase A) was added to a final concentration of 50 nM. RI was then added to a final concentration of 350 nM, and the resulting fluorescence change recorded. The Z'-factor was determined by preparing 96-well plates with 50 µL per well of DPBS containing fluorescein–RNase A or DEF–RNase A (100 nM; 2×) and BSA (0.1 mg/mL). The positive control plates also contained RNase A (10 µM; 2×). To these plates were added 50 µL per well of DPBS containing BSA (0.1 mg/mL), DTT (10 mM; 2×), and RI (100 nM; 2×). The fluorescence of each well was quantified after incubation at ambient temperature for 30 min. The Z'-factor was determined with eq A1.5 where σ^+ and σ^- are the standard deviations of the positive and negative controls, respectively, and μ^+ and μ^- are the means of the positive and negative controls (Zhang *et al.*, 1999).

$$Z' - factor = 1 - 3\frac{(\sigma^+ + \sigma^-)}{|\mu^+ - \mu^-|} \tag{A1.5}$$

A1.3.7 Determination of K_d Values

A serial dilution (2×) of the RNase A variant in DPBS with BSA (0.1 mg/mL) was prepared in Eppendorf Protein LoBind Tubes (Fisher Scientific). An aliquot (50 µL) of these serial dilutions was added to the wells of a 96-well plate. A solution (50 µL) of DEF–RNase A (100 nM; 2×) and RI (100 nM; 2×) in DPBS containing DTT (10 mM; 2×) and BSA (0.1 mg/mL) was then added to each well. The negative control contained no ribonuclease and the positive control contained excess RNase A (5 µM). The plate was incubated for 30 min at ambient temperature after which the fluorescence intensity was measured. The observed fluorescence intensity (I) is described by eq A1.6:

$$I = f_F I_F + f_B I_B \tag{A1.6}$$

where f_F and f_B are the fractions of the free and RI-bound form of the fluorescent conjugate, respectively, and I_F and I_B are the fluorescence intensities of the free and RI-bound states, respectively. The value of I_B was determined via linear regression using the intensities of the positive and negative controls, which represent 0% and 84.6% bound respectively based on a K_d value of 1.4 nM for the fluorophore-labeled G88R variant of RNase A (Rutkoski *et al.*, 2005). The fraction bound (f_B) was then calculated using eq A1.7:

$$f_B = \frac{I - I_F}{I_B - I_F} \tag{A1.7}$$

The value of K_d was calculated by plotting f_B against the concentration of competing ribonuclease and fitting the data to the mathematical expression for complete competitive binding of two different ligands (Wang, 1995; Roehrl et al., 2004).

A1.4 Results and Discussion

A1.4.1 pK$_a$ Values of Bound and Free Fluorescein-Labeled RNase A

Our binding assay utilizes the A19C/G88R variant of RNase A. Ala19 resides in a solvent-exposed loop that is not within the interface of the RI·RNase A complex (Kobe and Deisenhofer, 1996). Introduction of a thiol group at this position allows site-specific labeling that does not perturb other properties of the protein, such as enzymatic activity or binding to RI (Abel et al., 2002). The fluorescein label is attached covalently by reaction of the free thiol-containing protein with 5-iodoacetamidofluorescein (5-IAF) to give fluorescein-labeled RNase A (fluorecein–RNase A). The RI·RNase A complex exhibits extremely tight binding (K_d = 44 fM, (Lee et al., 1989)). Substitution at position 88 attenuates the binding constant of the complex by more than four orders of magnitude (K_d = 1.4 nM, (Rutkoski et al., 2005)) and thus allows for effective competition by other ribonucleases with K_d values at or above the nanomolar range. Our assay is typically performed in commercial Dulbecco's phosphate-buffered saline (DPBS) (Dulbecco and Vogt, 1954) at pH 7.12, which defines the target pH for assay optimization.

In the original report (Abel et al., 2002) of this assay system, we noted that the cause of the fluorescence change of the fluorescein conjugate of A19C/G88R RNase A (herein, fluorescein–RNase A) upon binding to RI was unclear, but we hypothesized that it arose

from a shift in the pK_a of the fluorescein label. To test this premise, and gain insight for assay optimization, we measured the pK_a values of both bound and free fluorescein–RNase A. A series of buffers were prepared from pH 4 to 10, and the fluorescence intensity of the conjugate in the absence and presence of a 7-fold molar excess of RI was measured and plotted against pH. This surfeit of RI is sufficient to bind >99.5% of the labeled ribonuclease based on the K_d value of 1.4 nM (Rutkoski *et al.*, 2005). The difference between the curves was also calculated, and the resulting data are shown in Figure A1.1A.

The data in Figure A1.1A conform to a model for pK_a shifts of fluorescein–protein conjugates described by Garel (Garel, 1976), including the bell-shaped difference trace. We note that at high pH values, complex formation causes only a minor decrease (<5%) in fluorescence intensity. The inhibition of the catalytic activity of RNase A by RI is known to be similar in solutions of different pH (Lee *et al.*, 1989), indicating that complex formation is unaffected by pH. Thus, the traces in Figure A1.1A suggest that the pK_a shift of fluorescein upon RI binding is the primary cause for the fluorescence modulation. The phenolic pK_a value of the free fluorescein–RNase A is 6.35 ± 0.03, and the pK_a value for RI-bound fluorescein–RNase A is 6.70 ± 0.02. The maximal difference is at pH 6.5, making that the solution pH at which our assay is most sensitive. Interestingly, the pK_a values for the free and RI-bound conjugates are both higher than our measured pK_a value for free fluorescein of 6.30 ± 0.03 (*vida infra*).

The phenolic pK_a value of fluorescein can change dramatically upon conjugation to a biomolecule (Klonis *et al.*, 1998), and it remains difficult to predict how the local

environment around the label will affect the pK_a of the dye. Nonetheless, the shift in pK_a value upon binding of fluorescein–RNase A by RI is intuitive, based on the net macromolecular charge of the two proteins. RNase A is a cationic protein (pI = 9.33, (Ui, 1971)), creating an electropositive field in which the ionization of fluorescein is relatively favorable. Binding of RNase A to the comparatively anionic RI (pI = 4.7, (Blackburn et al., 1977)) can neutralize much of this field (Lee et al., 1989), leading to an increased phenolic pK_a value for the fluorescein label.

The data in Figure A1.1A suggested to us an optimization strategy that involved "tuning" the phenolic pK_a value of the label through chemical synthesis. Changing the pK_a of fluorescein would, in effect, shift the pK_a curves of the free and RI-bound conjugate either higher or lower along the abscissa, causing the maximal difference between these two curves to align more closely with the desired assay pH. Such a shift could lead to a higher assay dynamic range at the preferred pH. Prior attempts to adjust the pK_a of fluorescein labels have focused on decreasing this value as much as possible to abolish pH sensitivity (Mchedlov-Petrossyan et al., 1992; Sun et al., 1997; Haugland et al., 2005). Conversely, our goal was to *increase* the pK_a so as to maximize the fluorescence change at the assay pH.

A1.4.2 Design and Synthesis of 2',7'-Diethylfluorescein

The proximity of the pK_a value of fluorescein to biologically relevant pH values allows its use as fluorescent pH indicator in certain experiments (Thomas et al., 1979; Graber et al., 1986; Wu et al., 2000). Alkyl substitution on the xanthenyl portion of

fluorescein can increase the phenolic pK_a of fluorescein, making it more sensitive to changes in pH near neutrality. Such substitution was exploited by Tsien and coworkers to prepare the widely used pH indicator 2',7'-*bis*-carboxyethyl-5(6)-carboxyfluorescein (BCECF) that possesses a pK_a near 7.0 (Paradiso *et al.*, 1984; Graber *et al.*, 1986). Hexyl-substituted fluoresceins also show an increase in the phenolic pK_a making them useful fluorescent pH sensors (Schroder *et al.*, 2005). Although these compounds show the desired increase in pK_a value, the relatively large appendages could cause unnecessary disruption of the protein if incorporated into a fluorescent label. Substitution with smaller, ethyl groups at the 2' and 7' positions can also increase the pK_a of fluorescein (Diwu *et al.*, 2004). We reasoned that the negligible perturbation of the fluorescein structure from such ethyl substituents would preserve its utility as a label.

To evaluate the effect of ethyl-group substitution, we synthesized 2',7'-diethylfluorescein (DEF) by the route shown in Scheme A1.2. This compound was reported in the 1930's by Novelli in research directed toward the development of fluorescein-based antiseptics (Novelli, 1932; Novelli, 1933). We used a more contemporary route, taking advantage of the commercial availability of 4-ethylresorcinol **A1.4**. This compound was condensed with phthalic anhydride **A1.5** in methanesulfonic acid (Sun *et al.*, 1997) to afford crude DEF. This material was acetylated with acetic anhydride in pyridine, and the resulting diacetate **A1.6** was purified via crystallization. We found that suspension of the crude **A1.6** in cold EtOH prior to crystallization removed a significant amount of polar impurities, thereby improving the yield. Hydrolysis of the ester groups with base followed by acidification gave DEF (**A1.7**).

A1.4.3 Spectral Properties of 2',7'-Diethylfluorescein

Both fluorescein and 2',7'-diethylfluorescein were evaluated to confirm the anticipated effect of alkylation on the pK_a value and to compare other spectral properties of these dyes in aqueous solution. The measured parameters are listed in Table A1.1. The pK_a values for both fluorescein and DEF were determined in the same buffer system used for the fluorescein–RNase A conjugate (see: Figure A1.2). The extinction coefficients and quantum yields of fluorescein and DEF were determined in 0.1 M NaOH to isolate the properties of the dianionic dye form.

The spectral values determined for the diethyl variant of fluorescein are close to those reported for other dialkyl derivatives (Schroder et al., 2005). The electron-donating character of the ethyl substituents increases the pK_a from 6.30 to 6.61. Our pK_a value for free fluorescein is slightly lower than the reported range of values (Mchedlov-Petrosyan, 1979; Diehl, 1989; Diehl and Markuszewski, 1989; Sjoback et al., 1995; Klonis and Sawyer, 1996; Smith and Pretorius, 2002) because of the relatively high ionic strength of our buffer system (Sjoback et al., 1995). The alkyl substitution also elicits bathochromic shifts of 10 nm for both absorption and emission maxima relative to fluorescein (Figure A1.2). The extinction coefficient at maximal absorption of DEF under basic conditions (0.1 M NaOH) is about 10% higher than the absorptivity of fluorescein. The quantum yield of diethylfluorescein is slightly lower than that of fluorescein, again in agreement with other reported dialkylfluorescein derivatives (Schroder et al., 2005). Overall, the ethyl group substitution confers the desired increase in pK_a value while causing only minor differences in absorption and fluorescence properties (Figure A1.3).

This similarity of optical characteristics of the two dyes allows for the use of standard fluorescein excitation and emission wavelengths for both dyes and their conjugates.

A1.4.4 Synthesis of 2',7'-Diethylfluorescein-5-iodoacetamide (DEFIA)

Having confirmed the elevated pK_a values of DEF, we next sought to prepare a thiol-reactive derivative for bioconjugation. To ensure an accurate comparison between fluorescein-labeled and DEF-labeled proteins, we designed an analogue of 5-IAF in which introduction of the ethyl groups was the only structural perturbation, thereby eliminating effects due to different linker lengths or conjugation chemistries. The synthesis of 5-aminofluorescein is well documented because of its intermediacy in the preparation of the widely-used fluorescent label: fluorescein-isothiocyanate (FITC) (Coons and Kaplan, 1950; McKinney et al., 1962; Steinbach, 1974). We were pleased to discover that this established chemistry is sufficiently pliable to allow for introduction of the desired ethyl substituents without dramatic changes in yield. To our knowledge, this is the first example of a fluorescein-derived label in which the phenolic pK_a is tuned to a higher rather than a lower value. In addition, this synthesis adds to the sparse reports in the primary scientific literature describing iodoacetamide derivatives of xanthene dyes (Krafft et al., 1988; Corrie and Craik, 1994).

The scheme for the synthesis of 2',7'-diethylfluorescein-5-iodoacetamide (DEFIA) is shown in Scheme A1.3. Condensation of 4-ethylresorcinol **A1.4** with commercially available 4-nitrophthalic anhydride **A1.8** gave fluorescein **A1.9** as a mixture of 5- and 6-nitro isomers. This material could be acetylated with acetic anhydride to yield a diacetate.

Separation of the two isomers via recrystallization (Coons and Kaplan, 1950) afforded

the single 5-nitro isomer **A1.10**. Hydrolysis of this diacetate with base gave free 5-nitro-

2',7'-diethylfluorescein **A1.11**. Reduction of the nitro group with sulfide (Steinbach,

1974) followed by crystallization from aqueous HCl gave the 5-aminofluorescein as the

HCl salt. Dissolving this intermediate HCl salt in basic solution followed by precipitation

of the free amine with acetic acid (McKinney *et al.*, 1962) afforded the 5-amino-2',7'-

diethylfluorescein **A1.12**. This material was treated with chloroacetic anhydride to give

an intermediate 5-amidofluorescein diester. Hydrolysis of the ester groups using NaOH in

the same pot gave chloroacetamide **A1.13**, which was taken on to DEFIA (**A1.14**) via

reaction with NaI in acetone.

A1.4.5 pK$_a$ Values of Free and RI-Bound DEF-labeled A19C/G88R RNase A

Thiol-containing A19C/G88R RNase A variant was reacted with DEFIA, and the

resulting conjugate was purified with cation-exchange chromatography. The fluorescence

intensity of the resulting 2',7'-diethylfluorescein conjugate of A19C/G88R RNase A

(herein, DEF–RNase A) was measured in the absence and presence of RI in buffered

aqueous solution over a pH range of 4–10, as with the fluorescein–RNase A conjugate.

The fluorescence values and fluorescence difference were plotted against pH as shown in

Figure A1.1B. The pK_a values of the free and RI-bound DEF–RNase A were calculated

to be 6.68 ± 0.03 and 7.29 ± 0.03, respectively. As with the fluorescein system, these

values are higher than those measured for unliganded DEF (pK_a = 6.61 ± 0.03). This shift

in pK_a values increases the maximum of the fluorescence difference to above 7.0.

The bound and free DEFIA conjugates exhibit a larger ΔpK_a value than did the fluorescein-labeled protein. This larger difference in pK_a likely arises from structural rather than electronic consequences of the two ethyl groups. For example, the DEF label could exist in a different orientation than the fluorescein label such that its pK_a value is affected to a greater degree upon binding to RI.

A1.4.6 Assay Comparison

A major goal of this work was to improve the assay performance and then investigate the utility of the enhanced system in a microplate format. To quantify the assay improvement, we first determined the maximum dynamic range by measuring the change in fluorescence upon RI binding under typical assay conditions. Addition of excess RI to fluorescein–RNase A elicits a 15% decrease in fluorescence, whereas the change in fluorescence intensity of the DEF–RNase A conjugate is a significantly larger 38% (Figure A1.4).

Having confirmed the enhancement of the assay, we then evaluated the utility of this assay in a microplate format. A common quantification of plate-based assay performance is the *Z'-factor* which uses the standard deviation of controls and the dynamic range to assign a numerical value to assay utility (Zhang *et al.*, 1999). We measured the *Z'-factor* using microplates containing the labeled conjugate and RI. The positive control also contained excess RNase A to liberate fully the fluorophore-labeled protein. As shown in Figure A1.5, the fluorescein system had *Z'-factor* = –0.17, signifying an overlap of the $\mu \pm 3\sigma$ levels for the positive and negative controls. In stark contrast, the

diethylfluorescein system had a Z'-factor of 0.69. An assay system with a Z'-factor >0.5 is considered to be "excellent" (Zhang et al., 1999) and therefore highly useful in microplate systems, including high-throughput screening (HTS) assays. Thus, in addition to improving assay performance, this new diethylfluorescein label could allow HTS to identify compounds that disrupt the RI–ribonuclease interaction.

A1.4.7 Microplate-Based Determination of K_d Values

The increase in assay dynamic range and superb Z'-factor prompted us to validate this microplate system to measure RI·ribonuclease dissociation constants. Pancreatic-type ribonucleases are cationic proteins that can enter cells via endocytosis (Haigis and Raines, 2003). The ubiquitous ribonuclease inhibitor has a high cytosolic concentration (4 μM) and can therefore protect cellular RNA from degradation by invading ribonucleases (Haigis et al., 2003). Amino acid substitutions that disrupt the RI–ribonuclease interface can endow an otherwise benign ribonuclease with cytotoxic activity (Rutkoski et al., 2005). Thus, the K_d value of a RI·ribonuclease complex is helpful in predicting the cytotoxicity of a novel ribonuclease variant.

We first determined the affinity of DEF–RNase A for RI by direct titration (Abel et al., 2002) and found that the ethyl groups did not cause any significant change in binding constant between the labeled protein and RI (data not shown). We then determined the K_d values for other variants of RNase A using DEF–RNase A in microplates (Figure A1.6). These values (± SE), which are listed in Table A1.2, are in gratifying agreement with those determined previously using the cuvette assay (Rutkoski et al., 2005). The new

system proved extremely facile and economical, requiring 5% of the protein and significantly less time compared to the original assay format.

A1.5 Conclusions

The ubiquity of fluorescein in biochemical, biological, and medicinal research demands a detailed grasp of the acid–base equilibria of this dye in aqueous solution. Our results show that a thorough understanding and application of the nuances of fluorescein can be useful in the optimization of assays. Shifts in the phenolic pK_a are a significant causal force behind many of the fluorescence modulations observed with fluorescein conjugates. Tuning this pK_a through chemical synthesis can have dramatic effects on assay dynamic range, leading to significant improvement in throughput and requisite sample volume.

This work could inspire the expansion of the current spectrum of fluorescent labels. A palette of reactive dyes with tuned pK_a values could prove useful in the development of new binding assays. In addition to fluorescein, other classes of fluorescent dyes are sensitive to pH and thus could be evaluated and optimized in a similar manner. Of particular interest are dye systems that exhibit a large spectral shift upon protonation (Whitaker *et al.*, 1991; Liu *et al.*, 2001). Use of these fluorophores could permit ratiometric measurement of binding events. Overall, properly tuned fluorescent labels hold the potential to improve existing systems and aid in the development of new assays for characterizing protein–protein interactions and other important biomolecular processes.

Table A1.1 Spectroscopic parameters of fluorescein and 2′,7′-diethylfluorescein (DEF)

Parameter	Fluorescein	DEF
pK_a	6.30 ± 0.02	6.61 ± 0.03
λ_{max} (nm)	491	501
ε (mM^{-1}cm^{-1})	89.8 ± 0.4	98.5 ± 0.4
λ_{em} (nm)	510	520
Φ	0.95 ± 0.03[a]	0.89 ± 0.03

[a] Value from ref (Lakowicz, 1999).

Table A1.2 Values of K_d for RI·ribonuclease complexes

RNase A	K_d^a (nM)
G88R	1.3 ± 0.2
K7A/G88R	80 ± 5
D38R/R39D/N67R/G88R	730 ± 40
K7A/D38R/R39D/G88R	3100 ± 200

^{a} Values of K_d ($\pm$ SE) were determined in microplate assays with DEF–RNase A at pH 7.12.

HO—⬡—O—⬡=O

CO₂H

A1.1

HO—⬡—O—⬡=O

CO₂⁻

A1.2

λ_{max} = 453, 472 nm
ε = 29,000–32,600 M⁻¹cm⁻¹
Φ = 0.36–0.37

∓H⁺
pK_a 6.31–6.80

⁻O—⬡—O—⬡=O

CO₂⁻

A1.3

λ_{max} = 490 nm
ε = 76,900–87,600 M⁻¹cm⁻¹
Φ = 0.92–0.95
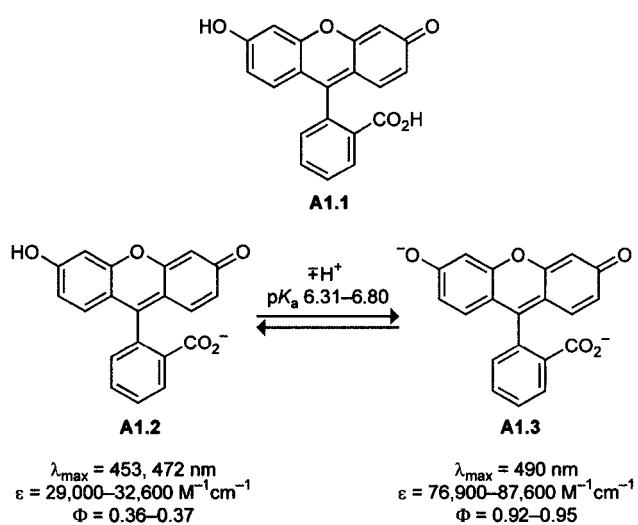
Scheme A1.1 Fluorescein and its principal ground-state species
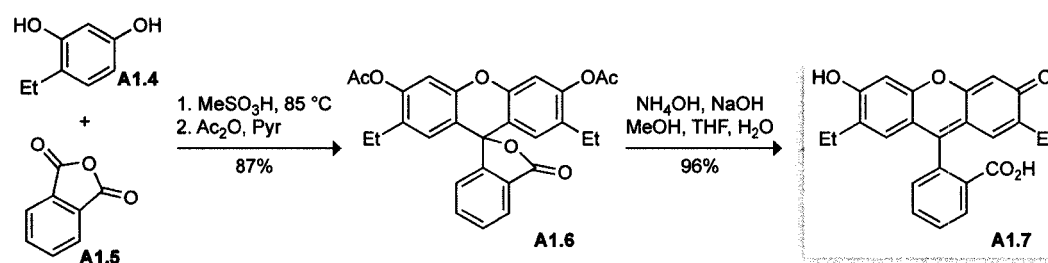
Scheme A1.2 Synthesis of 2′,7′-diethylfluorescein (DEF)
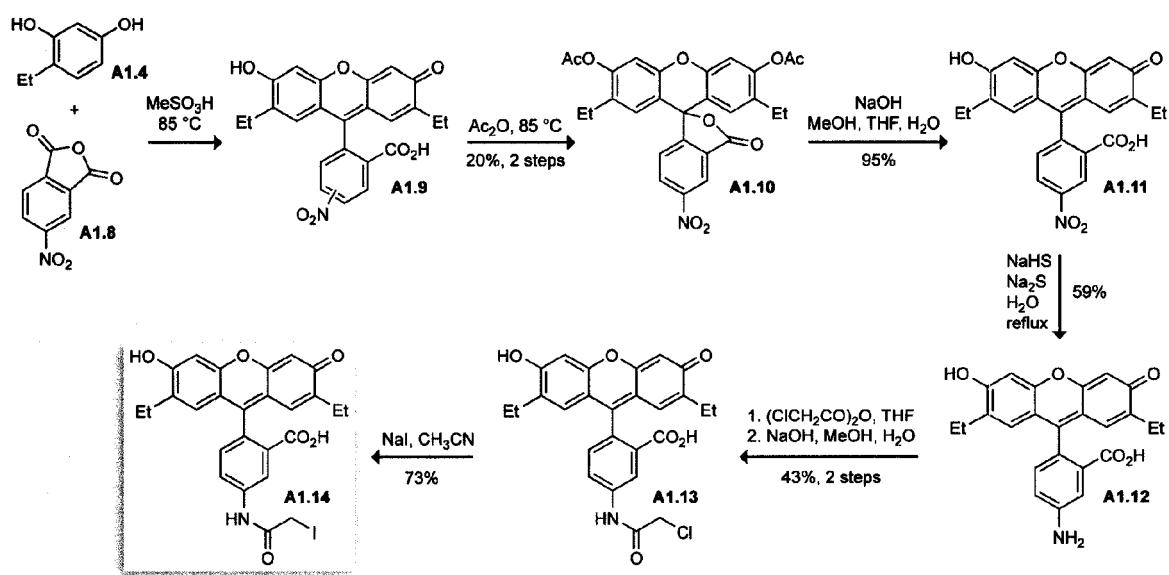
Scheme A1.3 Synthesis of 2′,7′-diethylfluorescein-5-iodoacetamide (DEFIA)
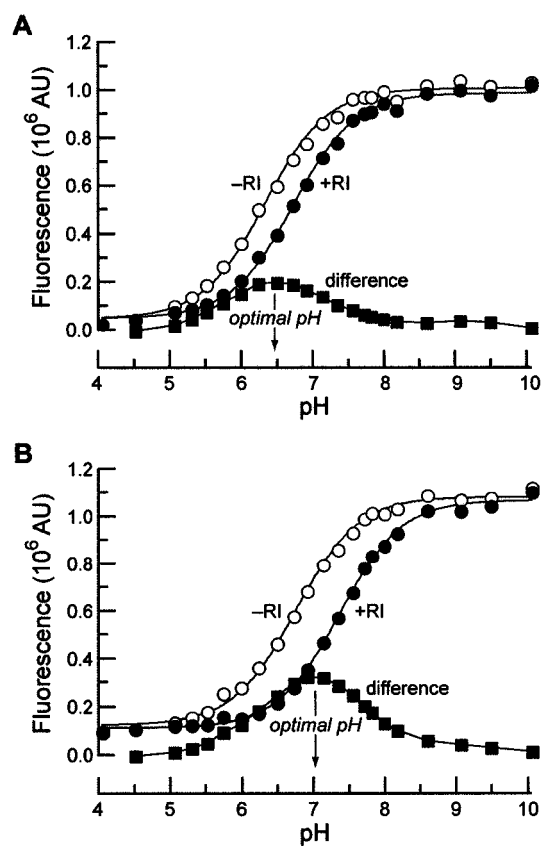
Figure A1.1 Effect of pH on the fluorescence (λ_{ex} = 493 nm, λ_{em} = 515 nm) of

fluorophore-labeled RNase A (50 nM) in the absence (O) or presence (●)

of excess RI (350 nM), and the difference (■). (A) Fluorescein–RNase A.

(B) DEF–RNase A.
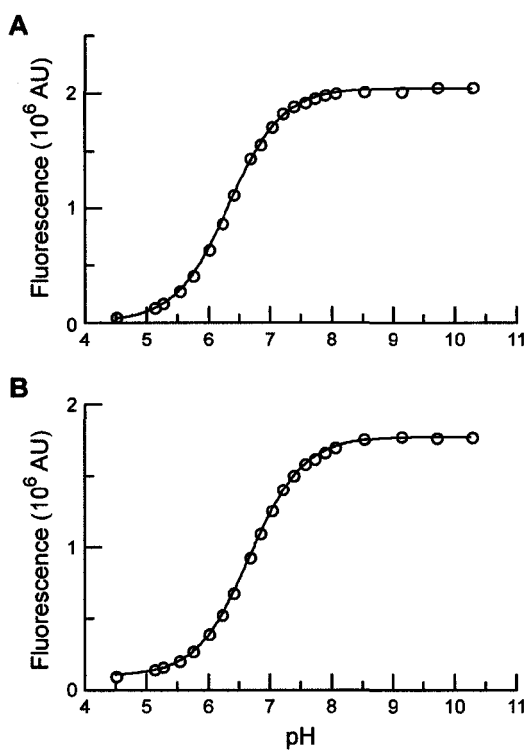
Figure A1.2 (A) pH-Dependence of the fluorescence of fluorescein (A1.1) and (B)

2',7'-diethylfluorescein (A1.7) (λ_{ex} = 493 nm, λ_{em} = 515 nm). Values of

pK_a were found to be 6.30 ± 0.02 for A1.1, and 6.61 ± 0.03 for A1.7.
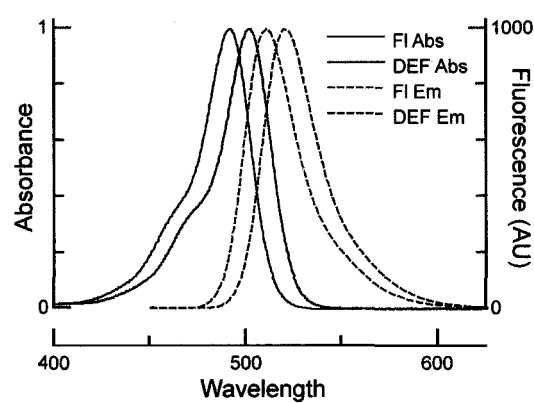
Figure A1.3 Normalized absorption and emission spectra of fluorescein (**A1.1**) and

2',7'-diethylfluorescein (**A1.7**) in 0.1 M NaOH.
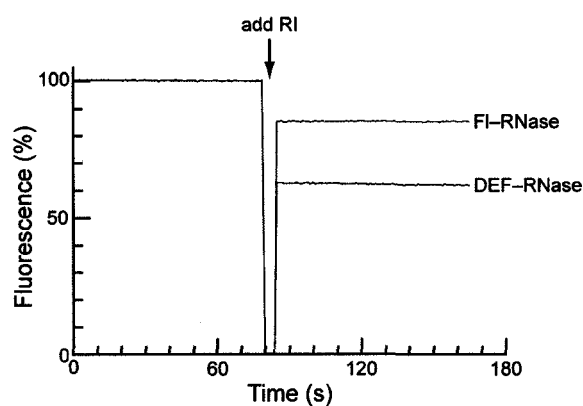
Figure A1.4   Comparison of the fluorescence change of Fl–RNase (red) and DEF–

RNase (blue) upon addition of excess RI (λ_{ex} = 493 nm, λ_{em} = 515 nm) in

DPBS containing BSA (2 µg/mL).
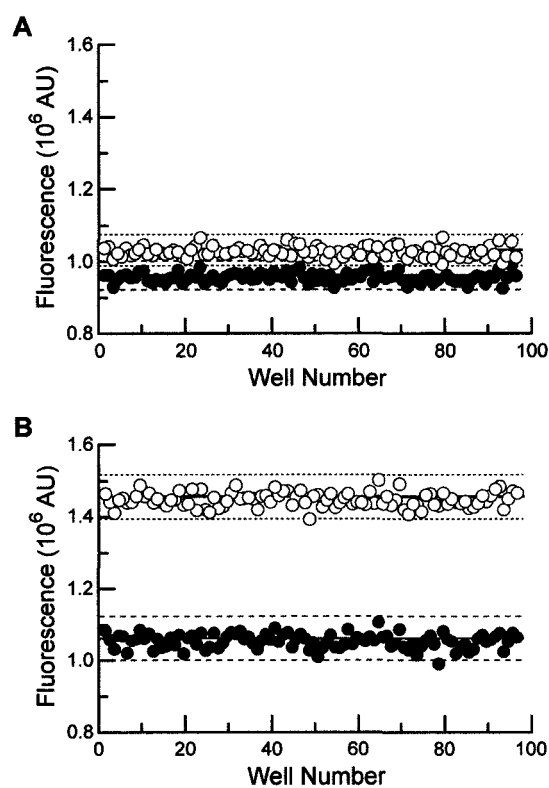
Figure A1.5 Fluorescence in microplate wells containing a fluorophore-labeled

ribonuclease (50 nM) and RI (50 nM) in the absence (O) or presence (●)

of excess RNase A (5 μM) at pH 7.12. Horizontal solid lines indicate the

mean value; horizontal dashed lines indicate the range (±3σ) of values. (A)

Fluorescein–RNase A (Z'-factor –0.17). (B) DEF–RNase A (Z'-factor

0.69).
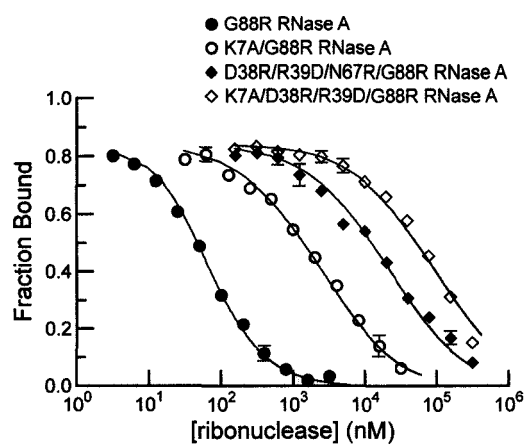
Figure A1.6 Data from microplate assays for determination of the K_d values of

RI·ribonuclease complexes in DPBS containing BSA (0.1 mg/mL).

APPENDIX 2

Increasing the Potency of a Cytotoxin with an Arginine Graft

A2.1 Abstract

Variants and homologs of bovine pancreatic ribonuclease (RNase A) can exhibit cytotoxic activity. This toxicity relies on cellular internalization of the enzyme. Residues Glu49 and Asp53 form an anionic patch on the surface of RNase A. We find that replacing these two residues with arginine does not affect catalytic activity or affinity for the cytosolic ribonuclease inhibitor protein (RI). This "arginine graft" does, however, increase the toxicity towards human cancer cells. Appending a nonaarginine domain to this cationic variant results in an additional increase in cytotoxicity, providing one of the most cytotoxic known variants of RNase A. These findings correlate the potency of a ribonuclease with its deliverance of ribonucleolytic activity to the cytosol, and indicate a rational means to enhance the efficacy of ribonucleases and other cytotoxic proteins.

A2.2 Introduction

Ribonucleases can be cytotoxic and thus have notable potential as chemotherapeutic agents (Youle and D'Alessio, 1997; Leland and Raines, 2001; Matoušek, 2001; Makarov and Ilinskaya, 2003; Benito et al., 2005; Arnold and Ulbrich-Hofmann, 2006). Bovine pancreatic ribonuclease (RNase A; EC 3.1.27.5) is the most-studied ribonuclease (Cuchillo et al., 1997; Raines, 1998). Although wild-type RNase A is not toxic to mammalian cells, properly engineered variants are cytotoxic (Rutkoski et al., 2005).

The cytotoxicity of a mammalian ribonuclease relies on several attributes (Bretscher et al., 2000; Dickson et al., 2003). First and foremost, ribonucleolytic activity is required for cytotoxicity (Ardelt et al., 1991; Kim et al., 1995a). The cytotoxicity of a ribonuclease also correlates with its ability to evade the cytosolic ribonuclease inhibitor (RI) protein (Haigis et al., 2003; Dickson et al., 2005; Rutkoski et al., 2005; Johnson et al., 2007c). Even single amino-acid substitutions that weaken the affinity for RI make RNase A cytotoxic (Leland et al., 1998). The potency of cytotoxic RNase A variants is increased by enhancing their conformational stability (Klink and Raines, 2000). Lastly, a ribonuclease must reach the cytoplasm to engage and then degrade RNA. Mammalian ribonucleases bind to the cell surface through Coulombic interactions between cationic residues and anionic cell-surface molecules (Notomista et al., 2006), and are then endocytosed through a dynamin-independent pathway without the need for a specific receptor (Haigis and Raines, 2003). The efficiency of internalization is thus a key determinant of cytotoxicity (Wu et al., 1995), and can be increased by fusion to transferrin (Suzuki et al., 1999) or by making noncovalent or covalent oligomers that

serve to increase molecular charge (Matoušek *et al.*, 2003a; Libonati, 2004; Leich *et al.*, 2006).

Cationic molecules are taken up readily by mammalian cells (Ryser and Hancock, 1965; Fuchs and Raines, 2006). By condensing the carboxyl groups of RNase A with ethylenediamine, Yamada and coworkers endowed the enzyme with cytotoxic activity but also diminished by 20-fold its enzymatic activity (Futami *et al.*, 2002). This dichotomous result highlights a severe limitation of chemical cationization—the reaction is non-specific, producing a complex mixture of products and compromising function by allowing the modification of residues important for substrate binding or catalysis. In addition, chemical cationization attenuated the affinity of RNase A for RI, making it difficult to tease apart the individual contributions of increased positive charge and decreased affinity for RI in enhancing cytotoxic activity.

Here, we employ a new approach, 'arginine grafting' (Fuchs and Raines, 2007), to create a more cell-permeable variant of RNase A. The premise is that installing a patch of arginine residues improves affinity for the cell surface and hence cellular internalization, without affecting other properties of the enzyme. The resulting variant is a single, well-defined protein that can be produced by recombinant DNA technology alone. Previously, replacing five dispersed acidic residues with lysine was shown to endow a microbial ribonuclease with cytotoxic activity (Ilinskaya *et al.*, 2002). By replacing only two proximal acidic residues with arginines, we create an arginine patch that increases the cytotoxicity of an RNase A variant. By also adding a protein transduction domain, we increase cytotoxicity even further.

A2.3 Experimental Procedures

A2.3.1 Cells and Chemicals

Escherichia coli strains BL21(DE3) pLysS and BL21(DE3) were from Novagen

(Madison, WI, USA). Human erythroleukemia cells (line K-562) were from the

American Type Culture Collection (Manassas, VA, USA). [methyl-^{3}H]Thymidine (6.7

Ci/mmol) was from NEN Life Science Products (Boston, MA, USA). All other chemicals

and reagents were of commercial reagent grade or better, and were used without further

purification.

A2.3.2 Instruments

The mass of each RNase A variant was ascertained by MALDI–TOF mass

spectrometry using a Voyager-DE-PRO Biospectrometry Workstation (Applied

Biosystems, Foster City, CA, USA) with 3,5-dimethoxy-4-hydroxycinnamic acid as a

matrix in the campus Biophysics Instrumentation Facility. Fluorescence measurements

were performed with a QuantaMaster 1 photon-counting fluorometer equipped with

sample stirring (Photon Technology International, South Brunswick, NJ, USA).

Radioactivity was quantified with a Microbeta TriLux liquid scintillation counter

(Perkin–Elmer, Wellesley, MA, USA). Electrostatic potential maps were created with the

program PyMol (DeLano Scientific, South San Francisco, CA, USA).

A2.3.3 Site-directed mutagenesis

Oligonucleotides were obtained from Integrated DNA Technology (Coralville, IA, USA). cDNA encoding variants of RNase A were created in plasmid pBXR, which directs the production of RNase A in *E. coli* (delCardayré *et al.*, 1995), by using the QuikChange mutagenesis kit from Stratagene (La Jolla, CA, USA). All variants of RNase A possessed either the native Lys1 residue (wild-type RNase A, G88R RNase A, E49/D53R RNase A, and E49/D53R/G88R RNase A) or an N-terminal methionine residue (R_9-tagged variants of RNase A), which has no effect on ribonucleolytic activity (Arnold *et al.*, 2002). The C-terminal R_9 tag was distanced from the remainder of a protein by a triglycine linker.

A2.3.4 Production and Purification of Protein Variants

Untagged variants of RNase A and Onconase [which is the most cytotoxic known homolog of RNase A (Matoušek *et al.*, 2003b)] were produced in *E. coli* BL21(DE3) and purified as described previously (Leland *et al.*, 1998). Variants of RNase A containing a C-terminal R_9 tag were produced in BL21(DE3)pLysS cells and purified as described previously (Fuchs and Raines, 2005).

A2.3.5 Assay of Enzymatic Activity

Ribonucleolytic activity was measured by monitoring the increase in the fluorescence of 6-FAM–dArU(dA)$_2$–6-TAMRA (Integrated DNA Technologies, Coralville, IA, USA) upon enzyme-catalyzed cleavage, as described previously (Kelemen *et al.*, 1999) with

minor modifications. Polyarginine-containing peptides are known to bind to glass surfaces (Chico *et al.*, 2003). We observed this phenomenon with RNase A (Fuchs and Raines, 2005), and so performed all enzymatic activity assays in 10 mM Bis-Tris–HCl buffer, pH 6.0, containing NaCl (0.50 M). In this high-salt buffer, the binding of protein to a quartz cuvette was found to be insignificant.

A2.3.6 Assay of Conformational Stability

As RNase A is denatured, its six tyrosine residues become exposed to solvent and its molar absorptivity at 287 nm decreases significantly (Hermans and Scheraga, 1961). Unfolding was monitored in PBS by the change in absorbance at 287 nm as the temperature was raised at a rate of 0.15 °C/min. Data were fitted to a two-state model to calculate the value of T_m (Pace *et al.*, 1998), which is the temperature at the midpoint of the transition between the folded and unfolded states.

A2.3.7 Assay of Ribonuclease Inhibitor Binding

The affinity of RNase A variants for human RI (hRI) was determined by using a competition binding assay reported recently (Lavis *et al.*, 2007). Unlike other assays (Abel *et al.*, 2002), this assay exhibits negligible protein loss by non-specific binding, allowing the determination of K_d values for the highly cationic R_9-tagged variants of RNase A.

A2.3.8 Assay of Cytotoxicity

The effect of ribonucleases on the proliferation of K-562 cells was determined by measuring the incorporation of [methyl-^{3}H]thymidine into cellular DNA as described previously (Leland *et al.*, 1998; Rutkoski *et al.*, 2005).

A2.4 Results and Discussion

A2.4.1 Design of Cationic RNase A Variants

The ability of polycations to effect the cellular internalization of a macromolecule has been known for over 40 years (Ryser and Hancock, 1965; Fuchs and Raines, 2006). Recently, we used an arginine "graft" to endow the green fluorescent protein from the jellyfish *Aequorea victoria* with cell permeability (Fuchs and Raines, 2007). We have now applied the arginine grafting strategy to RNase A, a mammalian protein that can be cytotoxic.

We used the cytotoxic activity of an RNase A variant as a measure of its cellular internalization. This measure, though indirect, requires the internalized ribonuclease to retain its catalytic activity (and, thus, its three-dimensional structure) to elicit cytotoxicity (Ardelt *et al.*, 1991; Kim *et al.*, 1995a). Accordingly, most of our variants contained the G88R substitution, which makes RNase A cytotoxic by raising the K_d value for the hRI·RNase A complex (Leland *et al.*, 1998).

We sought to increase the cationicity of RNase A without disrupting catalytic activity. In an electrostatic potential map of RNase A, we noted the presence of two acidic residues on its molecular surface (Figure A2.1A and A2.1B). These residues,

Glu49 and Asp53, are in close proximity to one another but remote from the active site. We hypothesized that replacing these acidic residues with basic ones would create a cationic patch without compromising catalytic activity. We chose to replace Glu49 and Asp53 with arginine, which is the most effective residue for facilitating cellular internalization (Mitchell *et al.*, 2000; Suzuki *et al.*, 2002). Recently, we showed that appending an R$_9$ tag to the C-terminus of RNase A increased its internalization (Fuchs and Raines, 2005). Hence, we also determined if an arginine graft and an R$_9$ tag have an additive effect on cytotoxic activity.

A2.4.2 Biochemical Properties of RNase A Variants

The E49R/D53R-containing variants of RNase A exhibited wild-type catalytic activity (Table A2.1), as expected. The conformational stability of the E49R/D53R and E49R/D53R/G88R variants (T_m = 54 °C) was, however, significantly lower than that of either wild-type RNase A (T_m = 64 °C) or the G88R variant (T_m = 60 °C). Appending an R$_9$ tag to either the E49R/D53R or E49R/D53R/G88R variant decreased their stability even further. Still, all variants were >99% folded at physiological temperature.

The ability to evade endogenous RI protein within mammalian cells is a strong determinant of ribonuclease cytotoxicity (Leland *et al.*, 1998; Rutkoski *et al.*, 2005; Johnson *et al.*, 2007c). Glu49 and Asp53 are remote from the molecular interface in the porcine RI·RNase A complex (Figure A2.1C). Nevertheless, we measured the affinity of both E49R/D53R/G88R RNase A and E49R/D53R/G88R RNase A–R$_9$ for RI

(Table A2.1), finding these affinities (K_d = 2.6 nM and K_d = 3.0 nM, respectively) to be comparable to that of G88R RNase A (K_d = 2.8 nM).

A2.4.3 Cytotoxicity of RNase A Variants

The toxicity of a ribonuclease increases as its cellular internalization becomes more efficient (Fuchs and Raines, 2005; Leich et al., 2007). We monitored the internalization of the RNase A variants by measuring their toxicity to K-562 cells (Figure A2.2; Table A2.1). Wild-type RNase A is not toxic to mammalian cells due to its high affinity for the cytosolic RI protein. The RI-evasive variant, G88R RNase A, had an IC_{50} value of 6.2 μM. Arginine grafting increased the cytotoxicity of this variant by 3-fold. In contrast, E49R/D53R RNase A was not toxic to K-562 cells.

Finally, the addition of an R_9-tag to either G88R RNase A or E49R/D53R/G88R RNase A increased cytotoxicity by an additional 3-fold, with G88R RNase A–R_9 and E49R/D53R/G88R RNase A–R_9 exhibiting IC_{50} values of 1.9 and 0.58 μM, respectively (Figure A2.2B; Table A2.1). Thus, the cumulative effect of arginine grafting and the addition of an R_9 tag increased cytotoxic activity by an order of magnitude. E49R/D53R/G88R RNase A–R_9 is one of the most toxic of known variants for K-562 cells (Rutkoski et al., 2005).

Surprisingly, E49R/D53R RNase A–R_9, which retains its high affinity for RI, exhibited cytotoxicity (IC_{50} = 6.0 μM) comparable to that of G88R RNase A. This result was unexpected because RNase A–R_9 (Z= +13) does not exhibit cytotoxic activity (Fuchs and Raines, 2005). We suspect that this highly cationic E49R/D53R RNase A–R_9

$(Z = +17)$ is internalized so efficiently that its concentration in the cytosol overwhelms endogenous RI. A similar explanation has been made to explain the cytotoxic activity of otherwise RI-sensitive RNases ((Leich *et al.*, 2006);(See also Section 1.7)) of which there have been several reports (Bosch *et al.*, 2004; Naddeo *et al.*, 2005; Notomista *et al.*, 2006).

A2.5 Conclusion

The cytotoxicity of a ribonuclease arises from its degradation of cellular RNA. Herein, we demonstrated that this cytotoxic activity can be enhanced by the installation of an arginine graft. The increased efficiency of internalization presumably afforded by the arginine graft can be used in conjunction with an R_9 protein transduction domain tag to achieve additive enhancements in cytotoxicity. In the absence of an R_9 tag, evasion of RI is necessary for a permeant variant to be cytotoxic. Accordingly, the potency of a ribonuclease correlates with its ability to manifest unfettered ribonucleolytic activity in the cytosol. These findings inform the design and engineering of ribonucleases with enhanced cytotoxic activity and clinical utility.

Biophysics Instrumentation Facility was established with Grants BIR-9512577 (NSF) and

RR13790 (NIH).

Table A2.1 Biochemical parameters of RNase A and its variants

Ribonuclease	pI [a]	T_m [b] (°C)	k_{cat}/K_M [c] ($10^6\ M^{-1}s^{-1}$)	IC_{50} [d] (μM)	K_d (nM)
RNase A	8.6	64 [e]	2.34 ± 0.09	>25	44 × 10^{-6} [f]
G88R RNase A	8.8	60 [e]	2.9 ± 0.1	6.2 ± 0.5	2.8 ± 0.1
E49R/D53R RNase A	9.2	54	2.21 ± 0.02	>25	<2.8 [g]
E49R/D53R/G88R RNase A	9.3	54	2.5 ± 0.1	1.9 ± 0.2	2.6 ± 0.8
RNase A-R9	9.6	56 [e]	1.0 ± 0.2 [e]	>25 [e]	ND
G88R RNase A-R9	9.8	54 [e]	9.6 ± 0.2 [e]	1.8 ± 0.1 [h]	ND
E49R/D53R RNase A-R9	10.0	48	1.55 ± 0.03	6.0 ± 0.3	<2.8 [g]
E49R/D53R/G88R RNase A-R9	10.1	49	3.59 ± 0.05	0.58 ± 0.02	3.0 ± 1.1

ND, not determined

[a] Values of pI were estimated from amino acid composition (Bjellqvist et al., 1993; Bjellqvist et al., 1994).

[b] Values of T_m (± 2 °C) were determined in PBS by ultraviolet spectroscopy.

[c] Values of k_{cat}/K_M (± SE) are for the catalysis of 6-FAM–dArU(dA)$_2$–6-TAMRA cleavage at 25 °C in 10 mM Bis-Tris–HCl buffer, pH 6.0, containing NaCl (0.50 M).

[d] Values of IC_{50} (± SE) are for the incorporation of [methyl-^{3}H]thymidine into the DNA of K-562 cells (Figure A2.2).

[e] Value from (Fuchs and Raines, 2005).

[f] Value from (Lee et al., 1989).

[g] Value was below the lower limit of detection for the assay.

[h] Raw data from (Fuchs and Raines, 2005) fitted in the manner of this work.
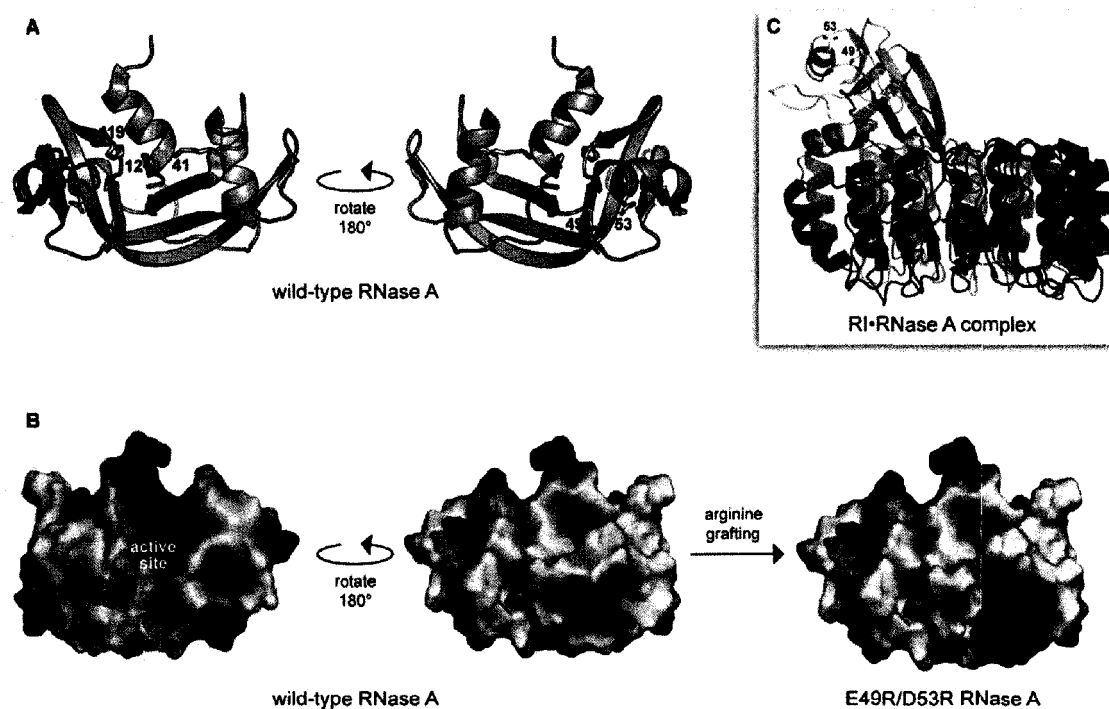
Figure A2.1 Arginine grafting of RNase A. (A) Ribbon diagram of RNase A based on

PDB entry 7rsa. The side chain of residues in the active site (His12,

Lys41, and His119) and Glu49 and Asp53 are shown explicitly. (B)

Electrostatic potential map of wild-type RNase A and its E49R/D53R

variant (blue = cationic; red = anionic). (C) Ribbon diagram of the porcine

RI·RNase A complex based on PDB entry 1dfj. Images were created with

the program PyMOL (DeLano Scientific, South San Francisco, CA)
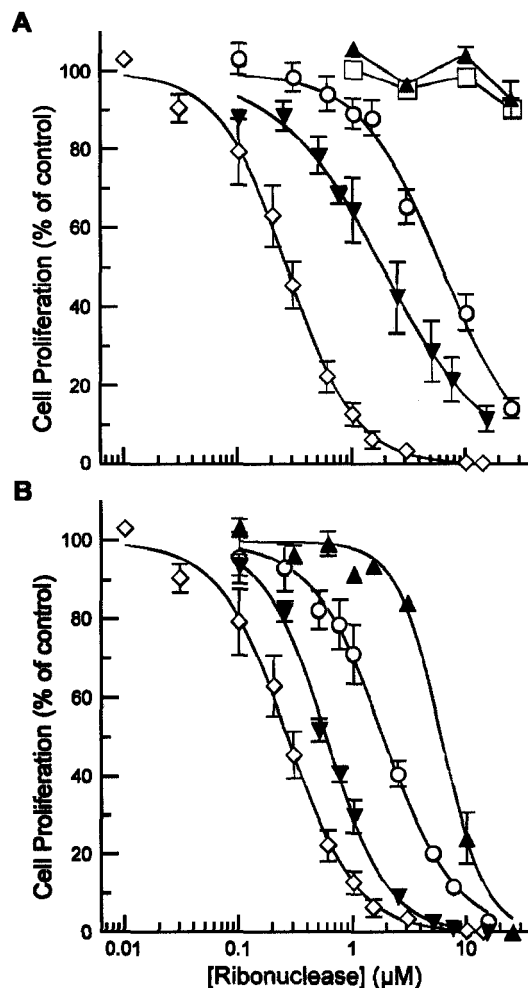
Figure A2.2 Cytotoxicity of Onconase (◊), wild-type RNase A (□), and its G88R (○),

E49R/D53R (▲), and E49R/D53R/G88R (▼) variants. Data in panel **(B)**

are for variants with a C-terminal R_9 tag. Data for Onconase are depicted

in both panels to facilitate comparisons. Cell viability was measured by

monitoring [methyl-^{3}H]thymidine incorporation into the DNA of K-562

cells after a 44-h incubation with a ribonuclease. Data points listed are for

the mean (± SE) of three experiments; values of IC_{50} are listed in Table

A2.1.

APPENDIX 3

Gadolinium(III)-Conjugates of Ribonuclease A for In Vivo Transport
Studies

Contribution: Protein expression, purification, conjugation to Gd·DO3A-MAL, conjugate purification, and biochemical analysis including assays of ribonucleolytic activity, RI-affinity, and cytotoxicity. Composition of this thesis chapter, preparation of figure drafts, and design of in vivo experiments were conducted with the assistance of M. J. Allen. Synthesis of **A3.2**, determination of longitudinal relaxivity values, and initial conception of the project was carried out by M. J. Allen. J. A. Kink assisted in the design and execution of the Gd·DO3A–G89C RNase 1 in vivo experiment.

Prepared for submission to *Bioconjugate Chemistry* as:
Rutkoski, T. J., Allen, M. J., Block, W. F., Kiessling, L. L., and Raines, R. T. (2008) Gadolinium(III)-conjugates of ribonuclease A for in vivo transport studies.

A3.1 Abstract

Cytotoxic ribonucleases demonstrate selectivity for cancer cells both in vitro and in vivo, however, the basis of this favorable preference is unknown. We describe a method to link covalently a derivative of the Gd(III) chelate 1,4,7,10-tetraazacyclododecane-1,4,7,10-tetraacetic acid (DOTA) to pancreatic-type ribonucleases. These conjugates retain wild-type ribonucleolytic activity and display attenuated affinity for the cytosolic ribonuclease inhibitor protein (RI), endowing these conjugates with cytotoxic activity toward cancer cells. The Gd(III)-ribonuclease conjugates effect a three-fold enhanced water proton longitudinal relaxivity ($r_1 = 15$ mM^{-1}s^{-1}) compared to [Gd(DOTA)]$^-$, which could enable the visualization of tumor-specific accumulation in vivo with magnetic resonance imaging (MRI), shedding light on the mechanism of ribonuclease-mediated cytotoxicity in whole animals. Here, we report on the synthesis, characterization, and in vivo properties of these conjugates. Attachment of a Gd(III)-complex to RNase A also portends a strategy for converting a potential anti-cancer therapeutic into a combined therapeutic–diagnostic agent.

A3.2 Introduction

Cytotoxic ribonucleases represent a promising biopharmaceutical alternative to chemotherapy and immunotherapy for the treatment of many forms of cancer (Arnold *et al.*, 2006). Their unique mechanism of action endows them with a significant degree of selectivity for cancer cells over non-cancerous cells although the origin of this discrimination is not yet fully understood (Rutkoski *et al.*, 2005). This selectivity is

especially important because the aforementioned standard therapies typically exhibit significant systemic toxicity among many other undesirable side effects which dramatically reduce the quality of life for patients undergoing anticancer treatment (Hampton, 2005; Yeoh *et al.*, 2006; Chen *et al.*, 2007; Hofman *et al.*, 2007; Schwartzberg, 2007). Onconase[®] (ONC), a pancreatic-type ribonuclease from the Northern leopard frog *Rana pipiens*, is currently in phase IIIb confirmatory trials for treatment of malignant mesothelioma in combination with doxorubicin and is poised to become the first ribonuclease-based cancer therapy (Pavlakis and Vogelzang, 2006). Significant progress has been made towards elucidating how ONC and other ribonucleases mediate cancer cell death (Haigis and Raines, 2003; Rodríguez *et al.*, 2007). Much of this insight is, however, at a cellular level, with little being known about how these enzymes inhibit the growth of solid tumors following their intravenous administration.

Magnetic resonance imaging (MRI), which is essentially three-dimensional clinical proton NMR spectroscopy used to map the chemical environment of water protons, has become an invaluable technique in radiologic practice and medicine for non-invasively visualizing anatomical structures at high spatial and temporal resolution (Brown and Semelka, 2003). Diagnostic applications of MRI include the identification of tumor lesions, the staging of various cancers, and the visualization of organ perfusion (Aime *et al.*, 2000b). For 3 out of 10 MRI exams performed worldwide, the utility of MRI is furthered by the use of contrast agents (CAs), such as $[Gd(DTPA)]^{2-}$ (gadopentetate dimeglumine; Magnevist®, Schering) in the U.S. and $[Gd(DOTA)]^{-}$ (gadoterate

meglumine; Dotarem®, Guerbet) in Europe, which increase the MRI signal by decreasing the relaxation time T_1 of water protons (*i.e.*, tissues with short relaxation times T_1 appear as more intense) (Caravan *et al.*, 1999; Gries, 2002). Thus, CAs themselves are not detected directly but instead exert their influence on nearby protons through dipolar interactions (Platzek *et al.*, 2007). Therefore, due to their high magnetic moments and relaxation efficiency, paramagnetic metal ions such as gadolinium (Gd^{3+}), which contains seven unpaired electrons, are generally employed as the functional part of the CA (Caravan *et al.*, 1999; Platzek *et al.*, 2007).

Due to the similarity in the size and charge of Gd^{3+} and Ca^{2+} ions, gadolinium is highly toxic if administered as the free salt—its toxicity stemming from the disruption of Ca^{2+}-mediated signaling pathways (Haley, 1965). For this reason, the potentially toxic metal is delivered within a macrocyclic chelate such as 1,4,7,10-tetraazacyclododecane-1,4,7,10-tetraacetic acid (DOTA). The extraordinary affinity of these chelates for metals such as gadolinium ($K_d \sim 10^{-25}$), renders them benign to animals during the timeframe that they persist in circulation (Cacheris *et al.*, 1987). Lanthanide ions exhibit high coordination numbers in aqueous solution. Gadolinium has a coordination state of nine—eight of which are occupied by the chelate in $[Gd(DOTA)]^-$. The remaining coordinate position is occupied by a water molecule, which exchanges freely with others from the bulk solution (See **A3.2** in Scheme A3.1). Good CAs possess a high proton relaxivity r_1 or r_{1p}, which is defined as the concentration dependence of $1/T_1$ ($mM^{-1}s^{-1}$). The three primary factors that influence CA relaxivity are: (1) the number of coordinated water

molecules (q), (2) the exchange rate of those water molecules, and (3) the tumbling motion time of the chelated metal (Delikatny and Poptani, 2005).

Conjugation of a CA to macromolecular species such as micelles, polysaccharides, dendrimers, polyamino acids, other polymers or protein is one way to achieve high relaxivity CAs by slowing the tumbling rate of the CA (Tilcock *et al.*, 1991; Aime *et al.*, 2001; Aime *et al.*, 2002). Bioconjugation of CAs to a targeting moiety such as an antibody (Wahl *et al.*, 1983b; Curtet *et al.*, 1986; Curtet *et al.*, 1988; Gohr-Rosenthal *et al.*, 1993; Matsumura *et al.*, 1994; Shahbazi-Gahrouei *et al.*, 2001; Kuriu *et al.*, 2006) or antibody fragment (Wahl *et al.*, 1983a; Curtet *et al.*, 1998) also has the benefit of effecting the accumulation of the CA within a desired structure, such as a solid tumor. Additionally, CAs have been coupled to proteins such as human serum albumin (HSA) for the purpose of altering the pharmacokinetics and biodistribution of the CA (Schmiedl *et al.*, 1987a; Schmiedl *et al.*, 1987b), for example compartmentalization as blood pool MR CAs (Unger *et al.*, 1999).

Here, we describe the conjugation of a maleimide-functionalized Gd·DOTA derivative to a variant of RNase A. The cytotoxic potential of RNase A is normally masked upon potent inhibition by the ubiquitous cytosolic ribonuclease inhibitor protein (RI), but can be overcome by disrupting the affinity of RI (Leland *et al.*, 1998; Rutkoski *et al.*, 2005); (See also CHAPTER 1). For this reason, the metal chelate is site-specifically attached through a free thiol residue introduced via site-directed mutagenesis within the RI-binding interface. We characterize both the MR (relaxivity) and biochemical (ribonucleolytic activity, affinity for RI, cytotoxicity) properties of this conjugate.

Finally, the results of several preliminary in vivo imaging experiments are described and the potential of CA–ribonuclease conjugates as dual purpose (imaging/therapeutic) molecules is discussed.

A3.3 Experimental Procedures

A3.3.1 Materials and Protein Production

1,4,7,10-Tetraazacyclododecane-1,4,7-tris-acetic acid-10-maleimidoethylacetamide (DO3A-MAL) **A3.1** was from Macrocyclics (Dallas, TX). Diethylenetriaminepentaacetic acid gadolinium(III) dihydrogen salt hydrate was from Sigma Chemical (St. Louis, MO). All other commercial chemicals were of reagent grade or better and used without further purification unless otherwise noted. Homozygous (*nu/nu*) Balb/c mice were obtained from Harlan Sprague Dawley (Indianapolis).

cDNA encoding ribonuclease variants was generated by Quickchange site-directed mutagenesis (Stratagene, La Jolla, CA) using plasmid pBXR (RNase A) (delCardayré *et al.*, 1995) or pHP-RNase (RNase 1) (Leland *et al.*, 2001). The production, folding, and purification of G88C RNase A and G89C RNase 1 were performed as described for other RNase A and RNase 1 variants (delCardayré *et al.*, 1995; Leland *et al.*, 1998; Leland *et al.*, 2001), but with several alterations to accommodate the presence of the unpaired cysteine residue, including protection of the free thiol with DTNB (described in the Experimental Procedures of CHAPTERS 3 and 4; Sections 3.3.4 and 4.3.3). Ribonuclease inhibitor (RI) was prepared as described previously (Rutkoski *et al.*, 2005; Smith, 2006).

Following purification, ribonucleases and ribonuclease inhibitor protein migrated as single bands during SDS–PAGE, confirming their purity and apparent molecular weight.

A3.3.2 Instrumentation

Cuvette-scale fluorescence measurements were carried out on a QuantaMaster1 photon-counting fluorometer from Photon Technology International (South Brunswick, NJ) equipped with sample stirring. Fluorescence-based competition binding assays performed in 96-well plate format were read with an EnVison 2100 Plate Reader (Perkin–Elmer, Waltham, MA) in the Keck Center for Chemical Genomics at the University of Wisconsin–Madison. Absorbance spectroscopy was performed using a Cary Model 50 spectrometer from Varian (Sugar Land, TX). Matrix-assisted laser desorption ionization—time-of-flight (MALDI–TOF) mass spectrometry was performed using a Voyager-DE-PRO Biospectrometry Workstation (Applied Biosystems, Foster City, CA) and a 3,5-dimethoxy-4-hydroxycinnamic acid matrix in the campus Biophysics Instrumentation Facility. Liquid chromatography and mass spectrometry (LC–MS) analysis was performed on a Shimadzu LC–MS containing a C18 column (Supelco Discovery, 2.1×150 mm) equilibrated with 0.4% (v/v) formic acid. Determinations of gadolinium concentration in solution were performed at Desert Analytics Laboratory (Tucson, AZ). The longitudinal water proton relaxation rate at 60 MHz was measured using a Bruker mq60 NMR Analyzer (Bruker Canada, Milton, Ont. Canada) operating at 1.5 T. MR scans/imaging were performed on a Varian 4.7 T horizontal bore imaging/spectroscopy system (7.0 cm ID) at the UW Carbone Cancer Center (UWCCC)

Small Animal Imaging Facility. MR phantom images (Figure A3.4) were acquired on a

GE short-bore whole body scanner operating at 3.0 T (T_R time: 3 sec; T_E time: 7.7 msec).

A3.3.3 Gadolinium(III) Metalation of DO3A-MAL (A3.2 synthesis)

To a solution of DO3A-MAL A3.1 (20.0 mg, 0.0254 mmol) in H_2O (0.25 mL) was

added a solution of $GdCl_3$ (9.45 mg, 0.0254 mmol) in H_2O (0.25 mL). The pH of the

resulting reaction mixture was brought to and maintained at 5.5 with 2 N NaOH. After

15 h at constant pH, product formation was verified by LC–MS (m/z_{calc} $C_{22}H_{31}GdN_6O_9$

$[M+H^+]^+$: 681.8 with Gd isotope pattern; m/z_{obs}: 681.9 with Gd isotope pattern). The

reaction mixture was used directly in coupling to G88C RNase A.

A3.3.4 Conjugation of Gd-DO3A-MAL to G88C RNase A (A3.3 synthesis)

The pH of the protein solution containing TNB-protected ribonucleases in the

HiTrap SP elution buffer was adjusted from 5.0 to ~8.0 by the addition to ~20% (v/v) of

1.0 M Tris–HCl buffer at pH 8.0. 5-Thio(2-nitrobenzoic acid) was released by adding

DTT (10-fold molar excess) and allowing the reaction to proceed at room temperature for

$\geq$5 min, resulting in the immediate generation of the yellow TNB^{2-} (Ellman, 1958). DTT

and salt were removed from the ribonucleases by chromatography using HiTrap desalting

resin that had been equilibrated with 1×DPBS containing EDTA (1 mM), yielding the

pure G88C RNase A at a concentration of ~50–100 μM.

A 10-fold molar excess of A3.2 was added, and the resulting reaction mixture was

incubated for 1 h at ambient temperature, protected from light, followed by a 15 h

incubation at 4 °C. Reactions were terminated by ~6-fold dilution with 50 mM MES–

NaOH buffer at pH 6.0 and application to a HiTrap SPHP cation-exchange resin that had

been equilibrated with the same buffer. The desired conjugate **A3.3** (3.3 mL, 50.7 μM,

77%) was eluted from the column with a linear gradient of NaCl (0–0.4 M) in 50 mM

MES–NaOH buffer at pH 6.0; MS (MALDI): m/z 14,401.48 (expected = 14,408.00).

MES–NaOH buffer at pH 6.0 was used instead of sodium acetate buffer at pH 5.0 to

avoid de-metalation of the chelate which can occur at pH <5.5 upon protonation of the

coordinating groups.

A3.3.5 Biochemical Assays

Cell proliferation was determined as described previously (Leland *et al.*, 1998). RI-

evasion assays were performed using a fluorescence-based assay as reported previously

(Lavis *et al.*, 2007). Average K_d values represent the mean of three experiments

performed in duplicate. Enzymatic activity of the G88C RNase A conjugate was

determined by assaying its ability to cleave the hypersensitive fluorogenic substrate

6-FAM–dArUdAdA–6-TAMRA (20 nM) (λ_{ex} = 493 nm; λ_{em} = 515 nm) as described

previously (Kelemen *et al.*, 1999). Reported values of k_{cat}/K_M are the mean of three

measurements ± SE.

A3.3.6 Longitudinal Water Proton Relaxation (PRE) Rate Measurements

The longitudinal water proton relaxation rate at 60 MHz was measured by means of

the standard inversion-recovery technique (20 data points, 8 scans each). A typical 90°-

pulse length was 6.16 μs, and the reproducibility of the T_1 data was ± 0.3%. Temperature

was maintained at 22 °C with a Haake G cooling circulator.

A3.3.7 In Vivo Imaging Studies

Both animal studies were performed using a Gd·DO3A–G89C RNase 1 conjugate due

to limiting amounts of the G88C RNase A conjugate. Gd·DO3A–G89C RNase 1

exhibited a similar longitudinal relaxivity to that of Gd·DO3A–G88C RNase A (data not

shown). For both studies, the tumors were implanted into the flanks of nude mice. The

tumor cell lines were chosen both for their ability to proliferate in mice and for their low

rate of spontaneous regression. Importantly, both tumors chosen represent a clinically

relevant target and are used frequently in the testing of new chemotherapeutic agents.

Single-pass/clearance study. A male A549 (human lung carcinoma) tumor-bearing

homozygous (*nu/nu*) Balb/c mouse was anesthetized by mask ventilation with isoflorane

throughout the duration of the imaging experiment. The heart rate of the mouse was

monitored and kept within an appropriate range via adjustment of the isoflorane.

Gd–ribonuclease conjugate was administrated intravenously (250 mg/kg) and T_1-

weigthed scans were performed f repeatedly or up to 2 h following the injection.

Multi-dosing/accumulation study. Human BxPC-3 pancreas adenocarcinoma cells

were implanted into the right rear flank of 5–6 week old male homozygous (*nu/nu*)

Balb/c mice. Tumors were allowed to grow to an average size of ≥500 mm³ before

treatment was initiated to create a sufficiently large target for visualization without

allowing the tumors to become so large that they become necrotic with poor vasculature.

Xenograft animals were divided into three treatment groups. All the test compounds were

diluted in PBS (drug vehicle) and, to serve as a negative control, one set of animals was

treated with vehicle alone. All treatments were administered by intraperitoneal (i.p.)

injection, and the volume of drug/vehicle injected was based upon the body weight of the

animal (10 μL/g). Tumor size was measured using calipers, and tumor volume was

determined by using the formula for an ellipsoid sphere (eq 3.4). Gd·DO3A–G89C

RNase 1 treatment was administered as a dose of 75 mg/kg (i.p.; 7 × wk; twice daily for

days 1 and 2, once daily for days 3–5; $n = 2$). A second group of animals ($n = 2$)

received an equivalent amount of Gd(III) on the same dosing schedule in the form of

Gd·DTPA.

A3.4 Results and Discussion

A3.4.1 Design and synthesis of Gd-ribonuclease conjugate

The synthesis of conjugate **A3.3** involved two major decisions: the choice of chelate

and the site of conjugation to ribonuclease. The chosen chelate was a maleimide-

containing derivative of DOTA (DO3A-MAL). Unmodified Gd(III) DOTA is a clinically

approved contrast agent in Europe (Caravan et al., 1999), and the modified chelate

contained a maleimide group that can selectively react with a thiol group over amines (Ji,

1983). The rationale for using sulfhydryl-reactive moieties for site-specific attachment of

prosthetic groups was described in greater detail in Section 1.6.2, Section 3.2, and

Section 4.2. For conjugation to ribonuclease, we chose the G88C variant of RNase A.

Position 88 of RNase A is within the RI-binding interface and therefore replacement of

the native glycine residue with either another amino acid (Leland *et al.*, 1998) or

chemical derivatization at this position can reduce the sensitivity of the enzyme to RI

(See Sections 1.6.1 and 3.4.1; Figures 3.2 and 4.1).

In our synthetic route (Scheme A3.1), we first metalated DO3A-MAL **A3.1** using

$GdCl_3$. The conditions that we used were slightly acidic (pH 5.5) as hydrolysis of the

maleimide functionality was observed at higher pH values (≥ 7). The metalated chelate

A3.2 was conjugated to G88C RNase A in pH 8.0 PBS buffer and purified by FPLC to

give the desired conjugate **A3.3** in good yield.

A3.4.2 Biochemical characterization of Gd-ribonuclease conjugate

Before the conjugate could be used in biological studies, we wanted to ensure that it

retained both its enzymic (activity, RI evasion, cytotoxicity) and magnetic (high

relaxivity) properties. The k_{cat}/K_M of the conjugate was found to be

$5.38\ (\pm\ 0.65) \times 10^7\ M^{-1}s^{-1}$. This value is within error of the wild-type enzymatic activity

of $4.40\ (\pm\ 0.78) \times 10^7\ M^{-1}s^{-1}$, demonstrating that the conjugate retains the ribonucleolytic

activity necessary for cytotoxicity (Kim *et al.*, 1995a).

As mentioned previously, the ability to evade RI is another important determinant of

ribonuclease cytotoxicity (Rutkoski *et al.*, 2005). Placement of the chelate at position 88

was anticipated to disrupt a key interaction between RNase A and RI in a manner similar

to that observed for the G88R amino acid substitution (Leland *et al.*, 1998). Indeed,

conjugate **A3.3**, displayed a K_d value of 2.2 nM (Figure A3.1), similar to that of G88R

RNase A ($K_d = 1.4$ nM). Thus, the affinity of the Gd·DO3A–G88C RNase A for hRI has

been diminished by 50,000-fold compared to wild-type RNase A (K_d = 44 fM) (Lee *et al.*, 1989).

Having successfully prepared a conjugate with high ribonucleolytic activity and reduced sensitivity to RI, which are two key attributes of a cytotoxic ribonuclease, we next measured the ability of Gd·DO3A–G88C RNase A to inhibit the proliferation of K-562 cells in vitro. The results, shown in Figure A3.2, indicate that conjugation of a gadolinium chelate to G88C RNase A endows it with cytotoxic activity (IC_{50} = 13 μM)— though the conjugate was nearly 4-fold less potent of a cytotoxin than G88R RNase A (IC_{50} = 3.6 μM). We attribute the comparatively lower cytotoxicity of the conjugate to its lower net charge (Z) relative to that of G88R RNase A as cationicity of the ribonuclease mediates cellular internalization (Futami *et al.*, 2002; Fuchs *et al.*, 2007; Johnson *et al.*, 2007a).

A3.4.3 Magnetic properties of Gd·DO3A–G88C RNase A

The longitudinal relaxivity r_1 of our contrast agent was measured at 60 MHz and found to be 15 mM^{-1}s^{-1} (Figure A3.3). The concentration of the conjugate used for the relaxivity calculation was determined by both UV absorption and gadolinium content. The relaxivity values were identical and independent of the method of conjugate quantitation, consistent with the stoichiometry of Gd·DO3A:G88C RNase A being 1:1. The relaxivity value for Gd·DO3A–G88C RNase A is similar to values obtained for other Gd–protein conjugates such as Gd·DTPA–albumin (Ogan *et al.*, 1987) and nearly three-fold higher than the value of free Gd(III)·DOTA (r_1 = 5.8 mM^{-1}s^{-1}; Figure A3.3). The

relaxivity value obtained for the free Gd(III)·DOTA chelate is comparable to values

obtained by other groups for similar compounds (3.5–4.8 $mM^{-1}s^{-1}$) (Caravan *et al.*, 1999;

Gries, 2002). Based on these relaxivity values, the conjugate would be expected to

provide greater image enhancement than that of the free chelate when administered at an

equivalent concentration. To demonstrate this property, MR phantoms were obtained

(Figure A3.4). The tube containing the Gd·DO3A–G88C RNase A conjugate shows

substantial contrast, but no contrast is seen in the tube containing Gd(III)·DOTA in this

T_1-weighted scan. These images verified the relaxivity measurements and also

demonstrated that the unmodified RNase A cannot be used as a contrast agent for MRI.

A3.4.4 Disposition of Gd·DO3A–ribonuclease in tumor-bearing mice

Cytotoxic ribonucleases exhibit selectivity for cancerous cells over normal cells both

in vitro (Rutkoski *et al.*, 2005) and in vivo (See CHAPTERS 3–5), though the basis for this

preferential bioactivity is largely unknown and at best speculative (Lee and Raines,

2008). Having established the potential utility for Gd·DO3A–ribonuclease as contrast

reagents (*i.e.*, high relaxivity), we sought to gain insight via MR imaging into how

ribonucleases mediate their effects on solid tumors using this new tool. Gd·DO3A–

ribonuclease was administered to an anesthetized nude (*nu/nu*) mouse bearing a solid

human A549 tumor (i.v.; 250 mg/kg) and immediately imaged (repeatedly) by MR (T_1-

weighted scans. No contrast enhancement was observed in the tumor at any point post-

injection (data not shown). Within minutes after i.v. administration, marked contrast was

observed in the kidneys (Figure A3.5B), consistent with the established method of ribonuclease clearance from circulation (Vasandani *et al.*, 1996; Maack, 2000).

Concerned that a rapidly-clearing single administration of ribonuclease might not be sufficient to allow visualization of accumulation at the site of the tumor, a second animal experiment was conducted in which Gd·DOTA–ribonuclease was administered multiple times over the course of a week and subsequently imaged. BxPC-3 tumor-bearing male *nu/nu* mice (3 groups; $n = 2$) received Gd·DO3A–ribonuclease (i.p.; 75 mg/kg; 7×wk), an equivalent molar amount of Gd(III)·DOTA in PBS, or vehicle (PBS) alone. The size of the tumors as well as the body weights of the animals were monitored during the week of test article administration (Figure A3.6A). Both Gd chelate and Gd chelate conjugated to ribonuclease were tolerated by the animals throughout the duration of the study as evidenced by their maintenance of body weight. Despite the short timeframe of the experiment, the ribonuclease conjugate appeared to inhibit the growth of the tumor compared to the animals receiving CA alone. Several hours following the final injection, the mice were scanned by MRI (T_1-weighted). No visible contrast enhancement was observed in any tissues (including the tumor) in either the CA-ribonuclease conjugate group or the CA alone group over that of the vehicle control group.
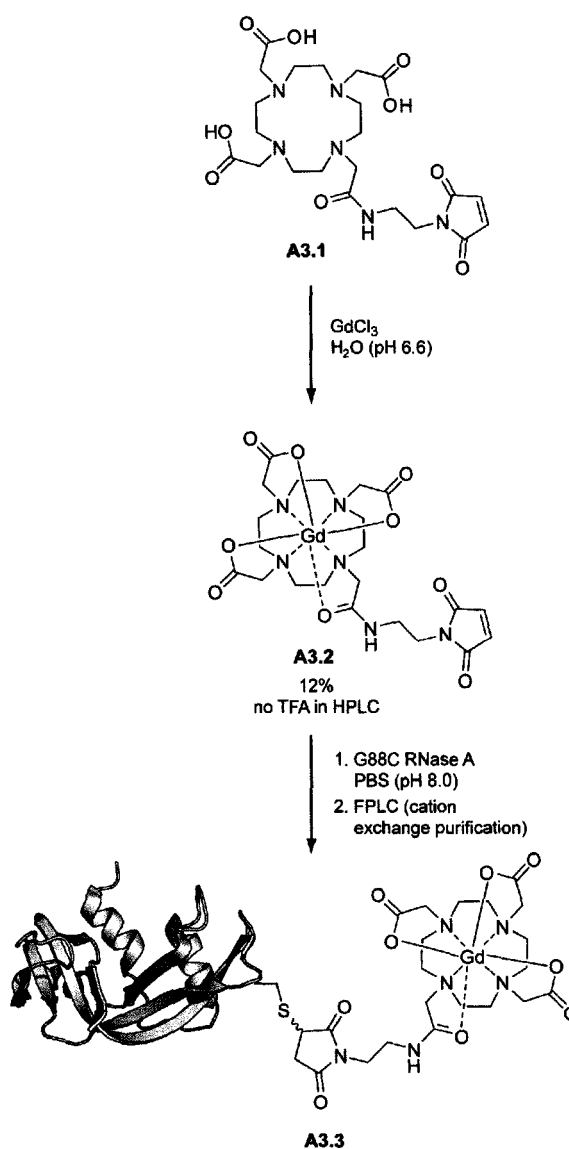
A3.5 Conclusions

We conclude that the amount of ribonuclease that localizes in solid tumors in mouse xenograft models and effects tumor growth inhibition (*e.g.*, Figure 3.5A–B), is too small to permit visualization using our Gd·DO3A–ribonuclease conjugate. It is established that

despite all of its merits, MRI does suffer from limited sensitivity (Aime et al., 2000a).

One gram of gadolinium (clinically approved, non-conjugated forms such as Gd·DTPA/

Gd·DOTA) is typically administered to a human subject immediately prior to MR

imaging (Caravan et al., 1999), which equates to 0.1 mmol/kg for useful contrast

(Shahbazi-Gahrouei et al., 2001). Although the doses used in our preliminary animal

studies were substantial (250 mg/kg ≈ 17 mmol/kg; 75 mg/kg ≈ 5 mmol/kg), apparently a

high enough degree of selective association with the tumor did not occur before the CA

was eliminated from the mouse. A substantial portion of the Gd·DO3A–ribonuclease

conjugate would have to accumulate preferentially in the tumor. Several groups have

attempted to calculate the minimum number of Gd-containing probes that would have to

localize to a particular cell to allow visualization (Nunn et al., 1997; Ahrens et al., 1998;

Aime et al., 2002). Aime et al. concluded that ~2 × 10^9 Gd(III) units (with relaxivities of

5–7 $mM^{-1}s^{-1}$) per cell was the minimum amount of CA needed to contribute detectable

contrast in an MR image (Aime et al., 2002). This hurdle was overcome by groups

developing CA–antibody conjugates by extensive labeling with as many as 28 metal ions

per antibody molecule (Curtet et al., 1998). This extensive degree of labeling would be

challenging for a protein as small as RNase A, not to mention the concern of

deleteriously affecting its ribonucleolytic activity or internalization efficiency.

Nonetheless, it might be possible using the multiple free thiol conjugation technique

described in CHAPTER 5 to attach several ligands with higher relaxivities than Gd·DO3A,

such as the HOPO ligands developed by Raymond and co-workers (Sunderland et al.,

2001), which have yielded relaxivities near 90 $mM^{-1}s^{-1}$ (Hajela et al., 2000).

Alternatively, the synthesis of ROMP-derived block co-polymers has been described in which Gd(III) chelates constitute a portion of the monomeric subunits and exhibit high relaxivity (Allen *et al.*, 2006). Attachment of such a polymeric contrast agent material to ribonuclease might permit their imaging in vivo. Finally, Gd(III) could be replaced with ^{64}Cu to allowing imaging using positron emission tomography (PET), which is more quantitative. Regardless of the strategy used, significant development of the technology is needed before it will bear any fruits lending insight into the mechanism of ribonuclease action in vivo. The endeavor would be worthwhile by its own right but could also enable the development of a dual MR diagnostic/therapeutic agent, of which there have been very few reports (Tatham *et al.*, 1999).

A3.1

GdCl$_3$
H$_2$O (pH 6.6)

A3.2
12%
no TFA in HPLC

1. G88C RNase A
   PBS (pH 8.0)
2. FPLC (cation
   exchange purification)

A3.3

Scheme A3.1 Synthesis and purification of Gd·DO3A–G88C RNase A.

Figure A3.1 Affinity of Gd·DO3A–G88C RNase A for hRI. The equilibrium

dissociation constant (K_d) for Gd·DO3A–G88C RNase A in complex with

hRI was determined using a fluorescence-based competition binding assay

described previously ((Lavis *et al.*, 2007); See also Appendix A2).
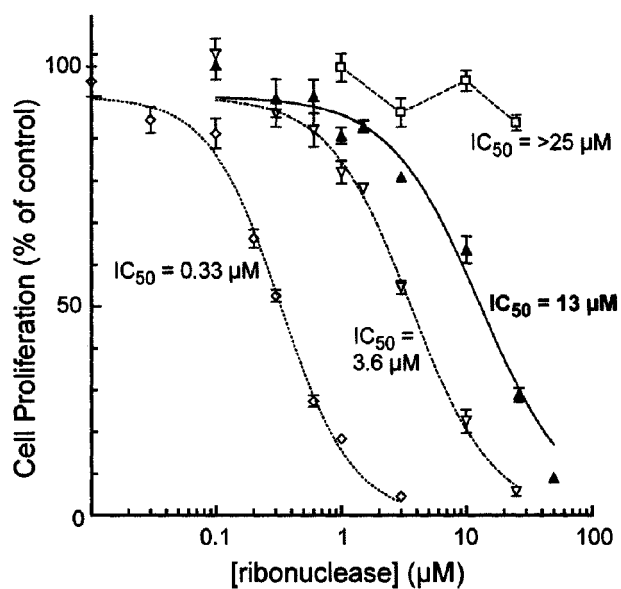
Figure A3.2 Effect of Gd·DO3A–G88C RNase A (▲) on the proliferation of K-562

cells. Data for wild-type RNase A (□), G88R RNase A (∇), and ONC (◊)

are shown as open symbols with curves fitted as broken lines. The

incorporation of [methyl-^{3}H]thymidine into cellular DNA was used to

monitor the proliferation of K-562 cells in the presence of ribonucleases.

Data points indicate the mean (± SE) of at least three separate experiments

carried out in triplicate.
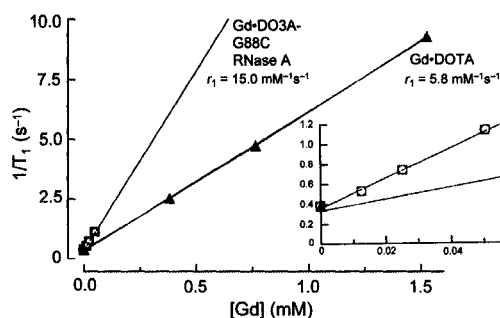
Figure A3.3 Effect of Gd·DOTA (triangles) and Gd·DO3A–G88C RNase A on water

proton relaxation in vitro. Values of longitudinal relaxivity (r_1) are

reported for both contrast reagents. The Gd·DO3A–G88C RNase A

conjugate exhibited a nearly 3-fold increase in relaxivity compared to

Gd·DOTA. The concentration of the Gd·DO3A–G88C RNase A conjugate

was determined both by protein concentration (UV spectroscopy; black

squares) and Gd(III) content (metal analysis; white circles). The value of

relaxivity obtained for Gd·DO3A–G88C RNase A was independent of the

quantitation method used, consistent with a 1:1 Gd·DO3A:ribonuclease

stoichiometry.
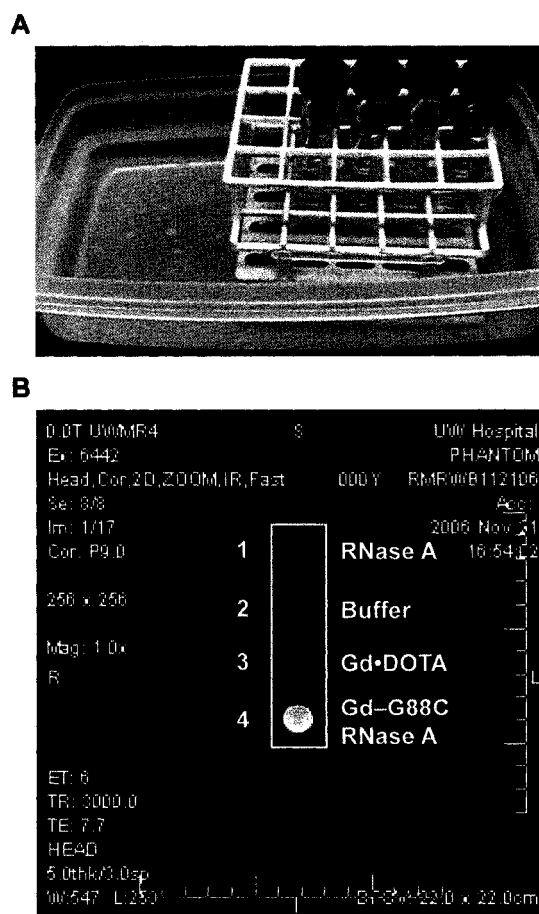
Figure A3.4 MR image illustrating the superior contrast afforded by Gd·DO3A–G88C

RNase A over Gd·DOTA owing to its increased longitudinal relaxivity

(r_1). (A) Photograph of the experimental setup used to image solutions

containing either (B) RNase A (1; 51 μM), buffer alone (3), Gd·DOTA (3;

51 μM), Gd·DO3A–G88C RNase A (4; 51 μM)
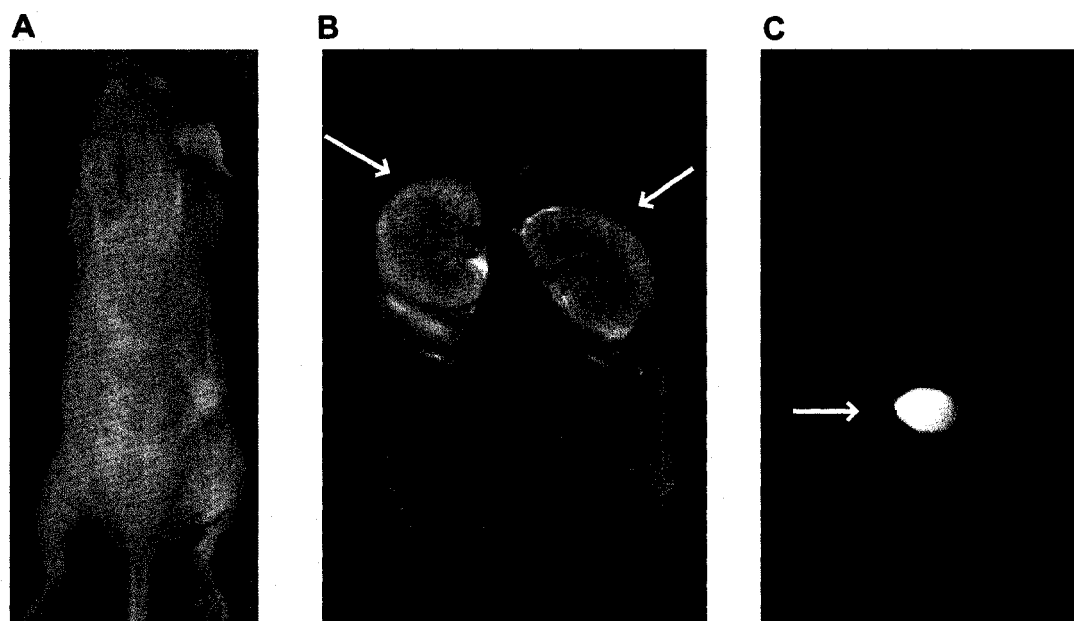
Figure A3.5 Renal clearance of Gd(III)·DO3A–G89C RNase 1 from a male A549

(non-small cell lung cancer) tumor-bearing homozygous (*nu/nu*) nude

mouse following intravenous administration (250 mg/kg) of the conjugate.

The photograph of the mouse in (**A**) gives the relative orientation of the

animal in the subsequent T_1-weighted MR images which are coronal

sections (head-top; tail-bottom). (**B**) Several minutes after administration

of the CA–RNase conjugate enhanced contrast (arrows) is observed in the

kidneys—consistent with the mechanism by which ribonucleases are

removed from circulation. (**C**) Within 30 min, marked enhancement is

visible in the bladder.
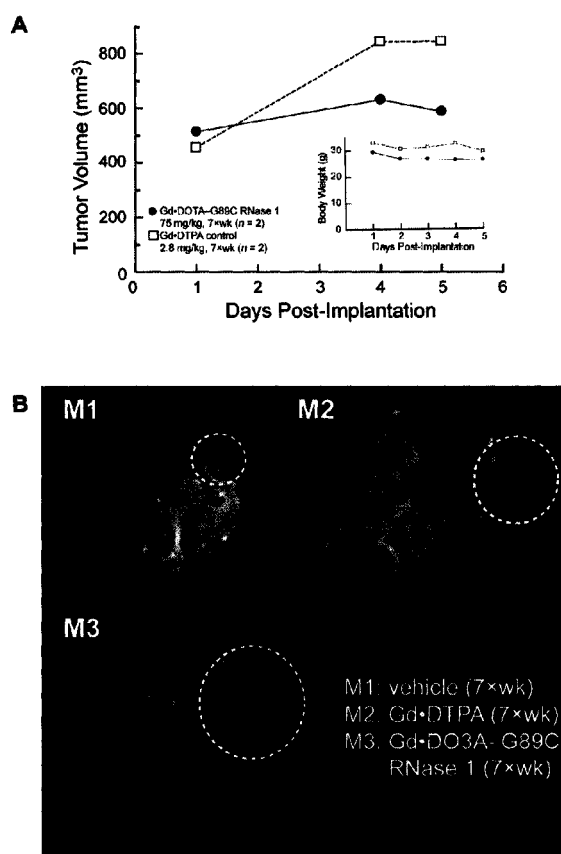
Figure A3.6 Disposition of Gd·DO3A–G89C RNase 1 in BxPC-3 tumor-bearing mice.

(A) Effect of Gd·DO3A–G89C RNase 1 (●) or Gd·DTPA (□) on tumor

volume and body weight (inset) of Balb/c mouse xenografts bearing

human BxPC-3 pancreas adenocarcinoma. Data plotted represent the mean

(± SE) for the number of animals indicated in the panel descriptions.

(B) T_1-weighted images of the mice after one-week dosing regimen. No

contrast enhancement is seen in the Gd·DO3A–G89C RNase 1 or

Gd·DTPA groups over that of the vehicle control group. A dotted white

line has been drawn around the solid tumors.

APPENDIX 4

Cover Art

Figure A4.1 *Journal of Molecular Biology* (2005) **354**(1) Cover Art.

Volume 354, Number 1, 18 November 2005   ISSN 0022-2836

JMB

JOURNAL OF MOLECULAR BIOLOGY

0022-2836(20051118)354:1;1-M
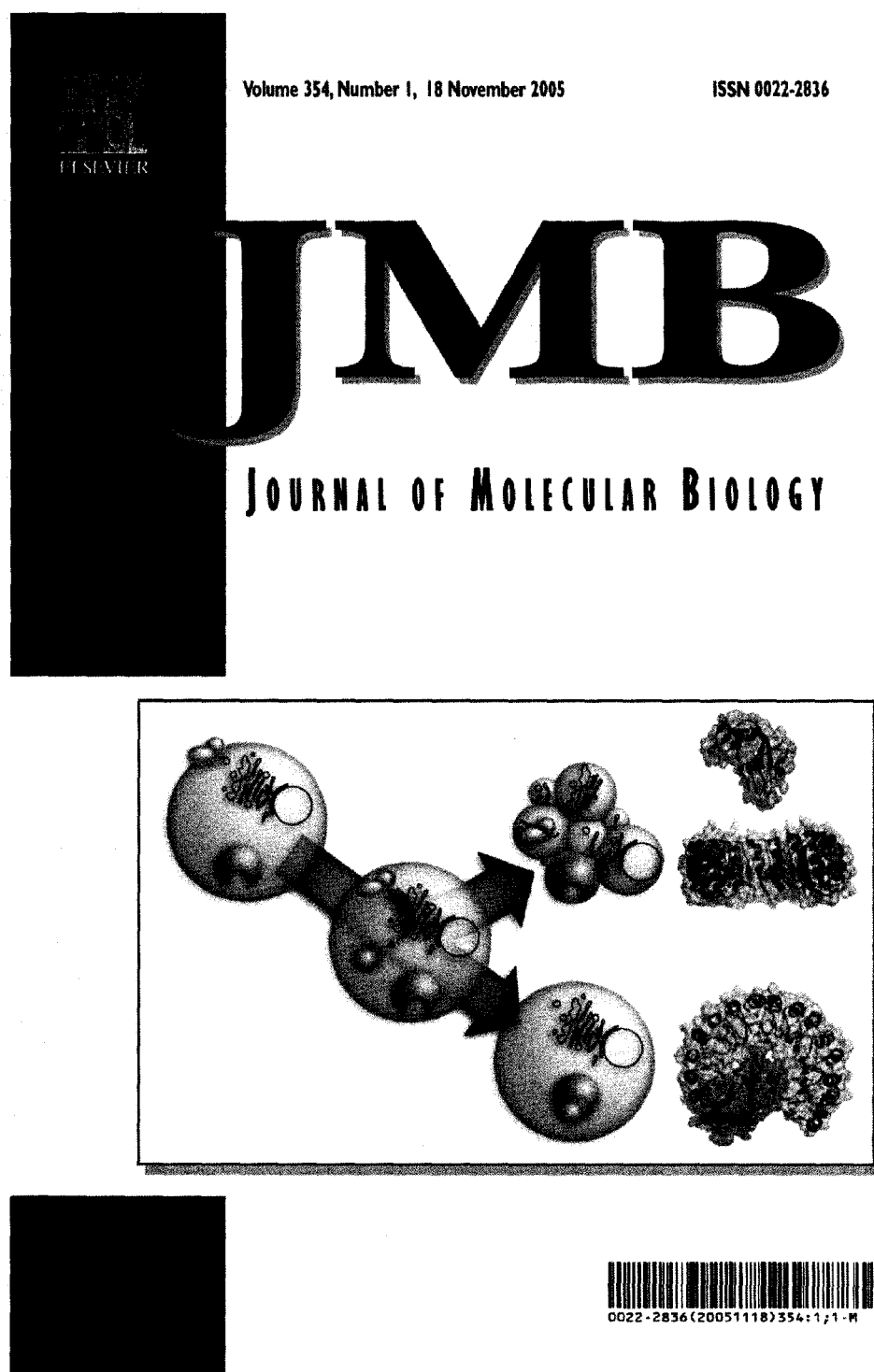
Figure A4.2 *Protein Engineering Design and Selection* (2007) **20**(10) Cover Art.
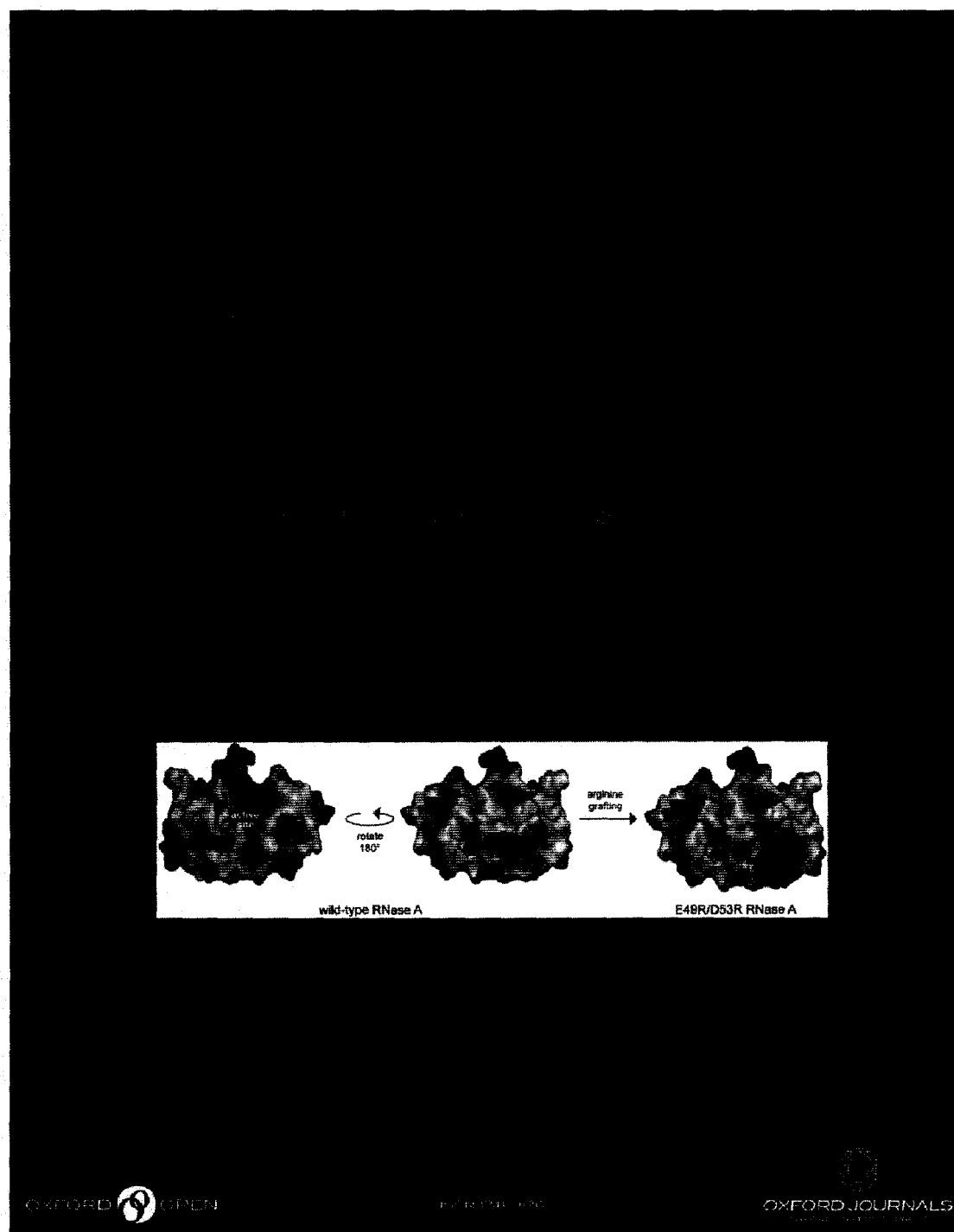
REFERENCES

List of Orphan Designations and Approvals. U.S. Food and Drug Administration/Office of Orphan Products Development.

Abel, R. L., Haigis, M. C., Park, C., Raines, R. T. (2002). Fluorescence assay for the binding of ribonuclease A to the ribonuclease inhibitor protein. *Anal. Biochem.* **306**, 100-107.

Agi, Y., Walt, D. R. (1997). Fluorescence monitoring of the microenvironmental pH of highly charged polymers. *J. Polym. Sci., Part A: Polym. Chem.* **35**, 2105-2110.

Ahrens, E. T., Rothbacher, U., Jacobs, R. E., Fraser, S. E. (1998). A model for MRI contrast enhancement using T1 agents. *Proc. Natl. Acad. Sci. U.S.A.* **95**, 8443-8448.

Aime, S., Botta, M., Garino, E., Crich, S. G., Giovenzana, G., Pagliarin, R., Palmisano, G., Sisti, M. (2000a). Non-covalent conjugates between cationic polyamino acids and GdIII chelates: A route for seeking accumulation of MRI-contrast agents at tumor targeting sites. *Chem. Eur. J.* **6**, 2609-2617.

Aime, S., Gianolio, E., Terreno, E., Giovenzana, G. B., Pagliarin, R., Sisti, M., Palmisano, G., Botta, M., Lowe, M. P., Parker, D. (2000b). Ternary Gd(III)L-HSA adducts: Evidence for the replacement of inner-sphere water molecules by coordinating groups of the protein. Implications for the design of contrast agents for MRI. *J. Biol. Inorg. Chem.* **5**, 488-497.

Aime, S., Botta, M., Fasano, M., Terreno, E. Protein-bound metal chealates. In: A. E. Merbach, E. Toth. (Eds.). The chemistry of contrast reagents in medical magnetic resonance imaging. John Wiley & Sons, Chichester. 2001. pp. 193.

Aime, S., Cabella, C., Colombatto, S., Geninatti Crich, S., Gianolio, E., Maggioni, F. (2002). Insights into the use of paramagnetic Gd(III) complexes in MR-molecular imaging investigations. *J. Magn. Reson. Imaging* **16**, 394-406.

Aleksandrowicz, J. (1958). Intracutaneous ribonuclease in chronic myelocytic leukaemia. *Lancet* **2**, 420.

Allen, M. J., Raines, R. T., Kiessling, L. L. (2006). Contrast agents for magnetic resonance imaging synthesized with ring-opening metathesis polymerization. *J. Am. Chem. Soc.* **128**, 6534-6535.

Anderson, N. L., Anderson, N. G. (2002). The human plasma proteome: History, character, and diagnostic prospects. *Mol. Cell. Proteomics* **1**, 845-867.

Antczak, C., Bauvois, B., Monneret, C., Florent, J. C. (2001). A new acivicin prodrug designed for tumor-targeted delivery. *Bioorg. Med. Chem.* **9**, 2843-2848.

Antignani, A., Naddeo, M., Cubellis, M. V., Russo, A., D'Alessio, G. (2001). Antitumor action of seminal ribonuclease, its dimeric structure, and its resistance to the cytosolic ribonuclease inhibitor. *Biochemistry* **40**, 3492-3496.

Arai, I., Sei, Y., Maramatsu, I. (1981). Preparation of 1,3,5-triaminobenzene by reduction of phloroglucinol trioxime. *J. Org. Chem.* **46**, 4597-4599.

Ardelt, B., Ardelt, W., Darzynkiewicz, Z. (2003). Cytotoxic ribonucleases and RNA interference (RNAi). *Cell Cycle* **2**, 22-24.

Ardelt, W., Mikulski, S. M., Shogen, K. (1991). Amino acid sequence of an anti-tumor protein from Rana pipiens oocytes and early embryos. Homology to pancreatic ribonucleases. *J. Biol. Chem.* **266**, 245-251.

Arnold, U., Hinderaker, M. P., Raines, R. T. (2002). Semisynthesis of ribonuclease A using intein-mediated protein ligation. *Sci. World J.* **2**, 1823-1827.

Arnold, U., Schulenburg, C., Schmidt, D., Ulbrich-Hofmann, R. (2006). Contribution of structural peculiarities of onconase to its high stability and folding kinetics. *Biochemistry* **45**, 3580-3587.

Arnold, U., Ulbrich-Hofmann, R. (2006). Natural and engineered ribonucleases as potential cancer therapeutics. *Biotechnol. Lett.* **28**, 1615-1622.

Avery, O. T., Dubos, R. (1931). The protective action of a specific enzyme against type III pneumococcus infection in mice. *J. Exp. Med.* **54**, 73-89.

Baeyer, A. (1871). Ueber eine neue klasse von farbstoffen. *Ber. Dtsch. Chem. Ges.* **4**, 555-558.

Barnard, E. A. (1969). Biological function of pancreatic ribonuclease. *Nature* **221**, 340-344.

Bartholeyns, J., Moore, S. (1974). Pancreatic ribonuclease: enzymic and physiological properties of a cross-linked dimer. *Science* **186**, 444-455.

Bartholeyns, J., Baudhuin, P. (1976). Inhibition of tumor cell proliferation by dimerized ribonuclease. *Proc. Natl. Acad. Sci. U.S.A.* **73**, 573-576.

Bartholeyns, J., Zenebergh, A. (1979). *In vitro* and *in vivo* antitumor effect of dimerized ribonuclease A. *Eur. J. Cancer* **15**, 85-91.

Beintema, J. J., Blank, A., Schieven, G. L., Dekker, C. A., Sorrentino, S., Libonati, M. (1988a). Differences in glycosylation pattern of human secretory ribonucleases. *Biochem. J.* **255**, 501-505.

Beintema, J. J., Schüller, C., Irie, M., Carsana, A. (1988b). Molecular evolution of the ribonuclease superfamily. *Prog. Biophys. Mol. Biol.* **51**, 165-192.

Beintema, J. J., Breukelman, H. J., Carsana, A., Furia, A. Evolution of vertebrate ribonucleases: Ribonuclease A superfamily. In: G. D'Alessio, J. F. Riordan. (Eds.). Ribonucleases: Structures and Functions. Academic Press, New York. 1997. pp. 245-269.

Benito, A., Ribó, M., Vilanova, M. (2005). On the track of antitumour ribonucleases. *Mol. Biosyst.* **1**, 294-302.

Berisio, R., Sica, F., De Lorenzo, C., Di Fiore, A., Piccoli, R., Zagari, A., Mazzarella, L. (2003). Crystal structure of the dimeric unswapped form of bovine seminal ribonuclease. *FEBS Lett.* **554**, 105-110.

Billeter, M. A., Weissmann, C., Warner, R. C. (1966). Replication of viral ribonucleic acid. IX. Properties of double-stranded RNA from *Escherichia coli* infected with bacteriophage MS2. *J. Mol. Biol.* **17**, 145-173.

Bjellqvist, B., Hughes, G. J., Pasquali, C., Paquet, N., Ravier, F., Sanchez, J. C., Frutiger, S., Hochstrasser, D. (1993). The focusing positions of polypeptides in immobilized pH gradients can be predicted from their amino acid sequences. *Electrophoresis* **14**, 1023-1031.

Bjellqvist, B., Basse, B., Olsen, E., Celis, J. E. (1994). Reference points for comparisons of two-dimensional maps of proteins from different human cell types defined in a pH scale where isoelectric points correlate with polypeptide compositions. *Electrophoresis* **15**, 529-539.

Blackburn, P., Wilson, G., Moore, S. (1977). Ribonuclease inhibitor from human placenta. Purification and properties. *J. Biol. Chem.* **252**, 5904-5910.

Blackburn, P., Moore, S. Pancreatic ribonuclease. The Enzymes. Vol. XV. Academic Press, Inc. 1982. pp. 317-433.

Blázquez, M., Fominaya, J. M., Hofsteenge, J. (1996). Oxidation of sulfhydryl groups of ribonuclease inhibitor in epithelial cells is sufficient for its intracellular degradation. *J. Biol. Chem.* **271**, 18638-18642.

Boix, E., Nogués, M. V., Schein, C. H., Benner, S. A., Cuchillo, C. M. (1994). Reverse transphosphorylation by ribonuclease A needs an intact p_2-binding site. *J. Biol. Chem.* **269**, 2529-2534.

Boix, E., Wu, Y., Vasandani, V. M., Saxena, S. K., Ardelt, W., Ladner, J., Youle, R. J. (1996). Role of the N terminus in RNase A homologues: Differences in catalytic activity, ribonuclease inhibitor interaction and cytotoxicity. *J. Mol. Biol.* **257**, 992-1007.

Boix, E., Leonidas, D. D., Nikolovski, Z., Nogués, M. V., Cuchillo, C. M., Acharya, K. R. (1999). Crystal structure of eosinophil cationic protein at 2.4 Å resolution. *Biochemistry* **38**, 16794-16801.

Bosch, M., Benito, A., Ribó, M., Puig, T., Beaumelle, B., Vilanova, M. (2004). A nuclear localization sequence endows human pancreatic ribonuclease with cytotoxic activity. *Biochemistry* **43**, 2167-2177.

Braschoss, S., Hirsch, B., Dubel, S., Stein, H., Durkop, H. M. (2007). New anti-CD30 human pancreatic ribonuclease-based immunotoxin reveals strong and specific cytotoxicity *in vivo*. *Leuk. Lymphoma* **48**, 1179-1186.

Brenner, B. M., Hostetter, T. H., Humes, H. D. (1978). Glomerular permselectivity: Barrier function based on discrimination of molecular size and charge. *Am. J. Physiol.* **234**, F455-F460.

Bretscher, L. E., Abel, R. L., Raines, R. T. (2000). A ribonuclease A variant with low catalytic activity but high cytotoxicity. *J. Biol. Chem.* **275**, 9893-9896.

Brown, M. A., Semelka, R. C. (2003). MRI: Basic principles and applications. Wiley-Liss.

Buckle, A. M., Fersht, A. R. (1994). Subsite binding in an RNase: Structure of a barnase-tetranucleotide complex at 1.76-Å resolution. *Biochemistry* **33**, 1644-1653.

Buckle, A. M., Schreiber, G., Fersht, A. R. (1994). Protein-protein recognition: Crystal structural analysis of a barnase-barstar complex at 2.0-Å resolution. *Biochemistry* **33**, 8878-8889.

Bugelski, P. J., Treacy, G. (2004). Predictive power of preclinical studies in animals for the immunogenicity of recombinant therapeutic proteins in humans. *Curr. Opin. Mol. Ther.* **6**, 10-16.

Cacheris, W. P., Nickle, S. K., Sherry, A. D. (1987). Thermodynamic study of lanthanide complexes of 1,4,7-triazacyclononane-N,N',N''-triacetic acid and 1,4,7,10-tetraazacyclododecane-N,N',N'',N'''-tetraacetic acid. *Inorg. Chem.* **26**, 958-960.

Caliceti, P., Schiavon, O., Veronese, F. M., Chaiken, I. M. (1990). Effects of monomethoxypoly(ethylene glycol) modification of ribonuclease on antibody

recognition, substrate accessibility and conformational stability. *J. Mol. Recognit.* **3**, 89-93.

Caravan, P., Ellison, J. J., McMurry, T. J., Lauffer, R. B. (1999). Gadolinium(III) chelates as MRI contrast agents: Structure, dynamics, and applications. *Chem. Rev.* **99**, 2293-2352.

Chalikian, T. V., Totrov, M., Abagyan, R., Breslauer, K. J. (1996). The hydration of globular proteins as derived from volume and compressibility measurements: Cross correlating thermodynamic and structural data. *J. Mol. Biol.* **260**, 588-603.

Chandran, S. S., Dickson, K. A., Raines, R. T. (2005). Latent fluorophore based on the trimethyl lock. *J. Am. Chem. Soc.* **127**, 1652-1653.

Chang, F. N., Flaks, J. G. (1972). The specific cross-linking of two proteins from the *Escherichia coli* 30 S ribosomal subunit. *J. Mol. Biol.* **68**, 177-180.

Chapman, A. P. (2002). PEGylated antibodies and antibody fragments for improved therapy: A review. *Adv. Drug Deliv. Rev.* **54**, 531-545.

Chen, C.-Z., Shapiro, R. (1997). Site-specific mutagenesis reveals differences in the structural bases for tight binding of RNase inhibitor to angiogenin and RNase A. *Proc. Natl. Acad. Sci. U.S.A.* **94**, 1761-1766.

Chen, C.-Z., Shapiro, R. (1999). Superadditive and subadditive effects of "hot spot" mutations within the interfaces of placental ribonuclease inhibitor with angiogenin and ribonuclease A. *Biochemistry* **38**, 9273-8285.

Chen, L. L., Rosa, J. J., Turner, S., Pepinsky, R. B. (1991). Production of multimeric forms of CD4 through a sugar-based cross-linking strategy. *J. Biol. Chem.* **266**, 18237-18243.

Chen, S. C., Nakamura, H., Tamura, Z. (1979). Supplemental studies on relationship between structure and spectrum of fluorescein. *Chem. Pharm. Bull.* **27**, 475-479.

Chen, Y., Jungsuwadee, P., Vore, M., Butterfield, D. A., St. Clair, D. K. (2007). Collateral damage in cancer chemotherapy: Oxidative stress in nontargeted tissues. *Mol. Interv.* **7**, 147-156.

Chico, D. E., Given, R. L., Miller, B. T. (2003). Binding of cationic cell-permeable peptides to plastic and glass. *Peptides* **24**, 3-9.

Cho, S., Beintema, J. J., Zhang, J. (2005). The ribonuclease A superfamily of mammals and birds: Identifying new members and tracing evolutionary histories. *Genomics* **85**, 208-220.

Cho, S. W., Joshi, J. G. (1989). Ribonuclease inhibitor from pig brain: Purification, characterization, and direct spectrophotometric assay. *Anal. Biochem.* **176**, 175-179.

Ciglic, M. I., Jackson, P. J., Raillard, S. A., Haugg, M., Jermann, T. M., Opitz, J. G., Trabesinger-Ruf, N., Benner, S. A. (1998). Origin of dimeric structure in the ribonuclease superfamily. *Biochemistry* **37**, 4008-4022.

Clackson, T., Wells, J. A. (1995). A hot spot of binding energy in a hormone-receptor interface. *Science* **267**, 383-386.

Collier, R. J. (2001). Understanding the mode of action of diphtheria toxin: A perspective on progress during the 20th century. *Toxicon* **39**, 1793-1803.

Coons, A. H., Kaplan, M. H. (1950). Localization of antigen in tissue cells. II. Improvements in a method for the detection of antigen by means of fluorescent antibody. *J. Exp. Med.* **91**, 1-13.

Corrie, J. E. T., Craik, J. S. (1994). Synthesis and characterization of pure isomers of iodoacetamidotetramethylrhodamine. *J. Chem. Soc., Perkin Trans. 1*, 2967-2973.

Cortney, M. A., Sawin, L. L., Weiss, D. D. (1970). Renal tubular protein absorption in the rat. *J. Clin. Invest.* **49**, 1-4.

Crestfield, A. M., Stein, W. H., Moore, S. (1962). On the aggregation of bovine pancreatic ribonuclease. *Arch. Biochem. Biophys.* **Supplement 1**, 217-222.

Crick, F. H. C. (1952). Is α-keratin a coiled coil? *Nature* **170**, 882-883.

Cuchillo, C. M., Vilanova, M., Nogués, M. V. Pancreatic ribonucleases. In: G. D'Alessio, J. F. Riordan. (Eds.). Ribonucleases: Structures and Functions. Academic Press, New York. 1997. pp. 271-304.

Curtet, C., Tellier, C., Bohy, J., Conti, M. L., Saccavini, J. C., Thedrez, P., Douillard, J. Y., Chatal, J. F., Koprowski, H. (1986). Selective modification of NMR relaxation time in human colorectal carcinoma by using gadolinium-diethylenetriaminepentaacetic acid conjugated with monoclonal antibody 19-9. *Proc. Natl. Acad. Sci. U.S.A.* **83**, 4277-4281.

Curtet, C., Bourgoin, C., Bohy, J., Saccavini, J. C., Thedrez, P., Akoka, S., Tellier, C., Chatal, J. F. (1988). Gd-25 DTPA-MAb, a potential NMR contrast agent for MRI in the xenografted nude mouse: Preliminary studies. *Int. J. Cancer Suppl.* **2**, 126-132.

Curtet, C., Maton, F., Havet, T., Slinkin, M., Mishra, A., Chatal, J. F., Muller, R. N. (1998). Polylysine-Gd-DTPA$_n$ and polylysine-Gd-DOTA$_n$ coupled to anti-CEA F(ab')$_2$ fragments as potential immunocontrast agents. Relaxometry, biodistribution, and magnetic resonance imaging in nude mice grafted with human colorectal carcinoma. *Invest. Radiol.* **33**, 752-761.

D'Alessio, G., Floridi, A., De Prisco, R., Pignero, A., Leone, E. (1972a). Bull semen ribonucleases 1. Purification and physico-chemical properties of the major component. *Eur. J. Biochem.* **26**, 153-161.

D'Alessio, G., Parente, A., Guida, C., Leone, E. (1972b). Dimeric structure of seminal ribonuclease. *FEBS Lett.* **27**, 285-288.

D'Alessio, G., Di Donato, A., Mazzarella, L., Piccoli, R. Seminal ribonuclease: The importance of diversity. In: G. D'Alessio, J. F. Riordan. (Eds.). Ribonucleases: Structures and Functions. Academic Press, New York. 1997. pp. 383-423.

D'Alessio, G., Riordan, J. F. (1997). Ribonucleases : Structures and Functions. Academic Press, San Diego.

Daniels, T. R., Delgado, T., Helguera, G., Penichet, M. L. (2006). The transferrin receptor part II: Targeted delivery of therapeutic agents into cancer cells. *Clin. Immunol.* **121**, 159-176.

Darzynkiewicz, Z., Carter, S. P., Mikulski, S. M., Ardelt, W. J., Shogen, K. (1988). Cytostatic and cytotoxic effect of Pannon (P-30 Protein), a novel anticancer agent. *Cell. Tissue Kinet.* **21**, 169-182.

Davidson, S. J., Hughes, W. L., Barnwell, A. (1971). Renal protein absorption into sub-cellular particles. I. Studies with intact kidneys and fractionated homogenates. *Exp. Cell Res.* **67**, 171-187.

de Beer, T., Vliengenthart, J. F., Loffler, A., Hofsteenge, J. (1995). The hexopyranosyl residue that is C-glycosidically linked to the side chain of tryptophan-7 in human RNase Us is alpha-mannopyranose. *Biochemistry* **34**, 11785-11789.

De Duve, C. (1966). The significance of lysosomes in pathology and medicine. *Proc. Inst. Med. Chic.* **26**, 73-76.

De Groot, A. S., Scott, D. W. (2007). Immunogenicity of protein therapeutics. *Trends Immunol.* **28**, 482-490.

De Lorenzo, C., Arciello, A., Cozzolino, R., Palmer, D. B., Laccetti, P., Piccoli, R., D'Alessio, G. (2004). A fully human antitumor immunoRNase selective for ErbB-2-positive carcinomas. *Cancer Res.* **64**, 4870-4874.

De Lorenzo, C., Di Malta, C., Calì, G., Troise, F., Nitsch, L., D'Alessio, G. (2007). Intracellular route and mechanism of action of ERB-hRNase, a human anti-ErbB2 anticancer immunoagent. *FEBS Lett.* **581**, 296-300.

DeLano, W. L. (2002). Unraveling hot spots in binding interfaces: Progress and challenges. *Curr. Opin. Struct. Biol.* **12**, 14-20.

delCardayré, S. B., Raines, R. T. (1994). Structural determinants of enzymatic processivity. *Biochemistry* **33**, 6031-6037.

delCardayré, S. B., Ribó, M., Yokel, E. M., Quirk, D. J., Rutter, W. J., Raines, R. T. (1995). Engineering ribonuclease A: Production, purification, and characterization of wild-type enzyme and mutants at Gln11. *Protein Eng.* **8**, 261-273.

Delgado, C., Francis, G. E., Fisher, D. (1992). The uses and properties of PEG-linked proteins. *Crit. Rev. Ther. Drug Carrier Syst.* **9**, 249-304.

Delikatny, E. J., Poptani, H. (2005). MR techniques for in vivo molecular and cellular imaging. *Radiol. Clin. North. Am.* **43**, 205-220.

Di Donato, A., Cafaro, V., D'Alessio, G. (1994). Ribonuclease A can be transformed into a dimeric ribonuclease with antitumor activity. *J. Biol. Chem.* **269**, 17394-17396.

Di Donato, A., Cafaro, V., Romeo, I., D'Alessio, G. (1995). Hints on the evolutionary design of a dimeric RNase with *special* bioactions. *Protein Sci.* **4**, 1470-1477.

Di Gaetano, S., D'Alessio, G., Piccoli, R. (2001). Second generation antitumour human RNase: Significance of its structural and functional features for the mechanism of antitumour action. *Biochem. J.* **358**, 241-247.

Dickson, K. A., Dahlberg, C. L., Raines, R. T. (2003). Compensating effects on the cytotoxicity of ribonuclease A variants. *Arch. Biochem. Biophys.* **415**, 172-177.

Dickson, K. A., Haigis, M. C., Raines, R. T. (2005). Ribonuclease inhibitor: Structure and function. *Prog. Nucleic Acid Res. Mol. Biol.* **80**, 349-374.

Diehl, H. (1989). Studies on fluorescein-VI: Absorbance of the various prototropic forms of yellow fluorescein in aqueous solution. *Talanta* **36**, 413-415.

Diehl, H., Markuszewski, R. (1989). Studies on fluorescein-VII: The fluorescence of fluorescein as a function of pH. *Talanta* **36**, 416-418.

Diwu, Z., Twu, J. J., Yi, G., Lavis, L. D., Chen, Y.-W., Cassutt, K. J. (2004) Fluorescent pH indicators for intracellular assays. U.S. Patent 6,800,765, October 5, 2004.

Dohi, S. R., Terzian, J. F., Widman, A., Brentani, R., Fausto, N., Liberman, B., Rabinovitch, M. (1959). Inactivation of serum ribonuclease by the kidney. *Am. J. Physiol.* **196**, 924-926.

Domachowske, J. B., Dyer, K. D., Adams, A. G., Leto, T. L., Rosenberg, H. F. (1998). Eosinophil cationic protein/RNase 3 is another RNase A-family ribonuclease with direct antiviral activity. *Nucleic Acids Res.* **26**, 3358-3363.

Dostál, J., Matoušek, J. (1973). Isolation and some chemical properties of aspermatogenic substance form bull seminal vesicle fluid. *J. Reprod. Fertil.* **33**, 263-274.

Dreher, M. R., Liu, W., Michelich, C. R., Dewhirst, M. W., Yuan, F., Chilkoti, A. (2006). Tumor vascular permeability, accumulation, and penetration of macromolecular drug carriers. *J. Natl. Cancer Inst.* **98**, 335-344.

Dulbecco, R., Vogt, M. (1954). Plaque formation and isolation of pure lines with poliomyelitis viruses. *J. Exp. Med.* **99**, 167-182.

Eberhardt, E. S., Wittmayer, P. K., Templer, B. M., Raines, R. T. (1996). Contribution of a tyrosine side chain to ribonuclease A catalysis and stability. *Protein Sci.* **5**, 1697-1703.

Ellman, G. L. (1958). A colorimetric method for determining low concentrations of mercaptans. *Arch. Biochem. Biophys.* **74**, 443-450.

Erickson, H. A., Jund, M. D., Pennell, C. A. (2006). Cytotoxicity of human RNase-based immunotoxins requires cytosolic access and resistance to ribonuclease inhibition. *Protein Eng. Des. Sel.* **19**, 37-45.

Evenson, M. A., Deutsch, H. F. (1978). Influence of fatty acids on the isoelectric point properties of human serum albumin. *Clin. Chim. Acta.* **89**, 341-354.

Fasold, H., Klappenberger, J., Meyer, C., Remold, H. (1971). Bifunctional reagents for the crosslinking of proteins. *Angew. Chem. Int. Ed. Engl.* **10**, 795-801.

Fee, C. J., Van Alstine, J. M. (2004). Prediction of the viscosity radius and the size exclusion chromatography behavior of PEGylated proteins. *Bioconjugate Chem.* **15**, 1304-1313.

Fee, C. J. (2007). Size comparison between proteins PEGylated with branched and linear poly(ethylene glycol) molecules. *Biotechnol. Bioeng.* **98**, 725-731.

Fishburn, C. S. (2008). The pharmacology of PEGylation: Balancing PD with PK to generate novel therapeutics. *J. Pharm. Sci.*

Fisher, B. M., Grilley, J. E., Raines, R. T. (1998a). A new remote subsite in ribonuclease A. *J. Biol. Chem.* **273**, 34134-34138.

Fisher, B. M., Ha, J.-H., Raines, R. T. (1998b). Coulombic forces in protein-RNA interactions: Binding and cleavage by ribonuclease A and variants at Lys7, Arg10, and Lys66. *Biochemistry* **37**, 12121-12132.

Floridi, A., D'Alessio, G. (1967). Compartamento chromatografico della ribonucleasi seminale. *Bull. Soc. Ital. Biol. Sper.* **43**, 32-36.

Floridi, A., D'Alessio, G., Leone, E. (1972). Bull semen ribonucleases. 2. Catalytic properties of the major component. *Eur. J. Biochem.* **26**, 162-167.

Fredens, K., Dahl, R., Venge, P. (1991). In vitro studies of the interaction between heparin and eosinophil cationic protein. *Allergy* **46**, 27-29.

Friedrich, K., Woolley, P. (1988). Electrostatic potential of macromolecules measured by pK_a shift of a fluorophore 1. The 3' terminus of 16S RNA. *Eur. J. Biochem.* **173**, 227-231.

Friedrich, K., Woolley, P., Steinhauser, K. G. (1988). Electrostatic potential of macromolecules measured by pK_a shift of a fluorophore 2. Transfer RNA. *Eur. J. Biochem.* **173**, 233-239.

Fu, C. H., Sakamoto, K. M. (2007). PEG-asparaginase. *Expert Opin. Pharmacother.* **8**, 1977-1984.

Fuchs, S. M., Raines, R. T. (2005). Polyarginine as a multifunctional fusion tag. *Protein Sci.* **14**, 1538-1544.

Fuchs, S. M., Raines, R. T. (2006). Internalization of cationic peptides: The road less (or more?) traveled. *Cell. Mol. Life Sci.* **63**, 1819-1822.

Fuchs, S. M., Raines, R. T. (2007). Arginine grafting to endow cell permeability. *ACS Chem. Biol.* **2**, 167-170.

Fuchs, S. M., Rutkoski, T. J., Kung, V. M., Groeschl, R. T., Raines, R. T. (2007). Increasing the potency of a cytotoxin with an arginine graft. *Protein Eng. Des. Sel.* **20**, 505-509.

Futami, J., Seno, M., Kosaka, M., Tada, H., Seno, S., Yamada, H. (1995). Recombinant human pancreatic ribonuclease produced in *E. coli*: Importance of the amino-terminal sequence. *Biochem. Biophys. Res. Commun.* **216**, 406-413.

Futami, J., Seno, M., Ueda, M., Tada, H., Yamada, H. (1999). Inhibition of cell growth by a fused protein of human ribonuclease 1 and human basic fibroblast growth factor. *Protein Eng.* **12**, 1013-1019.

Futami, J., Tada, H., Seno, M., Ishikami, S., Yamada, H. (2000). Stabilization of human RNase 1 by introduction of a disulfide bond between residues 4 and 118. *J. Biochem. (Tokyo)* **128**, 245-250.

Futami, J., Maeda, T., Kitazoe, M., Nukui, E., Tada, H., Seno, M., Kosaka, M., Yamada, H. (2001). Preparation of potent cytotoxic ribonucleases by cationization: Enhanced cellular uptake and decreased interaction with ribonuclease inhibitor by chemical modification of carboxyl groups. *Biochemistry* **26**, 7518-7524.

Futami, J., Nukui, K., Maeda, T., Kosaka, M., Tada, H., Seno, M., Yamada, H. (2002). Optimum modification for the highest cytotoxicity of cationized ribonuclease. *J. Biochem. (Tokyo)* **132**, 223-228.

Futami, J., Kitazoe, M., Maeda, T., Nukui, E., Sakaguchi, M., Kosaka, J., Miyazaki, M., Kosaka, M., Tada, H., Seno, M., Sasaki, J., Huh, N. H., Namba, M., Yamada, H. (2005). Intracellular delivery of proteins into mammalian living cells by polyethylenimine-cationization. *J. Biosci. Bioeng.* **99**, 95-103.

Gad, S. C. (2007). Handbook of Pharmaceutical Biotechnology. John Wiley and Sons, Inc., Hoboken, N.J.

Garel, J. R. (1976). pK changes of ionizable reporter groups as an index of conformational changes in proteins: A study of fluorescein-labelled ribonuclease A. *Eur. J. Biochem.* **70**, 179-189.

Gaudet, R., Bohm, A., Sigler, P. B. (1996). Crystal structure at 2.4 Å resolution of the complex of transducin βγ and its regulator, phosducin. *Cell* **87**, 577-588.

Gaur, D., Swaminathan, S., Batra, J. K. (2001). Interaction of human pancreatic ribonuclease with human ribonuclease inhibitor. Generation of inhibitor-resistant cytotoxic variants. *J. Biol. Chem.* **276**, 24978-24984.

Glukhov, B. N., Jerusalimsky, A. P., Canter, V. M., Salganik, R. I. (1976). Ribonuclease treatment of tick-borne encephalitis. *Arch. Neurol.* **33**, 598-603.

Gohr-Rosenthal, S., Schmitt-Willich, H., Ebert, W., Conrad, J. (1993). The demonstration of human tumors on nude mice using gadolinium-labelled monoclonal antibodies for magnetic resonance imaging. *Invest. Radiol.* **28**, 789-795.

Goldberg, J. M., Baldwin, R. L. (1998a). Kinetic mechanism of a partial folding reaction. 2. Nature of the transition state. *Biochemistry* **37**, 2556-2563.

Goldberg, J. M., Baldwin, R. L. (1998b). Kinetic mechanism of a partial folding reaction. 1. Properties of the reaction and effects of denaturants. *Biochemistry* **37**, 2546-2555.

Goldberg, J. M., Baldwin, R. L. (1999). A specific transition state for S-peptide combining with folded S-protein and then refolding. *Proc. Natl. Acad. Sci. U.S.A.* **96**, 2019-2024.

Goodson, R. J., Katre, N. V. (1990). Site-directed pegylation of recombinant interleukin-2 at its glycosylation site. *Biotechnology (New York)* **8**, 343-346.

Gotte, G., Testolin, L., Costanzo, C., Sorrentino, S., Armato, U., Libonati, M. (1997). Cross-linked trimers of bovine ribonuclease A: activity on double-stranded RNA and antitumor action. *FEBS Lett.* **415**, 308-312.

Gotte, G., Laurents, D. V., Libonati, M. (2006). Three-dimensional domain-swapped oligomers of ribonuclease A: Identification of a fifth tetramer, pentamers and hexamers, and detection of trace heptameric, octameric and nonameric species. *Biochim. Biophys. Acta.* **1764**, 44-54.

Graber, M. L., Dilillo, D. C., Friedman, B. L., Pastorizamunoz, E. (1986). Characteristics of fluoroprobes for measuring intracellular pH. *Anal. Biochem.* **156**, 202-212.

Grace, M. J., Lee, S., Bradshaw, S., Chapman, J., Spond, J., Cox, S., Delorenzo, M., Brassard, D., Wylie, D., Cannon-Carlson, S., Cullen, C., Indelicato, S., Voloch, M., Bordens, R. (2005). Site of pegylation and polyethylene glycol molecule size attenuate interferon-α antiviral and antiproliferative activities through the JAK/STAT signaling pathway. *J. Biol. Chem.* **280**, 6327-6336.

Green, N. M. (1975). Avidin. *Adv. Protein Chem.* **29**, 85-133.

Green, N. S., Reisler, E., Houk, K. N. (2001). Quantitative evaluation of the lengths of homobifunctional protein cross-linking reagents used as molecular rulers. *Protein Sci* **10**, 1293-1304.

Greenwald, R. B., Choe, Y. H., Conover, C. D., Shum, K., Royzen, M. (2000). Drug delivery systems based on trimethyl lock lactonization: Poly(ethylene glycol) prodrugs of amino-containing compounds. *J. Med. Chem.* **43**, 475-487.

Greenwald, R. B., Choe, Y. H., McGuire, J., Conover, C. D. (2003a). Effective drug delivery by PEGylated drug conjugates. *Adv. Drug Delivery Rev.* **55**, 217-250.

Greenwald, R. B., Yang, K., Zhao, H., Conover, C. D., Lee, S., Filpula, D. (2003b). Controlled release of proteins from their poly(ethylene glycol) conjugates: drug delivery systems employing 1,6-elimination. *Bioconjugate Chem.* **14**, 395-403.

Griep, M. A., Mchenry, C. S. (1990). Dissociation of the DNA polymerase III holoenzyme β_2 subunits is accompanied by conformational change at distal cysteines 333. *J. Biol. Chem.* **265**, 20356-20363.

Griep, M. A., Mesman, T. N. (1995). Fluorescent labeling of cysteine-39 on *Escherichia coli* primase places the dye near an active site. *Bioconjugate Chem.* **6**, 673-682.

Gries, H. Extracellular contrast agents based on gadolinium. In: W. Krause. (Ed.). Contrast Agents I: Magnetic Resonance Imaging. Vol. 221. Springer-Verlag, Heidelburg. 2002. pp. 1-24.

Haigis, M. C., Kurten, E. L., Abel, R. L., Raines, R. T. (2002). KFERQ sequence in ribonuclease A-mediated cytotoxicity. *J. Biol. Chem.* **277**, 11576-11581.

Haigis, M. C., Kurten, E. L., Raines, R. T. (2003). Ribonuclease inhibitor as an intracellular sentry. *Nucleic Acids Res.* **31**, 1024-1032.

Haigis, M. C., Raines, R. T. (2003). Secretory ribonucleases are internalized by a dynamin-independent endocytic pathway. *J. Cell Sci.* **116**, 313-324.

Hajela, S., Botta, M., Giraudo, S., Xu, J., Raymond, K. N., Aime, S. (2000). A tris-hydroxylmethyl-substituted derivative of Gd-TREN-Me-3,2-HOPO: An MRI relaxation agent with improved efficacy. *J. Am. Chem. Soc.* **122**, 11228-11229.

Haley, T. J. (1965). Pharmacology and toxicology of the rare earth elements. *J. Pharm. Sci.* **54**, 663-670.

Halicka, D. H., Pozarowski, P., Ita, M., Ardelt, W. J., Mikulski, S. M., Shogen, K., Darzynkiewicz, Z. (2002). Enhancement of activation-induced apoptosis of lymphocytes by the cytotoxic ribonuclease onconase (Ranpirnase). *Int. J. Oncol.* **21**, 1245-1250.

Hallahan, T. W., Shapiro, R., Vallee, B. L. (1991). Dual site model for the organogenic activity of angiogenin. *Proc. Natl. Acad. Sci. U.S.A.* **88**, 2222-2226.

Hampton, T. (2005). Cancer treatment's trade-off: Years of added life can have long-term costs. *JAMA* **294**, 167-168.

Haraldsson, B., Sorensson, J. (2004). Why do we not all have proteinuria? An update of our current understanding of the glomerular barrier. *News Physiol. Sci.* **19**, 7-10.

Harder, J., Schroder, J. M. (2002). RNase 7, a novel innate immune defense antimicrobial protein of healthy human skin. *J. Biol. Chem.* **277**, 46779-46784.

Harris, J. M., Zalipsky, S. (1997). Poly(ethylene glycol): Chemistry and Biological Applications. American Chemical Society, Washington, D.C.

Harris, J. M., Martin, N. E., Modi, M. (2001). Pegylation: A novel process for modifying pharmacokinetics. *Clin. Pharmacokinet.* **40**, 539-551.

Harris, J. M., Chess, R. B. (2003). Effect of pegylation on pharmaceuticals. *Nat. Rev. Drug Discov.* **2**, 214-221.

Harris, L. J., Larson, S. B., Hasel, K. W., McPherson, A. (1997). Refined structure of an intact IgG2a monoclonal antibody. *Biochemistry* **36**, 1581-1597.

Hartman, F. C., Wold, F. (1967). Cross-linking of bovine pancreatic ribonuclease A with dimethyl adipimidate. *Biochemistry* **6**, 2439-2448.

Haugland, R. P., Spence, M. T. Z., Johnson, I. D., Basey, A. (2005). The Handbook: A Guide to Fluorescent Probes and Labeling Technologies. Molecular Probes, Eugene, OR.

Hayashida, T., Ueda, M., Aiura, K., Tada, H., Onizuka, M., Seno, M., Yamada, H., Kitajima, M. (2005). Anti-angiogenic effect of an insertional fusion protein of human basic fibroblast growth factor and ribonuclease-1. *Protein Eng. Des. Sel.* **18**, 321-327.

Henderson, P. J. F. (1972). A linear equation that describes the steady-state kinetics of enzymes and subcellular particles interacting with tightly bound inhibitors. *Biochem. J.* **127**, 321-333.

Hermans, J., Jr., Scheraga, H. A. (1961). Structural studies of ribonuclease. V. Reversible change of configuration. *J. Am. Chem. Soc.* **83**, 3283-3292.

Hofman, M., Ryan, J. L., Figueroa-Moseley, C. D., Jean-Pierre, P., Morrow, G. R. (2007). Cancer-related fatigue: The scale of the problem. *Oncologist* **12 Suppl 1**, 4-10.

Hofsteenge, J. Ribonuclease inhibitor. In: G. D'Alessio, J. F. Riordan. (Eds.). Ribonucleases: Structures and Functions. Academic Press, New York. 1997. pp. 621-658.

Hofsteenge, J., Vicentini, A., Zelenko, O. (1998). Ribonuclease 4, an evolutionarily highly conserved member of the superfamily. *Cell. Mol. Life Sci.* **54**, 804-810.

Holcenberg, J. S., Roberts, R. (1977). Enzymes as drugs. *Ann. Rev. Pharmacol. Toxicol.* **17**, 97-116.

Hoshimoto, S., Ueda, M., Jinno, H., Kitajima, M., Futami, J., Seno, M. (2006). Mechanisms of the growth-inhibitory effect of the RNase-EGF fused protein against EGFR-overexpressing cells. *Anticancer Res.* **26**, 857-863.

Hsu, C.-H., Liao, Y.-D., Pan, Y.-R., Chen, L.-W., Wu, S.-H., Leu, Y.-J., Chen, C. (2003). Solution structure of the cytotoxic RNase 4 from oocytes of bullfrog *Rana catesbeiana. J. Mol. Biol.* **326**, 1189-1201.

Hu, G.-F., Strydom, D. J., Fett, J. W., Riordan, J. F., Vallee, B. L. (1993). Actin is a binding protein for angiogenin. *Proc. Natl. Acad. Sci. U.S.A.* **90**, 1217-1221.

Hu, G.-F., Riordan, J. F., Vallee, B. L. (1997). A putative angiogenin receptor in angiogenin-responsive human endothelial cells. *Proc. Natl. Acad. Sci. U.S.A.* **94**, 2204-2209.

Huang, Y.-C., Lin, Y.-M., Chang, T.-W., Wu, S.-J., Lee, Y.-S., Chang, M. D.-T., Chen, C., Wu, S.-H., Liao, Y.-D. (2007). The flexible and clustered lysine residues of human ribonuclease 7 are critical for membrane permeability and antimicrobial activity. *J. Biol. Chem.* **282**, 4626-4633.

Hubbard, S. J., Thornton, J. M. NACCESS. Department of Biochemistry and Molecular Biology, University College London, London, 1993.

Hutton, M., Willenbrock, F., Brocklehurst, K., Murphy, G. (1998). Kinetic analysis of the mechanism of interaction of full-length TIMP-2 and gelatinase A: Evidence for the existence of a low-affinity intermediate. *Biochemistry* 37, 10094-10098.

Ilinskaya, O., Decker, K., Koschinski, A., Dreyer, F., Repp, H. (2001). *Bacillus intermedius* ribonuclease as inhibitor of cell proliferation and membrane current. *Toxicology* 156, 101-107.

Ilinskaya, O. N., Dreyer, F., Mitkevich, V. A., Shaw, K. L., Pace, C. N., Makarov, A. A. (2002). Changing the net charge from negative to positive makes ribonuclease Sa cytotoxic. *Protein Sci* 11, 2522-2525.

Ilinskaya, O. N., Makarov, A. A. (2005). Why ribonucleases induce tumor cell death. *Mol. Biol. (Moscow)* 39, 1-10.

Iordanov, M. S., Ryabinina, O. P., Wong, J., Dinh, T. H., Newton, D. L., Rybak, S. M., Magun, B. E. (2000). Molecular determinants of apoptosis induced by the cytotoxic ribonuclease onconase: Evidence for cytotoxic mechanisms different from inhibition of protein synthesis. *Cancer Res.* 60, 1983-1994.

Iyer, S., Holloway, D. E., Kumar, K., Shapiro, R., Acharya, K. R. (2005). Molecular recognition of human eosinophil-derived neurotoxin (RNase 2) by placental ribonuclease inhibitor. *J. Mol. Biol.* 347, 637-655.

Jain, R. K. (1994). Barriers to drug delivery in solid tumors. *Sci. Am.* 271, 58-65.

Janin, J. (1995). Elusive affinities. *Proteins* 21, 30-39.

Ji, T. H. (1983). Bifunctional reagents. *Methods Enzymol.* 91, 580-609.

Johnson, R. J., Chao, T.-Y., Lavis, L. D., Raines, R. T. (2007a). Cytotoxic ribonucleases: The dichotomy of coulombic forces. *Biochemistry* 46, 10308-10316.

Johnson, R. J., Lavis, L. D., Raines, R. T. (2007b). Intraspecies regulation of ribonucleolytic activity. *Biochemistry* **46**, 13131-13140.

Johnson, R. J., McCoy, J. G., Bingman, C. A., Phillips, G. N., Jr., Raines, R. T. (2007c). Inhibition of human pancreatic ribonuclease by the human ribonuclease inhibitor protein. *J. Mol. Biol.* **368**, 434-449.

Jones, W. (1920). The action of boiled pancrease extract on yeast nucleic acid. *J. Am. Physiol.* **52**, 203-207.

Kalia, J., Raines, R. T. (2007). Catalysis of imido group hydrolysis in a maleimide conjugate. *Bioorg. Med. Chem. Lett.* **17**, 6286-6289.

Kamiya, Y., Oyama, F., Oyama, R., Sakakibara, F., Nitta, K., Kawauchi, H., Takayanagi, Y., Titani, K. (1990). Amino acid sequence of a lectin from Japanese frog (*Rana japonica*) eggs. *J. Biochem. (Tokyo)* **108**, 139-143.

Kawanomoto, M., Motojima, K., Sasaki, M., Hattori, H., Goto, S. (1992). cDNA cloning and sequence of rat ribonuclease inhibitor, and tissue distribution of mRNA. *Biochim. Biophys. Acta* **1129**, 335-338.

Kawashima, T., Berthet-Colominas, C., Wulff, M., Cusack, S., Leberman, R. (1996). The structure of the *Escherichia coli* EF-Tu•EF-Ts complex at 2.5 Å resolution. *Nature* **379**, 511-518.

Kelemen, B. R., Klink, T. A., Behlke, M. A., Eubanks, S. R., Leland, P. A., Raines, R. T. (1999). Hypersensitive substrate for ribonucleases. *Nucleic Acids Res.* **27**, 3696-3701.

Kim, B.-M., Kim, H., Raines, R. T., Lee, Y. (2004). Glycosylation of onconase increases its conformational stability and toxicity for cancer cells. *Biochem. Biophys. Res. Commun.* **315**, 976-983.

Kim, J.-S., Raines, R. T. (1993). Bovine seminal ribonuclease produced from a synthetic gene. *J. Biol. Chem.* **268**, 17392-17396.

Kim, J.-S., Raines, R. T. (1995). Dibromobimane as a fluorescent crosslinking reagent. *Anal. Biochem.* **225**, 174-176.

Kim, J.-S., Souček, J., Matoušek, J., Raines, R. T. (1995a). Catalytic activity of bovine seminal ribonuclease is essential for its immunosuppressive and other biological activities. *Biochem. J.* **308**, 547-550.

Kim, J.-S., Souček, J., Matoušek, J., Raines, R. T. (1995b). Structural basis for the biological activities of bovine seminal ribonuclease. *J. Biol. Chem.* **270**, 10525-10530.

Klink, T. A., Raines, R. T. (2000). Conformational stability is a determinant of ribonuclease A cytotoxicity. *J. Biol. Chem.* **275**, 17463-17467.

Klink, T. A., Vicentini, A. M., Hofsteenge, J., Raines, R. T. (2001). High-level soluble production and characterization of porcine ribonuclease inhibitor. *Protein Expression Purif.* **22**, 174-179.

Klonis, N., Sawyer, W. H. (1996). Spectral properties of the prototropic forms of fluorescein in aqueous solution. *J. Fluoresc.* **6**, 147-157.

Klonis, N., Clayton, A. H. A., Voss, E. W., Jr., Sawyer, W. H. (1998). Spectral properties of fluorescein in solvent-water mixtures: Applications as a probe of hydrogen bonding environments in biological systems. *Photochem. Photobiol.* **67**, 500-510.

Kobe, B., Deisenhofer, J. (1993). Crystal structure of porcine ribonuclease inhibitor, a protein with leucine-rich repeats. *Nature* **366**, 751-756.

Kobe, B., Deisenhofer, J. (1994). The leucine-rich repeat: A versatile binding motif. *Trends Biochem. Sci.* **19**, 415-421.

Kobe, B., Deisenhofer, J. (1995a). Proteins with leucine-rich repeats. *Curr. Opin. Struct. Biol.* **5**, 409-416.

Kobe, B., Deisenhofer, J. (1995b). A structural basis of the interactions between leucine-rich repeats and protein ligands. *Nature* **374**, 183-186.

Kobe, B., Deisenhofer, J. (1996). Mechanism of ribonuclease inhibition by ribonuclease inhibitor protein based on the crystal structure of its complex with ribonuclease A. *J. Mol. Biol.* **264**, 1028-1043.

Kothandaraman, S., Hebert, M. C., Raines, R. T., Nibert, M. L. (1998). No role for pepstatin-A-sensitive acidic proteinases in reovirus infections of L or MDCK cells. *Virology* **251**, 264-272.

Krafft, G. A., Sutton, W. R., Cummings, R. T. (1988). Photoactivable fluorophores. 3. Synthesis and photoactivation of fluorogenic difunctionalized fluoresceins. *J. Am. Chem. Soc.* **110**, 301-303.

Krol, M., Wrona, M., Page, C. S., Bates, P. A. (2006). Macroscopic pK_a calculations for fluorescein and its derivatives. *J. Chem. Theory Comput.* **2**, 1520-1529.

Krusemark, C. J., Ferguson, J. T., Wenger, C. D., Kelleher, N. L., Belshaw, P. J. (2008). Global amine and acid functional group modification of proteins. *Anal. Chem.* **80**, 713-720.

Kuhn, L. A., Siani, M. A., Pique, M. E., Fisher, C. L., Getzoff, E. D., Tainer, J. A. (1992). The interdependence of protein surface topography and bound water molecules revealed by surface accessibility and fractal density measures. *J. Mol. Biol.* **228**, 13-22.

Kumar, K., Brady, M., Shapiro, R. (2004). Selective abolition of pancreatic RNase binding to its inhibitor protein. *Proc. Natl. Acad. Sci. U.S.A.* **101**, 53-58.

Kunkel, T. A., Roberts, J. D., Zakour, R. A. (1987). Rapid and efficient site-specific mutagenesis without phenotypic selection. *Methods Enzymol.* **154**, 367-382.

Kurfürst, M. M. (1992). Detection and molecular weight determination of polyethylene glycol-modified hirudin by staining after sodium dodecyl sulfate-polyacrylamide gel electrophoresis. *Anal. Biochem.* **200**, 244-248.

Kuriu, Y., Otsuji, E., Kin, S., Nakase, Y., Fukuda, K., Okamoto, K., Hagiwara, A., Yamagishi, H. (2006). Monoclonal antibody conjugated to gadolinium as a

contrast agent for magnetic resonance imaging of human rectal carcinoma. *J. Surg. Oncol.* **94**, 144-148.

Kwaw, I., Sun, J., Kaback, H. R. (2000). Thiol cross-linking of cytoplasmic loops in the lactose permease of *Escherichia coli. Biochemistry* **39**, 3134-3140.

Labhardt, A. M., Ridge, J. A., Lindquist, R. N., Baldwin, R. L. (1983). Measurement of the refolding combination reaction between S-peptide and S-protein. *Biochemistry* **22**, 321-327.

Lakowicz, J. R. (1999). Principles of Fluorescence Spectroscopy. Plenum, New York.

Laskowski, R. A., Chistyakov, V. V., Thornton, J. M. (2005). PDBsum more: New summaries and analyses of the known 3D structures of proteins and nucleic acids. *Nucleic Acids Res.* **33**, D266-268.

Lavis, L. D., Chao, T. Y., Raines, R. T. (2006a). Latent blue and red fluorophores based on the trimethyl lock. *ChemBioChem* **7**, 1151-1154.

Lavis, L. D., Chao, T. Y., Raines, R. T. (2006b). Fluorogenic label for biomolecular imaging. *ACS Chem. Biol.* **1**, 252-260.

Lavis, L. D., Rutkoski, T. J., Raines, R. T. (2007). Tuning the pK_a of fluorescein to optimize binding assays. *Anal. Chem.* **79**, 6775-6782.

Lawrence, M. C., Colman, P. M. (1993). Shape complementarity at protein/protein interfaces. *J. Mol. Biol.* **234**, 946-950.

Lázníček, M., Schiavon, O., Caliceti, P., Veronese, F. M. (1993). Pharmacokinetics and distribution of ribonuclease and its monomethoxypoly(ethylene glycol) derivatives in rats. *Pharmacol. Res.* **28**, 153-161.

Ledoux, L., Baltus, E. (1954). Action de la ribonucléase sur les cellules du carcinome d'Ehrlich. *Experientia* **10**, 500-501.

Ledoux, L. (1955a). Action of ribonuclease on two solid tumours *in vivo*. *Nature* **176**, 36-37.

Ledoux, L. (1955b). Action of ribonuclease on certain ascites tumours. *Nature* **175**, 258-259.

Lee, B. K., Kwon, J. S., Kim, H. J., Yamamoto, S., Lee, E. K. (2007). Solid-phase PEGylation of recombinant interferon α-2a for site-specific modification: Process performance, characterization, and in vitro bioactivity. *Bioconjugate Chem.* **18**, 1728-1734.

Lee, F. S., Shapiro, R., Vallee, B. L. (1989). Tight-binding inhibition of angiogenin and ribonuclease A by placental ribonuclease inhibitor. *Biochemistry* **28**, 225-230.

Lee, F. S., Vallee, B. L. (1990). Kinetic characterization of two active mutants of placental ribonuclease inhibitor that lack internal repeats. *Biochemistry* **29**, 6633-6638.

Lee, F. S., Vallee, B. L. (1993). Structure and action of mammalian ribonuclease (angiogenin) inhibitor. *Prog. Nucleic Acid Res. Mol. Biol.* **44**, 1-30.

Lee, J. E., Raines, R. T. (2003). Contribution of active-site residues to the function of onconase, a ribonuclease with antitumoral activity. *Biochemistry* **42**, 11443-11450.

Lee, J. E., Raines, R. T. (2005). Cytotoxicity of bovine seminal ribonuclease: Monomer versus dimer. *Biochemistry* **44**, 15760-15767.

Lee, J. E., Raines, R. T. (2008). Ribonucleases as novel chemotherapeutics: The ranpirnase example. *BioDrugs* **22**, 53-58.

Lee, S., Greenwald, R. B., McGuire, J., Yang, K., Shi, C. (2001). Drug delivery systems employing 1,6-elimination: Releasable poly(ethylene glycol) conjugates of proteins. *Bioconjugate Chem.* **12**, 163-169.

Leich, F., Koditz, J., Ulbrich-Hofman, R., Arnold, U. (2006). Tandemization endows bovine pancreatic ribonuclease with cytotoxic activity. *J. Mol. Biol.* **358**, 1305-1313.

Leich, F., Stohr, N., Rietz, A., Ulbrich-Hofmann, R., Arnold, U. (2007). Endocytotic internalization as a crucial factor for the cytotoxicity of ribonucleases. *J. Biol. Chem.* **282**, 27640-27646.

Leland, P. A., Schultz, L. W., Kim, B.-M., Raines, R. T. (1998). Ribonuclease A variants with potent cytotoxic activity. *Proc. Natl. Acad. Sci. U.S.A.* **98**, 10407-10412.

Leland, P. A., Raines, R. T. (2001). Cancer chemotherapy—ribonucleases to the rescue. *Chem. Biol.* **8**, 405-413.

Leland, P. A., Staniszewski, K. E., Kim, B.-M., Raines, R. T. (2001). Endowing human pancreatic ribonuclease with toxicity for cancer cells. *J. Biol. Chem.* **276**, 43095-43102.

Lewis, M., Hunt, L., Barker, W. (1989). Striking sequence similarity among sialic acid-binding lectin, pancreatic ribonucleases and angiogenin: Possible structural and functional relationships. *Protein Sequences Data Anal.* **2**, 101-105.

Liao, Y.-D. (1992). A pyrimidine-guanine sequence-specific ribonuclease from *Rana catesbeiana* (bullfrog) oocytes. *Nucleic Acids Res.* **20**, 1371-1377.

Liao, Y.-D., Huang, H.-C., Leu, Y.-J., Wei, C.-W., Tang, P.-C., Wang, S.-C. (2000). Purification and cloning of cytotoxic ribonucleases from *Rana catesbeiana* (bullfrog). *Nucleic Acids Res.* **28**, 4097-4104.

Libonati, M., Floridi, A. (1969). Breakdown of double-stranded RNA by bull semen ribonuclease. *Eur. J. Biochem.* **8**, 81-87.

Libonati, M. (1971). Degradation of poly A and double-stranded RNA by aggregates of pancreatic ribonuclease. *Biochim. Biophys. Acta.* **228**, 440-445.

Libonati, M., Sorrentino, S., Galli, R., La Montagna, R., Di Donato, A. (1975). Degradation of DNA . RNA hybrids by aggregates of pancreatic ribonuclease. *Biochim. Biophys. Acta.* **407**, 292-298.

Libonati, M. (2004). Biological actions of the oligomers of ribonuclease A. *Cell. Mol. Life Sci.* **61**, 2431-2436.

Libonati, M., Gotte, G. (2004). Oligomerization of bovine ribonuclease A: Structural and functional features of its multimers. *Biochem. J.* **380**, 311-327.

Lindqvist, L. (1960). A flash photolysis study of fluorescein. *Ark. Kemi* **16**, 79-138.

Liu, J., Diwu, Z., Leung, W. Y. (2001). Synthesis and photophysical properties of new fluorinated benzo[c]xanthene dyes as intracellular pH indicators. *Bioorg. Med. Chem. Lett.* **11**, 2903-2905.

Liu, J., Qian, N., Morrical, S. W. (2006). Dynamics of bacteriophage T4 presynaptic filament assembly from extrinsic fluorescence measurements of Gp32-single-stranded DNA interactions. *J. Biol. Chem.* **281**, 26308-26319.

Liu, J. X., Diwu, Z. J., Klaubert, D. H. (1997). Fluorescent molecular probes III. 2',7'-bis-(3-carboxypropyl)-5-(and-6)-carboxyfluorescein (BCPCF): A new polar dual-excitation and dual-emission pH indicator with a pK_a of 7.0. *Bioorg. Med. Chem. Lett.* **7**, 3069-3072.

Lo Conte, L., Chothia, C., Janin, J. (1999). The atomic structure of protein-protein recognition sites. *J. Mol. Biol.* **285**, 2177-2198.

Lopez-Otin, C., Matrisian, L. M. (2007). Emerging roles of proteases in tumour suppression. *Nat. Rev. Cancer* **7**, 800-808.

Lou, Y.-C., Huang, Y.-C., Pan, Y.-R., Chen, C., Liao, Y.-D. (2006). Roles of N-terminal pyroglutamate in maintaining structural integrity and pK_a values of catalytic histidine residues in bullfrog ribonuclease 3. *J. Mol. Biol.* **355**, 409-421.

Lund, U., Rippe, A., Venturoli, D., Tenstad, O., Grubb, A., Rippe, B. (2003). Glomerular filtration rate dependence of sieving of albumin and some neutral proteins in rat kidneys. *Am. J. Physiol. Renal Physiol.* **284**, F1226-1234.

Maack, T. (1975). Renal handling of low molecular weight proteins. *Am. J. Med.* **58**, 57-64.

Maack, T., Johnson, V., Kau, S. T., Figueiredo, J., Sigulem, D. (1979). Renal filtration, transport, and metabolism of low-molecular-weight proteins: A review. *Kidney Int.* **16**, 251-270.

Maack, T., Park, H., Camargo, M. Renal filtration, transport and metabolism of proteins. In: D. W. Seldin, G. H. Giebisch. (Eds.). The Kidney : Physiology and Pathophysiology. Raven, New York. 1992. pp. 3005-3038.

Maack, T. Renal filtration, transport, and metabolism of proteins. In: D. W. Seldin, G. H. Giebisch. (Eds.). The Kidney : Physiology and Pathophysiology. Vol. 2. Lippincott Williams & Wilkins, Philadelphia, PA. 2000. pp. 2235-2267.

Maddox, D., Deen, W., Brenner, B. Glomerular filtration. Handbook of Physiology. Renal Physiology. Vol. I. Am. Physiol. Soc., Bethesda, MD. 1992. pp. 545-638.

Maeda, H., Seymour, L. W., Miyamoto, Y. (1992). Conjugates of anticancer agents and polymers: Advantages of macromolecular therapeutics *in vivo*. *Bioconjugate Chem.* **3**, 351-362.

Maeda, H., Wu, J., Sawa, T., Matsumura, Y., Hori, K. (2000). Tumor vascular permeability and the EPR effect in macromolecular therapeutics: A review. *J. Control. Release* **65**, 271-284.

Magde, D., Wong, R., Seybold, P. G. (2002). Fluorescence quantum yields and their relation to lifetimes of rhodamine 6G and fluorescein in nine solvents: Improved absolute standards for quantum yields. *Photochem. Photobiol.* **75**, 327-334.

Makarov, A. A., Ilinskaya, O. N. (2003). Cytotoxic ribonucleases: Molecular weapons and their targets. *FEBS Lett.* **540**, 15-20.

Marshall, G. R., Feng, J. A., Kustler, D. J. (2007). *Biopolymers*, In Press.

Martin, M. M., Lindqvist, L. (1975). The pH dependence of fluorescein fluorescence. *J. Lumin.* **10**, 381-390.

Matoušek, J., Kim, J.-S., Souček, J., Rihá, J., Ribó, M., Leland, P. A., Raines, R. T. (1997). Ribonucleases endowed with specific toxicity for spermatogenic layers. *Comp. Biochem. Physiol.* **118B**, 881-888.

Matoušek, J. (2001). Ribonucleases and their antitumor activity. *Comp. Biochem. Physiol.* **129C**, 175-191.

Matoušek, J., Poučková, P., Souček, J., Škvor, J. (2002). PEG chains increase aspermatogenic and antitumor activity of RNase A and BS-RNase enzymes. *J. Control. Release* **82**, 29-37.

Matoušek, J., Gotte, G., Poučková, P., Souček, J., Slavík, T., Vottariello, F., Libonati, M. (2003a). Antitumor activity and other biological actions of oligomers of ribonuclease A. *J. Biol. Chem.* **278**, 23817-23822.

Matoušek, J., Souček, J., Slavík, T., Tománek, M., Lee, J. E., Raines, R. T. (2003b). Comprehensive comparison of the cytotoxic activities of onconase and bovine seminal ribonuclease. *Comp. Biochem. Physiol. C: Toxicol. Pharmacol.* **136**, 343-356.

Matoušek, J., Poučková, P., Hloušková, D., Zadinová, M., Souček, J., Škvor, J. (2004). Effect of hyaluronidase and PEG chain conjugation on the biologic and antitumor activity of RNase A. *J. Control. Release* **94**, 401-410.

Matsumura, A., Shibata, Y., Nakagawa, K., Nose, T. (1994). MRI contrast enhancement by Gd-DTPA-monoclonal antibody in 9L glioma rats. *Acta. Neurochir. Suppl. (Wien)* **60**, 356-358.

Mazzarella, L., Capasso, S., Demasi, D., Di Lorenzo, G., Mattia, C. A., Zagari, A. (1993). Bovine seminal ribonuclease: Structure at 1.9 Å resolution. *Acta Crystallogr., Sect. D* **49**, 389-402.

Mchedlov-Petrossyan, N. O., Rubtsov, M. I., Lukatskaya, L. L. (1992). Ionization and tautomerism of chloro-derivatives of fluorescein in water and aqueous acetone. *Dyes Pigm.* **18**, 179-198.

Mchedlov-Petrosyan, N. O. (1979). Ionization constants of fluorescein. *Zh. Anal. Khim.* **34**, 1055-1059.

McKinney, R. M., Spillane, J. T., Pearce, G. W. (1962). Amino- and nitrofluorescein derivatives. *J. Org. Chem.* **27**, 3986-3988.

McLendon, G. (1977). A correlation between myoglobin thermodynamic stabilities and species metabolic rates. *Biochem. Biophys. Res. Commun.* **77**, 959-966.

McMurry, J. (1996). Organic Chemistry. Brooks/Cole Publishing Company, Pacific Grove, CA.

Messmore, J. M., Fuchs, D. N., Raines, R. T. (1995). Ribonuclease A: Revealing structure–function relationships with semisynthesis. *J. Am. Chem. Soc.* **117**, 8057-8060.

Michaelis, M., Cinatl, J., Poučková, P., Langer, K., Kreuter, J., J., M. (2002). Coupling of the antitumoral enzyme bovine seminal ribonuclease to polyethylene glycol chains increases its systemic efficacy in mice. *Anticancer Drugs* **13**, 149-154.

Mikulski, S. M., Ardelt, W., Shogen, K., Bernstein, E. H., Menduke, H. (1990). Striking increase of survival of mice bearing M109 Madison carcinoma treated with a novel protein from amphibian embryos. *J. Natl. Cancer Inst.* **82**, 151-153.

Mikulski, S. M., Grossman, A. M., Carter, P. W., Shogen, K., Costanzi, J. J. (1993). Phase I human clinical trial of ONCONASE (P-30 Protein) administered intravenously on a weekly schedule in cancer patients with solid tumors. *Int. J. Oncol.* **3**, 57-64.

Mikulski, S. M., Costanzi, J. J., Vogelzang, N. J., McCachren, S., Taub, R. N., Chun, H., Mittelman, A., Panella, T., Puccio, C., Fine, R., Shogen, K. (2002). Phase II trial of a single weekly intravenous dose of ranpirnase in patients with unresectable malignant mesothelioma. *J. Clin. Oncol.* **20**, 274-281.

Miller, S., Janin, J., Lesk, A. M., Chothia, C. (1987). Interior and surface of monomeric proteins. *J. Mol. Biol.* **196**, 641-656.

Mitchell, D. J., Kim, D. T., Steinman, L., Fathman, C. G., Rothbard, J. B. (2000). Polyarginine enters cells more efficiently than other polycationic homopolymers. *J. Pept. Res.* **56**, 318-325.

Mitchell, J. C., Kerr, R., Ten Eyck, L. F. (2001). Rapid atomic density methods for molecular shape characterization. *J. Mol. Graph. Model.* **19**, 325-330.

Mitchell, J. C., Shahbaz, S., Ten Eyck, L. F. (2004). Interfaces in molecular docking. *Mol. Simul.* **30**, 97-106.

Moenner, M., Vosoghi, M., Ryazantsev, S., Glitz, D. (1998). Ribonuclease inhibitor protein of human erythrocytes: Characterization, loss of activity in response to oxidative stress, and association with Heinz bodies. *Blood Cells Mol. Dis.* **24**, 149-164.

Monfardini, C., Schiavon, O., Caliceti, P., Morpurgo, M., Harris, J. M., Veronese, F. M. (1995). A branched monomethoxypoly(ethylene glycol) for protein modification. *Bioconjugate Chem.* **6**, 62-69.

Monkarsh, S. P., Spence, C., Porter, J. E., Palleroni, A., Nalin, C., Rosen, P., Bailon, P. Isolation of positional isomers of monopoly(ethylene glycol)ylated interferon/α-2a and the determination of their biochemical and biological characteristics. In: J. M. Harris, S. Zalipsky. (Eds.). Poly(ethylene glycol): Chemistry and Biological Applications. American Chemical Society, Washington, D.C. 1997. pp. 207-216.

Monti, D. M., D'Alessio, G. (2004). Cytosolic RNase inhibitor only affects RNases with intrinsic cytotoxicity. *J. Biol. Chem.* **279**, 39195-39198.

Monti, D. M., Montesano Gesualdi, N., Matoušek, J., Esposito, F., D'Alessio, G. (2007). The cytosolic ribonuclease inhibitor contributes to intracellular redox homeostasis. *FEBS Lett.* **581**, 930-934.

Moreira, I. S., Fernandes, P. A., Ramos, M. J. (2007). Hot spots—a review of the protein-protein interface determinant amino-acid residues. *Proteins* **68**, 803-812.

Moroianu, J., Riordan, J. F. (1994). Identification of the nucleolar targeting signal of human angiogenin. *Biochem. Biophys. Res. Commun.* **203**, 1765-1772.

Morpurgo, M., Veronese, F. M., Kachensky, D., Harris, J. M. (1996). Preparation of characterization of poly(ethylene glycol) vinyl sulfone. *Bioconjugate Chem.* **7**, 363-368.

Mosimann, S. C., Ardelt, W., James, M. N. G. (1994). Refined 1.7 Å X-ray crystallographic structure of P-30 protein, an amphibian ribonuclease with anti-tumor activity. *J. Mol. Biol.* **236**, 1141-1153.

Murthy, B. S., Sirdeshmukh, R. (1992). Sensitivity of monomeric and dimeric forms of bovine seminal ribonuclease to human placental ribonuclease inhibitor. *Biochem. J.* **281**, 343-348.

Murthy, B. S., De Lorenzo, C., Piccoli, R., D'Alessio, G., Sirdeshmukh, R. (1996). Effects of protein RNase inhibitor and substrate on the quaternary structures of bovine seminal RNase. *Biochemistry* **35**, 3880-3885.

Nadano, D., Yasuda, T., Takeshita, H., Uchide, K., Kishi, K. (1994). Purification and characterization of human brain ribonuclease inhibitor. *Arch. Biochem. Biophys.* **312**, 421-428.

Naddeo, M., Vitagliano, L., Russo, A., Gotte, G., D'Alessio, G., Sorrentino, S. (2005). Interactions of the cytotoxic RNase A dimers with the cytosolic ribonuclease inhibitor. *FEBS Lett.* **579**, 2663-2668.

Navarro, S., Aleu, J., Jimenez, M., Boix, E., Cuchillo, C. M., Nogués, M. V. (2008). The cytotoxicity of eosinophil cationic protein/ribonuclease 3 on eukaryotic cell lines takes place through its aggregation on the cell membrane. *Cell. Mol. Life Sci.* **65**, 324-337.

Nedergaard, M., Desai, S., Pulsinelli, W. (1990). Dicarboxy-dichlorofluorescein: A new fluorescent probe for measuring acidic intracellular pH. *Anal. Biochem.* **187**, 109-114.

Neumann, U., Hofsteenge, J. (1994). Interaction of semisynthetic variants of RNase A with ribonuclease inhibitor. *Protein Sci.* **3**, 248-256.

Newman, J. A contender? Quintessence Biosciences has a chance at success with its incipient cancer drug. Wisconsin State Journal, Madison, WI, 2007.

Newton, D. L., Nicholls, P. J., Rybak, S. M., Youle, R. J. (1994). Expression and characterization of recombinant human eosinophil-derived neurotoxin and eosinophil-derived neurotoxin-anti-transferrin receptor sFv. *J. Biol. Chem.* **269**, 26739-26745.

Nitta, K., Ozaki, K., Ishikawa, M., Furusawa, S., Hosono, M., Kawauchi, H., Sasaki, K., Takayanagi, Y., Tsuiki, S., Hakomori, S. (1994). Inhibition of cell proliferation by *Rana catesbeiana* and *Rana japonica* lectins belonging to the ribonuclease superfamily. *Cancer Res.* **54**, 920-927.

Noguchi, Y., Wu, J., Duncan, R., Strohalm, J., Ulbrich, K., Akaike, T., Maeda, H. (1998). Early phase tumor accumulation of macromolecules: A great difference in clearance rate between tumor and normal tissues. *Jpn. J. Cancer Res.* **89**, 307-314.

Nogués, M. V., Vilanova, M., Cuchillo, C. M. (1995). Bovine pancreatic ribonuclease A as a model of an enzyme with multiple substrate binding sites. *Biochim. Biophys. Acta* **1253**, 16-24.

Notomista, E., Mancheño, J. M., Crescenzi, O., Di Donato, A., Gavilanes, J., D'Alessio, G. (2006). The role of electrostatic interactions in the antitumor activity of dimeric RNases. *FEBS J.* **273**, 3687-3697.

Novelli, A. (1932). Alkyl fluoresceins. *Anales Farm. Bioquim.* **3**, 112-120.

Novelli, A. (1933). Antiseptics. Mercury salts of alkylfluoresceins. *Anales Farm. Bioquim.* **4**, 29-35.

Nunn, A. D., Linder, K. E., Tweedle, M. F. (1997). Can receptors be imaged with MRI agents? *Q. J. Nucl. Med.* **41**, 155-162.

Ogan, M. D., Schmiedl, U., Moseley, M. E., Grodd, W., Paajanen, H., Brasch, R. C. (1987). Albumin labeled with Gd-DTPA. An intravascular contrast-enhancing agent for magnetic resonance blood pool imaging: preparation and characterization. *Invest. Radiol.* **22**, 665-671.

Oishi, M., Nagasaki, Y., Itaka, K., Nishiyama, N., Kataoka, K. (2005). Lactosylated poly(ethylene glycol)-siRNA conjugate through acid-labile beta-thiopropionate linkage to construct pH-sensitive polyion complex micelles achieving enhanced gene silencing in hepatoma cells. *J. Am. Chem. Soc.* **127**, 1624-1625.

Olmo, N., Turnay, J., González de Buitrago, G., López de Silanes, I., Gavilanes, J. G., Lizarbe, M. A. (2001). Cytotoxic mechanism of the ribotoxin α-sarcin. Induction of cell death via apoptosis. *Eur. J. Biochem.* **268**, 2113-2123.

Olsnes, S., Kozlov, J. V. (2001). Ricin. *Toxicon* **39**, 1723-1728.

Omelyanenko, V. G., Jiskoot, W., Herron, J. N. (1993). Role of electrostatic interactions in the binding of fluorescein by antifluorescein antibody 4-4-20. *Biochemistry* **32**, 10423-10429.

Opitz, J. G., Ciglic, M. I., Haugg, M., Trautwein-Fritz, K., Raillard, S. A., Jermann, T. M., Benner, S. A. (1998). Origin of the catalytic activity of bovine seminal ribonuclease against double-stranded RNA. *Biochemistry* **37**, 4023-4033.

Owicki, J. C. (2000). Fluorescence polarization and anisotropy in high throughput screening: Perspectives and primer. *J. Biomol. Screen.* **5**, 297-306.

Pace, C. N. (1990). Measuring and increasing protein stability. *Trends Biotechnol.* **8**, 93-98.

Pace, C. N., Hebert, E. J., Shaw, K. L., Schell, D., Both, V., Krajcikova, D., Sevcik, J., Wilson, K. S., Dauter, Z., Hartley, R. W., Grimsley, G. R. (1998). Conformational stability and thermodynamics of folding of ribonucleases Sa, Sa2 and Sa3. *J. Mol. Biol.* **279**, 271-286.

Papageorgiou, A., Shapiro, R., Acharya, K. (1997). Molecular recognition of human angiogenin by placental ribonuclease inhibitor—an X-ray crystallographic study at 2.0 Å resolution. *EMBO J.* **16**, 5162-5177.

Paradiso, A. M., Tsien, R. Y., Machen, T. E. (1984). Na^+-H^+ exchange in gastric glands as measured with a cytoplasmic-trapped, fluorescent pH indicator. *Proc. Natl. Acad. Sci. U.S.A.* **81**, 7436-7440.

Park, C., Raines, R. T. (2003). Catalysis by ribonuclease A is limited by the rate of substrate association. *Biochemistry* **42**, 3509-3518.

Pasut, G., Veronese, F. M. (2007). Polymer drug conjugation, recent achievements and general strategies. *Prog. Polym. Sci.* **32**, 933-961.

Pavlakis, N., Vogelzang, N. J. (2006). Ranpirnase-an antitumour ribonuclease: Its potential role in malignant mesothelioma. *Expert Opin. Biol. Ther.* **6**, 391-399.

Pennell, C. A., Erickson, H. A. (2002). Designing immunotoxins for cancer therapy. *Immunol. Res.* **25**, 177-191.

Peters, K., Richards, F. M. (1977). Chemical cross-linking: Reagents and problems in studies of membrane structure. *Annu. Rev. Biochem.* **46**, 523-551.

Piccoli, R., Tamburrini, M., Piccialli, G., Di Donato, A., Parente, A., D'Alessio, G. (1992). The dual-mode quaternary structure of seminal RNase. *Proc. Natl. Acad. Sci. U.S.A.* **89**, 1870-1874.

Piccoli, R., Di Gaetano, S., De Lorenzo, C., Grauso, M., Monaco, C., Spalletti-Cernia, D., Laccetti, P., Cinatl, J., Matoušek, J., D'Alessio, G. (1999). A dimeric mutant of human pancreatic ribonuclease with selective cytotoxicity toward malignant cells. *Proc. Natl. Acad. Sci. U.S.A.* **96**, 7768-7773.

Pierce. (2006). Crosslinking Reagents Technical Handbook. Pierce Biotechnology, Inc., Rockford, IL.

Platzek, J., Schmitt-Willich, H., Michl, G., Frenzel, T., Sulzle, D., Bauer, H., Raduchel, B., Weinmann, H.-J., Schirmer, H. (2007) Conjugates of macrocycle metal complexes with biomolecules and their use for the productionof agents for NMR diagnosis and radiodiagnosis as well as radiotherapy. US 2007/0014725 A1, Jan. 18, 2007.

Plummer, T. H., Jr., Hirs, C. H. (1963). The isolation of ribounclease B, a glycoprotein, from bovine pancreatic juice. *J. Biol. Chem.* **238**, 1396-1401.

Plummer, T. H., Jr. (1968). Glycoproteins of bovine pancreatic juice. Isolation of ribonucleases C and D. *J. Biol. Chem.* **243**, 5961-5966.

Poučková, P., Zadinová, M., Hloušková, D., Strohalm, J., Plocová, D., Špunda, M., Olejár, T., Zitko, M., Matoušek, J., Ulbrich, K., Souček, J. (2004). Polymer-conjugated bovine pancreatic and seminal ribonucleases inhibit growth of human tumors in nude mice. *J. Control. Release* **95**, 83-92.

Pous, J., Canals, A., Terzyan, S. S., Guasch, A., Benito, A., Ribó, M., Vilanova, M., Coll, M. (2000). Three-dimensional structure of a human pancreatic ribonuclease variant, a step forward in the design of cytotoxic ribonucleases. *J. Mol. Biol.* **303**, 49-60.

Pous, J., Mallorqui-Fernandez, G., Peracaula, R., Terzyan, S. S., Futami, J., Tada, H., Yamada, H., Seno, M., de Llorens, R., Gomis-Ruth, F. X., Coll, M. (2001). Three-dimensional structure of human RNase 1 ΔN7 at 1.9 Å resolution. *Acta. Crystallogr., Sect D: Biol. Crystallogr.* **57**, 498-505.

Presta, L. G. (2006). Engineering of therapeutic antibodies to minimize immunogenicity and optimize function. *Adv. Drug Deliv. Rev.* **58**, 640-656.

Probst, J., Brechtel, S., Scheel, B., Hoerr, I., Jung, G., Rammensee, H. G., Pascolo, S. (2006). Characterization of the ribonuclease activity on the skin surface. *Genet. Vaccines Ther.* **4**, 4.

Rabinovitch, M., Dohi, S. R. (1956). Increase in serum ribonuclease activity after bilateral nephrectomy. *Am. J. Physiol.* **187**, 525-528.

Radzicka, A., Wolfenden, R. (1988). Comparing the polarities of the amino acids: Side-chain distribution coefficients between the vapor phase, cyclohexane, 1-octanol, and neutral aqueous solution. *Biochemistry* **27**, 1664-1670.

Raines, R. T. (1998). Ribonuclease A. *Chem. Rev.* **98**, 1045-1065.

Raines, R. T. Ribonuclease A: From model system to cancer chemotherapeutic. In: P. A. Frey, D. B. Northrop. (Eds.). Enzymatic Mechanisms. IOS Press, Washington, DC. 1999. pp. 235-249.

Raines, R. T. Active site of ribonuclease A. In: M. A. Zenkova. (Ed.). Artificial Nucleases. Springer–Verlag, Heidelberg, Germany. 2004. pp. 19-32.

Rajamani, D., Thiel, S., Vajda, S., Camacho, C. J. (2004). Anchor residues in protein-protein interactions. *Proc. Natl Acad. Sci. U.S.A.* **101**, 11287-11292.

Ramon, J., Saez, V., Baez, R., Aldana, R., Hardy, E. (2005). PEGylated interferon-α2b: a branched 40K polyethylene glycol derivative. *Pharm. Res.* **22**, 1374-1386.

Rappsilber, J., Siniossoglou, S., Hurt, E. C., Mann, M. (2000). A generic strategy to analyze the spatial organization of multi-protein complexes by cross-linking and mass spectrometry. *Anal. Chem.* **72**, 267-275.

Rejman, J., Oberle, V., Zuhorn, I. S., Hoekstra, D. (2004). Size-dependent internalization of particles via the pathways of clathrin- and caveolae-mediated endocytosis. *Biochem. J.* **377**, 159-169.

Renkin, E., Gilmore, J. Glomerular filtration. Handbook of Physiology. Renal Physiology. Am. Physiol. Soc., Washington, D.C. 1973. pp. 185-248.

Rennke, H. G., Patel, Y., Venkatachalam, M. A. (1978). Glomerular filtration of proteins: Clearance of anionic, neutral, and cationic horseradish peroxidase in the rat. *Kidney Int.* **13**, 278-288.

Richards, F. M., Wyckoff, H. W. Bovine Pancreatic Ribonuclease. The Enzymes. Vol. IV. 1971. pp. 647-806.

Rippe, B., Stelin, G. (1989). Simulations of peritoneal solute transport during CAPD. Application of two-pore formalism. *Kidney Int.* **35**, 1234-1244.

Rodríguez, M., Benito, A., Tubert, P., Castro, J., Ribó, M., Beaumelle, B., Vilanova, M. (2006). A cytotoxic ribonuclease variant with a discontinuous nuclear localization signal constituted by basic residues scattered over three areas of the molecule. *J. Mol. Biol.* **360**, 548-557.

Rodríguez, M., Torrent, G., Bosch, M., Rayne, F., Dubremetz, J.-F., Ribó, M., Benito, A., Vilanova, M., Beaumelle, B. (2007). Intracellular pathway of Onconase that enables its delivery to the cytosol. *J. Cell Sci.* **120**, 1405-1411.

Roehrl, M. H., Wang, J. Y., Wagner, G. (2004). A general framework for development and data analysis of competitive high-throughput screens for small-molecule inhibitors of protein-protein interactions by fluorescence polarization. *Biochemistry* **43**, 16056-16066.

Rojas, J., Taylor, R. P., Cunningham, M. R., Rutkoski, T. J., Vennarini, J., Jang, H., Graham, M. A., Geboes, K., Rousselle, S. D., Wagner, C. L. (2005). Formation, distribution, and elimination of infliximab and anti-infliximab immune complexes in cynomolgus monkeys. *J. Pharmacol. Exp. Ther.*

Rosenberg, H. F., Zhang, J., Liao, Y.-D., Dyer, K. D. (2001). Rapid diversification of RNase A superfamily ribonucleases from the bullfrog, *Rana catesbeiana*. *J. Mol. Evol.* **53**, 31-38.

Roth, J. S. (1958). Ribonuclease. VII. Partial purification and characterization of a ribonuclease inhibitor in rat liver supernatant fraction. *J. Biol. Chem.* **231**, 1085-1095.

Russell, R. B. (1994). Domain insertion. *Protein Eng.* **7**, 1407-1410.

Rutkoski, T. J., Kurten, E. L., Mitchell, J. C., Raines, R. T. (2005). Disruption of shape-complementarity markers to create cytotoxic variants of ribonuclease A. *J. Mol. Biol.* **354**, 41-54.

Rutkoski, T. J., Raines, R. T. (2008). Evasion of ribonuclease inhibitor as a determinant of ribonuclease cytotoxicity. *Curr. Pharmaceut. Biotech.*, In Press.

Rybak, S. M., Saxena, S. K., Ackerman, E. J., Youle, R. J. (1991). Cytotoxic potential of ribonuclease and ribonuclease hybrid proteins. *J. Biol. Chem.* **266**, 21202-21207.

Rybak, S. M., Hoogenboom, H. R., Meade, H. M., Raus, J. C., Schwartz, D., Youle, R. J. (1992). Humanization of immunotoxins. *Proc. Natl. Acad. Sci. U.S.A.* **89**, 3165-3169.

Rybak, S. M., Newton, D. L. (1999). Natural and engineered cytotoxic ribonucleases: Therapeutic potential. *Exp. Cell Res.* **253**, 325-335.

Ryser, H. J., Hancock, R. (1965). Histones and basic polyamino acids stimulate the uptake of albumin by tumor cells in culture. *Science* **150**, 501-503.

Sapsford, K. E., Berti, L., Medintz, I. L. (2006). Materials for fluorescence resonance energy transfer analysis: Beyond traditional donor-acceptor combinations. *Angew. Chem. Int. Ed.* **45**, 4562-4589.

Saxena, S. K., Rybak, S. M., Winkler, G., Meade, H. M., McGray, P., Youle, R. J., Ackerman, E. J. (1991). Comparison of RNases and toxins upon injection into *Xenopus* oocytes. *J. Biol. Chem.* **266**, 21208-21214.

Saxena, S. K., Shogen, K., Ardelt, W. (2003). ONCONASE® and its therapeutic potential. *Lab. Med.* **34**, 380-387.

Schein, C. H. (1997). From housekeeper to microsurgeon: The diagnostic and therapeutic potential of ribonucleases. *Nat. Biotechnol.* **15**, 529-536.

Schiavon, O., Caliceti, P., Sartore, L., Veronese, F. M. (1991). Surface modification of enzymes for therapeutic use: monomethoxypoly(ethylene glycol) derivatization of ribonuclease. *Farmaco* **46**, 967-978.

Schmiedl, U., Moseley, M. E., Sievers, R., Ogan, M. D., Chew, W. M., Engeseth, H., Finkbeiner, W. E., Lipton, M. J., Brasch, R. C. (1987a). Magnetic resonance

imaging of myocardial infarction using albumin-(Gd-DTPA), a macromolecular blood-volume contrast agent in a rat model. *Invest. Radiol.* **22**, 713-721.

Schmiedl, U., Ogan, M., Paajanen, H., Marotti, M., Crooks, L. E., Brito, A. C., Brasch, R. C. (1987b). Albumin labeled with Gd-DTPA as an intravascular, blood pool-enhancing agent for MR imaging: biodistribution and imaging studies. *Radiology* **162**, 205-210.

Schreiber, G., Fersht, A. R. (1993). Interaction of barnase with its polypeptide inhibitor barstar studied by protein engineering. *Biochemistry* **32**, 5145-5150.

Schroder, C. R., Weidgans, B. M., Klimant, I. (2005). pH Fluorosensors for use in marine systems. *Analyst* **130**, 907-916.

Schwartzberg, L. S. (2007). Chemotherapy-induced nausea and vomiting: Clinician and patient perspectives. *J. Support. Oncol.* **5**, 5-12.

Sela, M., Anfinsen, C. B., Harrington, W. F. (1957). The correlation of ribonuclease activity with specific aspects of tertiary structure. *Biochim. Biophys. Acta* **26**, 502-512.

Seno, M., Futami, J., Kosaka, M., Seno, S., Yamada, H. (1994). Nucleotide sequence encoding human pancreatic ribonuclease. *Biochim. Biophys. Acta* **1218**, 466-468.

Sevcik, J., Urbanikova, L., Leland, P. A., Raines, R. T. (2002). X-ray structure of two crystalline forms of a *Streptomycete* ribonuclease with cytotoxic activity. *J. Biol. Chem.* **277**, 47325-47330.

Shahbazi-Gahrouei, D., Williams, M., Rizvi, S., Allen, B. J. (2001). *In vivo* studies of Gd-DTPA-monoclonal antibody and gd-porphyrins: Potential magnetic resonance imaging contrast agents for melanoma. *J. Magn. Reson. Imaging.* **14**, 169-174.

Shapiro, R., Harper, J. W., Fox, E. A., Jansen, H. W., Hein, F., Uhlmann, E. (1988). Expression of Met-(-1) angiogenin in *Escherichia coli*: Conversion to the authentic <Glu-1 protein. *Anal. Biochem.* **175**, 450-461.

Shapiro, R., Ruiz-Gutierrez, M., Chen, C.-Z. (2000). Analysis of the interactions of human ribonuclease inhibitor with angiogenin and ribonuclease A by mutagenesis: Importance of inhibitor residues inside versus outside the C-terminal "Hot Spot". *J. Mol. Biol.* **302**, 497-519.

Shapiro, R. (2001). Cytoplasmic ribonuclease inhibitor. *Methods Enzymol.* **341**, 611-628.

Shaunak, S., Godwin, A., Choi, J. W., Balan, S., Pedone, E., Vijayarangam, D., Heidelberger, S., Teo, I., Zloh, M., Brocchini, S. (2006). Site-specific PEGylation of native disulfide bonds in therapeutic proteins. *Nat. Chem. Biol.* **2**, 312-313.

Sica, F., Di Fiore, A., Zagari, A., Mazzarella, L. (2003). The unswapped chain of bovine seminal ribonuclease: Crystal structure of the free and liganded monomeric derivative. *Proteins* **52**, 263-271.

Simons, B. L., Kaplan, H., Fournier, S. M., Cyr, T., Hefford, M. A. (2007). A novel cross-linked RNase A dimer with enhanced enzymatic properties. *Proteins* **66**, 183-195.

Singh, U. P., Ardelt, W., Saxena, S. K., Holloway, D. E., Vidunas, E., Lee, H.-S., Saxena, A., Shogen, K., Acharya, K. R. (2007). Enzymatic and structural characterisation of amphinase, a novel cytotoxic ribonuclease from Rana pipiens oocytes. *J. Mol. Biol.* **371**, 93-111.

Sjoback, R., Nygren, J., Kubista, M. (1995). Absorption and fluorescence properties of fluorescein. *Spectrochim. Acta, Part A* **51**, L7-L21.

Sjoback, R., Nygren, J., Kubista, M. (1998). Characterization of fluorescein-oligonucleotide conjugates and measurement of local electrostatic potential. *Biopolymers* **46**, 445-453.

Skoog, B. (1979). Determination of polyethylene glycols 4000 and 6000 in plasma protein preparations. *Vox. Sang.* **37**, 345-349.

Smeaton, J. R., Elliott, W. H., Coleman, G. (1965). An inhibitor in *Bacillus subtilis* of Its extracellular ribonuclease. *Biochem. Biophys. Res. Commun.* **18**, 36-42.

Smith, B. D., Soellner, M. B., Raines, R. T. (2003). Potent inhibition of ribonuclease A by oligo(vinylsulfonic acid). *J. Biol. Chem.* **278**, 20934-20938.

Smith, B. D. (2006). Ribonuclease Activity: Basis and Control. Biochemistry, University of Wisconsin-Madison. 249pp.

Smith, P. K., Krohn, R. I., Hermanson, G. T., Mallia, A. K., Gartner, F. H., Provenzano, M. D., Fujimoto, E. K., Goeke, N. M., Olson, B. J., Klenk, D. C. (1985). Measurement of protein using bicinchoninic acid. *Anal. Biochem.* **150**, 76-85.

Smith, S. A., Pretorius, W. A. (2002). Spectrophotometric determination of pK_a values for fluorescein using activity coefficient corrections. *Water SA* **28**, 395-402.

Soncin, F., Strydom, D. J., Shapiro, R. (1997). Interaction of heparin with human angiogenin. *J. Biol. Chem.* **272**, 9818-9824.

Sorrentino, S., Naddeo, M., Russo, A., D'Alessio, G. (2003). Degradation of double-stranded RNA by human pancreatic ribonuclease: Crucial role of noncatalytic basic amino acid residues. *Biochemistry* **42**, 10182-10190.

Sparano, B. A., Shahi, S. P., Koide, K. (2004). Effect of binding and conformation on fluorescence quenching in new 2',7'-dichlorofluorescein derivatives. *Org. Lett.* **6**, 1947-1949.

Stanton, S. G., Kantor, A. B., Petrossian, A., Owicki, J. C. (1984). Location and dynamics of a membrane-bound fluorescent hapten: A spectroscopic study. *Biochim. Biophys. Acta* **776**, 228-236.

Steinbach, G. (1974). Characterization of fluorescein isothiocyanate. Synthesis and testing methods for fluorescein isothiocyanate isomers. *Acta Histochem.* **50**, 19-34.

Sugio, S., Kashima, A., Mochizuki, S., Noda, M., Kobayashi, K. (1999). Crystal structure of human serum albumin at 2.5 Å resolution. *Protein Eng.* **12**, 439-446.

Sun, W.-C., Gee, K. R., Klaubert, D. H., Haugland, R. P. (1997). Synthesis of fluorinated fluoresceins. *J. Org. Chem.* **62**, 6469-6475.

Sunderland, C. J., Botta, M., Aime, S., Raymond, K. N. (2001). 6-carboxamido-5,4-hydroxypyrimidinones: a new class of heterocyclic ligands and their evaluation as gadolinium chelating agents. *Inorg. Chem.* **40**, 6746-6756.

Suzuki, M., Saxena, S. K., Boix, E., Prill, R. J., Vasandani, V. M., Ladner, J. E., Sung, C., Youle, R. J. (1999). Engineering receptor-mediated cytotoxicity into human ribonucleases by steric blockage of inhibitor interaction. *Nat. Biotechnol.* **17**, 265-270.

Suzuki, T., Futaki, S., Niwa, M., Tanaka, S., Ueda, K., Sugiura, Y. (2002). Possible existence of common internalization mechanisms among arginine-rich peptides. *J. Biol. Chem.* **277**, 2437-2443.

Swaney, J. B. (1986). Use of cross-linking reagents to study lipoprotein structure. *Methods Enzymol.* **128**, 613-626.

Tada, H., Onizuka, M., Muraki, K., Masuzawa, W., Futami, J., Kosaka, M., Seno, M., Yamada, H. (2004). Insertional-fusion of basic fibroblast growth factor endowed ribonuclease 1 with enhanced cytotoxicity by steric blockade of inhibitor interaction. *FEBS Lett.* **568**, 39-43.

Takakura, Y., Fujita, T., Hashida, M., Sezaki, H. (1990). Disposition characteristics of macromolecules in tumor-bearing mice. *Pharm. Res.* **7**, 339-346.

Tarnowski, G. S., Kassel, R. L., Mountain, I. M., Blackburn, P., Wilson, G., Wang, D. (1976). Comparison of antitumor activities of pancreatic ribonuclease and its cross-linked dimer. *Cancer Res.* **36**, 4074-4078.

Tatham, A. T., Nakamura, H., Wiener, E. C., Yamamoto, Y. (1999). Relaxation properties of a dual-labeled probe for MRI and neutron capture therapy. *Magn. Reson. Med.* **42**, 32-36.

Terzyan, S. S., Peracaula, R., de Llorens, R., Tsushima, Y., Yamada, H., Seno, M., Gomis-Ruth, F. X., Coll, M. (1999). The three-dimensional structure of human

RNase 4, unliganded and complexed with d(Up), reveals the basis for its uridine selectivity. *J. Mol. Biol.* **285**, 205-214.

Teufel, D. P., Kao, R. Y., Acharya, K. R., Shapiro, R. (2003). Mutational analysis of the complex of human RNase inhibitor and human eosinophil-derived neurotoxin (RNase 2). *Biochemistry* **42**, 1451-1459.

Thelen, M., Petrone, G., Oshea, P. S., Azzi, A. (1984). The use of fluorescein-dipalmitoylphosphatidylethanolamine for measuring pH-changes in the internal compartment of phospholipid vesicles. *Biochim. Biophys. Acta* **766**, 161-168.

Thomas, J. A., Buchsbaum, R. N., Zimniak, A., Racker, E. (1979). Intracellular pH measurements in Ehrlich ascites tumor cells utilizing spectroscopic probes generated *in situ*. *Biochemistry* **18**, 2210-2218.

Tilcock, C., Unger, E. C., Ahkong, Q. F., Fritz, T., Koenig, S. H., Brown, R. D., 3rd. (1991). Polymeric gastrointestinal MR contrast agents. *J. Magn. Reson. Imaging* **1**, 463-467.

Tojo, A., Endou, H. (1992). Intrarenal handling of proteins in rats using fractional micropuncture technique. *Am. J. Physiol.* **263**, F601-606.

Tracy, R. P., Currie, R. M., Kyle, R. A., Young, D. S. (1982). Two-dimensional gel electrophoresis of serum specimens from patients with monoclonal gammopathies. *Clin. Chem.* **28**, 900-907.

Ui, N. (1971). Isoelectric points and conformation of proteins. I. Effect of urea on the behavior of some proteins in isoelectric focusing. *Biochim. Biophys. Acta* **229**, 567-581.

Unger, E. C., Shen, D., Wu, G., Stewart, L., Matsunaga, T. O., Trouard, T. P. (1999). Gadolinium-containing copolymeric chelates—a new potential MR contrast agent. *MAGMA* **8**, 154-162.

Urano, Y., Kamiya, M., Kanda, K., Ueno, T., Hirose, K., Nagano, T. (2005). Evolution of fluorescein as a platform for finely tunable fluorescence probes. *J. Am. Chem. Soc.* **127**, 4888-4894.

Vasandani, V. M., Wu, Y.-N., Mikulski, S. M., Youle, R. J., Sung, C. (1996). Molecular determinants in the plasma clearance and tissue distribution of ribonucleases of the ribonuclease A superfamily. *Cancer Res.* **56**, 4180-4186.

Vellard, M. (2003). The enzyme as drug: application of enzymes as pharmaceuticals. *Curr. Opin. Biotechnol.* **14**, 444-450.

Venkatachalam, M. A., Rennke, H. G. (1978). The structural and molecular basis of glomerular filtration. *Circ. Res.* **43**, 337-347.

Venturoli, D., Rippe, B. (2005). Ficoll and dextran vs. globular proteins as probes for testing glomerular permselectivity: Effects of molecular size, shape, charge, and deformability. *Am. J. Physiol. Renal Physiol.* **288**, F605-613.

Veronese, F. M., Largajolli, R., Boccu, E., Benassi, C. A., Schiavon, O. (1985). Surface modification of proteins. Activation of monomethoxy-polyethylene glycols by phenylchloroformates and modification of ribonuclease and superoxide dismutase. *Appl. Biochem. Biotechnol.* **11**, 141-152.

Veronese, F. M., Caliceti, P., Schiavon, O. (1997). Branched and linear poly(ethylene glycol): Influence of the polymer structure on enzymological, pharmacokinetic, and immunological properties of protein conjugates. *J. Bioact. Compat. Pol.* **12**, 196-207.

Veronese, F. M. (2001). Peptide and protein PEGylation: A review of problems and solutions. *Biomaterials* **22**, 405-417.

Veronese, F. M., Pasut, G. (2005). *Drug Discov. Today* **10**, 1451-1458.

Veronese, F. M., Harris, J. M. (2008). Peptide and protein PEGylation III: advances in chemistry and clinical applications. *Adv. Drug Delivery Rev.* **60**, 1-2.

Vescia, S., Tramontano, D., Augusti-Tocco, G., D'Alessio, G. (1980). *In vitro* studies on selective inhibition of tumor cell growth by seminal ribonuclease. *Cancer Res.* **40**, 3740-3744.

Vicentini, A. M., Kieffer, B., Mathies, R., Meyhack, B., Hemmings, B. A., Stone, S. R., Hofsteenge, J. (1990). Protein chemical and kinetic characterization of recombinant porcine ribonuclease inhibitor expressed in *Saccharomyces cerevisiae*. *Biochemistry* **29**, 8827-8834.

Vincent, J. P., Lazdunski, M. (1972). Trypsin-pancreatic trypsin inhibitor association. Dynamics of the interaction and role of disulfide bridges. *Biochemistry* **11**, 2967-2977.

Wahl, R. L., Parker, C. W., Philpott, G. W. (1983a). Improved radioimaging and tumor localization with monoclonal $F(ab')_2$. *J. Nucl. Med.* **24**, 316-325.

Wahl, R. L., Philpott, G., Parker, C. W. (1983b). Monoclonal antibody radioimmunodetection of human-derived colon cancer. *Invest. Radiol.* **18**, 58-62.

Wallis, R., Moore, G. R., James, R., Kleanthous, C. (1995). Protein-protein interactions in colicin E9 DNase-immunity protein complexes. 1. Diffusion-controlled association and femtomolar binding for the cognate complex. *Biochemistry* **34**, 13743-13750.

Wang, D., Wilson, G., Moore, S. (1976). Preparation of cross-linked dimers of pancreatic ribonuclease. *Biochemistry* **15**, 660-665.

Wang, Z.-X. (1995). An exact mathematical expression for describing competitive binding of two different ligands to a protein molecule. *FEBS Lett.* **360**, 111-114.

Wells, J. A. (1991). Systematic mutational analyses of protein-protein interfaces. *Methods Enzymol.* **202**, 390-411.

Whitaker, J. E., Haugland, R. P., Prendergast, F. G. (1991). Spectral and photophysical studies of benzo[c]xanthene dyes: Dual emission pH sensors. *Anal. Biochem.* **194**, 330-344.

Wlodawer, A., Svensson, L. A., Sjölin, L., Gilliland, G. L. (1988). Structure of phosphate-free ribonuclease A refined at 1.26 Å. *Biochemistry* **27**, 2705-2717.

Wu, M. M., Llopis, J., Adams, S., McCaffery, J. M., Kulomaa, M. S., Machen, T. E., Moore, H. P., Tsien, R. Y. (2000). Organelle pH studies using targeted avidin and fluorescein-biotin. *Chem. Biol.* **7**, 197-209.

Wu, Y., Mikulski, S. M., Ardelt, W., Rybak, S. M., Youle, R. J. (1993). A cytotoxic ribonuclease. Study of the mechanism of onconase cytotoxicity. *J. Biol. Chem.* **268**, 10686-10693.

Wu, Y., Saxena, S. K., Ardelt, W., Gadina, M., Mikulski, S. M., De Lorenzo, V., D'Alessio, G., Youle, R. J. (1995). A study of the intracellular routing of cytotoxic ribonucleases. *J. Biol. Chem.* **270**, 17476-17481.

Yagi, H., Ueda, M., Jinno, H., Aiura, K., Mikami, S., Tada, H., Seno, M., Yamada, H., Kitajima, M. (2006). Anti-tumor effect in an *in vivo* model by human-derived pancreatic RNase with basic fibroblast growth factor insertional fusion protein through antiangiogenic properties. *Cancer Sci.* **97**, 1315-1320.

Yamamoto, Y., Tsutsumi, Y., Yoshioka, Y., Nishibata, T., Kobayashi, K., Okamoto, T., Mukai, Y., Shimizu, T., Nakagawa, S., Nagata, S., Mayumi, T. (2003). Site-specific PEGylation of a lysine-deficient TNF-α with full bioactivity. *Nat. Biotechnol.* **21**, 546-552.

Yamaoka, T., Tabata, Y., Ikada, Y. (1994). Distribution and tissue uptake of poly(ethylene glycol) with different molecular weights after intravenous administration to mice. *J. Pharm. Sci.* **83**, 601-606.

Yang, K., Basu, A., Wang, M., Chintala, R., Hsieh, M. C., Liu, S., Hua, J., Zhang, Z., Zhou, J., Li, M., Phyu, H., Petti, G., Mendez, M., Janjua, H., Peng, P., Longley, C., Borowski, V., Mehlig, M., Filpula, D. (2003). Tailoring structure-function and pharmacokinetic properties of single-chain Fv proteins by site-specific PEGylation. *Protein Eng.* **16**, 761-770.

Yeoh, A., Gibson, R., Yeoh, E., Bowen, J., Stringer, A., Giam, K., Logan, R., Keefe, D. (2006). Radiation therapy-induced mucositis: Relationships between fractionated radiation, NF-κB, COX-1, and COX-2. *Cancer Treat. Rev.* **32**, 645-651.

Youle, R. J., Newton, D., Wu, Y.-N., Gadina, M., Rybak, S. M. (1993). Cytotoxic ribonucleases and chimeras in cancer therapy. *Crit. Rev. Ther. Drug Carrier Syst.* **10**, 1-28.

Youle, R. J., D'Alessio, G. Antitumor RNases. In: G. D'Alessio, J. F. Riordan. (Eds.). Ribonucleases: Structures and Functions. Academic Press, New York. 1997. pp. 491-514.

Zanker, V., Peter, W. (1958). Die prototropen formen des fluoresceins. *Ber. Dtsch. Chem. Ges.* **91**, 572-580.

Zhang, J. H., Chung, T. D., Oldenburg, K. R. (1999). A simple statistical parameter for use in evaluation and validation of high-throughput screening assays. *J. Biomol. Screen.* **4**, 67-73.